iScience

CellPress

Article

Association of Halogen Bonding and Hydrogen Bonding in Metal Acetate-Catalyzed Asymmetric Halolactonization

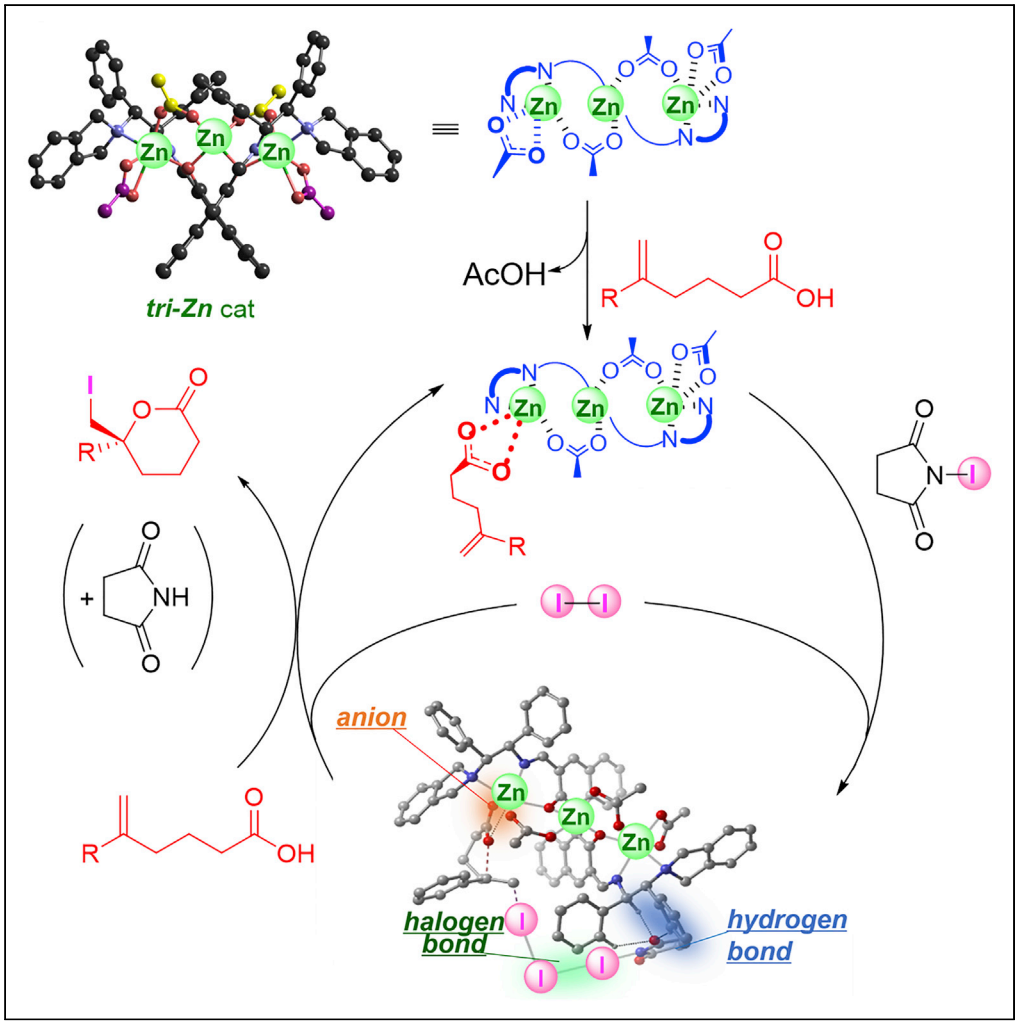

Takayoshi Arai, Kodai Horigane, Ohji Watanabe, ..., Yuto Kamei, Shinnosuke Yabe, Masahiro Yamanaka

tarai@faculty.chiba-u.jp (T.A.)
myamanak@rikkyo.ac.jp (M.Y.)

HIGHLIGHTS

Harmony of triple forces: actual iodination reagent is I_2 and not NIS

Arai et al., iScience 12, 280–292
February 22, 2019
https://doi.org/10.1016/j.isci.2019.01.029

iScience

CellPress

Article

Association of Halogen Bonding and Hydrogen Bonding in Metal Acetate-Catalyzed Asymmetric Halolactonization

Takayoshi Arai,[1,2,3,6,*] Kodai Horigane,[1] Ohji Watanabe,[1] Junki Kakino,[1] Noriyuki Sugiyama,[1] Hiroki Makino,[1] Yuto Kamei,[4] Shinnosuke Yabe,[4] and Masahiro Yamanaka[4,5,*]

SUMMARY

Cooperative activation using halogen bonding and hydrogen bonding works in metal-catalyzed asymmetric halolactonization. The $Zn_3(OAc)_4$-3,3′-bis(aminoimino)binaphthoxide (tri-Zn) complex catalyzes both asymmetric iodolactonization and bromolactonization. Carboxylic acid substrates are converted to zinc carboxylates on the tri-Zn complex, and the *N*-halosuccinimide (*N*-bromosuccinimide [NBS] or *N*-iodosuccinimide [NIS]) is activated by hydrogen bonding with the diamine unit of chiral ligand. Halolactonization is significantly enhanced by the addition of catalytic I_2. Density functional theory calculations revealed that a catalytic amount of I_2 mediates the alkene portion of the substrates and NIS to realize highly enantioselective iodolactonization. The *tri-Zn* catalyst activates both sides of the carboxylic acid and alkene moiety, so that asymmetric five-membered iodolactonization of prochiral diallyl acetic acids proceeded to afford the chiral γ-butyrolactones. In the total description of the catalytic cycle, iodolactonization using the NIS-I_2 complex proceeds with the regeneration of I_2, which enables the catalytic use of I_2. The actual iodination reagent is I_2 and not NIS.

INTRODUCTION

Electrostatic forces are fundamental forces that work in a wide range of molecular interactions. In catalysis, various metal cations act as the center of catalytic activity to enhance the reactivity of substrates (Figure 1A) (Yamamoto, 2001). Hydrogen bonding is the other representative electrostatic interaction observed between hydrogen (H) atoms with electronegative functionality (Figure 1B) (Pihko, 2009). Although these interactions have been widely utilized in the design and development of a wide range of catalysts, abundantly observed metal coordination and hydrogen bonding networks sometimes make the specific activation of substrates difficult. As a different type of noncovalent electrostatic interaction, halogen bonding has received much attention in organic chemistry. The origin of halogen bonding comes from the Lewis acidity of sigma holes that emerge on the opposite side of halogen-R sigma bonds, so that halogen bonding can effectively facilitate the direction of molecular recognition and can thus realize functional group selectivity (Figure 1C) (Cavallo et al., 2016).

Although the halogen bonding has been recently examined in several solution-phase catalyses, successful application in asymmetric reactions is limited (Beale et al., 2013; Bruckmann et al., 2008; Bulfield and Huber, 2016; Chan and Yeung, 2018; Coulembier et al., 2010; Dreger et al., 2018; Farina et al., 1999; Gliese et al., 2017; Haraguchi et al., 2018; He et al., 2014; Heiden et al., 2017; Heinen et al., 2018; Jungbauer et al., 2014; Jungbauer and Huber, 2015; Kaasik et al., 2017; Kazi et al., 2017; Kniep et al., 2013; Kuwano et al., 2018; Lim et al., 2016; Lindsay and Charette, 2012; Matsuzaki et al., 2018; Saito et al., 2017; Takeda et al., 2015; Zong et al., 2014). Here, halogen bonding and hydrogen bonding are merged with the metal-catalyzed asymmetric halolactonization (Castellanos and Fletcher, 2011; Chen and Ma, 2010; Cheng et al., 2014; Denmark et al., 2012; Hennecke, 2012; Tan et al., 2011a, 2011b, 2014).

RESULTS AND DISCUSSION

Structure-Activity Relationship of $Zn_3(OAc)_4$-3,3′-bis(aminoimino)binaphthoxide-Catalyzed Asymmetric Iodolactonization

Among the wide range of halogen chemistry, halolactonization has been well utilized in the stereoselective synthesis of versatile natural products, biologically significant pharmaceutical compounds, and agricultural chemicals. For the catalytic asymmetric version of iodolactonization, Gao reported a unique system of a

[1]Department of Chemistry, Graduate School of Science, Chiba University, 1-33 Yayoi, Inage, Chiba 263-8522, Japan

[2]Soft Molecular Activation Research Center (SMARC), Chiba University, 1-33 Yayoi, Inage, Chiba 263-8522, Japan

[3]Chiba Iodine Research Innovation Center (CIRIC), 1-33 Yayoi, Inage, Chiba 263-8522, Japan

[4]Department of Chemistry, Rikkyo University, 3-34-1 Nishi-Ikebukuro, Toshima-ku, Tokyo 171-8588, Japan

[5]Research Center for Smart Molecules, Rikkyo University, 3-34-1 Nishi-Ikebukuro, Toshima-ku, Tokyo 171-8588, Japan

[6]Lead Contact

*Correspondence: tarai@faculty.chiba-u.jp (T.A.), myamanak@rikkyo.ac.jp (M.Y.)

https://doi.org/10.1016/j.isci.2019.01.029

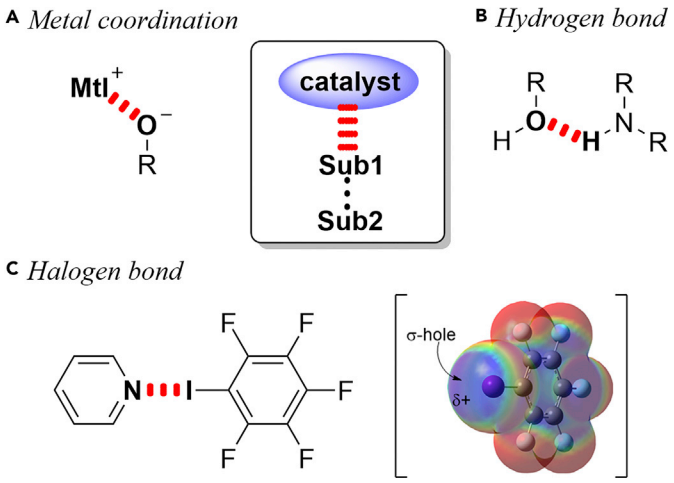

Figure 1. Classification of Electrostatic Molecular Interactions

(A) Metal coordination.

(B) Hydrogen bonding.

(C) Halogen bonding.

chiral salen-Co complex, in which I_2 was used as an I^+ source and the catalyst activity was enhanced by the addition of *N*-chlorosuccinimide (Ning et al., 2009). Jacobsen pioneered a tertiary aminourea-catalyzed asymmetric iodolactonization using *N*-iodo-4-fluorophthalimide as the I^+ source and I_2 as an additive (Veitch and Jacobsen, 2010). In the subsequently developed metal-catalyzed and organocatalyzed asymmetric iodolactonization reactions, the combined use of an I^+ source (e.g., *N*-iodosuccinimide [NIS]) with I_2 is often effective to improve the results (Arai et al., 2015a, 2015b; Brindle et al., 2013; Dobish and Johnston, 2012; Fang et al., 2012; Filippova et al., 2014; Kwon et al., 2008; Lu et al., 2018; Mizar et al., 2014; Murai et al., 2014a, 2014b; Nakatsuji et al., 2014; Toda et al., 2014; Tripathi and Mukherjee, 2013; Tungen et al., 2012; Sakakura et al., 2007; Suresh et al., 2018; Wang et al., 2012). In 2014, we also reported a highly efficient catalytic asymmetric iodolactonization using a 3,3′-bis(aminoimino)binaphthol ligand (**L1**) and $Zn(OAc)_2$. Only 1 mol% of trinuclear $Zn_3(OAc)_4$-3,3′-bis(aminoimino)binaphthoxide (**tri-Zn**) was required to catalyze the asymmetric iodolactonization using NIS with the catalytic assistance of I_2 to afford the products at up to over 99% enantiomeric excess (ee) (Figure 2) (Arai et al., 2014, 2015a, 2015b).

The structure-activity relationship of the aminoiminophenol ligands for Zn-catalyzed asymmetric iodolactonization is summarized in Table 1. The best ligand (**L1**) is prepared from (*R*, *R*)-diphenylethylenediamine and (*R*)-3,3′-diformylbinaphthol. The diastereomeric ligand (**L2**) prepared from (*S*, *S*)-diphenylethylenediamine and (*R*)-3,3′-diformylbinaphthol reduced asymmetric induction with 68% ee. Interestingly, a simple bis(aminoimino)binaphthol (**L3**) prepared using an achiral amine also provided an efficient chiral zinc catalyst to afford chiral **2a** with 98% ee. Thus the use of expensive chiral diamine is not essential for asymmetric induction. The catalyst prepared using (*R*, *R*)-diphenylethylenediamine-derived bis(aminoimino)biphenol (**L4**) gave (*R*)-enriched **2a** in 75% yield with 72% ee. From density functional theory (DFT) calculations of the **L4**-$Zn(OAc)_2$ complex, the conformation with the (*R*)-axis **L4**-Zn_3 complex is more stable by 6.0 kcal/mol than the (*S*)-axis configuration (Figure S1). The (*R*)-enriched formation of iodolactone **2a** from entry 1 to 4 shows the importance of axial chirality for the construction of an efficient asymmetric reaction sphere. 3-Aminoiminobinaphthol (**L6**) for the dinuclear Zn complex and aminoiminophenol (**L7**) for the mononuclear Zn complex resulted in low catalyst activity. Overall, high catalytic activity for asymmetric iodolactonization is obtained when the trinuclear zinc acetates are precisely arranged on the axially chiral bis(aminoimino)biphenol ligands (Shibasaki and Yamamoto, 2004).

Questions on Catalytic Asymmetric Halolactonization

Despite the success with a series of efficient catalysts for asymmetric iodolactonization, there are still unsolved problems in the catalyst behavior, especially with respect to the activation mode of the alkene moiety. Conventional catalysts for asymmetric iodolactonization generally result in low asymmetric

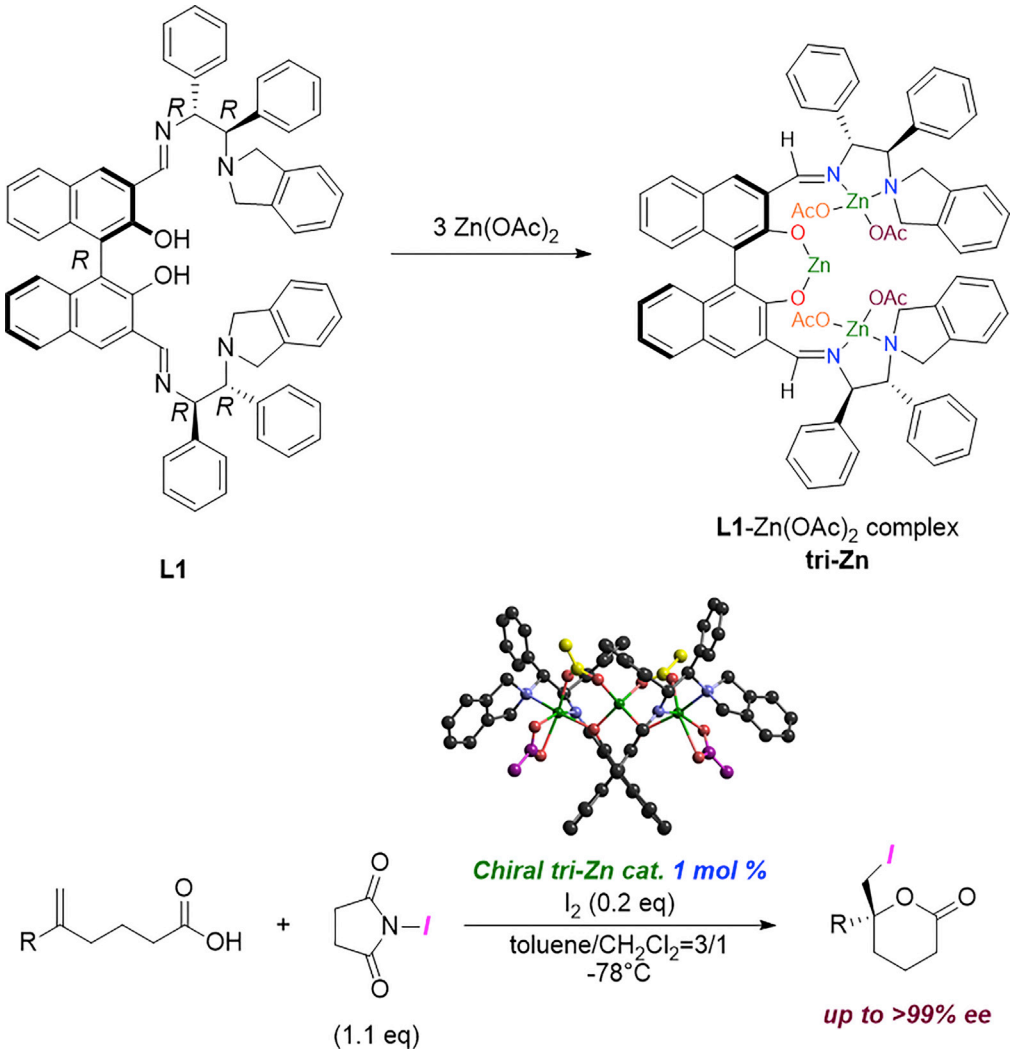

Figure 2. Chiral $Zn_3(OAc)_4$-3,3′-bis(aminoimino)binaphthoxide (tri-Zn) Catalyst for Asymmetric Iodolactonization

induction for other halolactonization (bromo-, chloro-, and fluorolactonization) reactions. The substrate scope is limited, and it is difficult to apply to rather complex molecules. For example, the catalyst developed for five-membered lactone formation tends to be unsuitable for the six-membered lactone system. The positive role of I_2 in asymmetric catalysis is also unclear. Without the addition of catalytic I_2, the **tri-Zn** catalyst gave **2a** in only 7% yield with 97% ee. The answer to the actual role of I_2 would provide realization of a true transition state, which would enable the appropriate selection of reaction substrates for the catalyst and the rational design of next-generation asymmetric catalysis.

Asymmetric Bromolactonization Using Tri-Zn Catalyst

The catalytic performance of the **tri-Zn** complex prepared using the best ligand (**L1**) was examined for asymmetric bromolactonization (Aursnes et al., 2016; Jiang et al., 2012, 2018; Murai et al., 2010; Tan et al., 2011a, 2011b; Zhou et al., 2010). When the reaction was conducted using *N*-bromosuccinimide (NBS) at −78 °C, 5 mol% **tri-Zn** complex catalyzed the bromolactonization to give the bromolactone **3a** in 38% yield with 92% ee (entry1, Table 2). Similar to the previously studied iodolactonization, the addition of I_2 or Br_2 enhanced the catalytic activity to give the bromolactone in higher chemical yields while maintaining the ees. However, interestingly, when 0.2 equiv. of I_2 was added to the bromolactonization of **1a**, 36% iodolactone **2a** (98% ee) was coproduced with 58% bromolactone **3a** (93% ee) shown in entry 2.

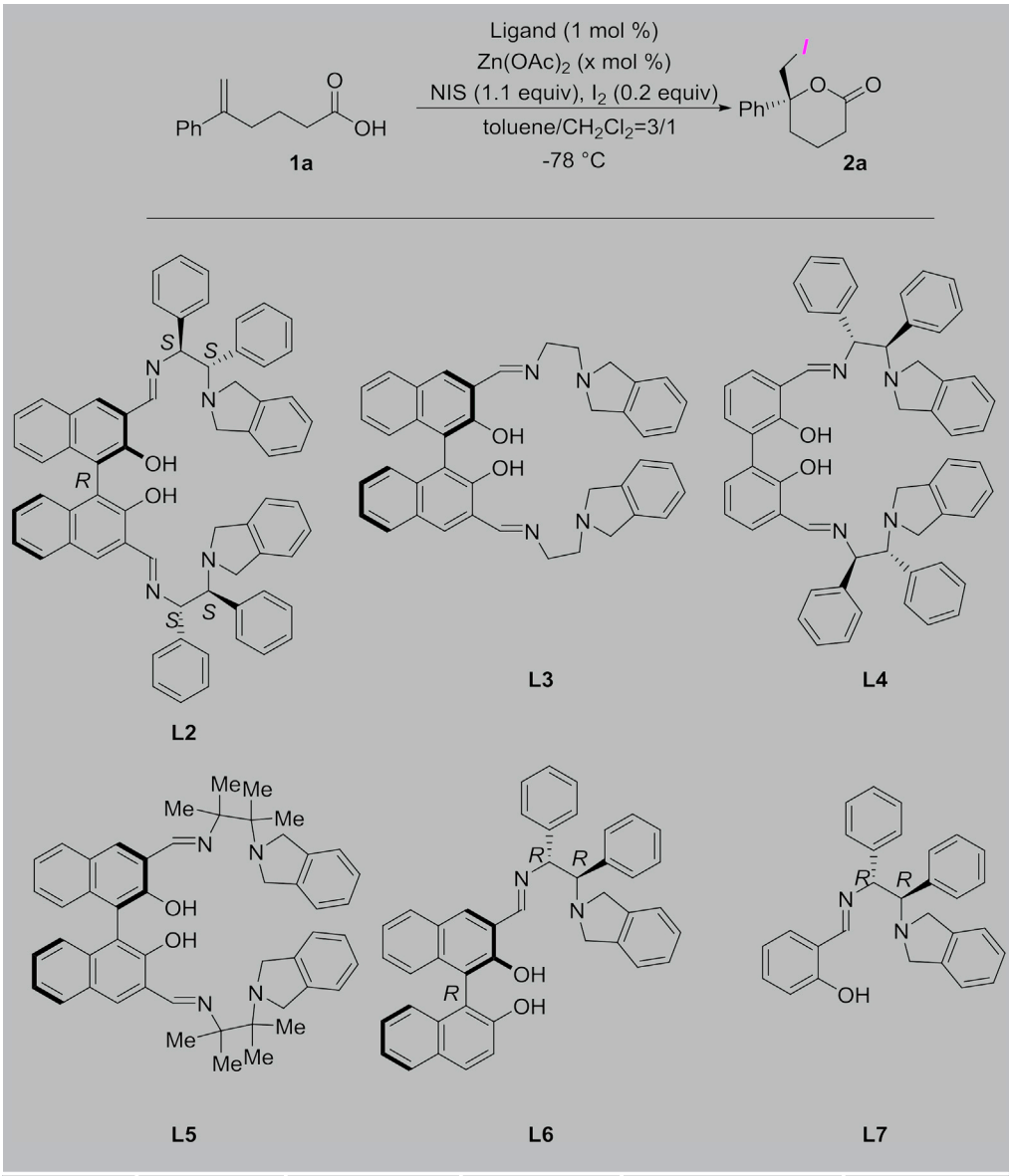

Entry	Ligand	X (mol %)	Time (h)	Yield of 2a (%)	ee of 2a (%)
1	L1	3	24	99	99.6 (*R*)
2	L2	3	24	99	68 (*R*)
3	L3	3	18	99	98 (*R*)
4	L4	3	24	75	72 (*R*)
5	L5	3	18	79	68 (*R*)
6	L6	2	24	34	89 (*R*)
7	L7	1	24	Trace	–

Table 1. Structure-Activity Relationship of the Aminoiminophenol Ligands for Zn-Catalyzed Asymmetric Iodolactonization

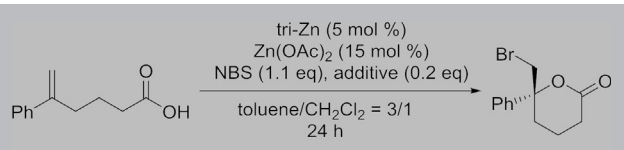

1a 3a

Entry	Additive	Additive	Temp (°C)	Yield (%)	ee (%)
1	–	–	−78	38	92
2	I_2	I_2	−78	58 (36)[a]	93 (98)[a]
3	Br_2	Br_2	−78	89	91
4	–	–	−40	99	94

Table 2. Catalytic Asymmetric Bromolactonization Using $Zn_3(OAc)_4$-3,3′-bis(aminoimino)binaphthoxide (tri-Zn) Catalyst

[a]Values in parentheses are yield or ee of iodolactone.

As a result of optimization for the bromolactonization, the reaction at −40°C without additive was selected to afford **3a** in quantitative yield with 94% ee. At this stage, it seems likely that the addition of I_2 (or Br_2) mainly contributes to accelerate the reaction and is not essential for asymmetric induction.

The scopes of both iodolactonization and bromolactonization were similar, and a comparison of bromolactonization and iodolactonization is summarized in Table S1.

DFT Calculation of the Transition State for Iodolactonization

DFT calculations were conducted to fully clarify the stereocontrol mechanism, the ligand structure-activity relationship, and the role of I_2 for Zn-catalyzed asymmetric iodolactonization. The addition of I_2 had a significant impact on the acceleration of the reaction, but no effect on stereochemical control. Therefore the transition state (**TS**)-**A** model for alkene activation by NIS was studied first (Figure 3A).

Negligible non-linear effect suggests the iodolactonization conducted on the unimolecular catalyst. In addition, a Job plot analysis suggests a 1: 1 interaction between **tri-Zn** complex and **1a** (Figure S3). This is consistent with the rational **TS-A** model for the **tri-Zn**-catalyzed asymmetric iodolactonization supposed by the previous experimental data and preliminary computational studies (Figures S6 and S7) (Arai et al., 2014). The **TS-A** model for the **tri-Zn**-catalyzed asymmetric iodolactonization involved the zinc carboxylate of **1a** replaced by the outer acetoxy anion on the **tri-Zn** complex. In $\mathbf{TS}_{major}$-**A**, to produce the preferentially obtained (*R*)-**2a**, bidentate and strong electrostatic interaction between the Zn atom and acetoxy anion of **1a** is formed to locate the bulky substituent (e.g., Ph group of **1a**) in the empty space of **tri-Zn**. The *anti*-addition to the alkene portion of **1a** locates NIS close to the aminoimino moiety of **L1** and forms a hydrogen bond with the imino-proton. The cooperative electrostatic or hydrogen bonding interactions stabilize $\mathbf{TS}_{major}$-**A**. In contrast, different structural features regarding these two interactions were found in $\mathbf{TS}_{minor}$-**A** to give the minor enantiomer (*S*)-**2a**. The bidentate Zn-carboxylate interaction is broken by the steric repulsion between the Ph group of **1a** and the naphthyl moiety of **L1**. The axial chirality plays a key role in the asymmetric induction rather than the terminal (*R*,*R*)-diphenylenediamine part of **L1**. These computational results are consistent with the experimentally observed structure-activity relationship (entries 1 and 3 in Table 1, Figure S2). In addition, NIS stays away from **tri-Zn** to lose the hydrogen bond. The changes in the attractive non-covalent interactions between **1a**, NIS, and tri-Zn are thus major factors in directing the stereochemical outcome. In addition, $\mathbf{TS}_{minor}$-**A** is 5.1 kcal/mol less stable than $\mathbf{TS}_{major}$-**A**.

However, there still remains a question with respect to the **tri-Zn**-catalyzed iodolactonization regarding the role of I_2. For the full description of the transition state, extensive studies with DFT calculations were conducted for the **TS-B** model involving the **tri-Zn** complex, **1a**, NIS, and I_2 in Figure 3B. The relative arrangement and electrostatic interaction between the **tri-Zn** complex and **1a** are well stored in the

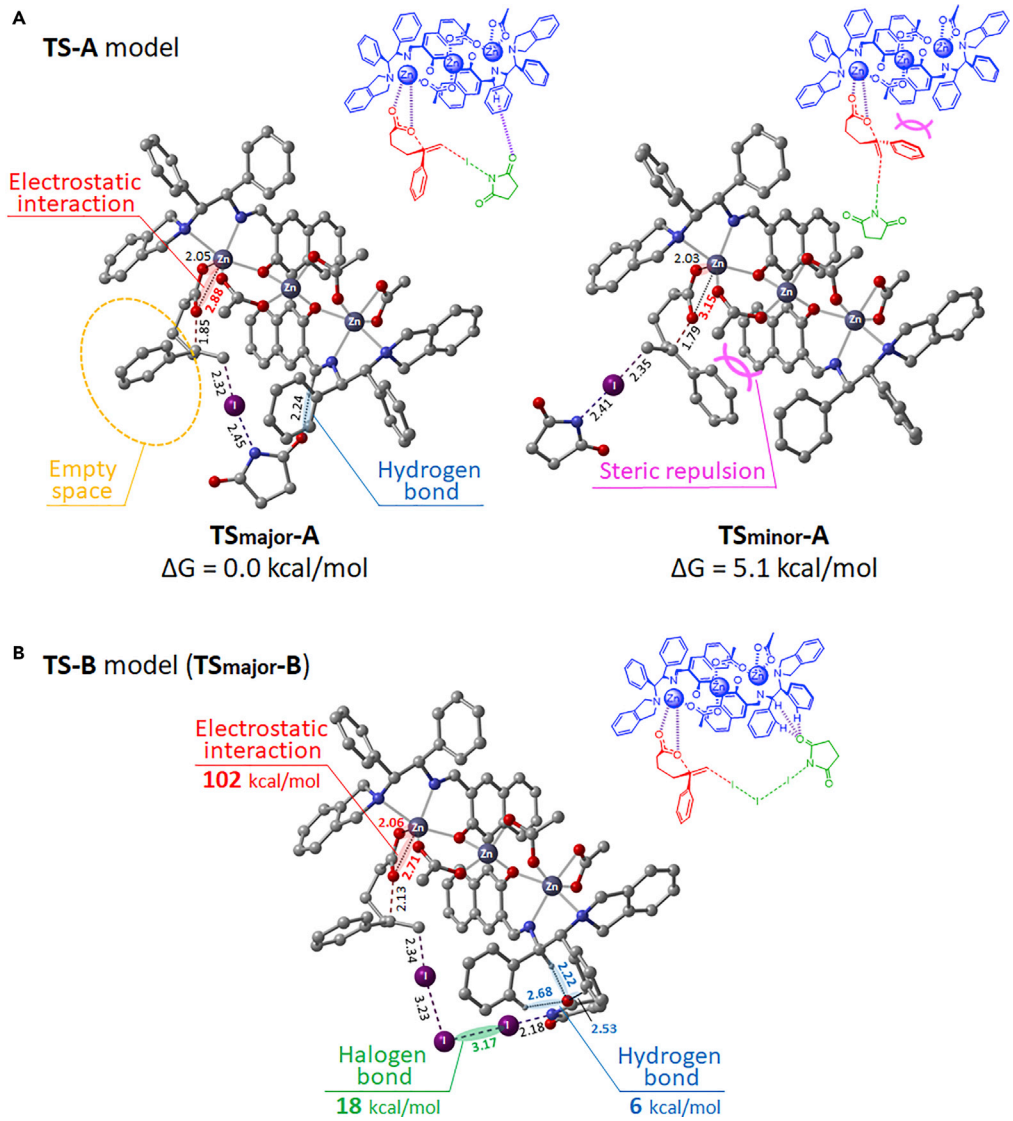

Figure 3. DFT Calculation of the Transition State for Iodolactonization

(A and B) Alkene activation by (A) NIS and (B) I_2/NIS in the **tri-Zn**-catalyzed iodolactonization. Bond lengths are in angstroms

TS-B model (TS_{major}-**B** in Figure 3B, TS_{minor}-**B** in Figure S8). Importantly, an I_2 molecule inserts between NIS and the alkene moiety of **1a** by forming a bent configuration. The bent interaction of I_2 with NIS is well explained by the halogen bonding observed in the I_3^+ species (Cavallo et al., 2016; Nakatsuji et al., 2014; Lu et al., 2018). The 1:1 interaction of the **tri-Zn** with the NIS-I_2 species was suggested by ultraviolet-visible analysis (Figure S4). One obvious difference from the **TS-A** model is the lack of hydrogen bonding interaction between NIS and the imine-proton. Owing to the insertion of I_2, NIS is moved to the right side and forms a new hydrogen bonding interaction with two methine protons of the diphenylethylenediamine framework and one proton on the benzene ring of diphenylethylenediamine. This plural hydrogen bonding scenario is well supported by the structure-activity relationship examined in Table 1 (entries 1, 3, and 5). The **tri-Zn** complex prepared from the simple ethanediamine-derived bis(aminoimino)binaphthol (**L3**)-**tri-Zn** catalyst gave **2a** with 98% ee, although the catalyst prepared from tetramethyl-substituted ethanediamine-derived bis(aminoimino)binaphthol (**L5**), which lacked the hydrogen-bonding-donating methine protons, gave **2a** with only 68% ee. In TS_{major}-**B**, the interaction energy analysis (Figure S9) clearly indicates that the electrostatic interaction (Zn carboxylate, 102 kcal/mol)

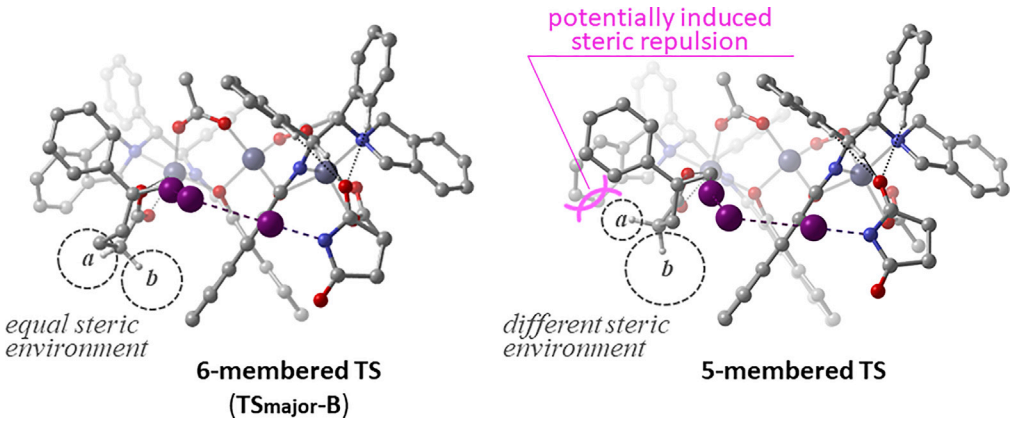

Figure 4. DFT Simulation of tri-Zn-Catalyzed Asymmetric Five-Membered Iodolactonization

is associated with hydrogen bonding (NIS-**tri-Zn**, 6 kcal/mol) and halogen bonding interactions (I_2-NIS, 18 kcal/mol). Overall, in the **tri-Zn**-catalyzed asymmetric iodolactonization, three types of attractive non-covalent interactions cooperatively stabilize the transition state to achieve high catalytic activity and almost perfect enantioselectivity.

Design of Asymmetric Five-Membered Iodolactonization Based on DFT Simulation

The five-membered lactone system was also computationally addressed (Figure 4) based on the rational TS model for formation of the six-membered lactone (Figure 3B).

There is no difference in the steric environment around the prochiral hydrogen atoms bonded to the α-carbon of the carboxyl group in the six-membered TS model (dotted circles around Ha and Hb in the left-hand side figure). On the five-membered TS model, the dotted circles around Ha and Hb in the right-hand side figure are differentiated in each space due to ring flipping. The introduction of a substituent at the prochiral hydrogen *Ha* would induce a repulsive interaction with the isoindoline moiety to increase the energy difference of the Ha- and Hb-substituted diastereomeric transition states and lead to high stereo-discrimination. Such transition state models predicted facilitation of the nucleophilic attack by the carboxylate anion to one side of the alkene moiety of the *meso*-substrate in the five-membered lactone system to yield the (3*S*, 5*R*)-product preferentially. These computational results prompted us to design the catalytic asymmetric iodolactonization of prochiral diallyl acetic acids as shown in Figure 5 (Ikeuchi et al., 2012; Jiang et al., 2018; Klosowski and Martin, 2018; Knowe et al., 2018; Murai et al., 2014a, 2014b; Wilking et al., 2013, 2016).

To accomplish the asymmetric reaction shown in Figure 5, the catalyst must recognize each side of the alkene moiety in an enantioselective manner. At the same time, the catalyst must allow incorporation of the bulky branched substrate into the asymmetric reaction sphere. This requirement can be satisfied with **tri-Zn** catalysis because the bulky substituent of the substrate remains in the empty space, as presented in Figure 4. The **tri-Zn** catalyst controlled the asymmetric iodolactonization efficiently to give the five-membered iodolactone **5** in a highly diastereo- and enantioselective manner. In agreement with the computational prediction, the absolute structure of chiral γ-butyrolactone **5a** was determined by X-ray crystallographic analysis to be (3*S*,5*R*)-5-(iodomethyl)-5-phenyl-3-(2-phenylallyl)dihydrofuran-2(3*H*)-one (see Supplemental Information, Data S1 for details.).

The synthetic utilities of the five-membered iodolactone **5** are demonstrated in Scheme 1. From 94% ee of **5a**, epoxyester **6a** and furan **7a** were obtained, which maintain the *exo*-olefine functionality. A radical cyclization of **5a** provided 7-oxabicyclo[4.2.1]nonan-8-one **8a**.

Discussion of the Catalytic Cycle of Asymmetric Iodolactonization

Based on the realization of the transition state in Figure 3B, the catalytic cycle of **tri-Zn**-catalyzed asymmetric iodolactonization can be described as shown in Figure 6A. The **tri-Zn** (**A**) would react with the

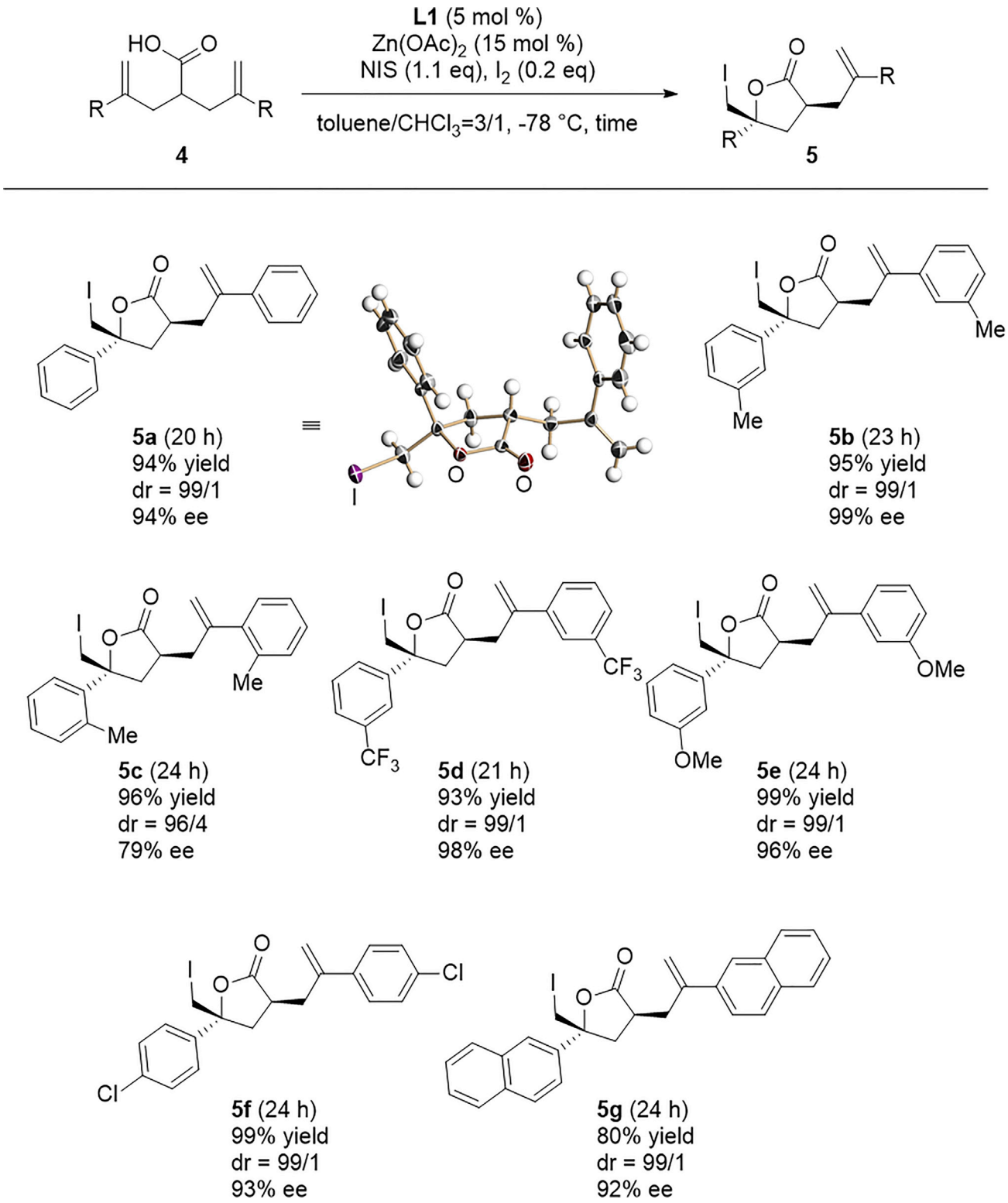

Figure 5. Catalytic Asymmetric Five-Membered Iodolactonization Using $Zn_3(OAc)_4$-3,3′-bis(aminoimino)binaphthoxide (tri-Zn) Catalyst

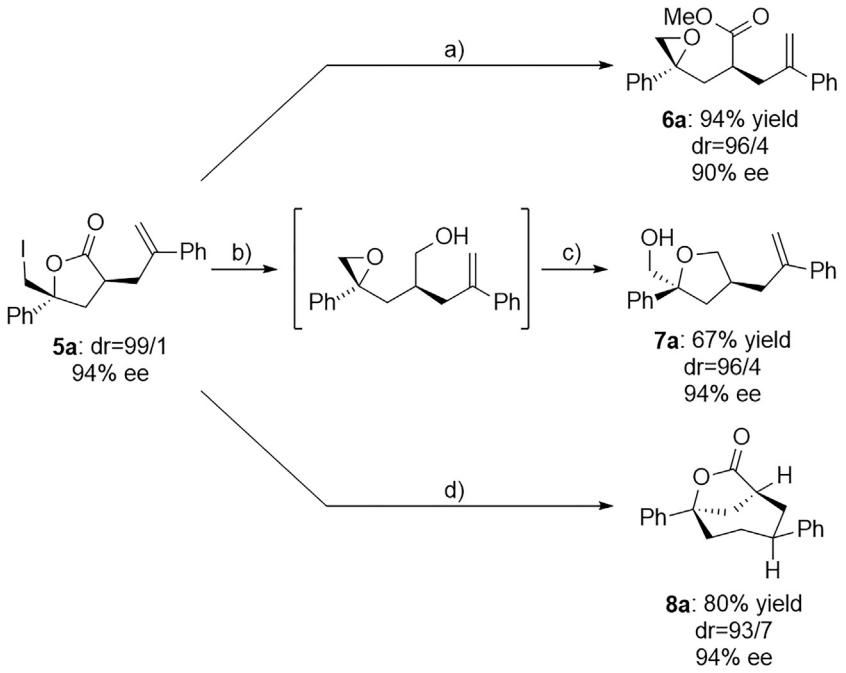

Scheme 1. Chemical Transformation of Iodolactone 5

(A) K_2CO_3 (2 equiv.), MeOH, rt, 30 min; (B) $LiBH_4$ (5 equiv.), THF/MeOH, rt, 5 h; (C) PPTS (0.1 equiv.), CH_2Cl_2, rt, 1 h; (D) AIBN (0.2 equiv.), Bu_3SnH (1.5 equiv.), toluene, 80°C, 6 h.

alkenoic acid substrate (**1**) to generate the Zn carboxylate (**B**). With the Zn carboxylate (**B**), the complex of NIS with I_2 (**C**) would activate the alkene moiety to give the model transition state (e.g., **TS-B** model). When the origin of the I-source is carefully considered (as marked by purple and green), the alkene moiety is activated by I_2, and not by NIS. However, by following the relay of arrows, the iodolactonization to yield product **2** would proceed with the co-production of *N*-succinimide and regeneration of I_2. From this mechanistic hypothesis, the **tri-Zn**-catalyzed reaction pathways with and without I_2 were compared (Figure 6B; black: with I_2, gray: without I_2). Ligand exchange process between **tri-Zn** and **1** readily proceeds without significant energy loss to generate the Zn carboxylate (**B**). Although additional I_2 entropically destabilizes the complex of NIS with I_2 (**C**) when compared with the complex of NIS without I_2 (**C′**), the **TS-B** model is −12.6 kcal/mol more stable than the **TS-A** model. By receiving the insertion of I_2, TS is significantly stabilized to accelerate the iodolactonization.

The halogen-incorporated reaction mechanism described in Figure 6A is strongly supported by the experimental results of entry 2 in Table 2, in which 36% yield of iodolactone is produced using 0.2 equiv. of I_2 for the NBS-promoted bromolactonization. This clearly indicates that both iodine atoms of I_2 are rapidly introduced to the product. The phenomenon is also well explained by the DFT simulation for the second catalytic cycle (Figure 7). In the first catalytic cycle based on the halogen-incorporated reaction mechanism, I-Br should be generated. When the I-Br is incorporated into the TS, the reaction should proceed from **TS-I** described on the left-hand side of Figure 7 to give the iodolactone.

Limitations of Study

This study is limited to catalytic asymmetric iodolactonization and bromolactonization. The method based on the current approach would be potentially applicable to other chlorolactonization or fluorolactonization.

Conclusions

Excellent catalytic activity of the **tri-Zn** catalyst to achieve highly enantioselective asymmetric halolactonization was realized. Both activation of the metal-carboxylate and hydrogen bonding activation of NIS

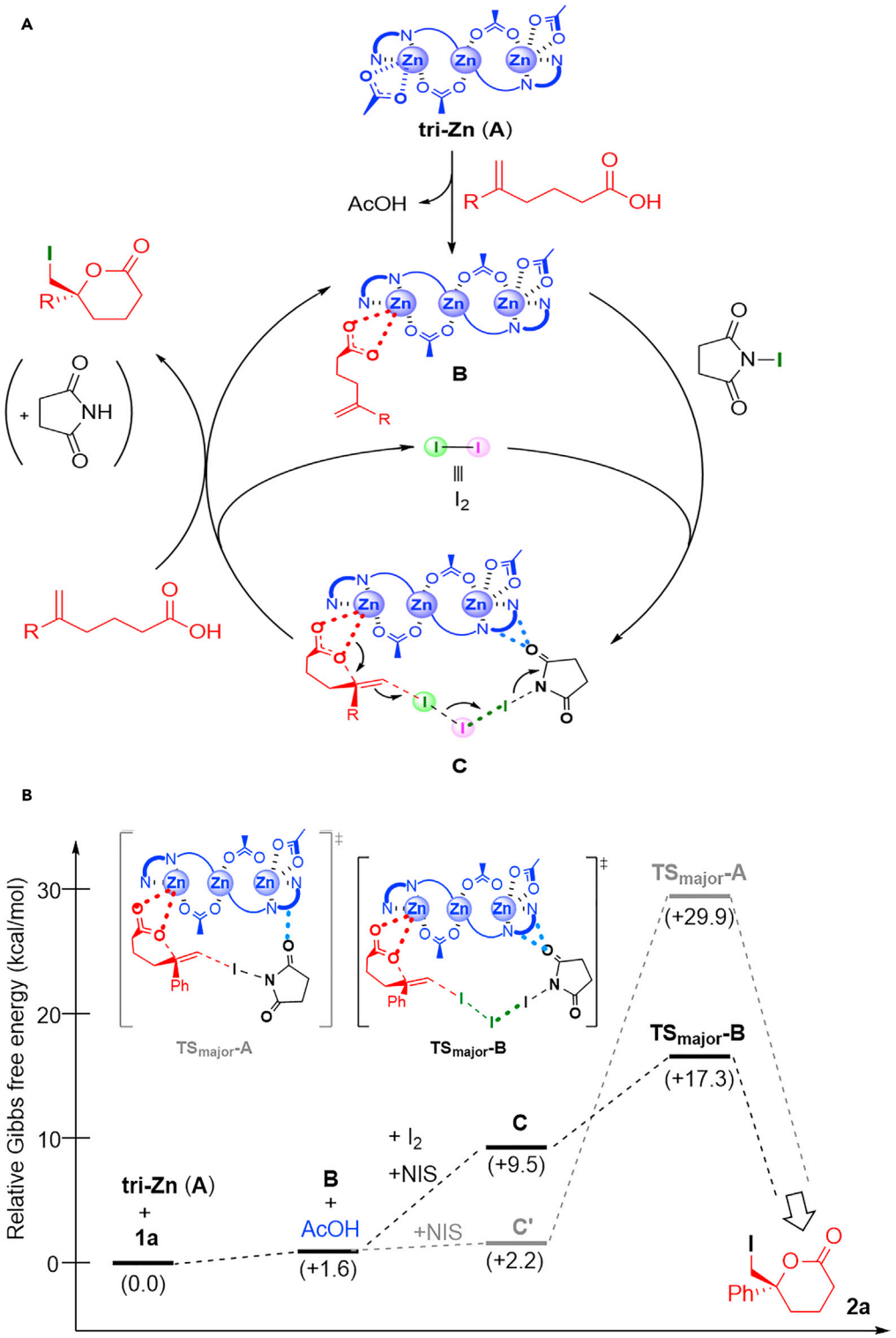

Figure 6. Reaction Mechanism of Asymmetric Iodolactonization

(A) Plausible catalytic cycle of **tri-Zn**-promoted asymmetric iodolactonization.

(B) Energy profile of plausible reaction pathways with I_2 (black) and without I_2 (gray).

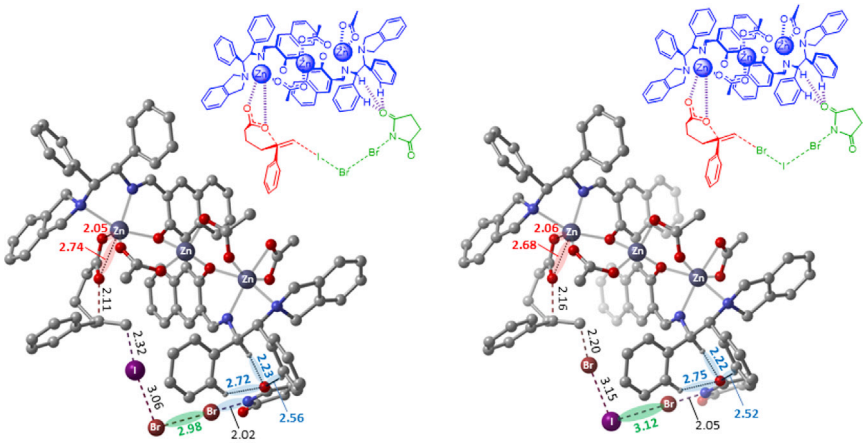

TS-I
ΔG = 0.0 kcal/mol

TS-Br
ΔG = 6.1 kcal/mol

Figure 7. Plausible Transition States for Alkene Activation by IBr with NBS in the tri-Zn-Catalyzed Halolactonization
Bond lengths are in angstroms.

are harmonized by the halogen bonding with I_2 to enable highly asymmetric iodolactonization. In the **tri-Zn**-catalyzed iodolactonization, the actual iodination reagent was identified for the first time; it is I_2, and not NIS.

METHODS

All methods can be found in the accompanying Transparent Methods supplemental file.

SUPPLEMENTAL INFORMATION

Supplemental Information includes Transparent Methods, 99 figures, 8 schemes, 1 table, and 2 data files and can be found with this article online at https://doi.org/10.1016/j.isci.2019.01.029.

ACKNOWLEDGMENTS

This research is supported by JSPS KAKENHI Grant Number JP16H01004 and JP18H04237 in Precisely Designed Catalysts with Customized Scaffolding, 17KT0011 in Development of Computationally Designed Diversity-Oriented Catalysis Based on Transition-State Control, and Workshop on Chirality at Chiba University (WCCU).

AUTHOR CONTRIBUTIONS

T.A. designed the experiments and wrote the paper; K.H., O.W., J.K., N.S., and H.M. conducted the experiments; Y.K., S.Y., and M.Y. performed all computational work.

DECLARATION OF INTERESTS

The authors declare no competing interests.

Received: September 7, 2018
Revised: December 26, 2018
Accepted: January 18, 2019
Published: February 22, 2019

REFERENCES

Arai, T., Kojima, T., Watanabe, O., Ito, T., and Kanoh, H. (2015a). Recyclable poly-$Zn_3(OAc)_4$-3,3′-bis(aminoimino)binaphthoxide catalyst for asymmetric iodolactonization. ChemCatChem *7*, 3234–3238.

Arai, T., Sugiyama, N., Masu, H., Kado, S., Yabe, S., and Yamanaka, M. (2014). A trinuclear $Zn_3(OAc)_4$-3,3′-bis(aminoimino)binaphthoxide complex for highly efficient catalytic asymmetric iodolactonization. Chem. Commun. (Camb). *50*, 8287–8290.

Arai, T., Watanabe, O., Yabe, S., and Yamanaka, M. (2015b). Catalytic asymmetric iodocyclization of N-tosyl alkenamides using aminoiminophenoxy copper carboxylate: a concise synthesis of chiral 8-oxa-6-azabicyclo [3.2.1]octanes. Angew. Chem. Int. Ed. *54*, 12767–12771.

Aursnes, M., Tungen, J.E., and Hansen, T.V. (2016). Enantioselective organocatalyzed bromolactonizations: applications in natural product synthesis. J. Org. Chem. *81*, 8287–8295.

Beale, T.M., Chudzinski, M.G., Sarwar, M.G., and Taylor, M.S. (2013). Halogen bonding in solution: thermodynamics and applications. Chem. Soc. Rev. *42*, 1667–1680.

Brindle, C.S., Yeung, C.S., and Jacobsen, E.N. (2013). Chiral β-iodoamines by urea-catalysed iodocyclization of trichloroacetimidates. Chem. Sci. *4*, 2100–2104.

Bruckmann, A., Pena, M.A., and Bolm, C. (2008). Organocatalysis through halogen-Bond activation. Synlett *2008*, 900–902.

Bulfield, D., and Huber, S.M. (2016). Halogen bonding in organic synthesis and organocatalysis. Chem. Eur. J. *22*, 14434–14450.

Castellanos, A., and Fletcher, S.P. (2011). Current methods for asymmetric halogenation of olefins. Chem. Eur. J. *17*, 5766–5776.

Cavallo, G., Metrangolo, P., Milani, R., Pilati, T., Priimagi, A., Resnati, G., and Terraneo, G. (2016). The halogen bond. Chem. Rev. *116*, 2478–2601.

Chan, Y.-C., and Yeung, Y.-Y. (2018). Halogen bond catalyzed bromocarbocyclization. Angew. Chem. Int. Ed. *57*, 3483–3487.

Chen, G.F., and Ma, S.M. (2010). Enantioselective halocyclization reactions for the synthesis of chiral cyclic compounds. Angew. Chem. Int. Ed. *49*, 8306–8308.

Cheng, Y.A., Yu, W.Z., and Yeung, Y.-Y. (2014). Recent advances in asymmetric intra- and intermolecular halofunctionalizations of alkenes. Org. Biomol. Chem. *12*, 2333–2343.

Coulembier, O., Meyer, F., and Dubois, P. (2010). Controlled room temperature ROP of L-lactide by ICl_3: a simple halogen-bonding catalyst. Polym. Chem. *1*, 434–437.

Denmark, S.E., Kuester, W.E., and Burk, M.T. (2012). Catalytic, asymmetric halofunctionalization of alkenes—a critical perspective. Angew. Chem. Int. Ed. *51*, 10938–10953.

Dobish, M.C., and Johnston, J.N. (2012). Achiral counterion control of enantioselectivity in a Brønsted acid-catalyzed iodolactonization. J. Am. Chem. Soc. *134*, 6068–6071.

Dreger, A., Engelage, E., Mallick, B., Beer, P.D., and Huber, S.M. (2018). The role of charge in 1,2,3-triazol(ium)-based halogen bonding activators. Chem. Commun. (Camb). *54*, 4013–4016.

Fang, C., Paull, D.H., Hethcox, J.C., Shugrue, C.R., and Martin, S.F. (2012). Enantioselective iodolactonization of disubstituted olefinic acids using a bifunctional catalyst. Org. Lett. *14*, 6290–6293.

Farina, A., Meille, S.V., Messina, M.T., Metrangolo, P., Resnati, G., and Vecchio, G. (1999). Resolution of racemic 1,2-dibromohexafluoropropane through halogen-bonded supramolecular helices. Angew. Chem. Int. Ed. *38*, 2433–2436.

Filippova, L., Stenstrfm, Y., and Hansen, T.V. (2014). An asymmetric iodolactonization reaction catalyzed by a zinc bis-proline–phenol complex. Tetrahedron Lett. *55*, 419–422.

Gliese, J.-P., Jungbauer, S.H., and Huber, S.M. (2017). A halogen-bonding-catalyzed Michael addition reaction. Chem. Commun. (Camb). *53*, 12052–12055.

Haraguchi, R., Hoshino, S., Sakai, M., Tanazawa, S., Morita, Y., Komatsu, T., and Fukuzawa, S. (2018). Bulky iodotriazolium tetrafluoroborates as highly active halogen-bonding-donor catalysts. Chem. Commun. (Camb). *54*, 10320–10323.

He, W., Ge, Y.C., and Tan, C.H. (2014). Halogen-bonding-induced hydrogen transfer to C=N bond with Hantzsch ester. Org. Lett. *16*, 3244–3247.

Heiden, D.V.D., Bozkus, S., Klussmann, M., and Breugst, M. (2017). Reaction mechanism of iodine-catalyzed michael additions. J. Org. Chem. *82*, 4037–4043.

Heinen, F., Engelage, E., Dreger, A., Weiss, R., and Huber, S.M. (2018). Iodine(III) derivatives as halogen bonding organocatalysts. Angew. Chem. Int. Ed. *57*, 3830–3833.

Hennecke, U. (2012). New catalytic approaches towards the enantioselective halogenation of alkenes. Chem. Asian J. *7*, 456–465.

Ikeuchi, K., Ido, S., Yoshimura, S., Asakawa, T., Inai, M., Hamashima, Y., and Kan, T. (2012). Catalytic desymmetrization of cyclohexadienes by asymmetric bromolactonization. Org. Lett. *14*, 6016–6019.

Jiang, X., Liu, S., Yang, S., Jing, M., Xu, L., Yu, P., Wang, Y., and Yeung, Y.-Y. (2018). Enantioselective bromolactonization of deactivated olefinic acids. Org. Lett. *20*, 3259–3262.

Jiang, X., Tan, C.K., Zhou, L., and Yeung, Y.-Y. (2012). Enantioselective bromolactonization using an S-alkyl thiocarbamate catalyst. Angew. Chem. Int. Ed. *51*, 7771–7775.

Jungbauer, S.H., Walter, S.M., Schindler, S., Rout, L., Kniep, F., and Huber, S.M. (2014). Activation of a carbonyl compound by halogen bonding. Chem. Commun. (Camb). *50*, 6281–6284.

Jungbauer, S.H., and Huber, S.M. (2015). Cationic multidentate halogen-bond donors in halide abstraction organocatalysis: catalyst optimization by preorganization. J. Am. Chem. Soc. *137*, 12110–12120.

Kaasik, M., Kaabel, S., Kriis, K., Jarving, I., Aav, R., Rissanen, K., and Kanger, T. (2017). Synthesis and characterisation of chiral triazole-based halogen-bond donors: halogen bonds in the solid state and in solution. Chem. Eur. J. *23*, 7337–7344.

Kazi, I., Guha, S., and Sekar, G. (2017). CBr_4 as a halogen bond donor catalyst for the selective activation of benzaldehydes to synthesize α,β-unsaturated ketones. Org. Lett. *19*, 1244–1247.

Klosowski, D.W., and Martin, S.F. (2018). Enantioselective synthesis of F-ring fragments of Kibdelone C via desymmetrizing bromolactonization of 1,4-dihydrobenzoic acid. Synlett *2018*, 430–432.

Kniep, F., Jungbauer, S.H., Zhang, Q., Walter, S.M., Schindler, S., Schnapperelle, I., Herdtweck, E., and Huber, S.M. (2013). Organocatalysis by neutral multidentate halogen-bond donors. Angew. Chem. Int. Ed. *52*, 7028–7032.

Knowe, M.T., Danneman, M.W., Sun, S., Pink, M., and Johnston, J.N. (2018). Biomimetic desymmetrization of a carboxylic acid. J. Am. Chem. Soc. *140*, 1998–2001.

Kuwano, S., Suzuki, T., Hosaka, Y., and Arai, T. (2018). A chiral organic base catalyst with halogen-bonding-donor functionality: asymmetric Mannich reactions of malononitrile with N-Boc aldimines and ketimines. Chem. Commun. (Camb). *54*, 3847–3850.

Kwon, H.Y., Park, C.M., Lee, S.B., Youn, J.-H., and Kang, S.H. (2008). Asymmetric iodocyclization catalyzed by salen–$Cr^{III}Cl$: its synthetic application to swainsonine. Chem. Eur. J. *14*, 1023–1028.

Lim, J.Y.C., Marques, I., Ferreira, L., Fèlix, V., and Beer, P.D. (2016). Enhancing the enantioselective recognition and sensing of chiral anions by halogen bonding. Chem. Commun. (Camb). *52*, 5527–5530.

Lindsay, V.N.G., and Charette, A.B. (2012). Design and synthesis of chiral heteroleptic rhodium(II) carboxylate catalysts: experimental investigation of halogen bond rigidification effects in asymmetric cyclopropanation. ACS Catal. *2*, 1221–1225.

Lu, Y., Nakatsuji, H., Okumura, Y., Yao, L., and Ishihara, K. (2018). Enantioselective halo-oxy- and halo-azacyclizations induced by chiral amidophosphate catalysts and halo-Lewis acids. J. Am. Chem. Soc. *140*, 6039–6043.

Matsuzaki, K., Uno, H., Tokunaga, E., and Shibata, N. (2018). Fluorobissulfonylmethyl iodides: an efficient scaffold for halogen bonding catalysts with an sp^3-hybridized carbon−iodine moiety. ACS Catal. *8*, 6601–6605.

Mizar, P., Burrelli, A., Gunther, E., Softje, M., Farooq, U., and Wirth, T. (2014). Organocatalytic stereoselective iodoamination of alkenes. Chem. Eur. J. *20*, 13113–13116.

Murai, K., Matsushita, T., Nakamura, A., Fukushima, S., Shimura, M., and Fujioka, H. (2010). Asymmetric bromolactonization catalyzed by a C_3-symmetric chiral trisimidazoline. Angew. Chem. Int. Ed. *49*, 9174–9177.

Murai, K., Nakajima, J., Nakamura, A., Hyogo, N., and Fujioka, H. (2014a). Enantioselective, desymmetrizing, bromolactonization reactions of symmetric olefinic dicarboxylic acids. Chem. Asian J. *9*, 3511–3517.

Murai, K., Shimizu, N., and Fujioka, H. (2014b). Enantioselective iodolactonization of allenoic acids. Chem. Commun. (Camb). *50*, 12530–12533.

Nakatsuji, H., Sawamura, Y., Sakakura, A., and Ishihara, K. (2014). Cooperative activation with chiral nucleophilic catalysts and N-haloimides: enantioselective iodolactonization of 4-arylmethyl-4-pentenoic acids. Angew. Chem. Int. Ed. *53*, 6974–6977.

Ning, Z., Jin, R., Ding, J., and Gao, L. (2009). Enantioselective iodolactonizations of 4-pentenoic acid derivatives mediated by chiral salen-Co(II) complex. Synlett *2009*, 2291–2294.

Pihko, P.M., ed. (2009). Hydrogen Bonding in Organic Synthesis (Wiley-VCH).

Saito, M., Kobayashi, Y., Tsuzuki, S., and Takemoto, Y. (2017). Electrophilic activation of iodonium ylides by halogen-bond-donor catalysis for cross-enolate coupling. Angew. Chem. Int. Ed. *56*, 7653–7657.

Sakakura, A., Ukai, A., and Ishihara, K. (2007). Enantioselective halocyclization of polyprenoids induced by nucleophilic phosphoramidites. Nature *445*, 900–903.

Shibasaki, M., and Yamamoto, Y., eds. (2004). Multimetallic Catalysts in Organic Synthesis (Wiley-VCH).

Suresh, R., Simlandy, A.K., and Mukherjee, S. (2018). A catalytic enantioselective iodocyclization route to dihydrooxazines. Org. Lett. *20*, 1300–1303.

Takeda, Y., Hisakuni, D., Lin, C.H., and Minakata, S. (2015). 2-Halogenoimidazolium salt catalyzed aza-Diels–Alder reaction through halogen-bond formation. Org. Lett. *17*, 318–321.

Tan, C.K., Zhou, L., and Yeung, Y.-Y. (2011a). Organocatalytic enantioselective halolactonizations: strategies of halogen activation. Synlett *2011*, 1335–1339.

Tan, C.K., Zhou, L., and Yeung, Y.-Y. (2011b). Aminothiocarbamate-catalyzed asymmetric bromolactonization of 1,2-disubstituted olefinic acids. Org. Lett. *13*, 2738–2741.

Tan, C.K., Yu, W.Z., and Yeung, Y.-Y. (2014). Stereoselective bromofunctionalization of alkenes. Chirality *26*, 328–343.

Toda, Y., Pink, M., and Johnston, J.N. (2014). Brønsted acid catalyzed phosphoramidic acid additions to alkenes: diastereo- and enantioselective halogenative cyclizations for the synthesis of C- and P-chiral phosphoramidates. J. Am. Chem. Soc. *136*, 14734–14737.

Tripathi, C.B., and Mukherjee, S. (2013). Catalytic enantioselective iodoetherification of oximes. Angew. Chem. Int. Ed. *52*, 8450–8453.

Tungen, J.E., Nolsøe, J.M.J., and Hansen, T.V. (2012). Asymmetric iodolactonization utilizing chiral squaramides. Org. Lett. *14*, 5884–5887.

Veitch, G.E., and Jacobsen, E.N. (2010). Tertiary aminourea-catalyzed enantioselective iodolactonization. Angew. Chem. Int. Ed. *49*, 7332–7335.

Wang, Y.-M., Wu, J., Hoong, C., Rauniyar, V., and Toste, F.D. (2012). Enantioselective halocyclization using reagents tailored for chiral anion phase-transfer catalysis. J. Am. Chem. Soc. *134*, 12928–12931.

Wilking, M., Daniliuc, C.G., and Hennecke, U. (2016). Monomeric cinchona alkaloid-based catalysts for highly enantioselective bromolactonisation of alkynes. Chem. Eur. J. *22*, 18601–18607.

Wilking, M., Muck-Lichtenfeld, C., Daniliuc, C.G., and Hennecke, U. (2013). Enantioselective, desymmetrizing bromolactonization of alkynes. J. Am. Chem. Soc. *135*, 8133–8136.

Yamamoto, H., ed. (2001). In Lewis Acids in Organic Synthesis, *Vol. 1 & 2* (Wiley-VCH).

Zhou, L., Tan, C.K., Jiang, X., Chen, F., and Yeung, Y.-Y. (2010). Asymmetric bromolactonization using amino-thiocarbamate catalyst. J. Am. Chem. Soc. *132*, 15474–15476.

Zong, L., Ban, X., Kee, C.W., and Tan, C.H. (2014). Catalytic enantioselective alkylation of sulfenate anions to chiral heterocyclic sulfoxides using halogenated pentanidium salts. Angew. Chem. Int. Ed. *53*, 11849–11853.

ISCI, Volume *12*

Supplemental Information

Association of Halogen Bonding and Hydrogen Bonding in Metal Acetate-Catalyzed Asymmetric Halolactonization

Takayoshi Arai, Kodai Horigane, Ohji Watanabe, Junki Kakino, Noriyuki Sugiyama, Hiroki Makino, Yuto Kamei, Shinnosuke Yabe, and Masahiro Yamanaka

Contents

Transparent Methods

1. General

Dry solvents were purchased from commercial suppliers and used without further purification. Analytical thin-layer chromatography (TLC) was performed on glass plates coated with 0.25 mm 230-400 mesh silica gel containing a fluorescent indicator (Merck, #1.05715.0009). Silica-gel column chromatography was performed on Kanto silica gel 60 (spherical, 100-210 μm). IR spectra were recorded on JASCO FT/IR-4100 using ATR. ^{1}H-NMR spectra were recorded on JEOL ECS-400 (400MHz), ECA-500 (500MHz), ECX-400 (400MHz) spectrometers. Chemical shifts of ^{1}H-NMR spectra were reported relative to tetramethyl silane (δ 0). ^{13}C-NMR spectra were recorded on JEOL ECS-400 (100MHz), ECA-500 (125MHz), ECX-400 (100MHz) spectrometers. Chemical shifts of ^{13}C-NMR spectra were reported relative to $CDCl_3$ (δ 77.0). Splitting patterns were reported as s, singlet; d, doublet; t, triplet; q, quartet; m, multiplet; br, broad.

2. Synthesis and analytical data of aminoimine ligands

***(R)*-3,3'-bis((*E*)-(((*1R*,*2R*)-2-(isoindolin-2-yl)-1,2-diphenylethyl)imino)methyl)-[1,1'-binaphthalene]-2,2'-diol (L1)** (Arai et al., 2014)

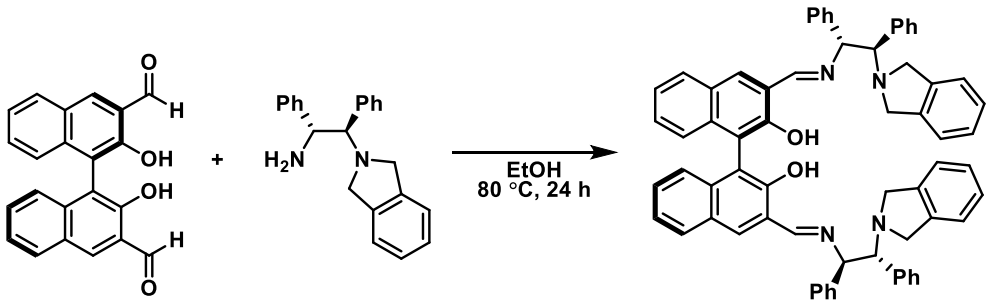

Scheme S1. Synthesis of **L1**, related to **Figure 2**.

A mixture of (*R*)-2,2'-dihydroxy-[1,1'-binaphthalene]-3,3'-dicarbaldehyde (Belkon et al., 2006) (61.0 mg, 0.195 mmol) and (*1R,2R*)-2-(isoindolin-2-yl)-1,2-diphenylethanamine (0.41 mmol) (Arai et al., 2007) in ethanol (30 mL) was heated to reflux. After being stirred for 24 hours, the solvent was removed under reduced pressure and the resulting residue was washed with cold ethanol to give bis(aminoimino)binaphthol as a yellow brown solid. ^{1}H NMR (500 MHz, $CDCl_3$) δ 8.78 (s, 2H), 7.96 (s, 2H), 7.88 (d, *J*=7.73 Hz, 2H), 7.37-7.30 (m, 6H), 7.14-7.00 (m, 30 H), 4.95 (d, *J*=7.45 Hz, 2H), 4.25 (d, *J*=7.45 Hz, 2H), 4.05 (d, *J*=11.46 Hz, 4H), 3.98 (d, *J*=11.46 Hz, 4H); ^{13}C NMR (125MHz,$CDCl_3$)δ164.97, 154.57, 139.89, 139.48, 138.02, 135.27, 133.92, 129.54, 128.89, 128.26, 128.11, 127.93, 127.74, 127.62, 127.22, 127.06, 126.58, 124.94, 123.35, 122.12, 121.09, 116.59, 78.70, 77.54, 58.32;HRMS calced for $C_{66}H_{55}O_2N_4$ $(M+H)^+$: 935.4320, found: *m/z* 935.4314; $[\alpha]_D^{20.0}$= +30.6 (c=0.115, $CHCl_3$); IR (neat) 3696, 3028, 2870, 2783, 1628, 1494, 1464, 1451, 1384, 1341, 1316, 1299, 1263, 1176, 1149, 1119, 1073, 1053, 1028, 934 cm^{-1}.

3,3'-bis((E)-(((1R,2R)-2-(isoindolin-2-yl)-1,2-diphenylethyl)imino)methyl)-[1,1'-biphenyl]-2,2'-diol (L4)

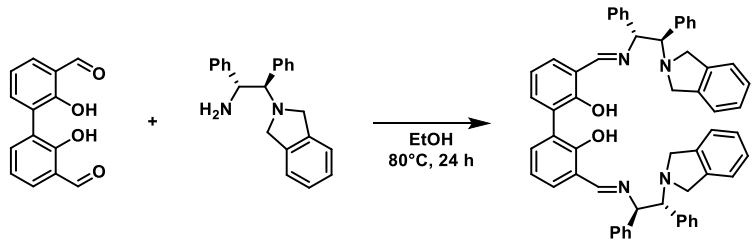

Scheme S2. Synthesis of **L4**, related to **Table 1**.

A mixture of 2,2'-dihydroxy-[1,1'-biphenyl]-3,3'-dicarbaldehyde (Wünnemann et al., 2008) (0.195 mmol) and (*1R,2R*)-2-(isoindolin-2-yl)-1,2-diphenylethanamine (0.41 mmol) (Arai et al., 2007) in ethanol (30 mL) was stirred for 24 hours at 80 °C. Then the solvent was removed under reduced pressure and the resulting residue was washed with cold ethanol to give bis(aminoimino)biphenol **L4** as a brown solid.

TLC R*f* = 0.50 (Hexane/ethyl acetate = 4/1); ^{1}H NMR (400 MHz, $CDCl_3$) δ 8.55 (s, 2H), 7.51 (dd, *J* = 7.52, 1.57 Hz, 2H), 7.27 (dd, *J* = 7.63, 1.57 Hz, 2H), 7.13-7.04 (m, 28H), 6.98 (dd, *J* = 7.63, 7.52 Hz, 2H), 4.89 (d, *J* = 6.96 Hz, 2H), 4.17 (d, *J* = 6.96 Hz, 2H), 3.97 (d, *J* = 11.67 Hz, 4H), 3.92 (d, *J* = 11.67 Hz, 2H); ^{13}C NMR (100 MHz, $CDCl_3$) δ 165.1, 158.7, 140.4, 139.5, 138.4, 134.5, 131.2, 129.4, 127.9, 127.8, 127.7, 127.1, 126.9, 126.5, 125.6, 122.2, 119.1, 118.2, 78.1, 75.6, 58.3; HRMS calced for $C_{58}H_{51}N_4O_2$ $(M+H)^+$: 835.4007, found: *m/z* 835.4014; $[\alpha]_D^{19.0}$ = + 95.67 (c = 0.1, $CHCl_3$); IR (neat) 3029, 2784, 1626, 1452, 1127, 908, 748, 704 cm^{-1}.

2-(isoindolin-2-yl)ethan-1-amine

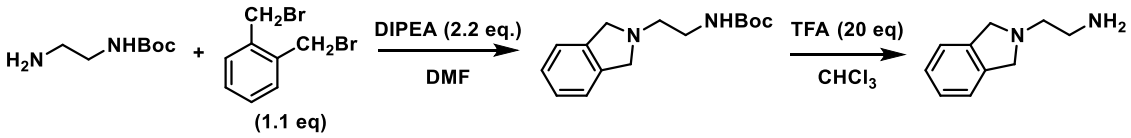

Scheme S3. Synthesis of 2-(isoindolin-2-yl)ethan-1-amine, related to **Table 1**.

A mixture of *tert*-butyl (2-aminoethyl)carbamate (Hoffmann and Kazmaier, 2014) (3 mmol) and DIPEA (6.6 mmol) in DMF (15 mL) were heated to 40 °C. *o*-xylylenedibromide (3.3 mmol) was added to the solution and stirred for 24h at the same temperature. Then, the reaction mixture was quenched by water, and extracted with ethyl acetate in three times. The corrected organic layer was washed with brine, and dried over Na_2SO_4. After removal of the solvent under reduced pressure, the residue was purified by silica-gel column chromathography (hexane/ethyl acetate = 1/1) to afford the *tert*-butyl (2-(isoindolin-2-yl)ethyl)carbamate.TLC R*f* = 0.2 (Hexane/ethyl acetate = 2/1); ^{1}H NMR (400 MHz, $CDCl_3$) δ 7.20 (s, 4H), 5.15 (br, 1H), 3.94 (s, 4H), 3.31 (dt, *J* = 5.61, 5.39 Hz, 2H), 2.86 (t, *J* = 5.39 H, 2H), 1.44 (s, 9H); ^{13}C NMR (100 MHz, $CDCl_3$) δ 156.0, 139.7, 126.7, 122.1, 78.9, 58.6, 54.6, 38.9, 28.3; HRMS calcd for $C_{15}H_{23}N_2O_2$ $(M+H)^+$: 263.1754, found: *m/z* 263.1750; IR (neat) 3431, 2975, 1706, 1489, 1158, 1051, 748 cm^{-1}.

To a solution of the *tert*-butyl (2-(isoindolin-2-yl)ethyl)carbamate (1.8 mmol) in chloroform (12 mL) was added TFA (36 mmol). The resulting mixture was stirred overnight, then quenched by saturated K_2CO_3 aq. The organic layer was extracted with chloroform and collected organic layer was dried over Na_2SO_4. The solvent was removed *in vacuo* to give 2-(isoindolin-2-yl)ethan-1-amine.

TLC R*f* = 0.1 (Chloroform/methanol = 10/1) ^{1}H NMR (400 MHz, $CDCl_3$) δ 7.20 (s, 4H), 3.95 (s, 4H), 2.88-2.81 (m, 4H); ^{13}C NMR (100 MHz, $CDCl_3$) δ; 139.9, 126.6, 122.1, 59.0, 58.9, 40.8; HRMS calcd for $C_{10}H_{15}N_2$ $(M+H)^+$:163.1230, found: *m/z* 163.1228; IR (neat) 2933, 2774, 1467, 1353, 1148, 1094, 931, 870, 744 cm^{-1}.

3-(isoindolin-2-yl)-2,3-dimethylbutan-2-amine

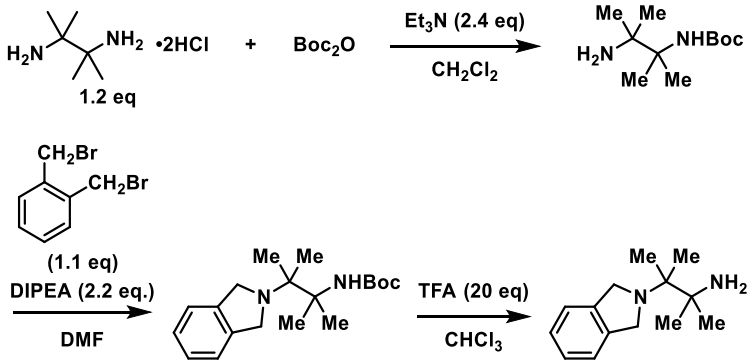

Scheme S4. Synthesis of 3-(isoindolin-2-yl)-2,3-dimethylbutan-2-amine, related to **Table 1**.

To a mixture of 2,3-Dimethyl-2,3-butanediamine dihydrochloride (2.4 mmol) and Et_3N (4.8 mmol) in dichloromethane (20 mL), Boc_2O (2 mmol) in dichloromethane (20 mL) was slowly added over 3h at room temperature. After concentration and addition of Na_2CO_3 solution (20%, 3 mL), the mixture was extracted with dichloromethane and dried over Na_2SO_4 affording *tert*-butyl (3-amino-2,3-dimethylbutan-2-yl)carbamate.

TLC R*f* = 0.1 (chloroform/methanol = 20/1); ^{1}H NMR (400 MHz, $CDCl_3$) δ 5.69 (br, 1H), 1.67 (br, 2H), 1.43 (s, 9H), 1.33 (s, 6H), 1.15 (s, 6H); ^{13}C NMR (100 MHz, $CDCl_3$) δ 155.5, 78.2, 57.3, 54.9, 28.4, 26.4, 21.8; HRMS calcd for $C_{11}H_{25}N_2O_2$ $(M+H)^+$: 217.1911, found: *m/z* 217.1906; IR (neat) 2993, 2806, 1705, 1555, 1354, 1165, 839 cm^{-1}.

A mixture of *tert*-butyl (3-amino-2,3-dimethylbutan-2-yl)carbamate (0.2 mmol) and DIPEA (0.44 mmol) in DMF (1 mL) were heated to 40 °C. *o*-xylylenedibromide (0.22 mmol) was added to the solution and stirred for 24h at the same temperature. Then, the reaction mixture was quenched by water, and extracted with ethyl acetate in three times. The corrected organic layer was washed with brine, and dried over Na_2SO_4. After removal of the solvent under reduced pressure, the residue was purified by silica-gel column chromathography (hexane/ethyl acetate = 4/1) to afford the *tert*-butyl (3-(isoindolin-2-yl)-2,3-dimethylbutan-2-yl)carbamate.

TLC R*f* = 0.5 (Hexane/ethyl acetate = 2/1); ^{1}H NMR (400 MHz, $CDCl_3$) δ 7.22 (s, 4H), 6.34 (br, 1H), 4.14 (s, 4H), 1.45 (s, 6H), 1.41 (s, 9H), 1.15 (s, 6H); ^{13}C NMR (100 MHz, $CDCl_3$) δ155.2, 139.3, 126.6, 122.2, 78.1, 61.2, 57.0, 54.3, 28.6, 24.7, 18.7; HRMS calcd for $C_{19}H_{31}N_2O_2$ $(M+H)^+$: 319.2380, found: *m/z* 319.2387; IR (neat) 3436, 2978, 1709, 1492, 1162, 1049, 742 cm^{-1}.

To a solution of the *tert*-butyl (3-(isoindolin-2-yl)-2,3-dimethylbutan-2-yl)carbamate (0.17 mmol) in chloroform (1.2 mL) was added TFA (3.4 mmol). The resulting mixture was stirred overnight, and then quenched by saturated K_2CO_3 aq. The organic layer was extracted with chloroform and collected organic layer was dried over Na_2SO_4. The solvent was removed *in vacuo* to give 3-(isoindolin-2-yl)-2,3-dimethylbutan-2-amine.
TLC R*f* = 0.1 (Chloroform/methanol = 20/1) ^{1}H NMR (400 MHz, $CDCl_3$) δ 7.19 (s, 4H), 4.21 (s, 2H), 2.03 (br, 2H), 1.22 (s, 6H), 1.21 (s, 6H); ^{13}C NMR (100 MHz, $CDCl_3$) δ139.9, 126.4, 122.0, 60.7, 57.1, 54.6, 28.0, 20.0; HRMS calcd for $C_{14}H_{23}N_2$ $(M+H)^+$: 219.1856, found: *m/z* 219.1854; IR (neat) 2984, 2806, 1555,1353, 1162, 742 cm^{-1}.

3. Procedures of structure-activity relationship study on the catalytic asymmetric iodolactonization (Fig. 2B)

[For entry 1]

A mixture of 3,3'-bis(aminoimino)binaphthol **L1** (0.001 mmol) and $Zn(OAc)_2$ (0.003 mmol) was stirred for 0.5 hour in anhydrous dichloromethane (1.0 ml) at rt. After cooling the mixture to -78 °C, 5-phenylhex-5-enoic acid (0.1 mmol) in toluene (3.0 ml) was slowly added to the resulting yellow solution and stirred for 0.5 hour at the same temperature. Then, *N*-iodosuccinimide (NIS) (24.6 mg, 0.11 mmol) and I_2 (5.0 mg, 0.02 mmol) were added to the reaction mixture. After being stirred for appropriate time, the reaction mixture was quenched with saturated Na_2SO_3 aq and 1*N* NaOH aq, and then the products were extracted with dichloromethane in 3 times. The collected organic layer was dried over Na_2SO_4. After removal of the solvent under reduced pressure, the residue was purified by silica-gel column chromathography (hexane/ethyl acetate = 5/1) to afford the iodolactone. The enantiomeric excesses of the products were determined by chiral stationary phase HPLC using a Daicel Chiralpak AD-H column.

[For entries 6, 7]

A mixture of corresponding aldehydes ((*R*)-bisformylbinaphthol for **L2**, (*R*)-monoformylbinaphthol for **L6** and salicylaldehydefor **L7**) (0.001 mmol) and 2-(isoindolin-2-yl)-1,2-diphenylethan-1-amine (0.002 mmol of (*1S*,*2S*)-configuration for **L2**, 0.001mmol (*1R*,*2R*)-configuration for **L6** and **L7**) was stirred for 2 hours in anhydrous dichloromethane (1.0 ml) at rt. Then added $Zn(OAc)_2$ (0.003 mmol for **L2**, 0.002 mmol for **L6** and 0.001mmol for **L7**) and stirred for 0.5 hour in the same temperature to afford Zn complex solution.

To a solution of *in situ* prepared Zn-complex as describe above, 5-phenylhex-5-enoic acid (0.1 mmol) in toluene (3.0 ml) was added and stirred for 0.5 hour at –78 °C. Then, *N*-iodosuccinimide (NIS) (0.11 mmol) and I_2 (0.02 mmol) were added to the reaction mixture. After being stirred for 24 h, the reaction mixture was quenched with saturated Na_2SO_3 aq and then the products were extracted with dichloromethane in three times. The collected organic layer was dried over Na_2SO_4. After removal of the solvent under reduced pressure, the residue was purified by silica-gel column chromathography (hexane/ethyl acetate=5/1) to afford the iodolactone. The enantiomeric excesses of the products were determined by chiral stationary phase HPLC using a Daicel Chiralpak AD-H column.

[For entries 3, 5]

A mixture of (*R*)-bisformylbinaphthol and corresponding diamine (0.005 mmol) was stirred for 2 hours in anhydrous dichloromethane (1.0 ml) at rt. Then added $Zn(OAc)_2$ (0.015 mmol) and stirred for 0.5 hour in same temperature to afford Zn complex solution. 5-phenylhex-5-enoic acid (0.1 mmol) in toluene (3.0 ml) was added and stirred for 0.5 hour at –78°C. Then, *N*-iodosuccinimide (NIS) (0.11 mmol) and I_2 (0.02 mmol) were added to the

reaction mixture. After being stirred for 24h, the reaction mixture was quenched with saturated Na_2SO_3 aq and then the products were extracted with dichloromethane in three times. The collected organic layer was dried over Na_2SO_4. After removal of the solvent under reduced pressure, the residue was purified by silica-gel column chromathography (hexane/ethyl acetate=5/1) to afford the iodolactone. The enantiomeric excesses of the products were determined by chiral stationary phase HPLC using a Daicel Chiralpak AD-H column.

[For entry 4]

A mixture of 3,3'-bis(aminoimino)biphenol **L4** (0.005 mmol) and $Zn(OAc)_2$ (0.015 mmol) was stirred for 0.5 hour in anhydrous dichloromethane (1.0 ml) at rt. After cooling the mixture to -78 °C, 5-phenylhex-5-enoic acid (0.1 mmol) in toluene (3.0 ml) was slowly added to the resulting yellow solution and stirred for 0.5 hour at the same temperature. Then, *N*-iodosuccinimide (NIS) (24.6 mg, 0.11 mmol) and I_2 (5.0 mg, 0.02 mmol) were added to the reaction mixture. After being stirred for appropriate time, the reaction mixture was quenched with saturated Na_2SO_3 aq and 1*N* NaOH aq, and then the products were extracted with dichloromethane in 3 times. The collected organic layer was dried over Na_2SO_4. After removal of the solvent under reduced pressure, the residue was purified by silica-gel column chromathography (hexane/ethyl acetate = 5/1) to afford the iodolactone. The enantiomeric excesses of the products were determined by chiral stationary phase HPLC using a Daicel Chiralpak AD-H column.

4. DFT calculations of the L4-$Zn(OAc)_2$ complex (Figure S1)

In the DFT calculation of **L4**-$Zn(OAc)_2$ complex, the conformation having (*R*)-axis **L4**-Zn_3 complex is stable in 6.0 kcal/mol to the (*S*)-axis configuration (**Fig. S1**). Details of computational method are described in the section 11.

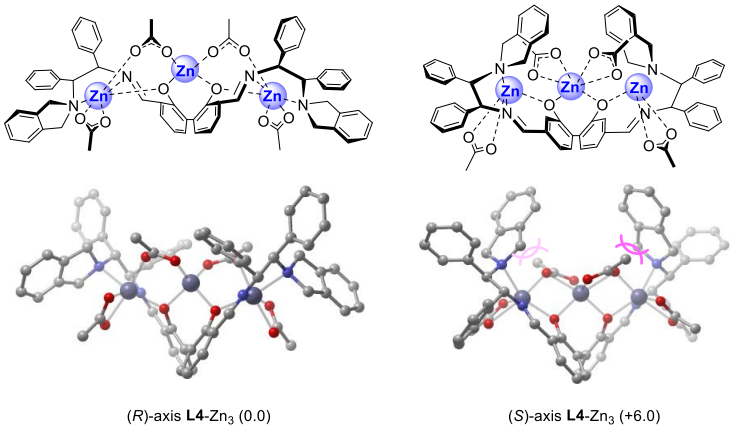

Figure S1. Gibbs free energy difference (kcal/mol) between (*R*)-axis **L4**-Zn and (*S*)-axis **L4**-Zn, related to **Table 1**.

5. Enantioselective iodolactonization and bromolactonization

(1) Enantioselective iodolactonization

A mixture of 3,3'-bis(aminoimino)binaphthol (0.001 mmol) and $Zn(OAc)_2$ (0.003 mmol) was stirred for 0.5 hour in anhydrous dichloromethane (1.0 ml) at rt. After cooling the mixture to -78 °C, carboxylic acid (0.1 mmol) in toluene (3.0 ml) was slowly added to the resulting yellow solution and stirred for 0.5 hour at the same temperature. Then, *N*-iodosuccinimide (NIS) (24.6 mg, 0.11 mmol) and I_2 (5.0 mg, 0.02 mmol) were added to the reaction mixture. After being stirred for appropriate time, the reaction mixture was quenched with saturated Na_2SO_3 aq and 1*N* NaOH aq, and then the products were extracted with dichloromethane in 3 times. The collected organic layer was dried over Na_2SO_4. After removal of the solvent under reduced pressure, the residue was purified by silica-gel column chromathography (hexane/acetone=8/1) to afford the iodolactone. The enantiomeric excesses of the products were determined by chiral stationary phase HPLC using a Daicel Chiralcel OD-H and Chiralpak AD-H column.

(2) Enantioselective bromolactonization

A mixture of 3,3'-bis(aminoimino)binaphthol (0.005 mmol) and $Zn(OAc)_2$ (0.015 mmol) was stirred for 0.5 hour in anhydrous dichloromethane (1.0 ml) at rt. After cooling the mixture to -40 °C, carboxylic acid (0.1 mmol) in toluene (3.0 ml) was slowly added to the resulting yellow solution and stirred for 0.5 hour at the same temperature. Then, *N*-bromosuccinimide (NBS) (19.6 mg, 0.11 mmol) was added to the reaction mixture. After being stirred for appropriate time, the reaction mixture was quenched with saturated Na_2SO_3 aq and 1*N* NaOH aq, and then the products were extracted with dichloromethane in 3 times. The collected organic layer was dried over Na_2SO_4. After removal of the solvent under reduced pressure, the residue was purified by silica-gel column chromathography (hexane/acetone=8/1) to afford the bromolactone. The enantiomeric excesses of the products were determined by chiral stationary phase HPLC using a Daicel Chiralcel OD-H and Chiralpak AD-H column.

Table S1. Catalytic asymmetric halolactonization using $Zn_3(OAc)_4$-3,3'-bis(aminoimino)binaphthoxide (tri-Zn) catalyst, related to **Table 2**. For **2**, X= 1 at -78 °C with 0.2 equiv of I_2. For **3**, X= 5 at -40 ºC.

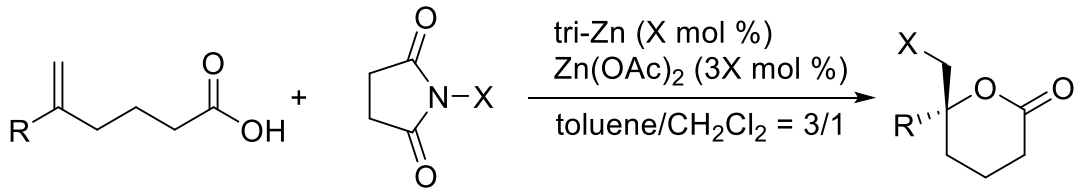

NIS (1.1 eq) for **2**
NBS (1.1 eq) for **3**

2: X = I
3: X = Br

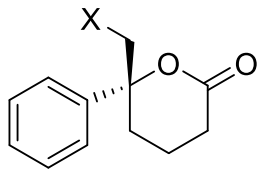

2a: >99% yield, 99.5% ee
3a: 99% yield, 94% ee

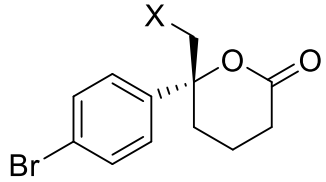

2b: >99% yield, 99.8% ee
3b: 99% yield, 92% ee

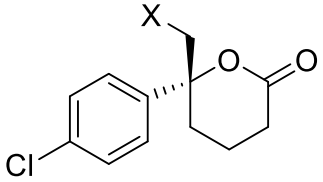

2c: >99% yield, 99.8% ee
3c: 91% yield, 95% ee

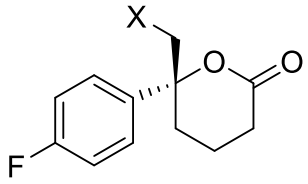

2d: >99% yield, 94% ee
3d: 90% yield, 90% ee

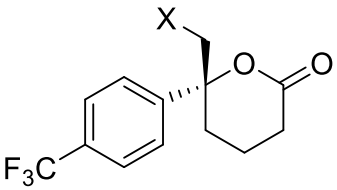

2e: >99% yield, 99.9% ee
3e: 92% yield, 99% ee

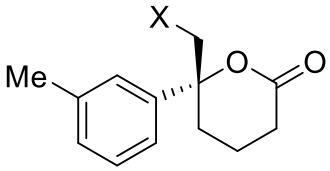

2f: >99% yield, 99.7% ee
3f: 99% yield, 92% ee

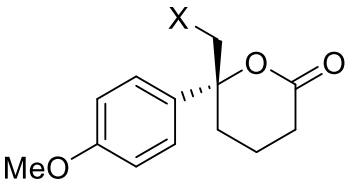

2g: >99% yield, 82% ee
3g: 89% yield, 95% ee

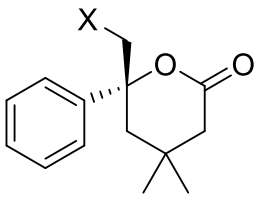

2h: 74% yield, 99% ee
3h: 88% yield, 87% ee

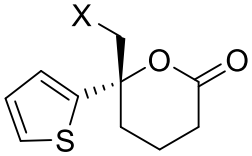

2i: 93% yield, 45% ee
3i: 56% yield, 72% ee

6. Non-linear effect on the catalytic asymmetric iodolactonization

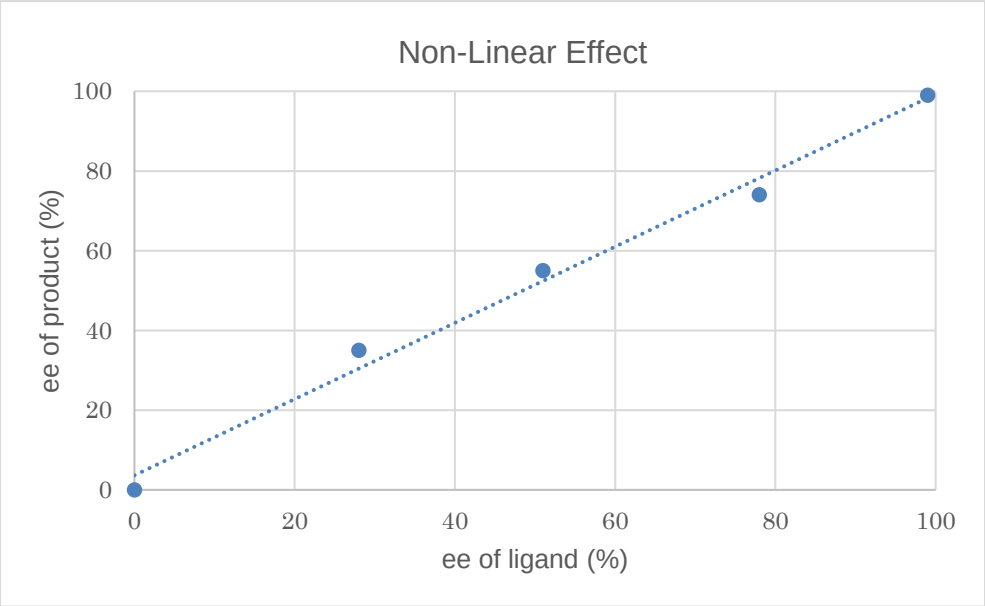

ee(%)					
ligand	0	28	51	78	99
product	0	35	55	74	99

Figure S2. Non-linear effect on asymmetric iodolactonization, related to **Figure 3**.

7. Job plot analysis on the interaction between tri-Zn catalyst and carboxylic acid (1a)

The ^{1}H-NMR spectra were collected at -40 ℃ in toluene-d_8. The analysis was conducted using the chemical shift of the imine proton of the **tri-Zn** catalyst.

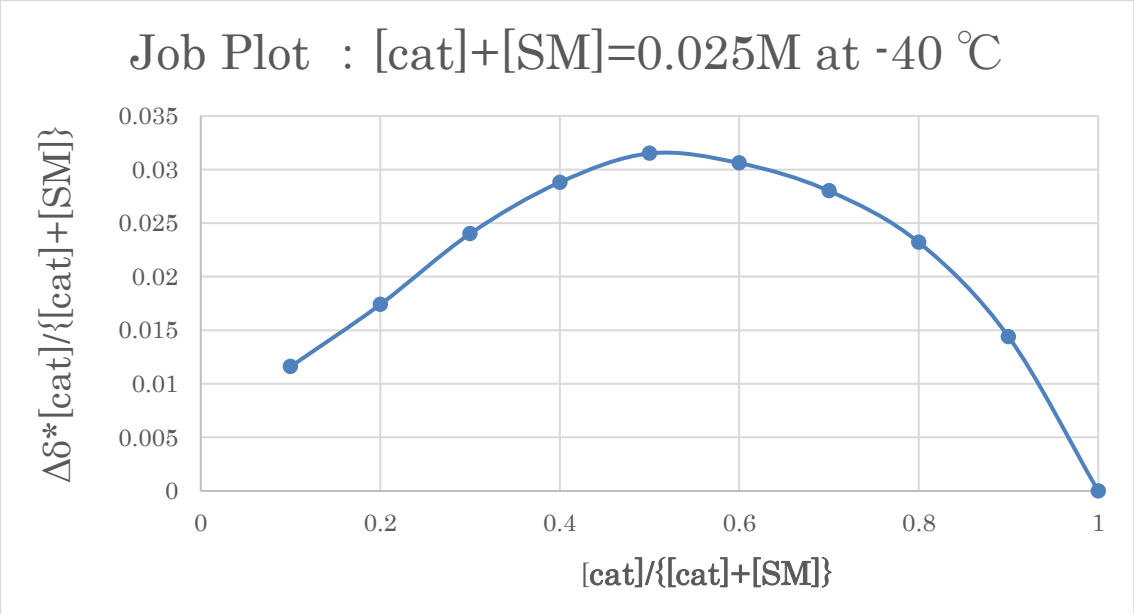

sample number	0	1	2	3	4	5	6	7	8	9
[cat]/{[cat]+[SM]}	1	0.9	0.8	0.7	0.6	0.5	0.4	0.3	0.2	0.1
Δ δ*[cat]/{[cat]+[SM]}	0	0.0144	0.0232	0.028	0.0306	0.0315	0.0288	0.024	0.0174	0.0116
Δ δ	0	0.016	0.029	0.04	0.051	0.063	0.072	0.08	0.087	0.116
peak(imine)	8.528	8.544	8.557	8.568	8.579	8.591	8.6	8.608	8.615	8.644

Figure S3. Job plot analysis on the interaction between tri-Zn catalyst and carboxylic acid (**1a**), related to **Figure 3**.

8. UV-Vis analysis on the interaction between tri-Zn catalyst and NIS-I_2 complex

In this analysis, tri-Zn catalyst prepared from **L4** was used for avoiding a fluorescence effects caused by the tri-Zn catalyst prepared from **L1**.

The UV-Vis spectra were collected at room temperature in dehydrated CH_2Cl_2, and concentration of **tri-Zn** catalyst was constant at 5.0*10^-5 M.

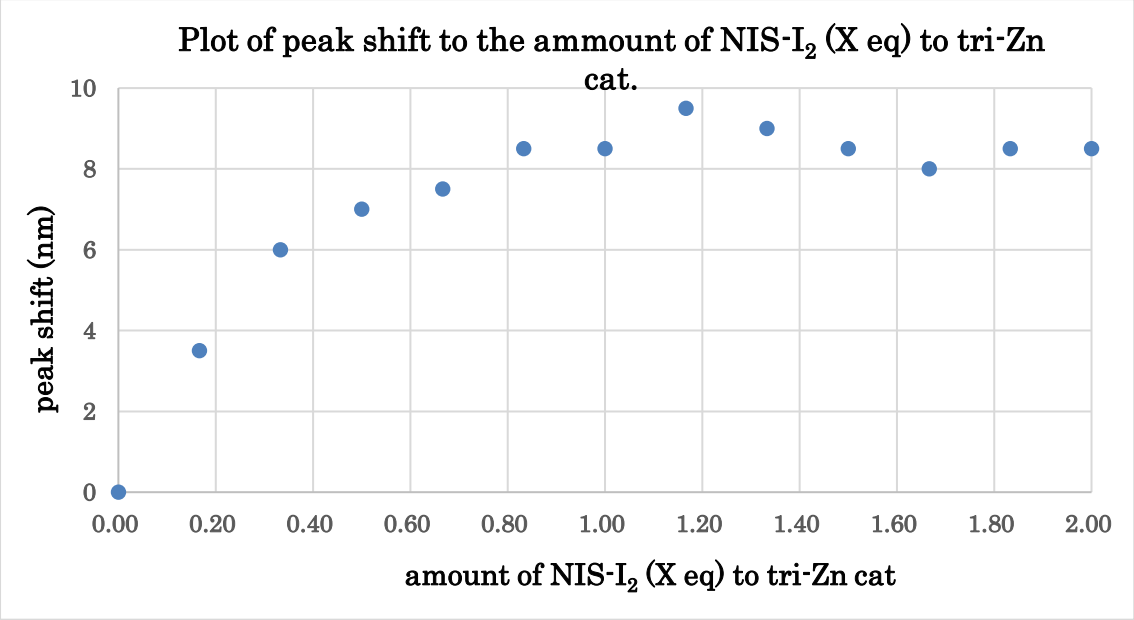

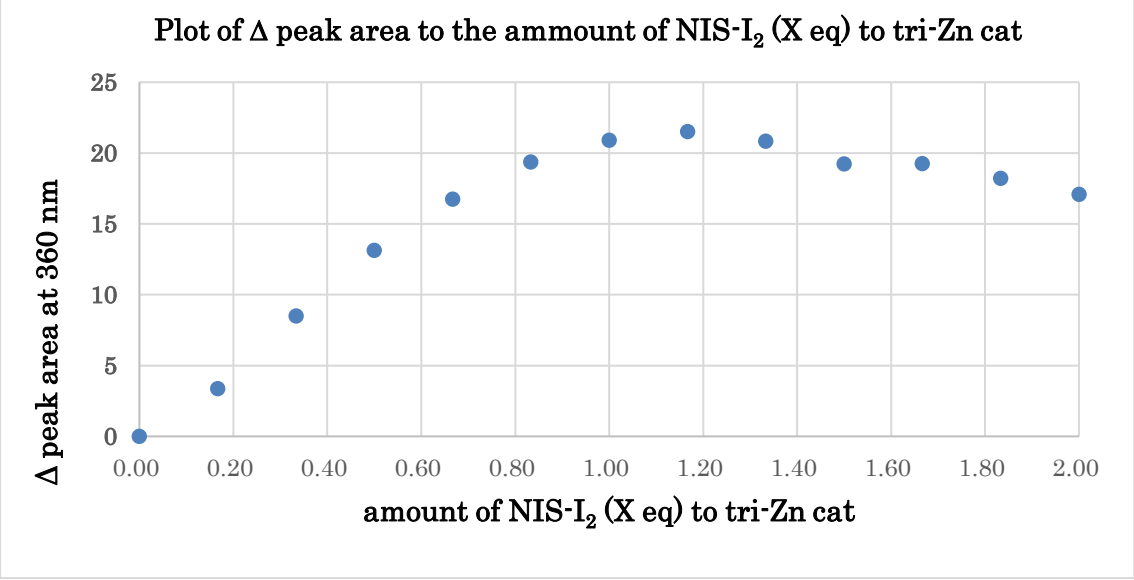

ammount of NIS-I_2 (X eq) to *tri-Zn* cat	0.00	0.17	0.33	0.50	0.67	0.83	1.00	1.17	1.33	1.50	1.67	1.83	2.00
Δ peak area at 360 nm	0	3.3727	8.4866	13.1135	16.7317	19.3522	20.8882	21.5095	20.8234	19.2229	19.2541	18.2141	17.0843
peak area at 360 nm	14.6943	18.067	23.1809	27.8078	31.426	34.0465	35.5825	36.2038	35.5177	33.9172	33.9484	32.9084	31.7786
peak shift (nm)	0	3.5	6	7	7.5	8.5	8.5	9.5	9	8.5	8	8.5	8.5
peak (nm)	357	360.5	363	364	364.5	365.5	365.5	366.5	366	365.5	365	365.5	365.5

Figure S4. UV-Vis analysis on the interaction between tri-Zn catalyst and NIS-I_2 complex, related to **Figure 3**.

9. Analytical data for product of iodolactonization and bromolactonization

(*R*)-6-(iodomethyl)-6-phenyltetrahydro-*2H*-pyran-2-one (2a)

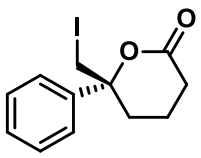

TLC R*f* = 0.40 (hexane : ethyl acetate = 2:1), ^{1}H NMR (400 MHz, $CDCl_3$) δ 7.44-7.33 (m, 5H), 3.57 (dd, *J*=11.3, 11.1 Hz, 2H), 2.55-2.30 (m, 4H), 1.87-1.79 (m, 1H), 1.63-1.56 (m, 1H); ^{13}C NMR (100 MHz, $CDCl_3$) δ 170.4, 140.1, 129.0, 128.4, 125.1, 84.4, 32.0, 28.9, 17.7, 16.5; HRMS calced for $C_{12}H_{14}O_2I$ $(M+H)^+$: 317.0033, found: *m/z* 317.0031; Enantiomeric excess was determined by HPLC with a Chiralpack AD-H column (95:5 hexane: 2-propanol, 1.0 mL/min, 254 nm); minor enantiomer t_r = 14.5 min, major enantiomer t_r = 16.3 min; 99.5% ee; $[\alpha]_D^{22.0}$= -31.6 (c=1.0, $CHCl_3$, 99.5% ee) ; IR (neat) 2956, 2933, 2863, 1734, 1682, 1575, 1388, 1276, 1130, 879 cm^{-1}

(*R*)-6-(bromomethyl)-6-phenyltetrahydro-2*H*-pyran-2-one (3a)

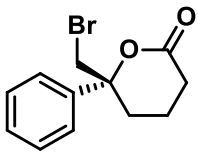

TLC R*f* = 0.41 (hexane : ethyl acetate = 2:1), ^{1}H NMR (400 MHz, $CDCl_3$) δ 7.45-7.33 (m, 5H), 3.66 (dd, *J*=19.7 Hz, 11.1 Hz, 2H), 2.55-2.33 (m, 4H), 1.88-1.80 (m, 1H), 1.65-1.53 (m, 1H); ^{13}C NMR (100MHz, $CDCl_3$) δ 170.4, 140.2, 129.0, 128.5, 125.3, 85.1, 41.5, 30.0, 29.6, 29.0, 16.2; HRMS calced for $C_{12}H_{13}O_2BrNa$ $(M+Na)^+$: 290.9991, found: *m/z* 290.9990; Enantiomeric excess was determined by HPLC with a Chiralcel OD-H column (92:8 hexane: 2-propanol, 1.0 mL/min, 210 nm); minor enantiomer t_r = 13.2 min, major enantiomer t_r = 17.5 min; 94% ee; $[\alpha]_D^{19.0}$= -15.2 (c=1.0, $CHCl_3$, 94% ee) ; IR (neat) 2361, 1736, 1447, 1261, 1231, 1180, 1011, 1045, 932, 766, 702 cm^{-1}

(*R*)-6-(bromomethyl)-6-(*p*-bromophenyl)tetrahydro-*2H*-pyran-2-one (3b)

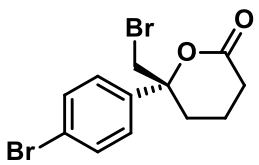

TLC R*f* = 0.41 (hexane : ethyl acetate = 2:1), ^{1}H NMR (400 MHz, $CDCl_3$) δ 7.54 (d, *J*=8.30 Hz, 2H), 7.28 (d, *J*=8.53 Hz, 2H), 3.68-3.59 (m, 2H), 2.56-2.31 (m, 4H), 1.92-1.82 (m, 1H), 1.68-1.55 (m, 1H); ^{13}C NMR (100MHz, $CDCl_3$) δ 170.0, 139.3, 132.1, 127.2, 122.8, 84.8, 41.0, 30.0, 29.0, 16.2; HRMS calced for $C_{12}H_{12}O_2Br_2Na$ $(M+Na)^+$: 368.9096, found: *m/z* 368.9092; Enantiomeric excess was determined by HPLC with a Chiralpack AD-H column (92:8 hexane: 2-propanol, 1.0 mL/min, 210 nm); minor enantiomer t_r = 12.6 min, major enantiomer t_r = 15.7 min; 92% ee; $[\alpha]_D^{17.0}$= -13.4 (c=1.0, $CHCl_3$, 92% ee) ; IR (neat) 2963, 2251, 1744, 1732, 1489, 1231, 1180, 1045, 1009 cm^{-1}

(*R*)-6-(bromomethyl)-6-(4-chlorophenyl)tetrahydro-2*H*-pyran-2-one (3c)

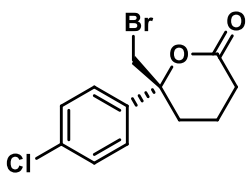

TLC R*f* = 0.41 (hexane : ethyl acetate = 2:1), ^{1}H NMR (400 MHz, $CDCl_3$) δ 7.42-7.32 (m, 4H), 3.65 (d, *J*=11.2 Hz, 1H), 3.60 (d, *J*=11.2 Hz, 1H), 2.56-2.31 (m, 4H), 1.91-1.82 (m, 1H), 1.65-1.52 (m, 1H); ^{13}C NMR (100MHz, $CDCl_3$) δ 170.0, 138.8, 134.6, 129.2, 126.9, 84.8, 41.1, 30.0, 29.1, 16.2; HRMS calced for $C_{12}H_{12}O_2BrClNa$ $(M+Na)^+$: 324.9601, found: *m/z* 324.9595; Enantiomeric excess was determined by HPLC with a Chiralpack AD-H column (95:5 hexane: 2-propanol, 1.0 mL/min, 254 nm); minor enantiomer t_r = 14.8 min, major enantiomer t_r = 18.8 min; 90% ee; $[\alpha]_D^{18.7}$= -5.0 (c=1.0, $CHCl_3$, 90% ee) ; IR (neat) 2987, 1725, 1491, 1444, 1232, 1043, 886, 821, 664 cm^{-1}

(*R*)-6-(bromomethyl)-6-(*p*-fluorophenyl)tetrahydro-*2H*-pyran-2-one (3d)

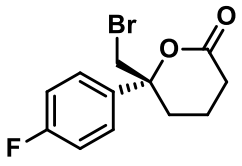

TLC R*f* = 0.41 (hexane : ethyl acetate = 2:1), ^{1}H NMR (400 MHz, $CDCl_3$) δ 7.41-7.36 (m, 2H), 7.13-7.07 (m, 2H), 3.63 (dd, *J*=23.3, 11.2 Hz, 2H), 2.57-2.32 (m, 4H), 1.91-1.77 (m, 1H), 1.68-1.54 (m, 1H); ^{13}C NMR (100MHz, $CDCl_3$) δ 170.1, 161.3, 136.1, 127.4, 127.3, 116.1, 115.8, 84.8, 41.4, 30.0, 29.1, 16.2; HRMS calced for $C_{12}H_{12}O_2BrNaF$ $(M+Na)^+$: 308.9897, found: *m/z* 308.9897; Enantiomeric excess was determined by HPLC with a Chiralpack AD-H column (92:8 hexane: 2-propanol, 1.0 mL/min, 210 nm); minor enantiomer t_r = 11.6 min, major enantiomer t_r = 13.9 min; 94% ee; $[\alpha]_D^{19.0}$= -12.2 (c=1.0, $CHCl_3$, 94% ee) ; IR (neat) 2963, 1730, 1603, 1510, 1300, 1261, 1234, 1044, 932, 833 cm^{-1}

(*R*)-6-(bromomethyl)-6-(*p*-(trifluoromethyl)phenyl)tetrahydro-*2H*-pyran-2-one (3e)

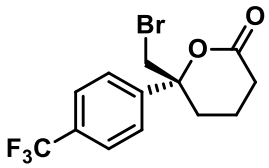

TLC R*f* = 0.41 (hexane : ethyl acetate = 2:1), ^{1}H NMR (400 MHz, $CDCl_3$) δ 7.70 (d, *J*=8.30 Hz, 2H), 7.56 (d, *J*=8.30 Hz, 2H), 3.70-3.64 (m, 2H), 260-2.38 (m, 4H), 1.96-1.86 (m, 1H), 1.64-1.54 (m, 1H); ^{13}C NMR (100MHz, $CDCl_3$) δ 169.7, 144.3, 131.0, 130.6, 126.0, 125.9, 125.1, 122.3, 84.8, 40.8, 30.3, 29.1, 16.2; HRMS calced for $C_{12}H_{12}O_2BrF_3Na$ $(M+Na)^+$: 358.9865, found: *m/z* 358.9864; Enantiomeric excess was determined by HPLC with a Chiralpack AD-H column (92:8 hexane: 2-propanol, 1.0 mL/min, 210 nm); minor enantiomer t_r = 10.7 min, major enantiomer t_r = 14.0 min; 99.9% ee; $[\alpha]_D^{19.0}$= -7.2 (c=1.0, $CHCl_3$, 99.9% ee) ; IR (neat) 2963, 1744, 1410, 1327, 1263, 1231, 1071, 1045, 1017, 934, 837 cm^{-1}

(*R*)-6-(bromomethyl)-6-(*m*-tolyl)tetrahydro-2*H*-pyran-2-one (3f)

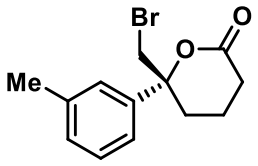

TLC R*f* = 0.41 (hexane : ethyl acetate = 2:1), ^{1}H NMR (400 MHz, $CDCl_3$) δ 7.33-7.27 (m, 1H), 7.24-7.15 (m, 3H), 3.65 (dd, *J*=11.0, 18.3 Hz, 2H), 2.57-2.18 (m, 7H), 1.91-1.72 (m, 1H), 1.66-1.53 (m, 1H); ^{13}C NMR (100MHz, $CDCl_3$) δ 170.6, 140.2, 138.8, 129.2, 128.8, 126.0, 122.4, 85.1, 41.6, 30.0, 29.1, 21.6, 16.2; HRMS calced for $C_{13}H_{16}O_2Br$ $(M+H)^+$: 283.0328, found: *m/z* 283.0327; Enantiomeric excess was determined by HPLC with a Chiralpack AD-H column (95:5 hexane: 2-propanol, 1.0 mL/min, 254 nm); minor enantiomer t_r = 13.3 min, major enantiomer t_r = 14.3 min; 94% ee; $[\alpha]_D^{18.5}$= -8.5 (c=1.0, $CHCl_3$, 94% ee) ; IR (neat) 2988, 1743, 1264, 1234, 1183, 1106, 1046, 931, 789, 711 cm^{-1}

(*R*)-6-(bromomethyl)-6-(4-methoxyphenyl)tetrahydro-2*H*-pyran-2-one (3g)

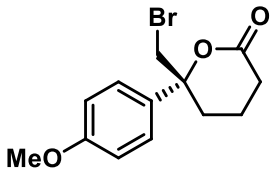

TLC R*f* = 0.41 (hexane : ethyl acetate = 2:1), ^{1}H NMR (400 MHz, $CDCl_3$) δ 7.37-7.27 (m, 2H), 6.94-6.93 (m, 2H), 3.82 (s, 3H), 3.67 (d, *J*=11.0 Hz, 1H), 3.60 (d, *J*=11.2 Hz, 1H), 2.57-2.31 (m, 4H), 1.88-1.80 (m, 1H), 1.75-1.56 (m, 1H); ^{13}C NMR (100MHz, $CDCl_3$) δ 170.6, 159.5, 132.0, 126.7, 114.2, 84.9, 55.3, 41.7, 29.7, 29.0, 16.2; HRMS calced for $C_{13}H_{15}O_3BrNa$ $(M+Na)^+$: 321.0097, found: *m/z* 321.0091; Enantiomeric excess was determined by HPLC with a Chiralpack AD-H column (95:5 hexane: 2-propanol, 1.0 mL/min, 254 nm);

minor enantiomer t_r = 20.4 min, major enantiomer t_r = 22.5 min; 97% ee; $[\alpha]_D^{18.1}$= -9.0 (c=1.0, $CHCl_3$, 97% ee) ; IR (neat) 2988, 2957, 1742, 1610, 1512, 1461, 1306, 1253, 1181, 1045, 931, 833, 734 cm^{-1}

(*R*)-6-(bromomethyl)-4,4-dimethyl-6-phenyltetrahydro-*2H*-pyran-2-one (3h)

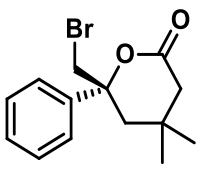

TLC R*f* = 0.65 (hexane : ethyl acetate = 2:1), ^{1}H NMR (400 MHz, $CDCl_3$) δ 7.56-7.17 (m, 5H), 3.63-3.53 (m, 2H), 2.48 (d, 1H), 2.36-2.25 (m, 2H), 2.19 (d, 1H), 1.11 (s, 3H), 0.73 (s, 3H); ^{13}C NMR (100 MHz, $CDCl_3$) δ 170.1, 141.5, 129.0, 128.5, 125.3, 84.0, 43.6, 42.6, 31.7, 30.6, 28.5; HRMS calced for $C_{14}H_{17}O_2BrNa$ $(M+Na)^+$: 319.0304, found: *m/z* 319.0301; Enantiomeric excess was determined by HPLC with a Chiralpack AD-H column (92:8 hexane: 2-propanol, 1.0 mL/min, 210 nm); minor enantiomer t_r = 7.4 min, major enantiomer t_r = 8.3 min; 87% ee; $[\alpha]_D^{18.0}$= -23.1 (c=1.0, $CHCl_3$, 87% ee) ; IR (neat) 2961, 1746, 1447, 1265, 1244, 1211, 1175, 1146, 1053, 764, 704 cm^{-1}

(*R*)-6-(iodomethyl)-6-(thiophen-*2*-yl)tetrahydro-2*H*-pyran-2-one (2i)

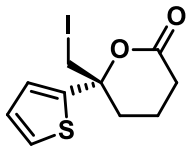

TLC R*f* = 0.46 (hexane : ethyl acetate = 2:1), ^{1}H NMR (500 MHz, $CDCl_3$) δ 7.33-7.32 (m, 1H), 7.05-7.00 (m, 2H), 3.68-3.57 (m, 2H) 2.56-2.32 (m, 4H), 1.96-1.75 (m, 2H); ^{13}C NMR (125MHz, $CDCl_3$) δ 169.6, 143.8, 127.3, 125.9, 125.1, 83.2, 33.1, 29.0, 17.7, 16.9; HRMS calced for $C_{10}H_{12}O_2IS$ $(M+H)^+$: 322.9597, found: *m/z* 322.9589; Enantiomeric excess was determined by HPLC with a Chiralpack AD-H column (95:5 hexane: 2-propanol, 1.0 mL/min, 254 nm); minor enantiomer t_r = 13.6 min, major enantiomer t_r = 15.1 min; 45% ee; $[\alpha]_D^{27.0}$= -29.0 (c=1.0, $CHCl_3$, 45% ee) ; IR (neat) 2956, 1738 cm^{-1}

(*R*)-6-(bromomethyl)-6-(thiophen-2-yl)tetrahydro-2*H*-pyran-2-one (3i)

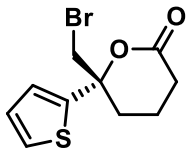

TLC R*f* = 0.65 (hexane : ethyl acetate = 2:1), ^{1}H NMR (400 MHz, $CDCl_3$) δ 7.34 (dd, *J*=1.35, 5.05 Hz, 1H), 7.07-7.01 (m, 2H), 3.77 (d, *J*=11.2 Hz, 1H), 3.64 (d, *J*=11.0 Hz, 1H), 2.59-2.44 (m, 3H), 2.34-2.28 (m, 1H), 1.96-1.74 (m, 2H); ^{13}C NMR (100 MHz, $CDCl_3$) δ 169.7, 144.0, 127.4, 126.1, 125.3, 84.0, 41.6, 31.2, 29.1, 16.6; HRMS calced for $C_{10}H_{12}O_2Br$ $(M+H)^+$: 274.9736, found: *m/z* 274.9731; Enantiomeric excess was determined by HPLC with a Chiralpack OD-H column (90:10 hexane: 2-propanol, 1.0 mL/min, 254 nm); minor enantiomer t_r = 12.8 min, major enantiomer t_r = 15.9 min; 78% ee; $[\alpha]_D^{18.6}$= -2.3 (c=1.0, $CHCl_3$, 78% ee) ; IR (neat) 2988, 1747, 1444, 1351, 1329, 1267, 1178, 1037, 709 cm^{-1}

10. Substrate preparation for desymmetric asymmetric iodolactonization

a. General procedure for preparation of diolefinic acid 4

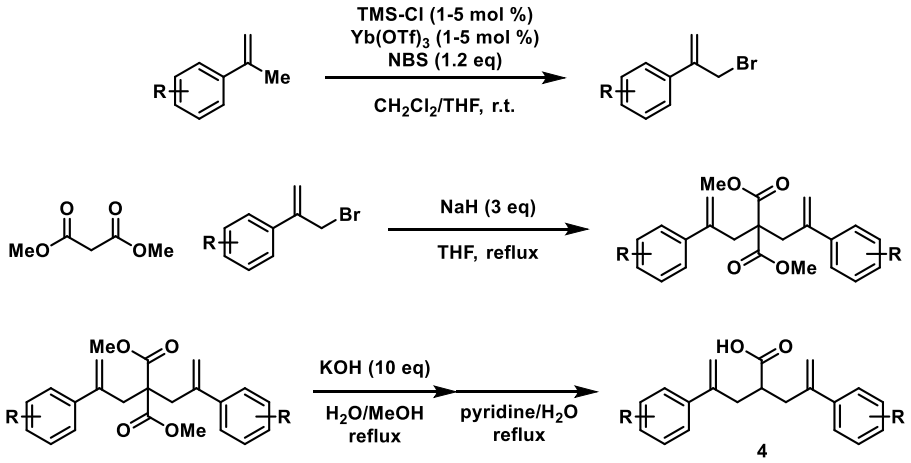

Scheme S5. Synthetic routes of diolefinic acid **4**, related to **Figure 5**.

Diolefinic acid **4** was prepared from α-methylstyrene derivatives and dimethyl malonate according to the procedure (Pratch and Overmann, 2015; Tay et al. 2014).

b. Analytical data for substrate 4

4-phenyl-2-(2-phenylallyl)pent-4-enoic acid (4a)

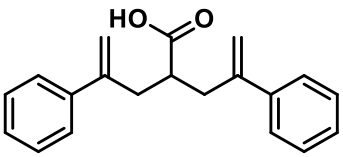

TLC R*f* = 0.32 (hexane : ethyl acetate = 2:1), ^{1}H NMR (400 MHz, $CDCl_3$) δ 7.30-7.24 (m, 10H), 5.33 (s, 2H), 5.11 (s, 2H), 2.90-2.83 (m, 2H), 2.74-2.67 (m, 3H) The NMR spectra was identical to those previously reported (Niu et al. 2015).

4-(m-tolyl)-2-(2-(m-tolyl)allyl)pent-4-enoic acid (4b)

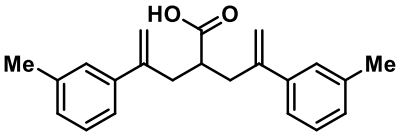

TLC R*f* = 0.42 (hexane : ethyl acetate = 2:1), ^{1}H NMR (400 MHz, $CDCl_3$) δ 7.16-7.04 (m, 8H), 5.31 (d, *J*=0.8 Hz, 2H), 5.09 (s, 2H), 2.87-2.80 (m, 2H), 2.74-2.67 (m, 3H); ^{13}C NMR (100 MHz, $CDCl_3$) δ 181.4, 145.3, 139.9, 137.8, 128.4, 128.2, 126.8, 123.2, 114.6, 42.7, 37.4, 21.5; HRMS calced for $C_{22}H_{23}O_2$ $(M-H)^-$: 319.1704, found: *m/z* 319.1711; IR (neat) 2925, 1708, 1446, 1240, 897, 795, 713 cm^-

4-(o-tolyl)-2-(2-(o-tolyl)allyl)pent-4-enoic acid (4c)

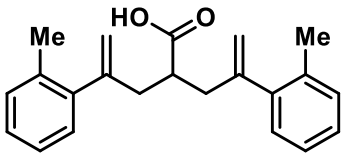

TLC R*f* = 0.48 (hexane : ethyl acetate = 2:1), ^{1}H NMR (400 MHz, $CDCl_3$) δ 7.17-7.13 (m, 4H), 7.11-7.04 (m, 2H), 6.95 (d, *J*=7.6 Hz), 5.18 (s, 1H), 4.91 (d, *J*=1.6 Hz, 2H), 2.75-2.68 (m, 2H), 2.58-2.50 (m, 3H), 2.24 (s, 6H); ^{13}C NMR (100 MHz, $CDCl_3$) δ 181.8, 146.6, 141.6, 134.8, 130.1, 128.5, 127.1, 125.4, 116.3, 42.2, 39.7, 19.7; HRMS calced for $C_{22}H_{23}O_2$ $(M-H)^-$: 319.1704, found: *m/z* 319.1707; IR (neat) 2945, 1708, 1444, 1240, 907, 768, 725 cm^{-1}

4-(3-(trifluoromethyl)phenyl)-2-(2-(3-(trifluoromethyl)phenyl)allyl)pent-4-enoic acid (4d)

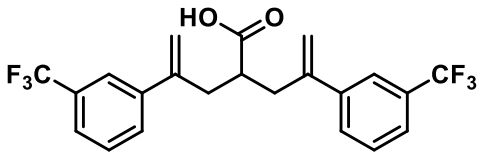

TLC R*f* = 0.27 (hexane : ethyl acetate = 2:1), ^{1}H NMR (400 MHz, $CDCl_3$) δ 7.56 (s, 2H), 7.50 (d, *J*=7.6 Hz, 2H), 7.43-7.35 (m, 4H), 5.38 (s, 2H), 5.20 (d, *J*=0.8 Hz, 2H), 2.89 (dd, *J*=14.4 Hz, 8.4 Hz, 2H), 2.73 (dd, *J*=14.2 Hz, 5.6 Hz, 2H), 2.62-2.54 (m, 1H); ^{13}C NMR (100 MHz, $CDCl_3$) δ 181.1, 144.1, 140.8, 130.8 (q, J_{CF}=31.9 Hz), 129.3, 128.9, 124.4 (q, J_{CF}=3.8 Hz), 124.0 (q, J_{CF}=276.6 Hz), 122.9 (q, J_{CF}=3.8 Hz), 116.6, 42.8, 37.2; HRMS calced for $C_{22}H_{17}O_2F_6$ $(M-H)^-$: 427.1138, found: *m/z* 427.1143 ; IR (neat) 3005, 1709, 1333, 1165, 1120, 1073, 902, 696 cm^{-1}

4-(3-methoxyphenyl)-2-(2-(3-methoxyphenyl)allyl)pent-4-enoic acid (4e)

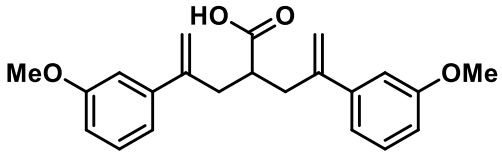

TLC R*f* = 0.31 (hexane : ethyl acetate = 2:1), ^{1}H NMR (400 MHz, $CDCl_3$) δ 7.18-7.14 (m, 2H), 6.86-6.84 (m, 4H), 6.79-6.76 (m, 2H), 5.32 (d, *J*=1.2 Hz, 2H), 5.09 (s, 2H), 3.77 (s, 6H), 2.83 (dd, *J*=16.4 Hz, 9.2 Hz, 2H), 2.73-2.66 (m, 3H); ^{13}C NMR (100 MHz, $CDCl_3$) δ 181.3, 159.5, 145.2, 141.6, 129.3, 118.6, 115.0, 113.0, 112.0, 55.1, 42.8, 37.5; HRMS calced for $C_{22}H_{23}O_4$ $(M-H)^-$: 351.1602, found: *m/z* 351.1610; IR (neat) 2948, 1706, 1576, 1228, 1044, 879, 781 cm^{-1}

4-(4-chlorophenyl)-2-(2-(4-chlorophenyl)allyl)pent-4-enoic acid (4f)

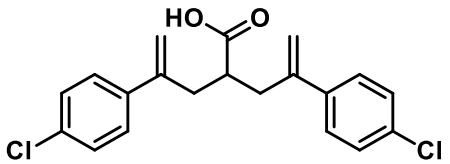

TLC R*f* = 0.32 (hexane : ethyl acetate = 2:1), ^{1}H NMR (400 MHz, $CDCl_3$) δ 7.26-7.22 (m, 4H), 7.20-7.17 (m, 4H), 5.30 (s, 2H), 5.11 (s, 2H), 2.83 (dd, *J*=14.4 Hz, 8.0 Hz, 2H), 2.68-2.54 (m, 3H); ^{13}C NMR (100 MHz, $CDCl_3$) δ 181.2, 144.1, 138.3, 133.5, 128.5, 127.4, 115.5, 42.6, 37.1; HRMS calced for $C_{20}H_{17}O_2Cl_2$ $(M-H)^-$: 359.0611, found: *m/z* 359.0623; IR (neat) 2968, 1698, 1494, 1241, 903, 835 cm^{-1}

4-(naphthalen-2-yl)-2-(2-(naphthalen-2-yl)allyl)pent-4-enoic acid (4g)

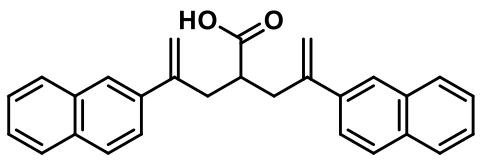

TLC R*f* = 0.30 (hexane : ethyl acetate = 2:1), ^{1}H NMR (400 MHz, $CDCl_3$) δ 7.75 (d, *J*=8.0 Hz, 2H), 7.67-7.65 (m, 4H), 7.53 (d, *J*=8.0 Hz, 2H), 7.46-7.35 (m, 6H), 5.49 (d, *J*=0.8 Hz, 2H), 5.24 (s, 2H), 3.00 (dd, *J*=13.8 Hz, 8.0 Hz, 2H), 2.90-2.78 (m, 3H);

^{13}C NMR (100 MHz, $CDCl_3$) δ 180.3, 145.0, 137.0, 133.2, 132.8, 128.1, 128.0, 127.4, 126.1, 125.9, 124.8, 124.4, 115.6, 42.6, 37.4; HRMS calced for $C_{28}H_{23}O_2$ $(M-H)^-$: 391.1704, found: *m/z* 391.1716; IR (neat) 3044, 1695, 1433, 1289, 915, 857, 739 cm^{-1}

11. General procedure of catalytic desymmetric asymmetric iodolactonization

A mixture of 3,3'-bis(aminoimino)binaphthol (4.7 mg, 0.005 mmol) and $Zn(OAc)_2$ (2.8 mg, 0.015 mmol) was stirred for 1 hour in anhydrous $CHCl_3$ (1.0 ml) at rt, the reaction mixture was added carboxylic acid (0.1 mmol) and toluene (3.0 ml). After cooling the mixture to -78 °C, the reaction mixture was stirred for 0.5 hour at the same temperature. Then, *N*-iodosuccinimide (NIS) (24.7 mg, 0.11 mmol) and I_2 (5.1 mg, 0.02 mmol) were added to the reaction mixture. After being stirred for appropriate time, the reaction mixture was quenched with saturated Na_2SO_3 aq and then the products were extracted with CH_2Cl_2 in 3 times. The collected organic layer was dried over Na_2SO_4. After removal of the solvent under reduced pressure, the residue was purified by silica-gel column chromatography (hexane/ethyl acetate=20/1~10/1) to afford the iodolactone. The enantiomeric excesses of the products were determined by chiral stationary phase HPLC using a Daicel Chiralcel OD-H and Chiralpak AD-3, AS-H and Chiralpak IC-3 column.

12. Analytical data for product of desymmetric iodolactonization

(3*S*,5*R*)-5-(iodomethyl)-5-phenyl-3-(2-phenylallyl)dihydrofuran-2(3H)-one (5a)

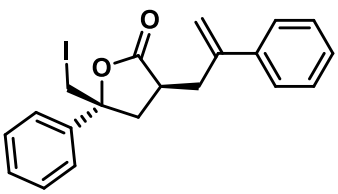

TLC R*f* = 0.74 (hexane : ethyl acetate = 2:1), ^{1}H NMR (400 MHz, $CDCl_3$) δ 7.38-7.24 (m, 10H), 5.34 (s, 1H), 5.15 (s, 1H), 3.61 (d, *J*=11.2 Hz, 1H), 3.55 (d, *J*=11.2 Hz, 1H), 3.38-3.27 (m, 1H), 2.71-2.57 (m, 3H), 2.41-2.30 (m, 1H); ^{13}C NMR (100 MHz, $CDCl_3$) δ 176.8, 145.1, 139.7, 139.4, 128.8, 128.5, 127.9, 126.0, 124.8, 114.7, 84.0, 40.1, 39.0, 36.2, 16.9; HRMS calced for $C_{20}H_{19}O_2INa$ $(M+Na)^+$: 441.0322, found: *m/z* 441.0313; Enantiomeric excess was determined by HPLC with a Chiralpack AS-H column (90:10 hexane: 2-propanol, 1.0 mL/min, 254 nm); minor enantiomer t_r = 16.5 min, major enantiomer t_r = 9.6 min; 94% ee; $[\alpha]_D^{25.3}$= -12.5 (c=1.0, $CHCl_3$, 99/1 diastereomixture, 94% ee); IR (neat) 3060, 3940, 1772, 1440, 1143, 908, 701 cm^{-1}

(3*S*,5*R*)-5-(iodomethyl)-5-(m-tolyl)-3-(2-(m-tolyl)allyl)dihydrofuran-2(3H)-one (5b)

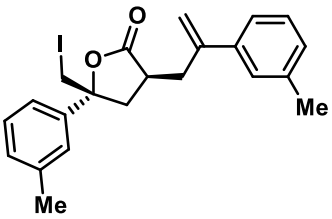

TLC R*f* = 0.75 (hexane : ethyl acetate = 2:1), ^{1}H NMR (400 MHz, $CDCl_3$) δ 7.25-7.07 (m, 8H), 5.33 (d, *J*=0.4 Hz, 1H), 5.13 (s, 1H), 3.61 (d, *J*=11.2 Hz, 1H), 3.55 (d, *J*=11.2 Hz, 1H), 3.33-3.30 (m, 1H), 2.70-2.55 (m, 3H), 2.38-2.34 (m, 1H), 2.32 (s, 3H), 2.31 (s, 3H); ^{13}C NMR (100 MHz, $CDCl_3$) δ 177.1, 145.2, 139.7, 139.5, 138.6, 138.1, 129.3, 128.7, 128.6, 128.4, 126.7, 125.5, 123.2, 121.9, 114.5, 84.0, 40.1, 38.9, 36.3, 21.49, 21.46, 17.2; HRMS calced for $C_{22}H_{27}O_2NI$ $(M+NH_4)^+$: 464.1081, found: *m/z* 464.1072; Enantiomeric excess was determined by HPLC with a Chiralpack AS-H column (95:5 hexane: 2-propanol, 1.0 mL/min, 254 nm); minor enantiomer t_r = 16.9 min, major enantiomer t_r = 8.8 min; 99% ee; $[\alpha]_D^{26.1}$= -12.6 (c=1.0, $CHCl_3$, 99/1 diastereomixture, 99% ee); IR (neat) 3033, 2925, 1776, 1604, 1452, 1146, 903, 787, 724, 705 cm^{-1}

(3*S*,5*R*)-5-(iodomethyl)-5-(o-tolyl)-3-(2-(o-tolyl)allyl)dihydrofuran-2(3H)-one (5c)

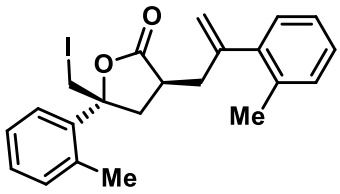

TLC R*f* = 0.74 (hexane : ethyl acetate = 2:1), ^{1}H NMR (400 MHz, $CDCl_3$) δ 7.39 (d, *J*=8.0 Hz, 1H), 7.26-7.09 (m, 6H), 7.02 (d, *J*=7.2 Hz, 1H), 5.30 (d, *J*=1.2 Hz, 1H), 4.99 (d, *J*=0.8 Hz, 1H), 3.75 (d, *J*=11.6 Hz, 1H), 3.69 (d, *J*=11.6 Hz, 1H), 3.15-3.11 (m, 1H), 2.77 (dd, *J*=13.2 Hz, 9.6 Hz, 1H), 2.66-2.48 (m, 2H), 2.38 (s, 3H), 2.35-2.26 (m, 4H); ^{13}C NMR (100 MHz, $CDCl_3$) δ 176.8, 146.6, 140.8, 137.5, 134.9, 133.8, 132.8, 130.4, 128.6, 128.3, 127.4, 126.3, 125.63, 125.58, 116.5, 84.7, 39.5, 38.6, 38.5, 21.3, 19.8, 16.0; HRMS calced for $C_{22}H_{27}O_2NI$ $(M+NH_4)^+$: 464.1081, found: *m/z* 464.1072; Enantiomeric excess was determined by HPLC with a Chiralpack AS-H column (99:1 hexane: 2-propanol, 1.0 mL/min, 254 nm); minor enantiomer t_r = 46.9 min, major enantiomer t_r = 19.3 min; 79% ee; $[\alpha]_D^{26.1}$= +19.8 (c=1.0, $CHCl_3$, 96/4 diastereomixture, 79% ee); IR (neat) 3060, 2929, 1774, 1487, 1240, 1148, 908, 728 cm^{-1}

(3*S*,5*R*)-5-(iodomethyl)-5-(3-(trifluoromethyl)phenyl)-3-(2-(3-(trifluoromethyl)phenyl)allyl)dihydrofuran-2(3H)-one (5d)

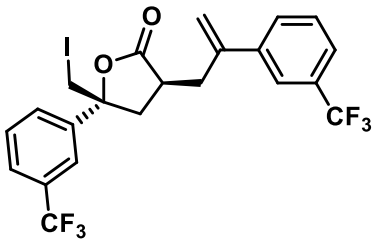

TLC R*f* = 0.70 (hexane : ethyl acetate = 2:1), ^{1}H NMR (500 MHz, $CDCl_3$) δ 7.62-7.44 (m, 8H), 5.43 (s, 1H), 5.27 (s, 1H), 3.62 (d, *J*=11.0 Hz, 1H), 3.56 (d, *J*=11.0 Hz, 1H), 3.33 (d, *J*=12.5 Hz, 1H), 2.73-2.58 (m, 3H), 2.45-2.37 (m, 1H); ^{13}C NMR (100 MHz, $CDCl_3$) δ 176.0, 143.8, 140.8, 140.4, 131.4 (q, J_{CF}=32.5 Hz), 131.0 (q, J_{CF}=32.4 Hz), 129.5, 129.3, 129.2, 128.3, 125.7 (q, J_{CF}=3.0 Hz), 124.7 (q, J_{CF}=3.9 Hz), 123.9 (q, *J*=276.6 Hz), 123.6 (q, *J*=276.8 Hz), 122.9 (q, J_{CF}=3.8 Hz), 121.8 (q, J_{CF}=3.8 Hz), 116.5, 83.6, 40.0, 38.8, 35.9, 16.0; HRMS calced for $C_{22}H_{17}O_2F_6INa$ $(M+Na)^+$: 577.0070, found: *m/z* 577.0055; Enantiomeric excess was determined by HPLC with two Chiralcel OD-H columns (95:5 hexane: 2-propanol, 1.0 mL/min, 254 nm); minor enantiomer t_r = 18.8 min, major enantiomer t_r = 26.6 min; 98% ee; $[\alpha]_D^{26.2}$= -7.2 (c=1.0, $CHCl_3$, 99/1 diastereomixture, 98% ee); IR (neat) 1779, 1332, 1165, 1119, 1073, 805, 701 cm^{-1}

(3*S*,5*R*)-5-(iodomethyl)-5-(3-methoxyphenyl)-3-(2-(3-methoxyphenyl)allyl)dihydrofuran-2(3H)-one (5e)

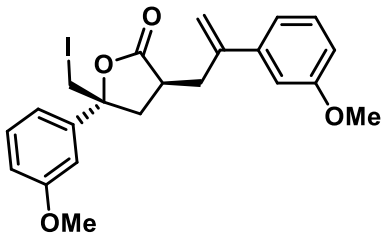

TLC R*f* = 0.63 (hexane : ethyl acetate = 2:1), ^{1}H NMR (400 MHz, $CDCl_3$) δ 7.27-7.20 (m, 2H), 6.97-6.95 (m, 1H), 6.91-6.90 (m, 1H), 6.87-6.81 (m, 4H), 5.35 (s, 1H), 5.16 (s, 1H), 3.80 (s, 3H), 3.78 (s, 3H), 3.62 (d, *J*=11.2 Hz, 1H), 3.56 (d, *J*=11.6 Hz, 1H), 3.33-3.29 (m, 1H), 2.72-2.56 (m, 3H), 2.35 (dd, *J*=12.6 Hz, 11.2 Hz, 1H); ^{13}C NMR (100 MHz, $CDCl_3$) δ 176.8, 159.8, 159.6, 145.0, 141.3, 141.0, 129.9, 129.5, 118.5, 117.0, 114.9, 113.7, 113.1, 112.0, 110.9, 83.9, 55.3, 55.2, 40.1, 38.9, 36.2, 16.8; HRMS calced for $C_{22}H_{27}O_4NI$ $(M+NH_4)^+$: 496.0979, found: *m/z* 496.0967; Enantiomeric excess was determined by HPLC with a Chiralpack IC-3 column (95:5 hexane: 2-propanol, 1.0 mL/min, 254 nm); minor enantiomer t_r = 22.9 min, major enantiomer t_r = 24.1 min; 96% ee; $[\alpha]_D^{26.0}$= -18.1 (c=1.0,

$CHCl_3$, 99/1 diastereomixture, 96% ee); IR (neat) 1774, 1578, 1487, 1290, 1229, 1145, 908, 728 cm^{-1}

(3*S*,5*R*)-5-(4-chlorophenyl)-3-(2-(4-chlorophenyl)allyl)-5-(iodomethyl)dihydrofuran-2(3H)-one (5f)

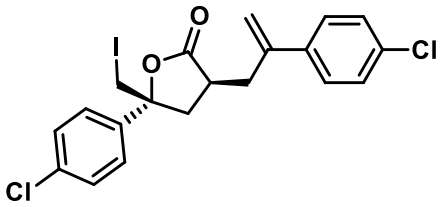

TLC R*f* = 0.72 (hexane : ethyl acetate = 2:1), ^{1}H NMR (400 MHz, $CDCl_3$) δ 7.34-7.24 (m, 8H), 5.35 (s, 1H), 5.17 (s, 1H), 3.59 (d, *J*=11.2 Hz, 1H), 3.53 (d, *J*=11.2 Hz, 1H), 3.32-3.24 (m, 1H), 2.61-2.53 (m, 3H), 2.61-2.53 (m, 1H); ^{13}C NMR (100 MHz, $CDCl_3$) δ 176.4, 144.0, 138.3, 137.9, 134.8, 134.0, 129.2, 128.9, 127.5, 126.5, 115.5, 83.7, 40.3, 39.0, 36.2, 16.4; HRMS calced for $C_{20}H_{21}O_2NCl_2I$ $(M+NH_4)^+$: 503.9989, found: *m/z* 503.9978; Enantiomeric excess was determined by HPLC with a Chiralpack AS-H column (90:10 hexane: 2-propanol, 1.0 mL/min, 254 nm); minor enantiomer t_r = 21.5 min, major enantiomer t_r = 12.4 min; 93% ee; $[\alpha]_D^{25.8}$= -25.5 (c=1.0, $CHCl_3$, 99/1 diastereomixture, 93% ee); IR (neat) 3087, 2950, 1775, 1491, 1139, 1011, 907, 831, 727 cm^{-1}

(3*S*,5*R*)-5-(iodomethyl)-5-(naphthalen-2-yl)-3-(2-(naphthalen-2-yl)allyl)dihydrofuran-2(3H)-one (5g)

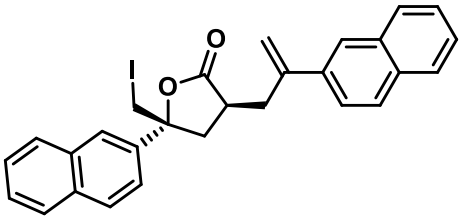

TLC R*f* = 0.72 (hexane : ethyl acetate = 2:1), ^{1}H NMR (400 MHz, $CDCl_3$) δ 7.80-7.69 (m, 8H), 7.52 (dd, *J*=8.6 Hz, 1.6 Hz, 1H), 7.46-7.42 (m, 4H), 7.29 (dd, *J*=8.8 Hz, 1.6 Hz, 1H), 5.50 (s, 1H), 5.27 (s, 1H), 3.70 (d, *J*=11.2 Hz, 1H), 3.66 (d, *J*=11.2 Hz, 1H), 3.53-3.45 (m, 1H), 2.79-2.68 (m, 3H), 2.49-2.42 (m, 1H); ^{13}C NMR (100 MHz, $CDCl_3$) δ 177.0, 144.8, 136.7, 136.5, 133.2, 132.9, 132.8, 132.7, 128.9, 128.25, 128.20, 128.1, 127.5, 126.7, 126.3, 126.1, 124.7, 124.2, 124.1, 122.2, 115.3, 84.2, 40.1, 39.1, 36.1. 16.6; HRMS calced for $C_{28}H_{27}O_2NI$ $(M+NH_4)^+$: 536.1081, found: *m/z* 536.1070; Enantiomeric excess was determined by HPLC with a Chiralpack AS-H column (90:10 hexane: 2-propanol, 1.0 mL/min, 254 nm); minor enantiomer t_r = 22.6 min, major enantiomer t_r = 17.0 min; 92% ee; $[\alpha]_D^{25.7}$= -42.7 (c=0.25, $CHCl_3$, 99/1 diastereomixture, 92% ee); IR (neat) 3057, 2930, 1773, 1167, 1134, 905, 819, 750, 730 cm^{-1}

13. Transformation of iodolactone 5a

13-1. Transformation to epoxyester 6a

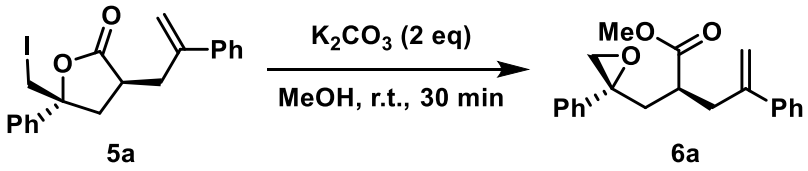

Scheme S6. Transformation to epoxyester **6a**, related to **Scheme 1**.

A mixture of iodolactone 5a (41.8 mg, 0.1 mmol, 99/1 diastereomixture, 94% ee) and K_2CO_3 (27.6 mg, 0.2 mmol) in MeOH (1 ml) was stirred for 30 min at rt. After the completion of the reaction, the reaction mixture was partitioned H_2O and Et_2O. The organic layer was dried over Na_2SO_4 and concentrated in vacuo. The residue was purified by silica-gel column chromatography (hexane/ethyl acetate = 8/1) to afford the epoxyester 6a (94% yield, 96/4 diastereomixture, 90% ee).

methyl (S)-4-phenyl-2-(((R)-2-phenyloxiran-2-yl)methyl)pent-4-enoate (6a)

TLC R*f* = 0.63 (hexane : ethyl acetate = 2:1), ^{1}H NMR (400 MHz, $CDCl_3$) δ 7.31-7.17 (m, 10H), 5.30 (s, 1H), 5.06 (s, 1H), 3.58 (s, 3H), 2.89-2.82 (m, 2H), 2.65-2.55 (m, 3H), 2.44 (dd, *J*=15.0 Hz, 3.6 Hz, 1H), 2.12-2.05 (m, 1H); ^{13}C NMR (100 MHz, $CDCl_3$) δ 175.9, 145.5, 140.2, 139.3, 128.5, 128.4, 127.8, 127.6, 126.3, 125.9, 115.1, 59.2, 55.6, 51.7, 40.3, 38.6, 37.2; HRMS calced for $C_{21}H_{22}O_3Na$ $(M+Na)^+$: 345.1461, found: *m/z* 345.1456; Enantiomeric excess was determined by HPLC with a Chiralpack IC-3 column (70:30 hexane: 2-propanol, 1.0 mL/min, 254 nm); minor enantiomer t_r = 5.6 min, major enantiomer t_r = 6.4 min; 90% ee; $[\alpha]_D^{22.4}$= -23.4 (c=1.0, $CHCl_3$, 96/4 diastereomixture, 90% ee); IR (neat) 1732, 1435, 1223, 1193, 1166, 899, 779, 760, 736, 698 cm^{-1}

13-2. Transformation to furan 7a

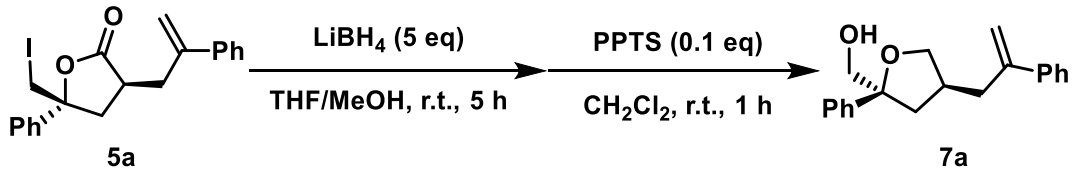

Scheme S7. Transformation to furan **7a**, related to **Scheme 1**.

A solution of iodolactone 5a (41.8 mg, 0.1 mmol, 99/1 diastereomixture, 94% ee) in THF/MeOH (2/1, 0.9 ml) was added $LiBH_4$ (12.1 mg, 0.5 mmol) at 0℃ and the reaction mixture was stirred for 5 h at rt. The reaction mixture was quenched by 1 M NaOH aq. and extracted with CH_2Cl_2. The organic layer was dried over Na_2SO_4 and concentrated in vacuo. To the solution of crude epoxyalcohol in CH_2Cl_2 (1 ml) was added PPTS (2.5 mg, 0.01 mmol) and stirred for 1 h at rt. The reaction mixture was quenched by sat. $NaHCO_3$ aq. and extracted with CH_2Cl_2. The organic layer was dried over Na_2SO_4 and concentrated in vacuo. The residue was purified by silica-gel column chromatography (hexane/ethyl acetate = 4/1) to afford the furan 7a (67% yield, 96/4 diastereomixture, 94% ee).

((2S,4S)-2-phenyl-4-(2-phenylallyl)tetrahydrofuran-2-yl)methanol (7a)

TLC R*f* = 0.48 (hexane : ethyl acetate = 2:1), ^{1}H NMR (400 MHz, $CDCl_3$) δ 7.37-7.25 (m, 10H), 5.21 (s, 1H), 4.92 (s, 1H), 4.05 (dd, *J*=8.6 Hz, 6.8 Hz, 1H), 3.60-3.49 (m, 3H), 2.55-2.39 (m, 4H), 2.02 (dd, *J*=8.0 Hz, 6.0 Hz, 1H), 1.87 (m, 1H); ^{13}C NMR (100 MHz, $CDCl_3$) δ 147.1, 145.0, 140.8, 128.48, 128.45, 127.7, 127.1, 126.2, 125.3, 113.7, 87.5, 73.4, 70.1, 41.1, 39.3, 38.9; HRMS calced for $C_{20}H_{26}O_2N$ $(M+NH_4)^+$: 312.1958, found: *m/z* 312.1955; Enantiomeric excess was determined by HPLC with a Chiralpack OJ-H column (90:10 hexane:2-propanol, 1.0 mL/min, 254 nm); minor enantiomer t_r = 12.0 min, major enantiomer t_r = 14.4 min; 90% ee; $[\alpha]_D^{22.2}$= +18.1 (c=0.5, $CHCl_3$, 96/4 diastereomixture, 90% ee); IR (neat) 3439, 3056, 2936,2863, 1493, 1445, 1044, 1028, 896, 778, 699 cm^{-1}

13-3. Transformation to bicyclic lactone 8a

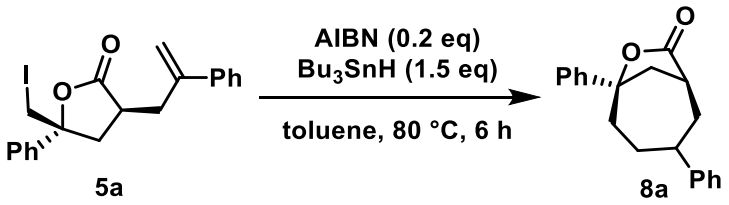

Scheme S8. Transformation to bicyclic lactone **8a**, related to **Scheme 1**.

To the solution of iodolactone 5a (41.8 mg, 0.1 mmol, 99/1 diastereomixture, 90% ee) in toluene (2.5 ml) was added AIBN (3.3 mg, 0.02 mmol) and Bu_3SnH (0.15 ml, 0.15 mmol) at 0 ℃. The reaction mixture was stirred for 6 h at 80 ℃. After cooling to rt, the reaction mixture was concentrated in vacuo and purified by silica-gel column chromatography (hexane/ethyl acetate = 8/1) to afford the bicyclic lactone 8a (80% yield, 93/7 diastereomixture, 94% ee).

(1S,6R)-3,6-diphenyl-7-oxabicyclo[4.2.1]nonan-8-one (8a)

TLC R*f* = 0.45 (hexane : ethyl acetate = 4:1), ^{1}H NMR (400 MHz, $CDCl_3$) δ 7.45-7.17 (m, 10H), 3.05-2.99 (m, 1H), 2.96-2.88 (m, 1H), 2.82 (d, *J*=13.2 Hz, 1H), 2.57 (dd, *J*=13.2 Hz, 9.0 Hz, 1H), 2.38-2.11 (m, 4H), 2.07-1.99 (m, 1H), 1.89 (dt, *J*=2.8 Hz, 13.3 Hz, 1H); ^{13}C NMR (100 MHz, $CDCl_3$) δ 178.3, 147.0, 146.1, 128.8, 128.6, 127.5, 126.6, 126.5, 123.9, 90.3, 41.7, 41.62, 41.55, 40.7, 37.9, 33.3; HRMS calced for $C_{20}H_{21}O_2$ $(M+H)^+$: 293.1536, found: *m/z* 293.1534; Enantiomeric excess was determined by HPLC with a Chiralpack IC-3 column (90:10 hexane: 2-propanol, 1.0 mL/min, 254 nm); minor enantiomer t_r = 24.2 min, major enantiomer t_r = 21.9 min; 94% ee; $[\alpha]_D^{22.1}$= +45.5 (c=1.0, $CHCl_3$, 93/7 diastereomixture, 94% ee); IR (neat) 1766, 1266, 1239, 1186, 1101, 971, 956, 755, 733, 698 cm^{-1}

14. Details of DFT calculations

All calculations were performed with the Gaussian 09 package (Frisch et al. 2013). The promising TS model was explored first using the simplified chemical model. Based on the rationale TS model, the origin of high enantioselectivity and the role of I_2 were clarified using the realistic chemical model. All geometries were optimized by B3LYP/LANL2DZ for Zn, LANL2DZdp for I, 6-31G* for the rest. Frequency analyses were also carried out to identify the stationary points (TS: one imaginary frequency) and to estimate thermodynamic properties and Gibbs free energies at 298.15 K and 1atm. To evaluate more reliable non-bonding attractive interaction energies (especially halogen bond), **TS_{major}-B** was also optimized by M06/SDD for Zn, aug-cc-pVTZ and SDB pseudopotential for I, 6-31G* for the rest. (Zhao and Truhlar, 2008; Kee and Wong, 2016) The molecular structures were depicted by using the CYLview v1.0.561 β. (Legault, 2009)

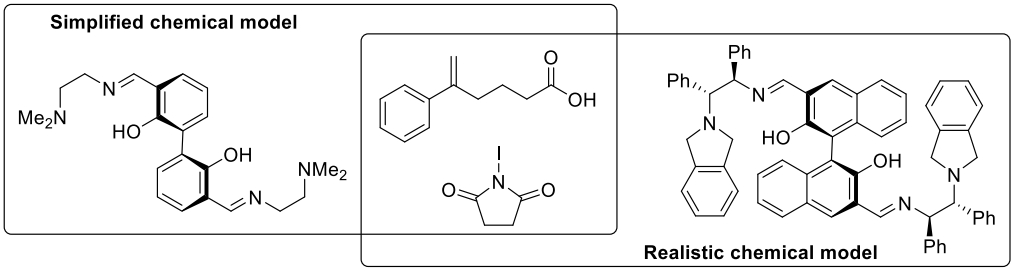

Figure S5. Realistic chemical model and simplified chemical model, related to **Figure 3**.

As a preliminary study, possible diastereomeric TS structures corresponding to facial-selectivity (major: **TSr**, minor: **TSs**), coordination position/nucleophilic oxygen atom in carboxylate anion (terminal: **TS_a1**, **TS_a2**, central: **TS_b1**, **TS_b2**), and six-membered ring structures in char-like TS (olefin in axial site: **TS-1**, equatorial site: **TS-2**) were compared using simplified chemical models (Fig. S6). In agreement with our previously reported experimental result, in which the terminal acetate anion was replaced by the carboxylate anion of **1a**, **TS_a** series were found to be energetically more stable than **TS_b** series. To clarify the ligand structure-activity relationship, the rationale TS_a series were expanded to the corresponding realistic chemical models (brackets in Fig. S6). **TSr_a1_2** (= **TS_{major}-A**) is energetically most stable in consistent with the experimentally observed major enantiomer. Relative Gibbs free energies showed a similar tendency in both simplified and realistic chemical models. This indicates that the chiral diamine framework at 3,3'-positions are not essential for asymmetric induction as observed in the experimentally observed ligand structure-activity relationship.

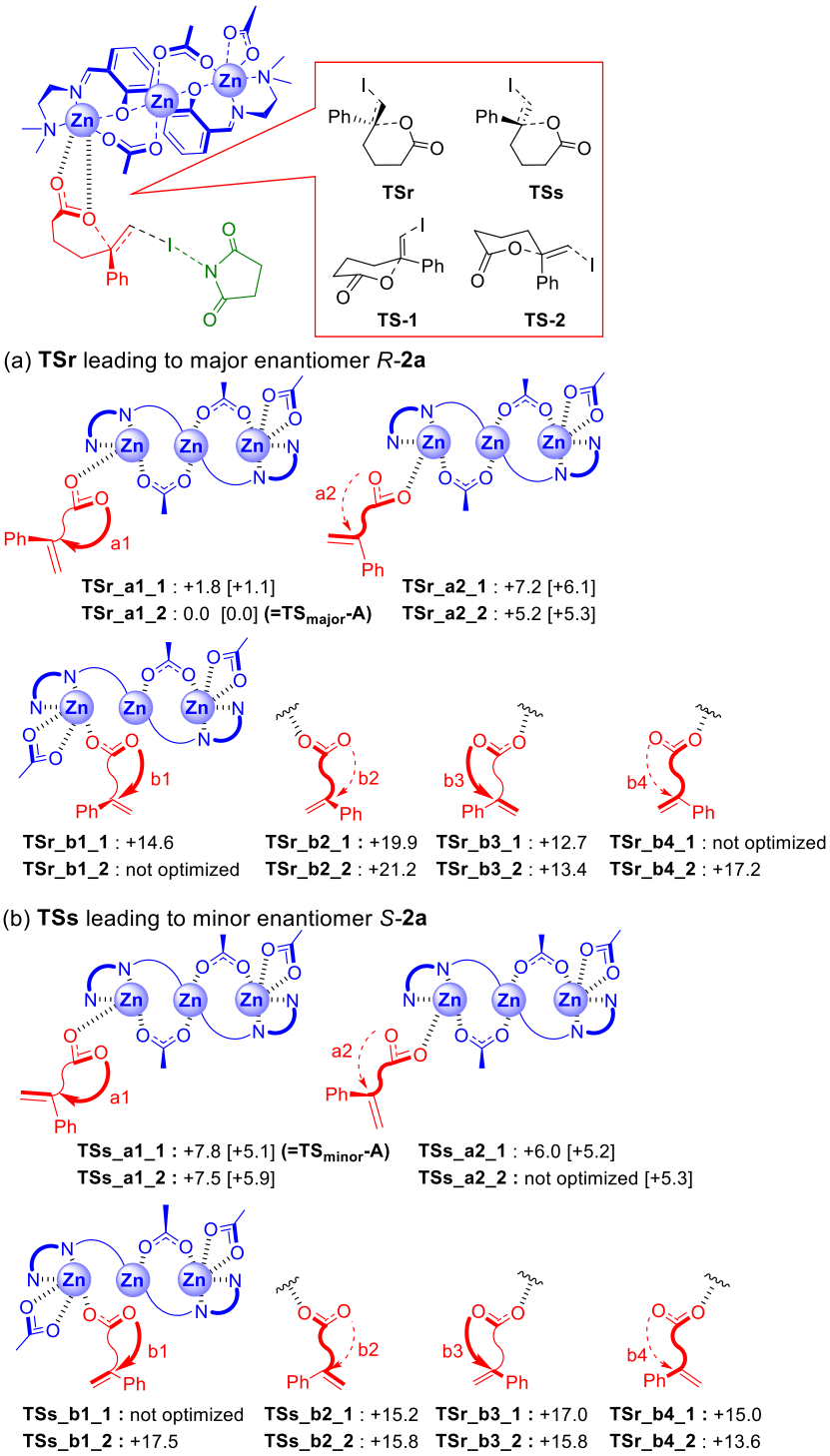

Figure S6. Schematic diastereomeric TS structures and relative Gibbs free energies (kcal/mol) of simplified chemical models (realistic chemical models in brackets), related to **Figure 3**.

To identify the rationale TS model involving I_2, various coordination modes of I_2 were explored based on the most stable **TSr_a1_2** (Fig. S7). Detailed screening of various TS models allowed us to find two possible functions of additional I_2; iodine source for iodination (**TS_IN**) and Lewis acid activation (**TS_NI**). The computational results of energetically more favored **TS_IN** than **TS_NI** indicate that additional I_2 act as the

iodine source for iodination. Therefore, further screening of **TS_IN** model was conducted for **TSr_a1** series and **TSs_a** series located within 1 kcal/mol. **TSr_a1_2_IN1** (= **TS$_{major}$-B**) is 3.3-kcal/mol more stable than **TSs_a1_2_IN2** (= **TS$_{minor}$-B**). Both stable TSs have similar gross structures of **TS-A** models with slightly different hydrogen bonding network of NIS-**tri-Zn**. Steric repulsion between the Ph group of **1a** and the naphthyl moiety of **L1** significantly destabilizes **TSs_a1_2_IN2**, albeit with the presence of halogen bonding and hydrogen bonding interactions with NIS (Fig. S8).

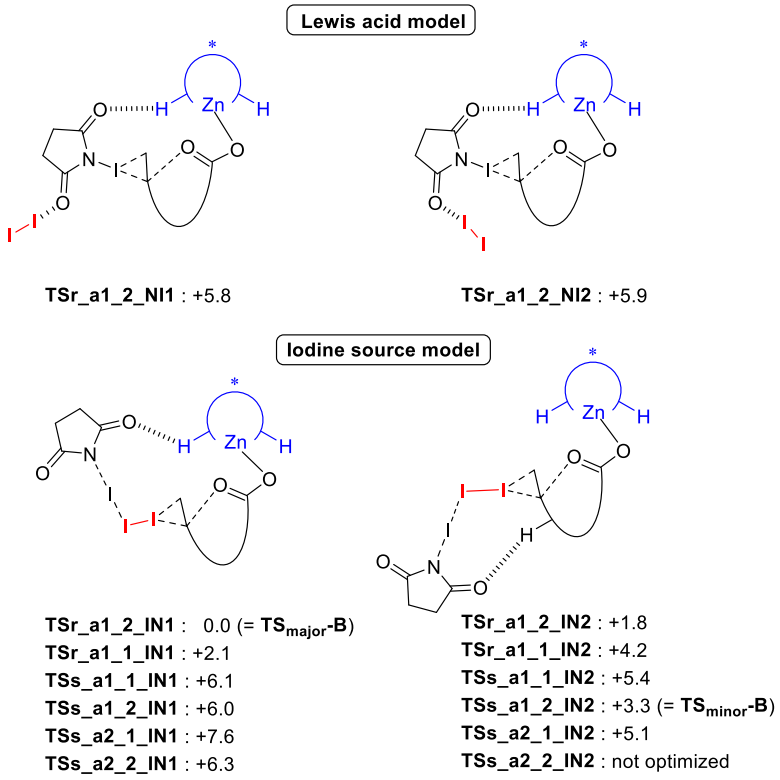

Figure. S7. Relative Gibbs free energies (kcal/mol) of TS models involving I_2, related to **Figure 3**.

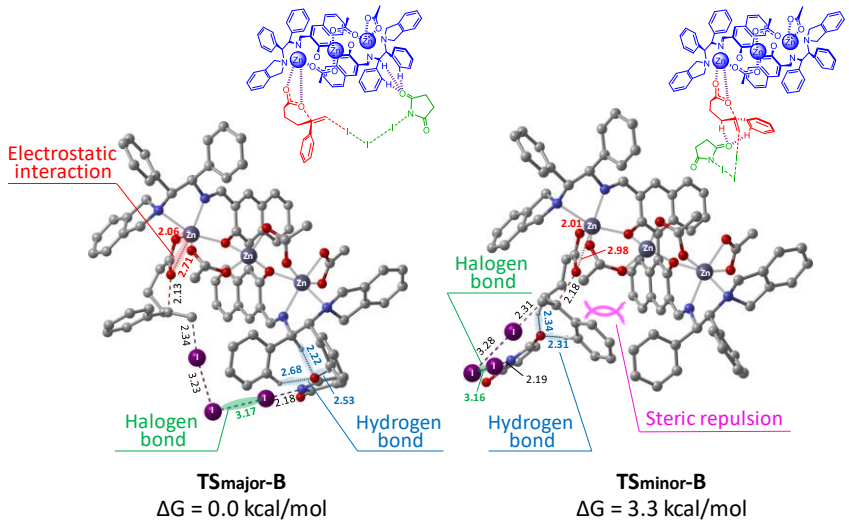

Figure S8. The most stable diastereomeric TS models of I_2/NIS in the **tri-Zn**-catalyzed iodolactonization. Bond lengths are in angstroms, related to **Figure 3**.

The details of three types of attractive non-covalent interactions in **TS$_{major}$-B**, each interaction energy (E_{int}) was estimated using the counterpoise method at the same level as geometry optimization. **TS$_{major}$-B** was dissected into three fragments (**1a**-I_2, NIS, and **tri-Zn**), of which single-point energies were compared with those of partial components (**tri-Zn**/**1a**-I_2, **tri-Zn**/NIS, **1a**-I_2/NIS,), estimating each interaction energy (Fig. S9A). Eelectrostatic interaction (101.5 kcal/mol) was found to be a major factor in attractive non-covalent interactions in **TS$_{major}$-B**. Both hydrogen bond (5.8 kcal/mol) and halogen bond (17.9 kcal/mol) act cooperatively in stabilizing **TS$_{major}$-B**. To evaluate more reliable non-bonding attractive interaction energies (especially halogen bond), **TS$_{major}$-B** was also optimized by M06/SDD for Zn, aug-cc-pVTZ and SDB pseudopotential for I, 6-31G* for the rest (Fig. S9B). TS structure optimized by the M06 method has almost the same gross structure as that by the B3LYP method. Contribution of three types of interaction energies (electrostatic interaction: 12.8 kcal/mol, hydrogen bond: 18.4 kcal/mol, halogen bond: 22.2 kcal/mol) is not fundamentally changed by the M06 method, albeit with the slightly different hydrogen bonding network in the NIS moiety.

(**A**) Interaction energy analysis

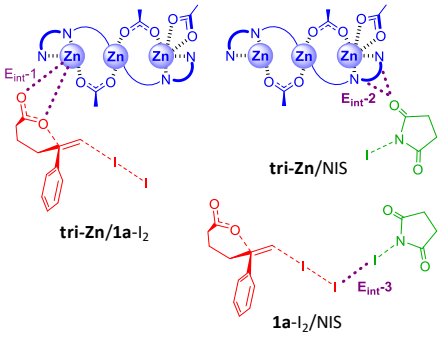

	E_{int} (kcal/mol)	
	B3LYP	M06
tri-Zn/**1a**-I_2 (E_{int}-1)	101.5	126.8
tri-Zn/NIS (E_{int}-2)	5.8	18.4
1a-I_2/NIS (E_{int}-3)	17.9	22.2

(**B**) **TS$_{major}$-B** (M06)

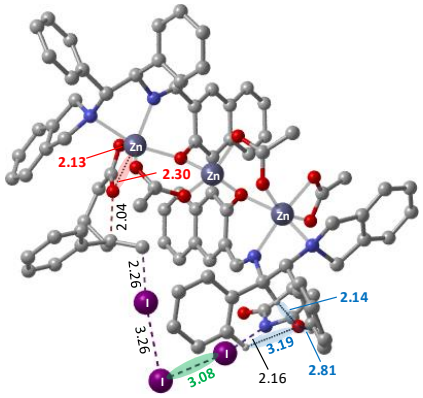

Figure S9. (A) Interaction energy analysis and (B) **TS$_{major}$-B** optimized by M06/SDD for Zn, aug-cc-pVTZ and SDB pseudopotential for I, 6-31G* for the rest, related to **Figure 3**.

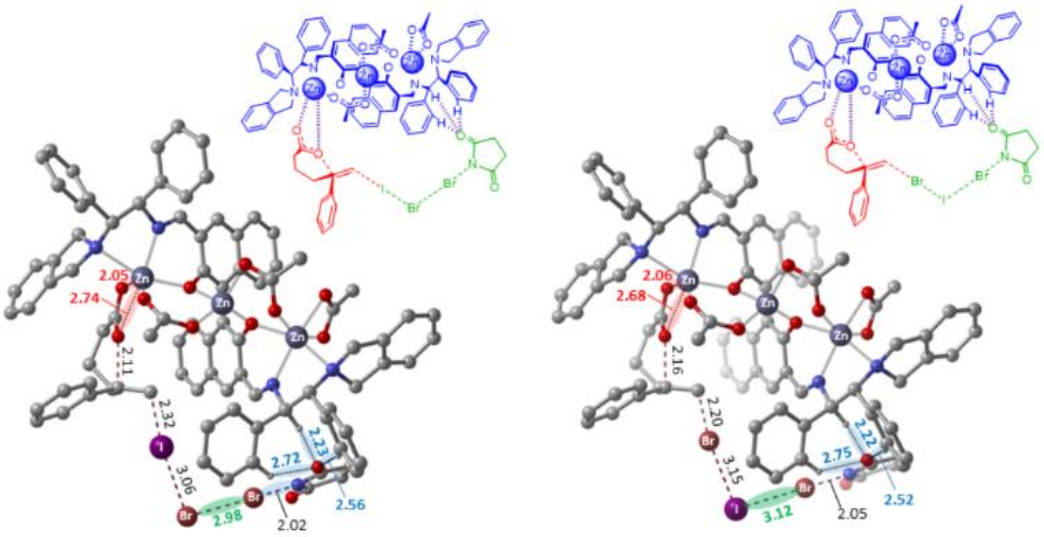

Figure S10 DFT simulations on the second catalytic cycle of **Tri-Zn**-catalyzed bromocyclization using NBS and I_2 (entry 2 in Table 2), related to **Figure 7**.

In the first catalytic cycle based on the halogen-incorporated reaction mechanism (Figure 6a), I-Br should be generated after the first catalytic cycle of the **Tri-Zn**-catalyzed bromocyclization using NBS and I_2 (entry 2 in Table 2). When the I-Br is incorporated into the TS for the second catalytic cycle, the reaction should proceed from **TS-I** described in the left side of the Figure S10 to give the iodolactone.

15. ^{1}H-NMR and ^{13}C-NMR spectra

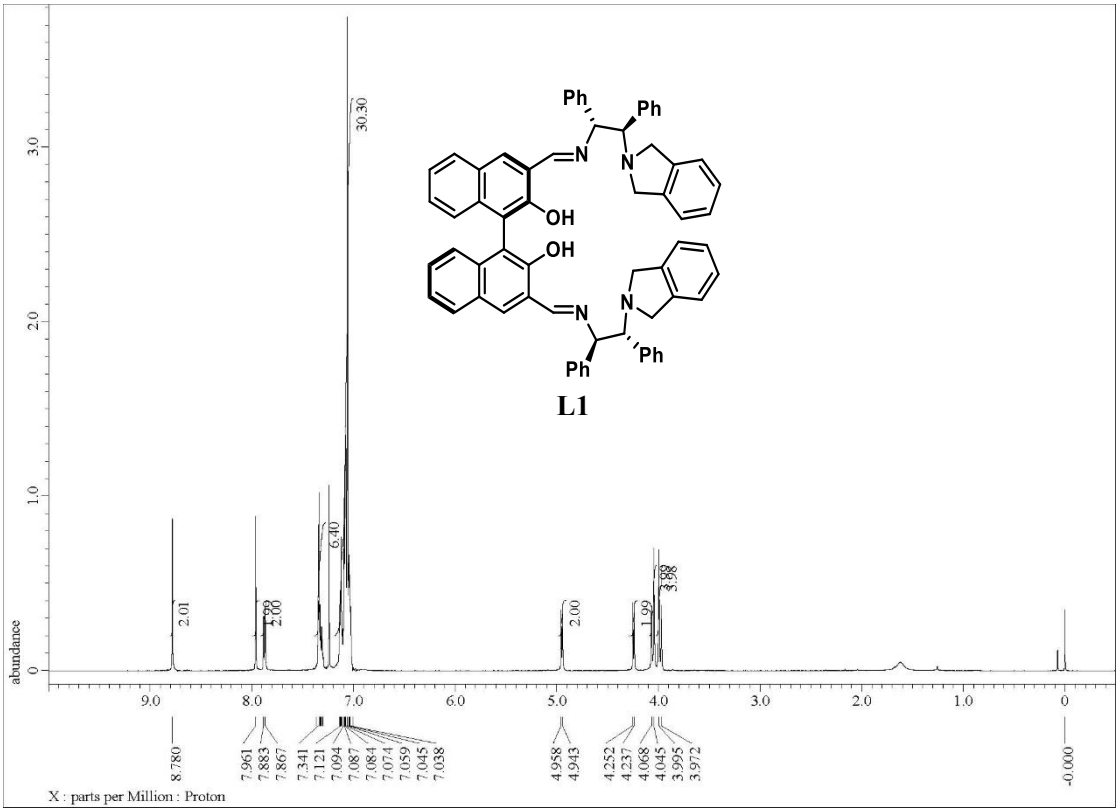

Figure S11. ^{1}H-NMR of **L1**, related to **Figure 2**.

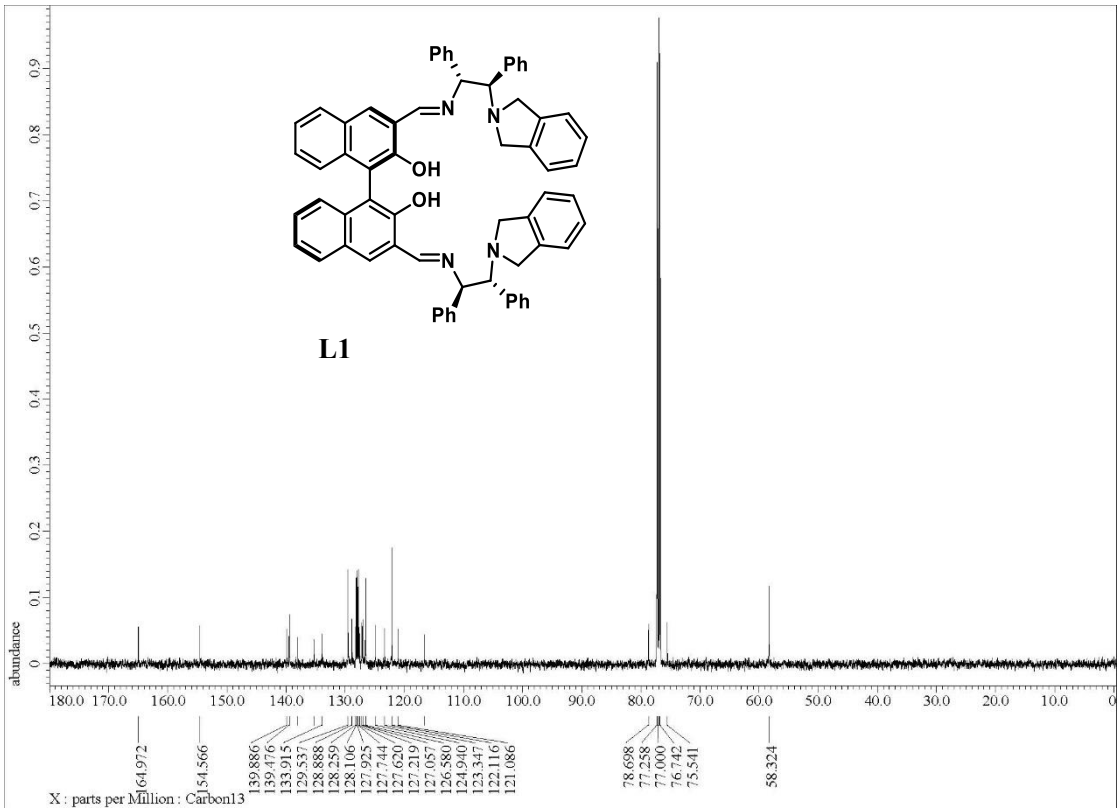

Figure S12. ^{13}C-NMR of **L1**, related to **Figure 2**.

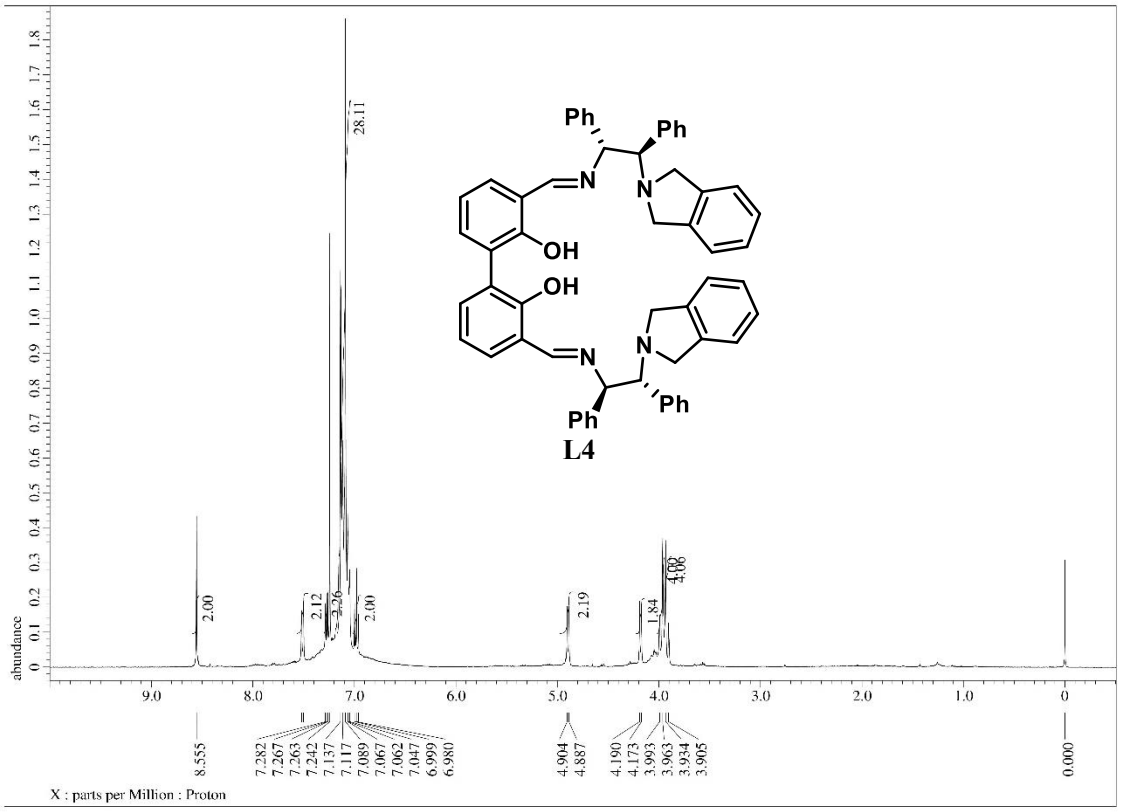

Figure S13. ^{1}H-NMR of **L4**, related to **Table 1**.

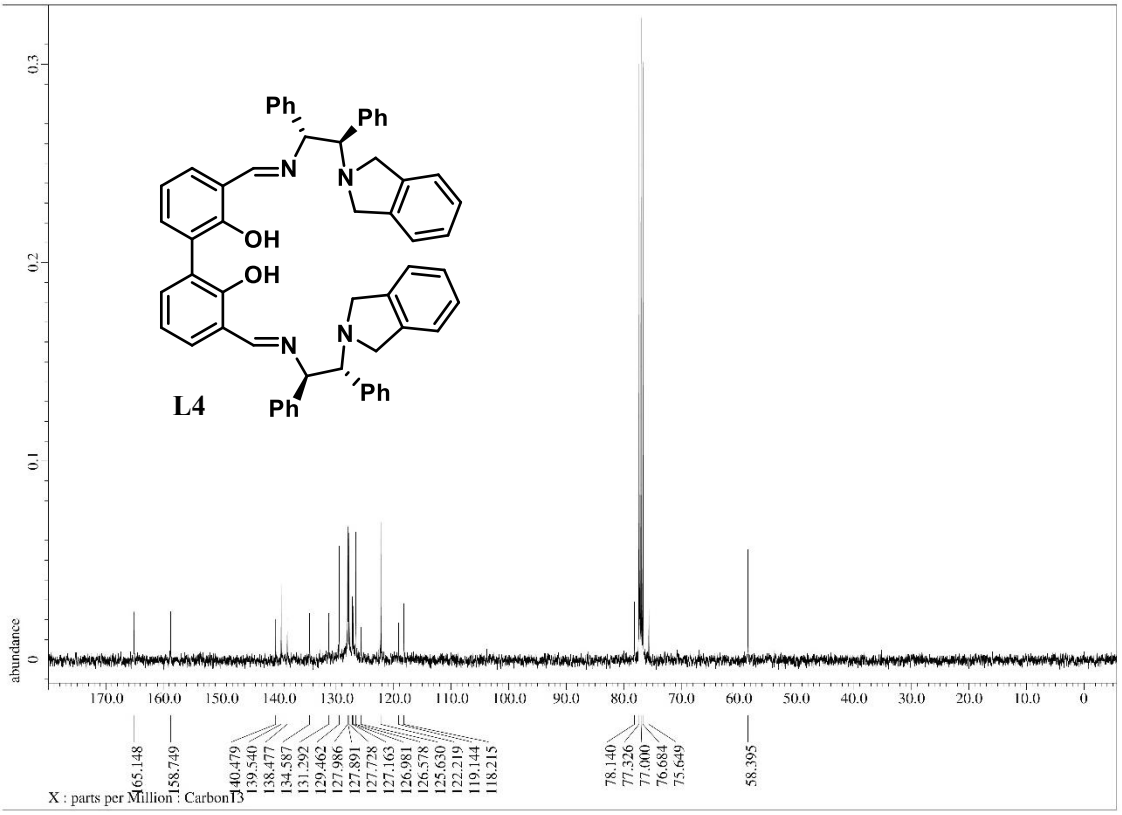

Figure S14. ^{13}C-NMR of **L4**, related to **Table 1**.

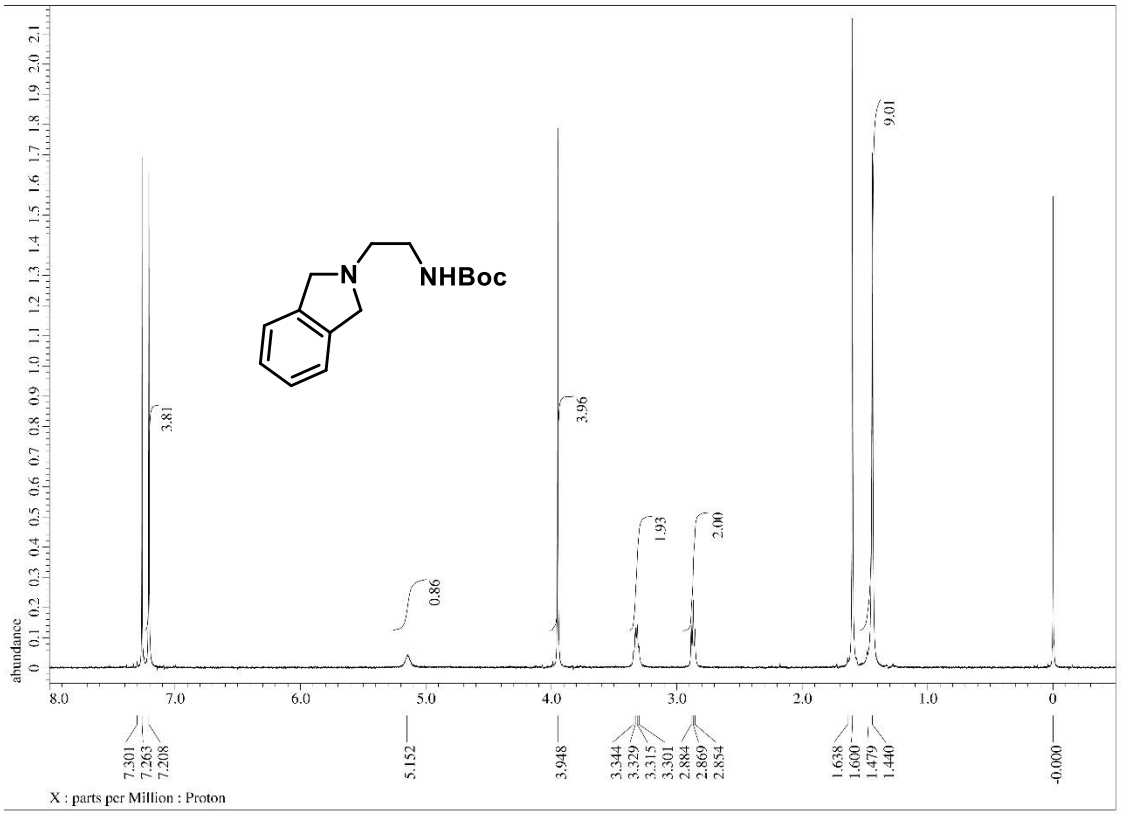

Figure S15. ^{1}H-NMR of *tert*-butyl (2-(isoindolin-2-yl)ethyl)carbamate, related to **Table 1**.

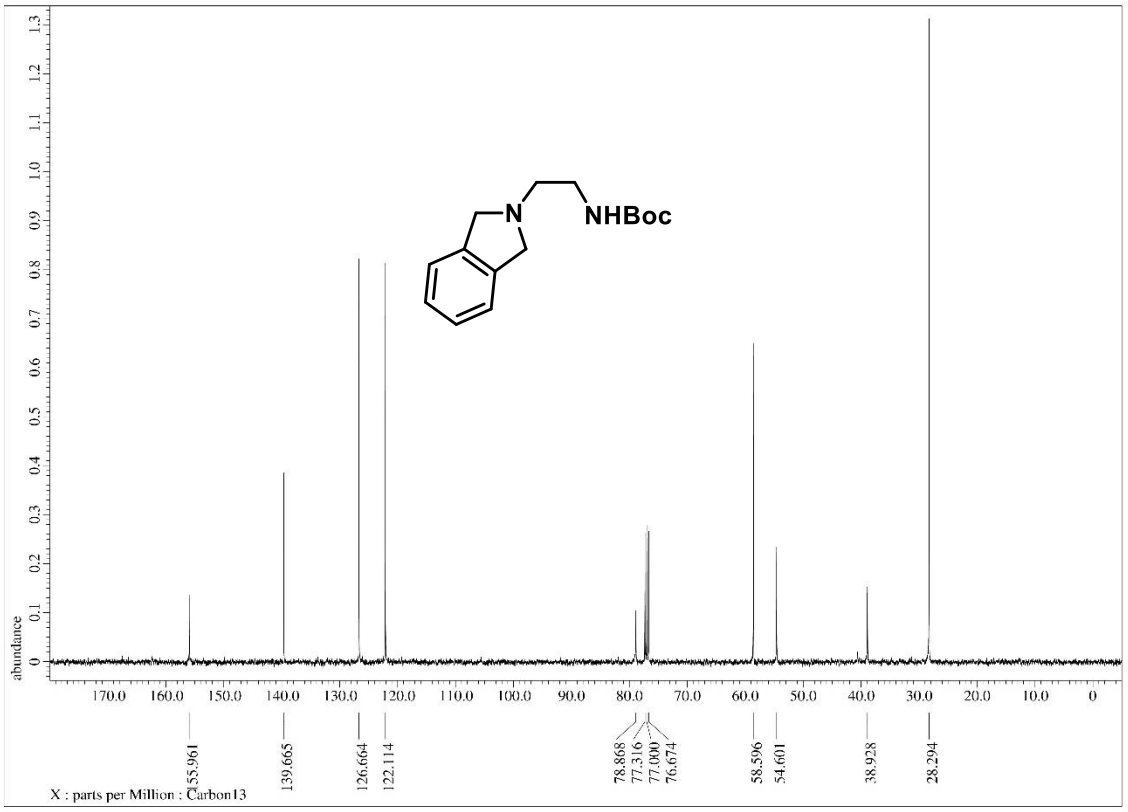

Figure S16. ^{13}C-NMR of *tert*-butyl (2-(isoindolin-2-yl)ethyl)carbamate, related to **Table 1**.

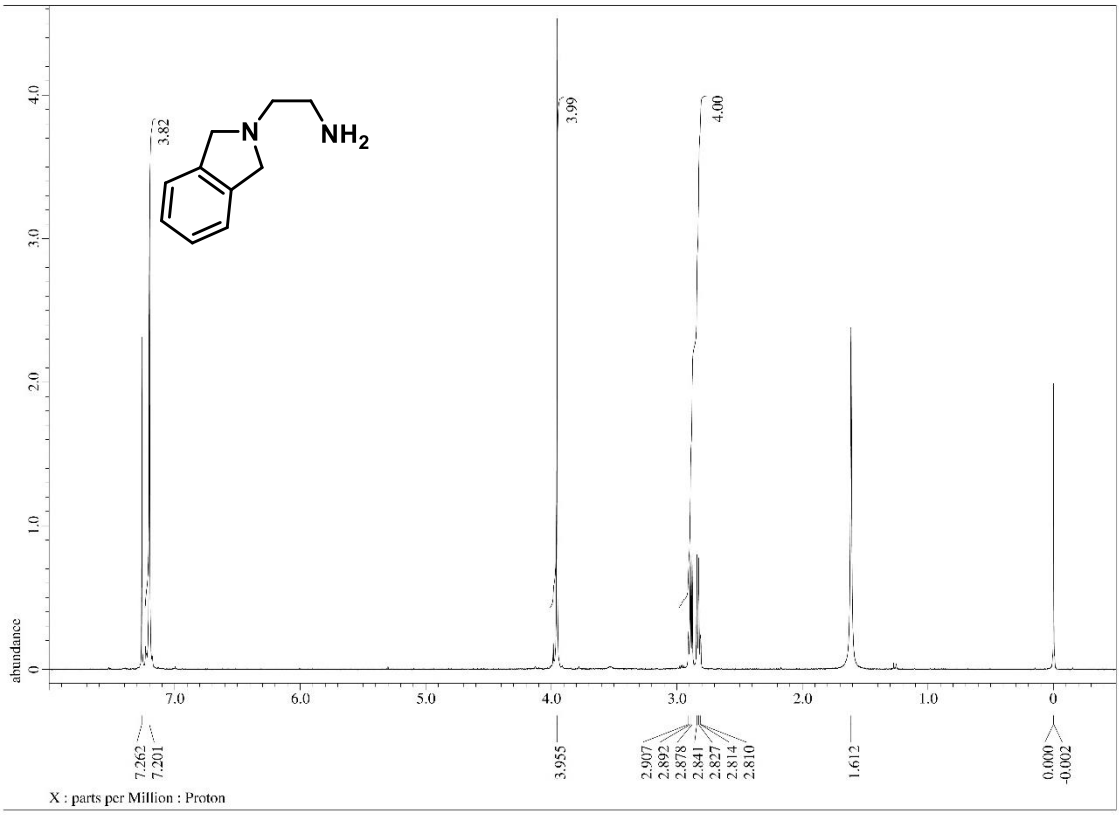

Figure S17. [1]H-NMR of 2-(isoindolin-2-yl)ethan-1-amine, related to **Table 1**.

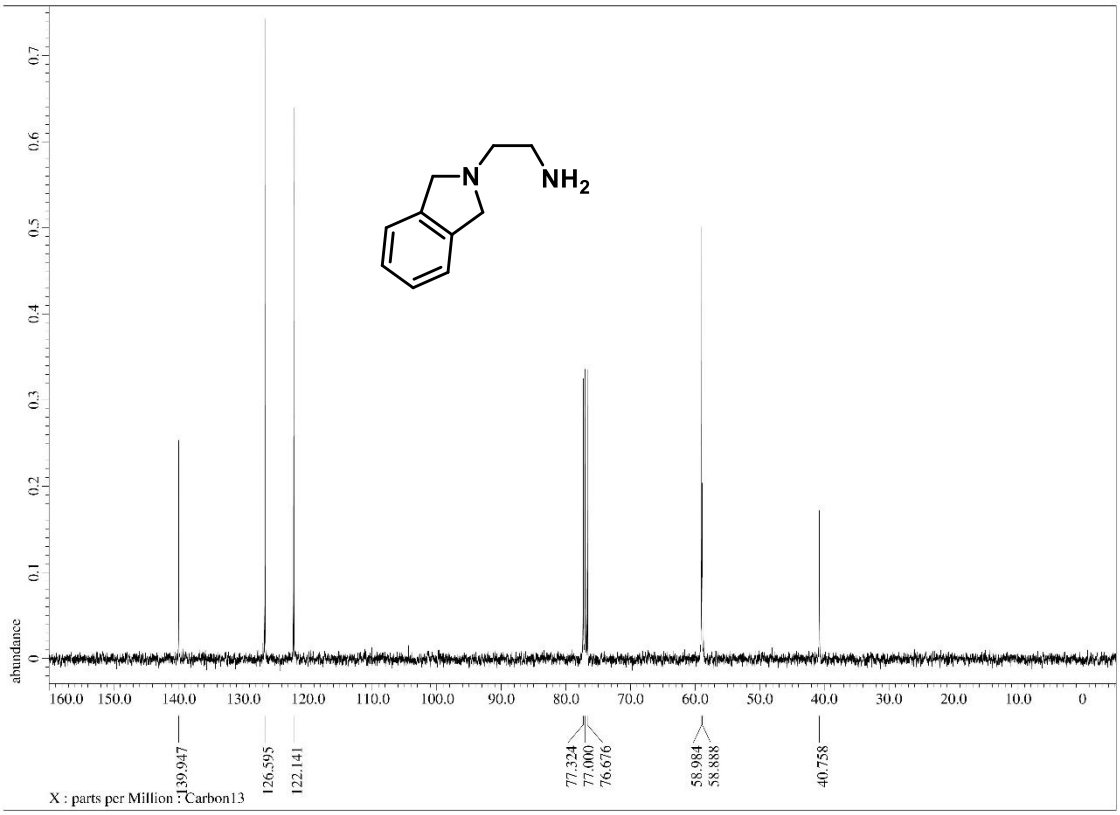

Figure S18. [13]C-NMR of 2-(isoindolin-2-yl)ethan-1-amine, related to **Table 1**.

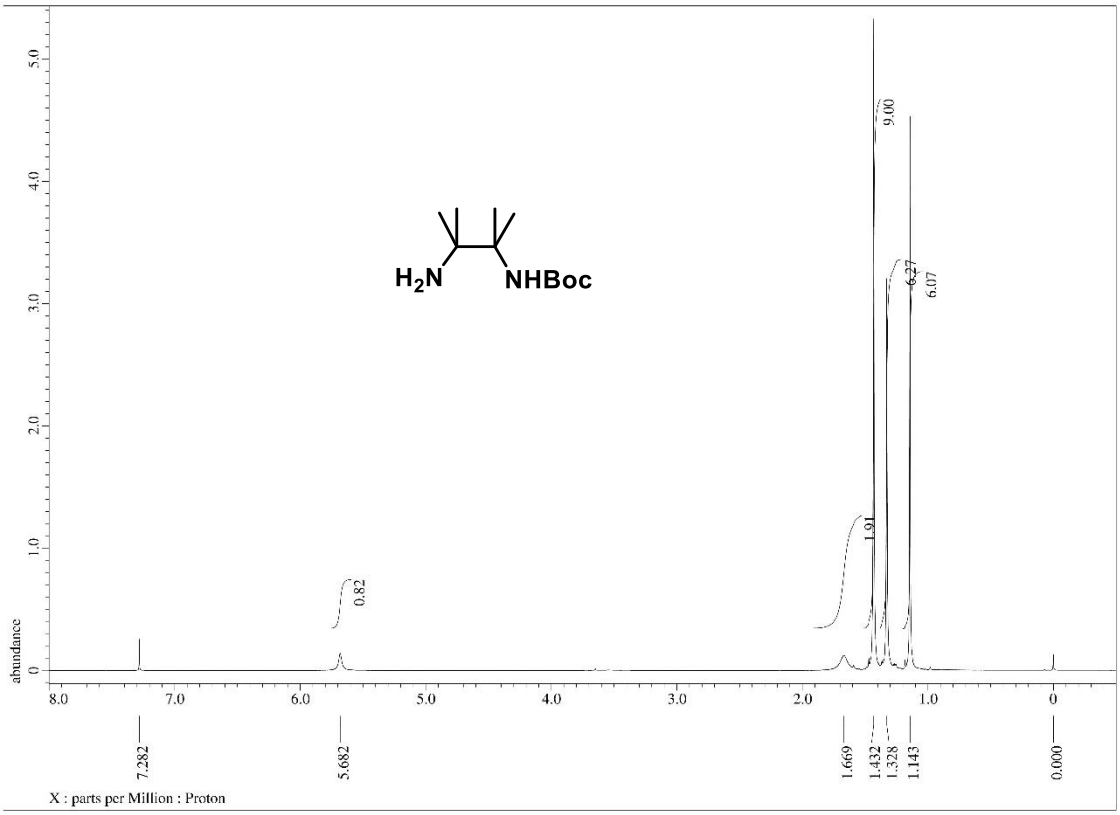

Figure S19. [1]H-NMR of *tert*-butyl (3-amino-2,3-dimethylbutan-2-yl)carbamate, related to **Table 1**.

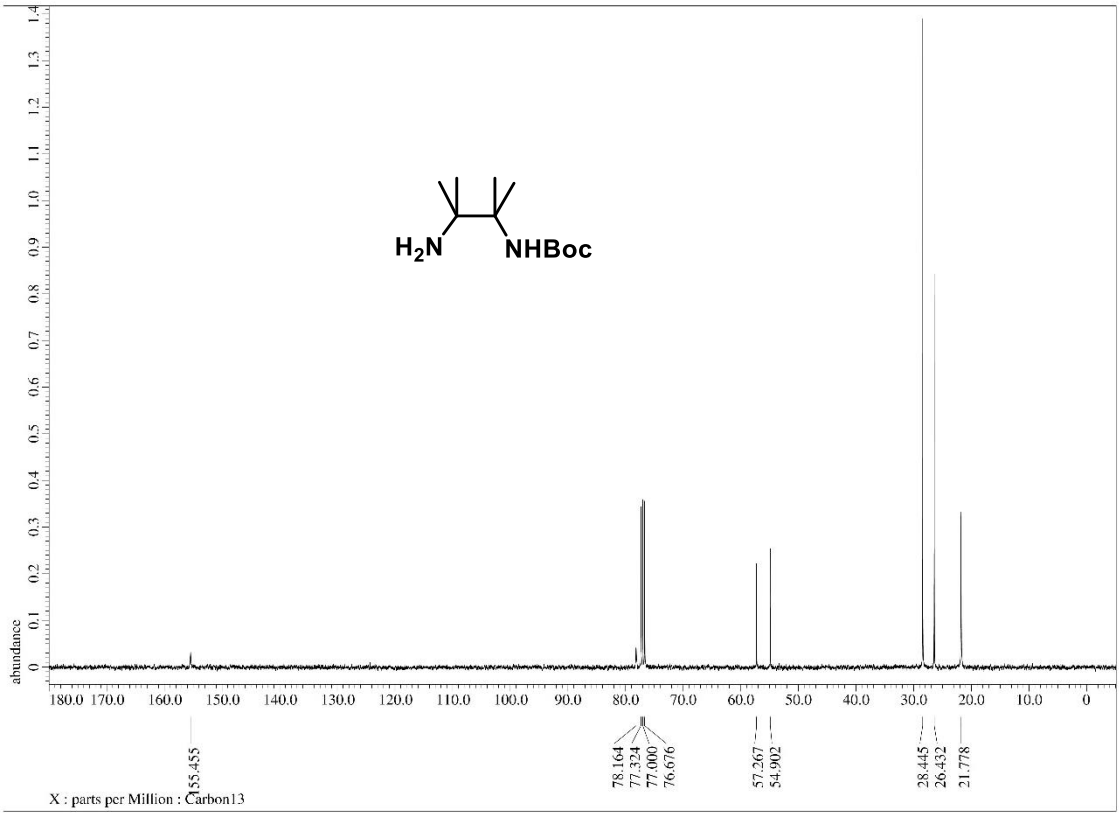

Figure S20. [13]C-NMR of *tert*-butyl (3-amino-2,3-dimethylbutan-2-yl)carbamate, related to **Table 1**.

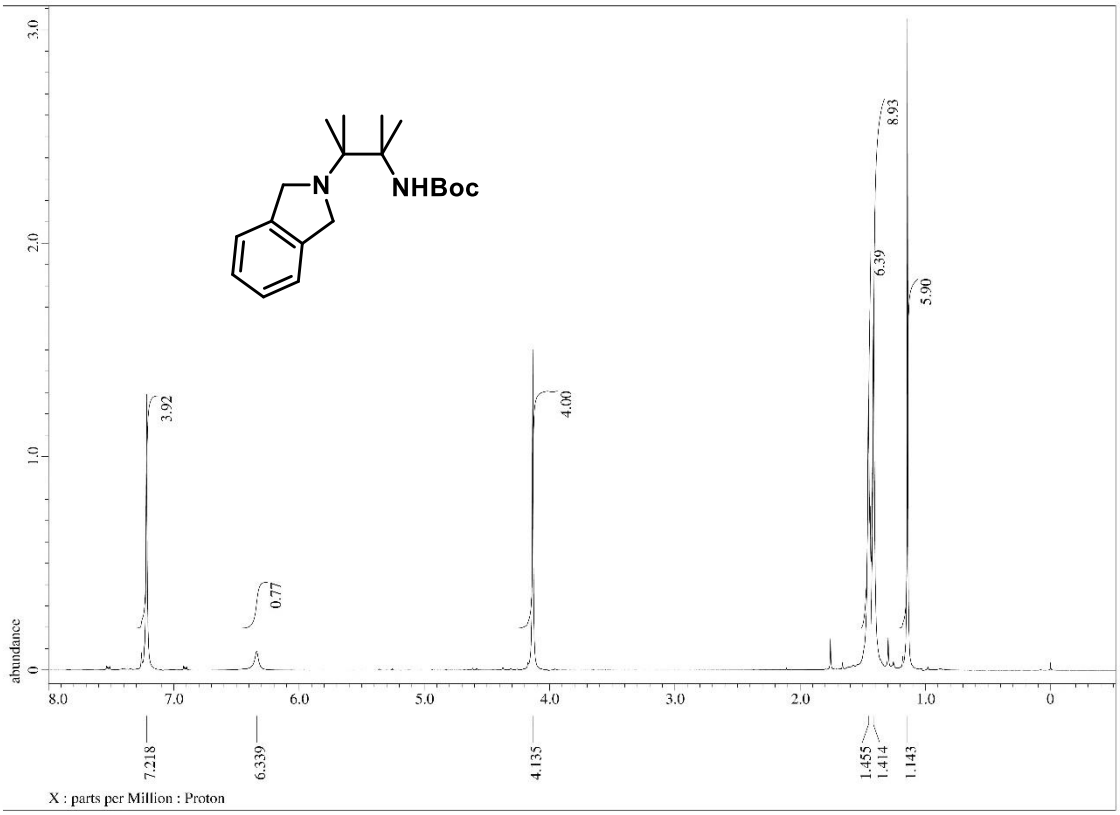

Figure S21. [1]H-NMR of *tert*-butyl (3-(isoindolin-2-yl)-2,3-dimethylbutan-2-yl)carbamate, related to **Table 1**.

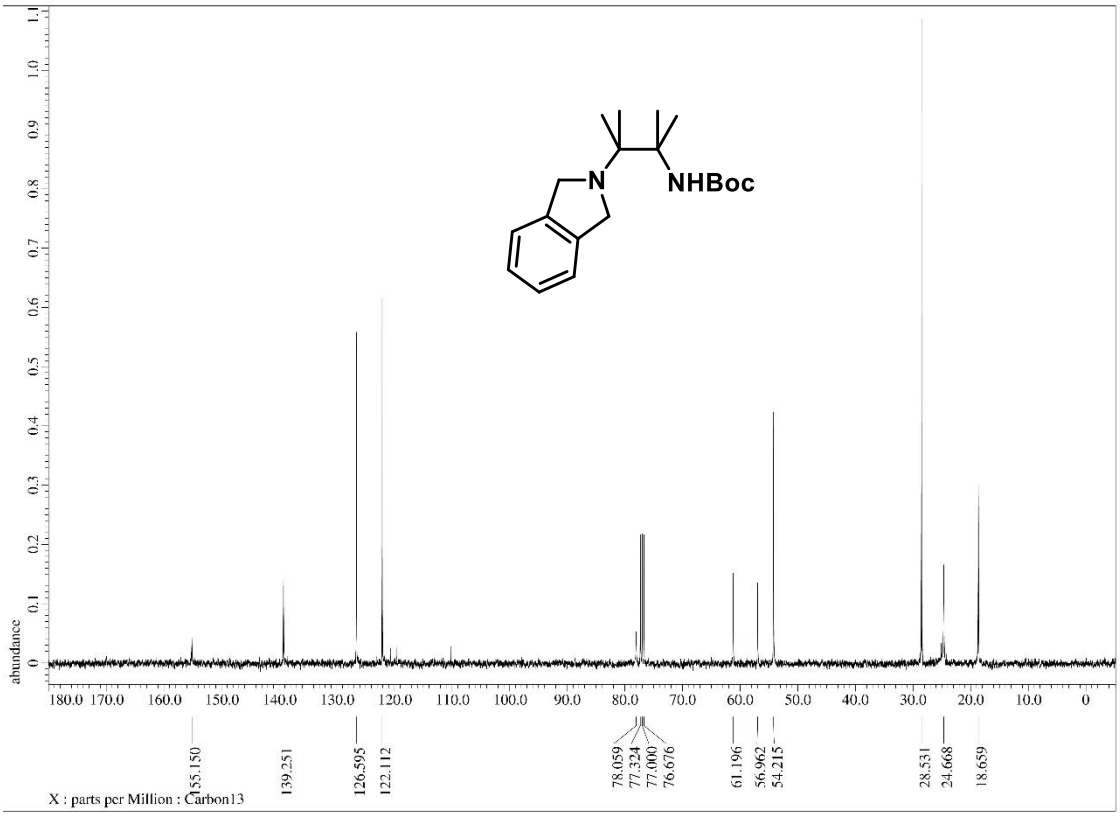

Figure S22. [13]C-NMR of *tert*-butyl (3-(isoindolin-2-yl)-2,3-dimethylbutan-2-yl)carbamate, related to **Table 1**.

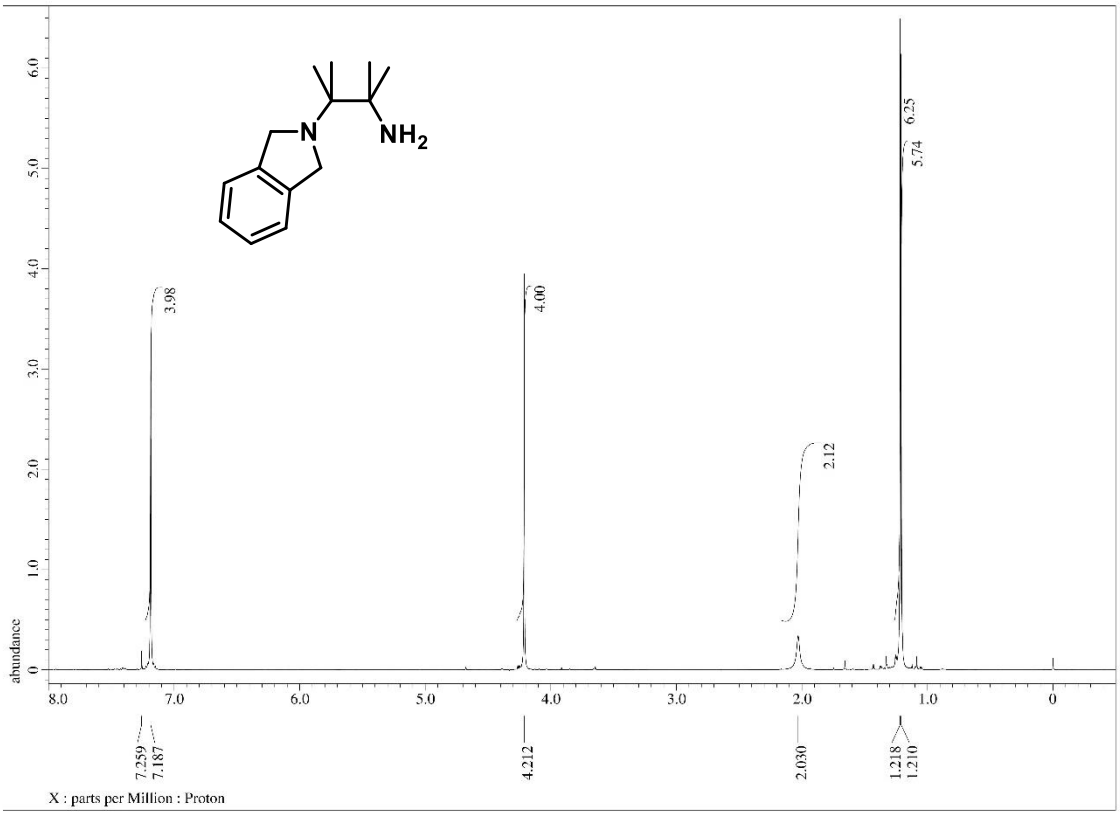

Figure S23. [1]H-NMR of 3-(isoindolin-2-yl)-2,3-dimethylbutan-2-amine, related to **Table 1**.

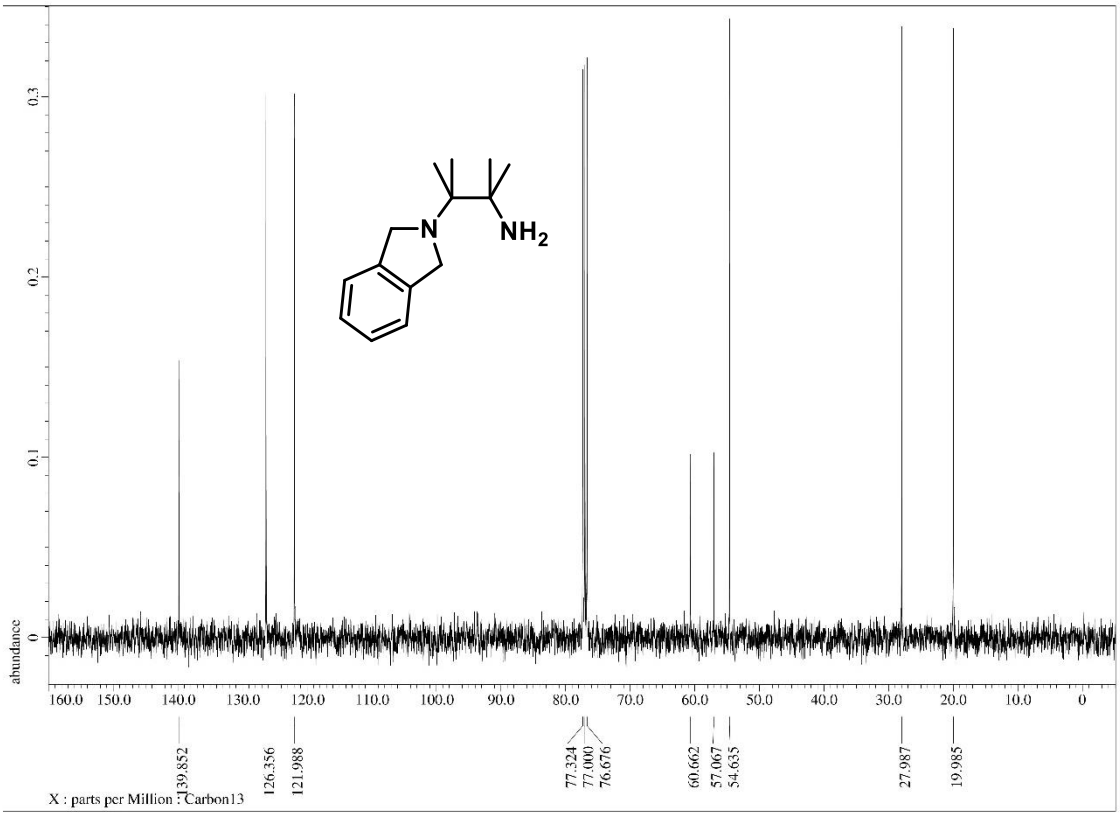

Figure S24. [13]C-NMR of 3-(isoindolin-2-yl)-2,3-dimethylbutan-2-amine, related to **Table 1**.

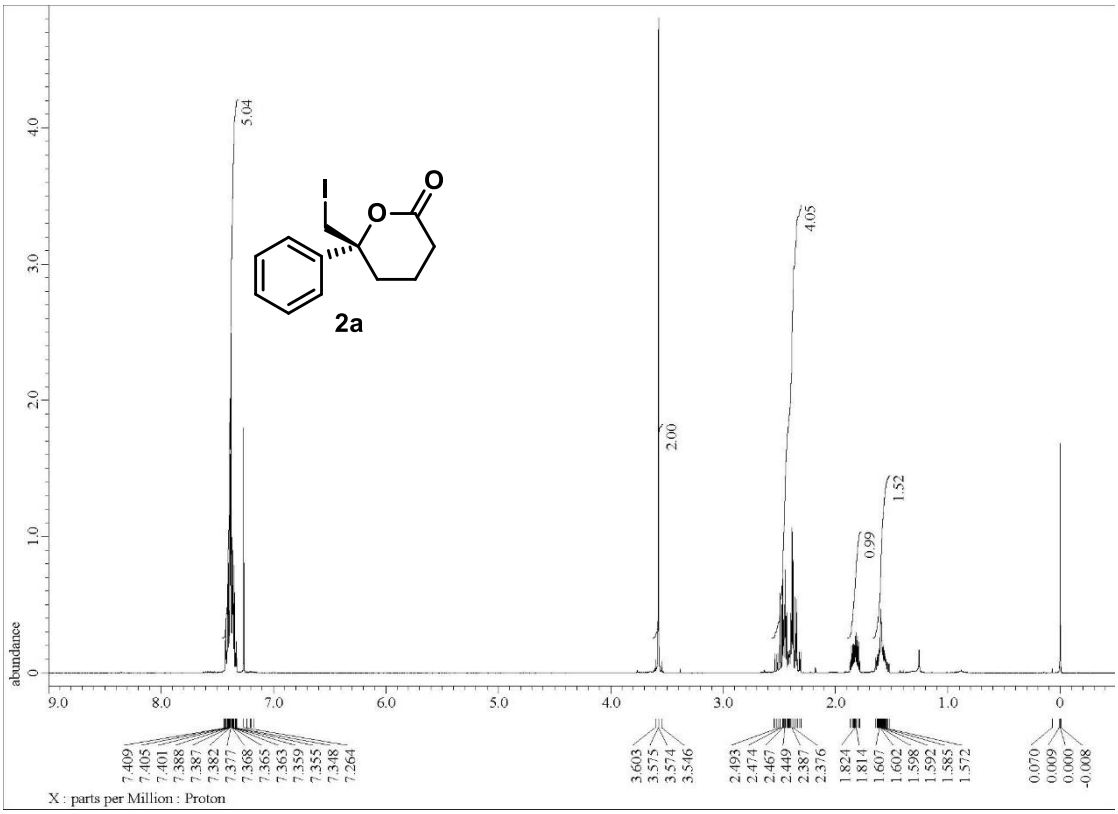

Figure S25. ^{1}H-NMR of **(*R*)-2a**, related to **Table 1**.

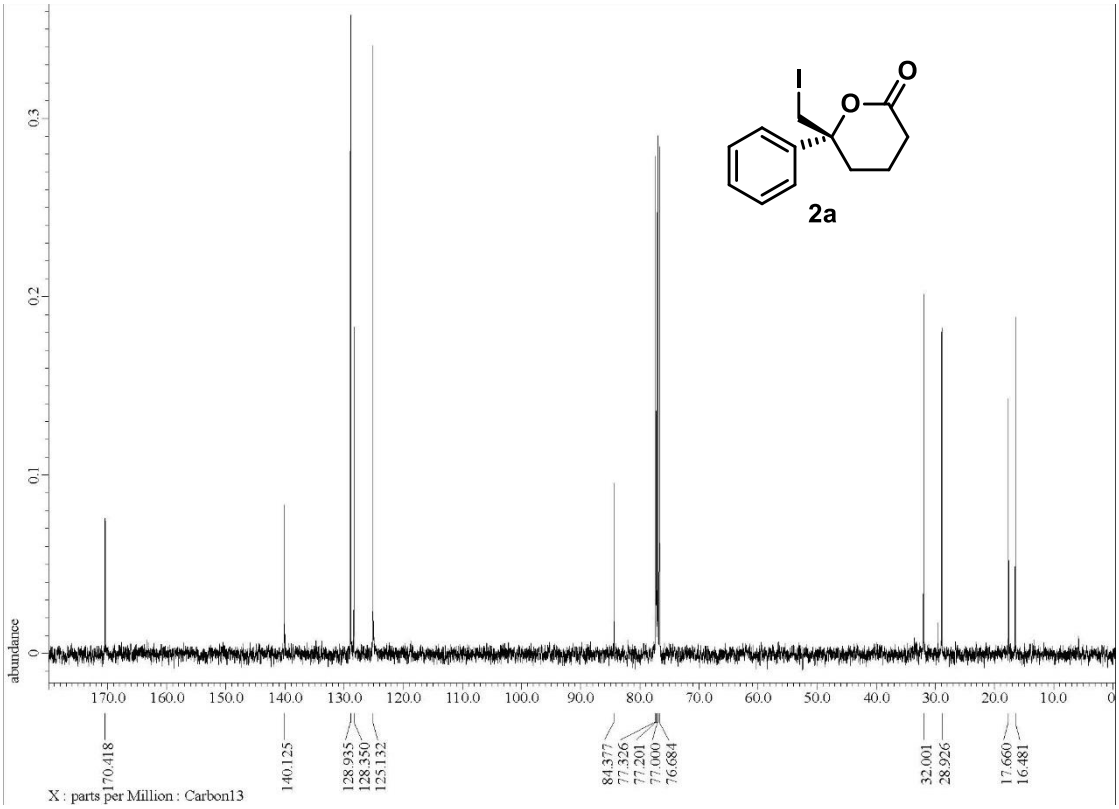

Figure S26. ^{13}C-NMR of **(*R*)-2a**, related to **Table 1**.

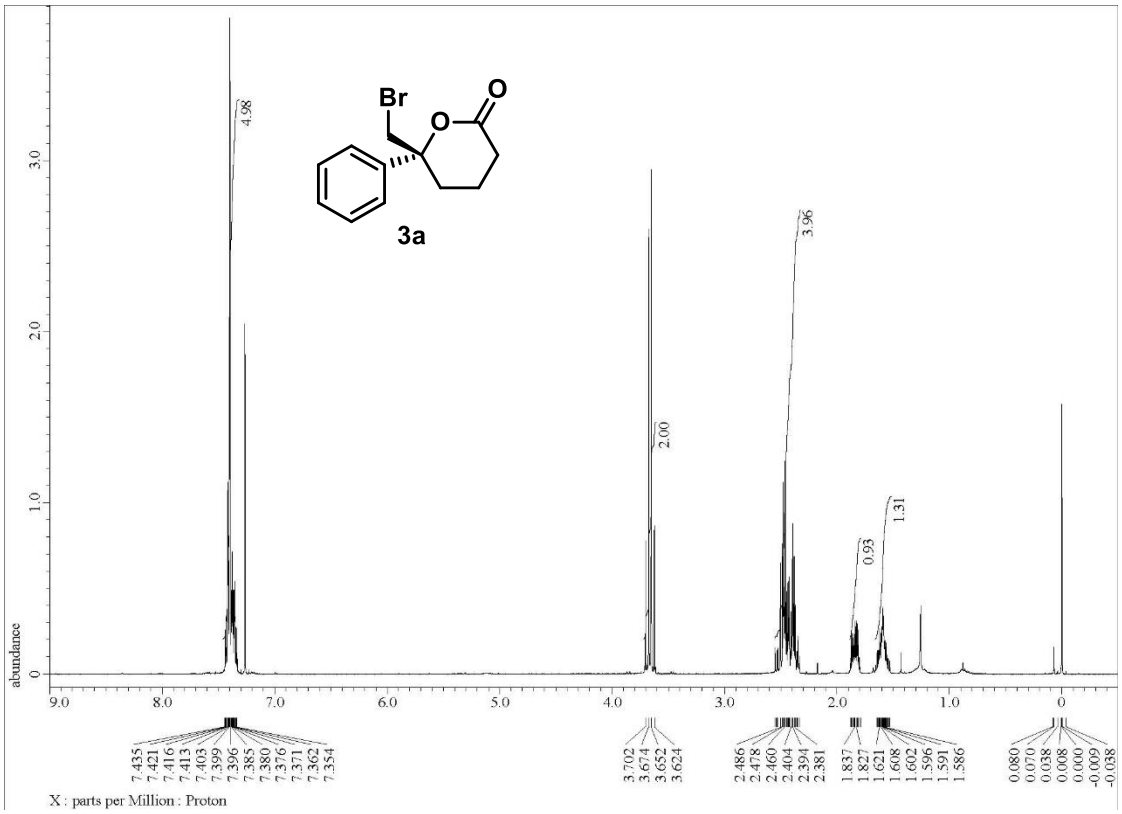

Figure S27. ^{1}H-NMR of **(*R*)-3a**, related to **Table 2**.

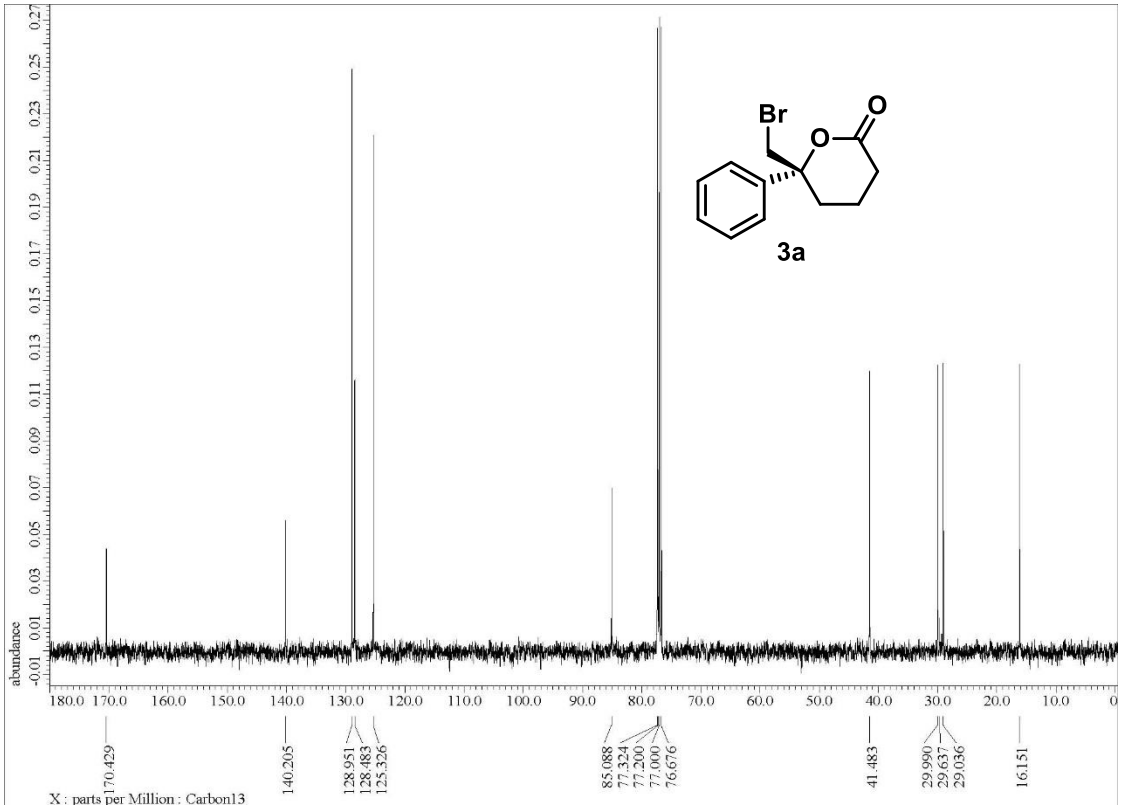

Figure S28. ^{13}C-NMR of **(*R*)-3a**, related to **Table 2**.

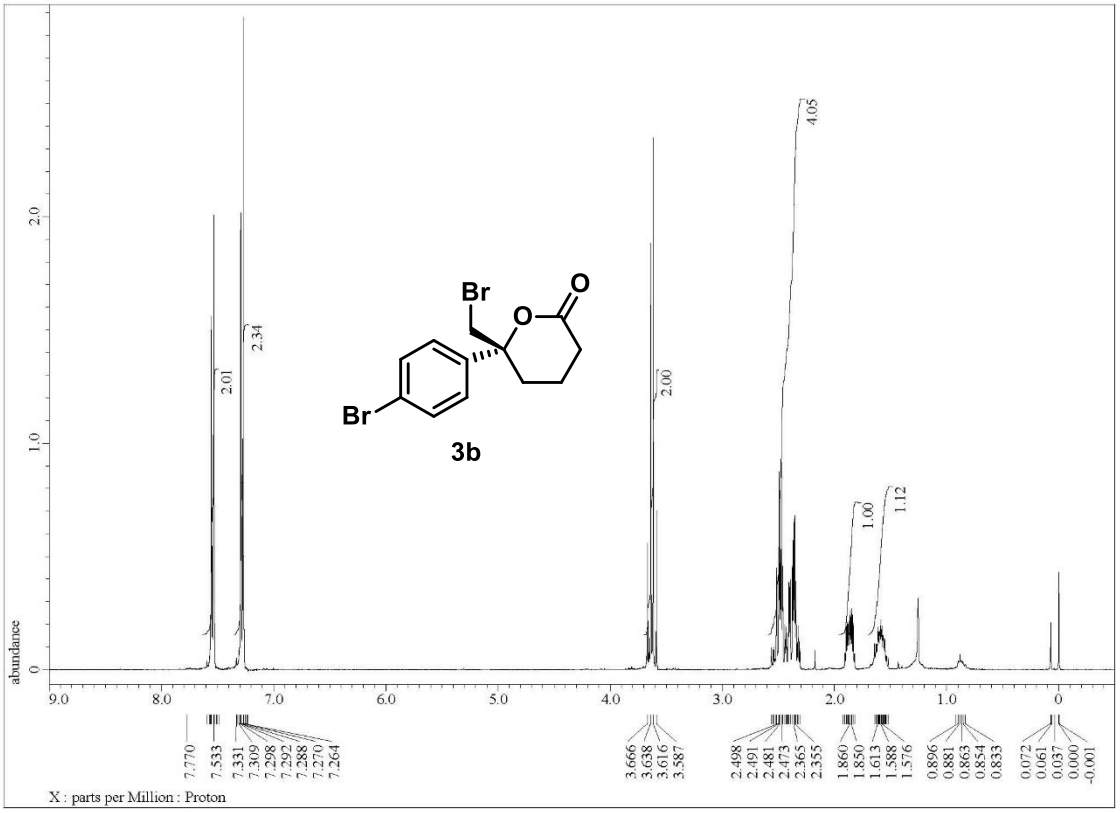

Figure S29. [1]H-NMR of **(*R*)-3b**, related to **Table S2**.

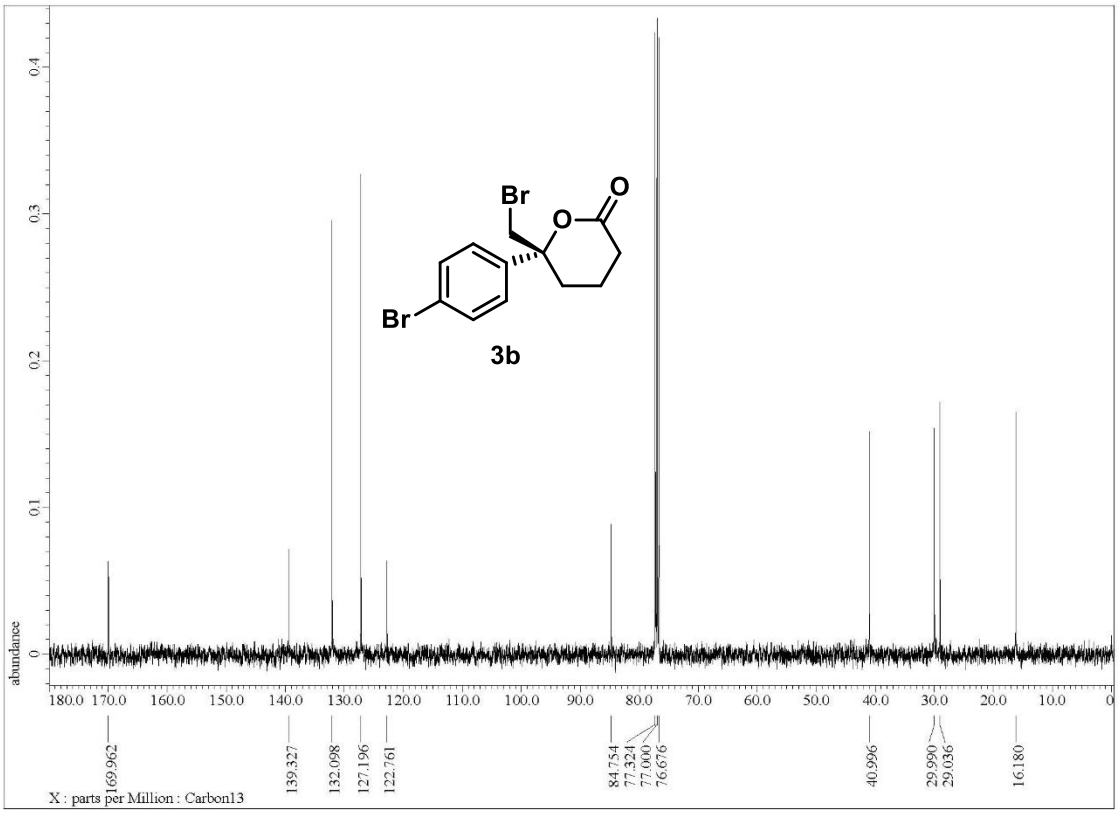

Figure S30. [13]C-NMR of **(*R*)-3b**, related to **Table S2**.

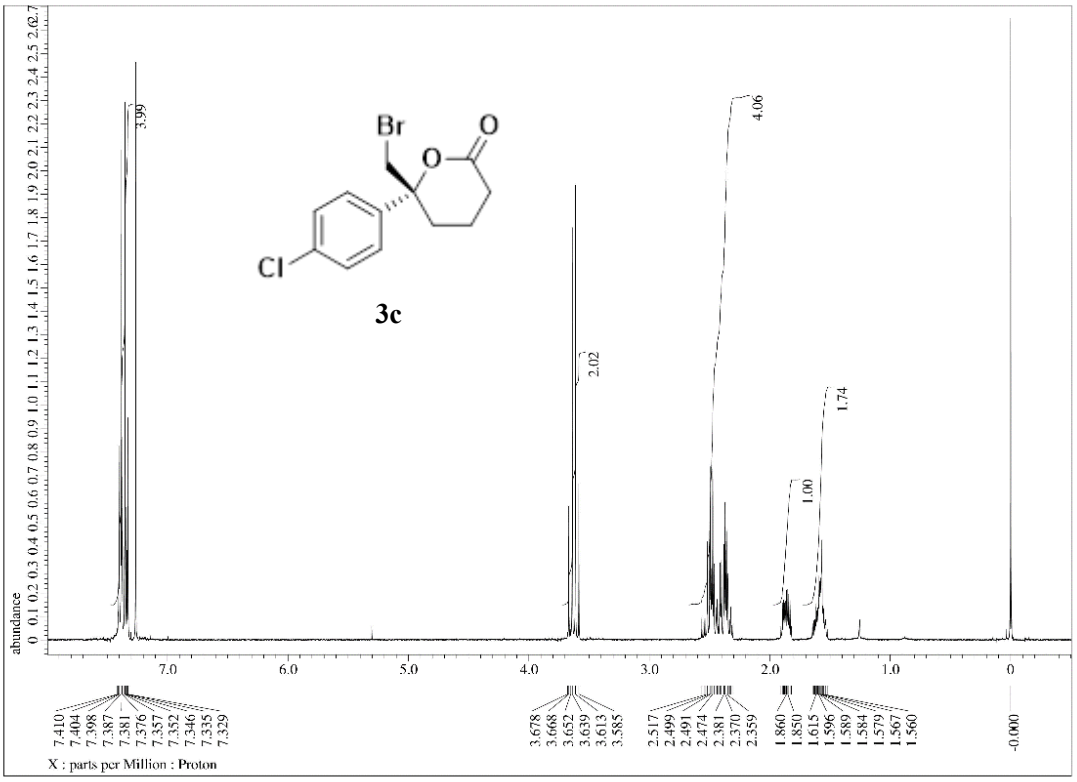

Figure S31. ^{1}H-NMR of **(*R*)-3c**, related to **Table S2**.

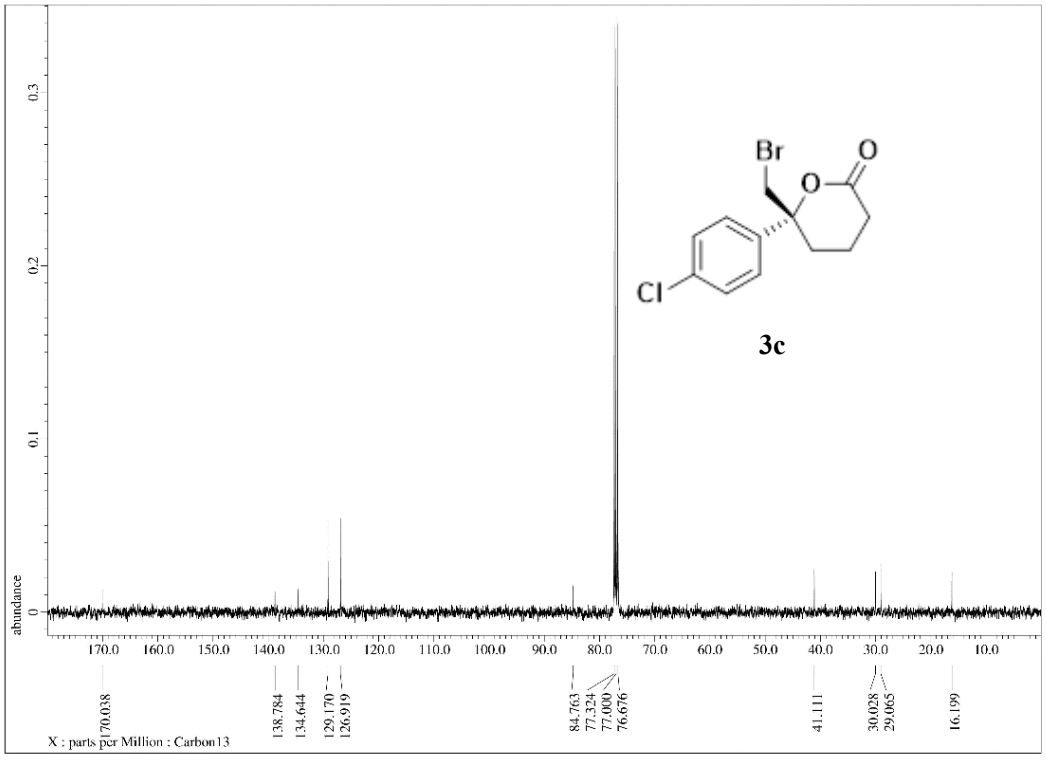

Figure S32. ^{13}C-NMR of **(*R*)-3c**, related to **Table S2**.

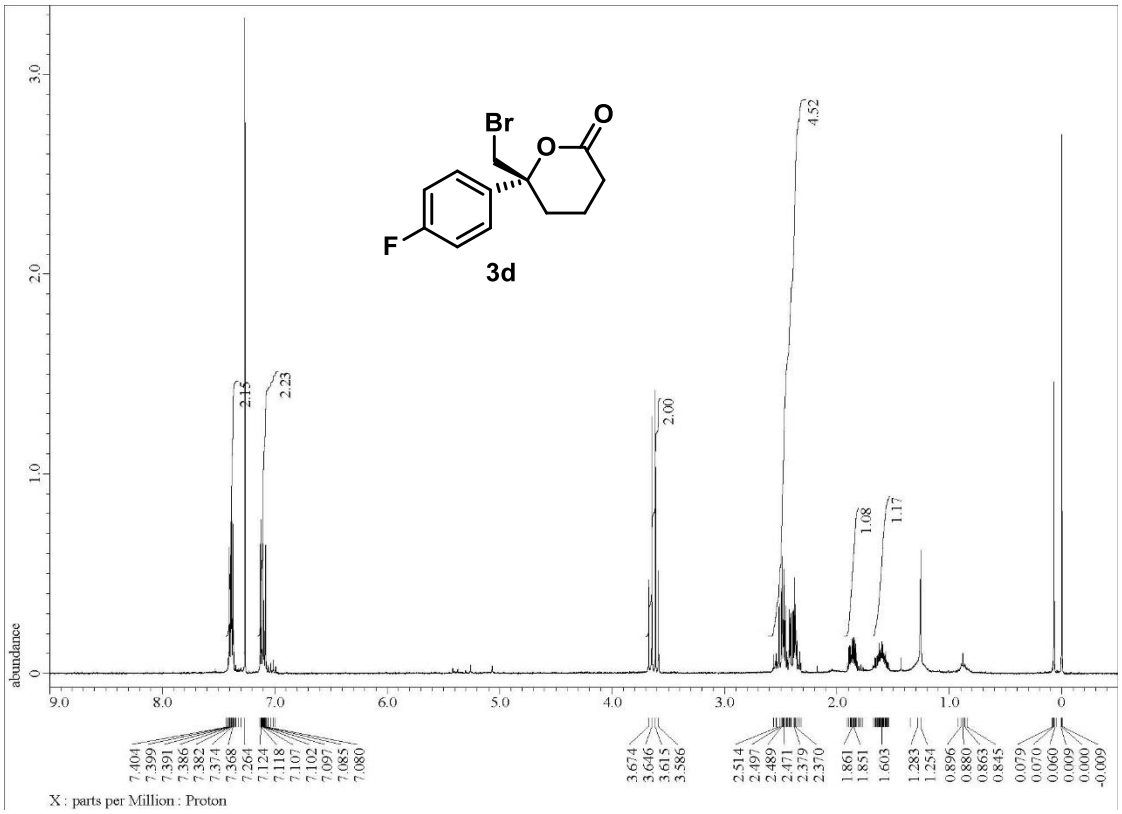

Figure S33. [1]H-NMR of **(*R*)-3d**, related to **Table S2**.

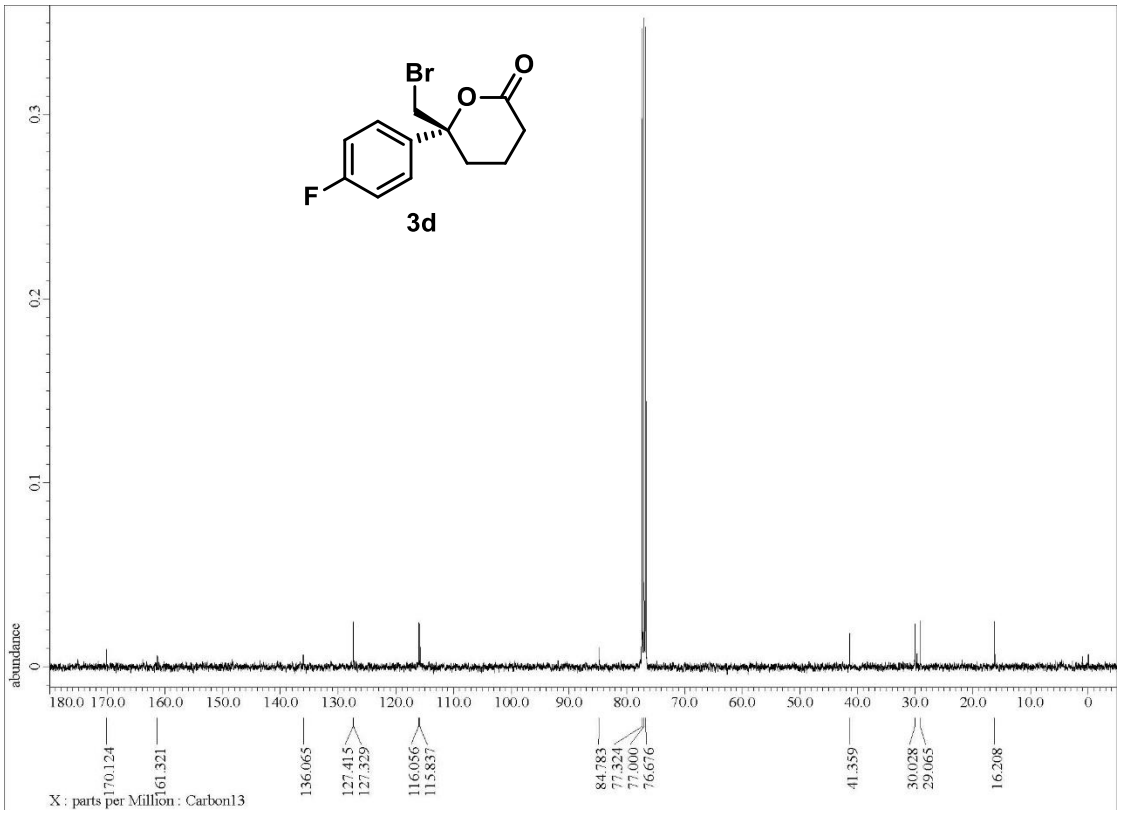

Figure S34. [13]C-NMR of **(*R*)-3d**, related to **Table S2**.

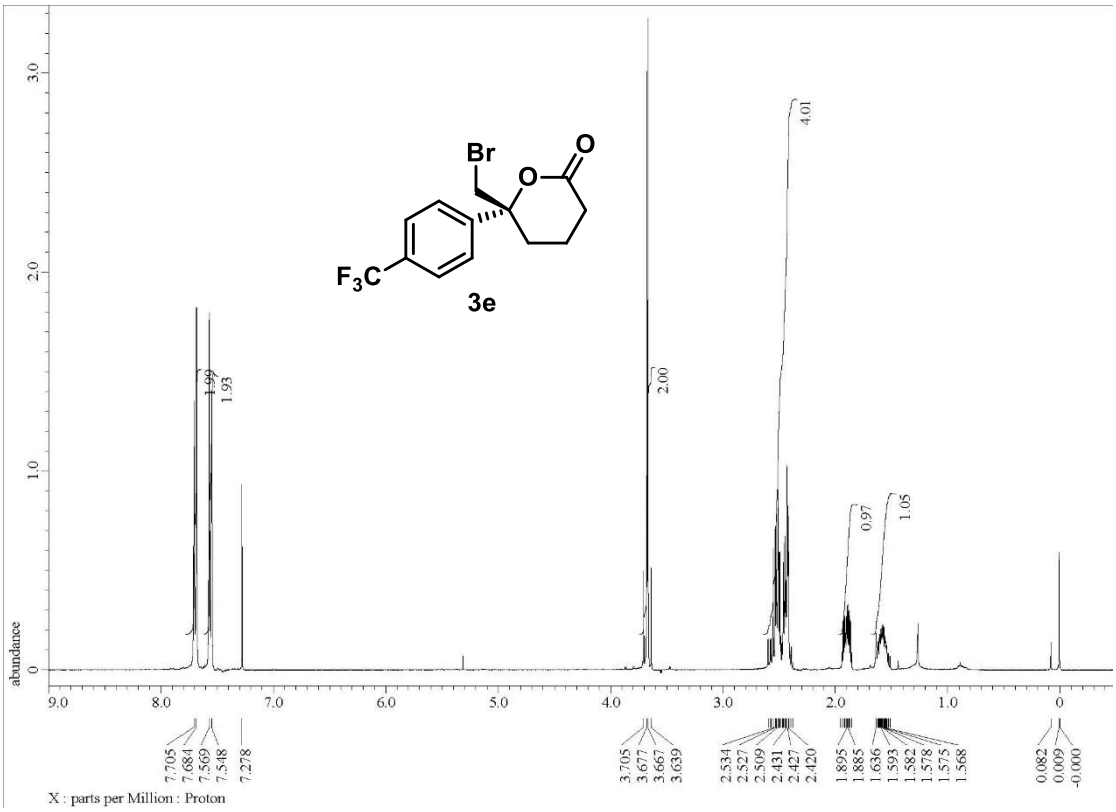

Figure S35. [1]H-NMR of **(*R*)-3e**, related to **Table S2**.

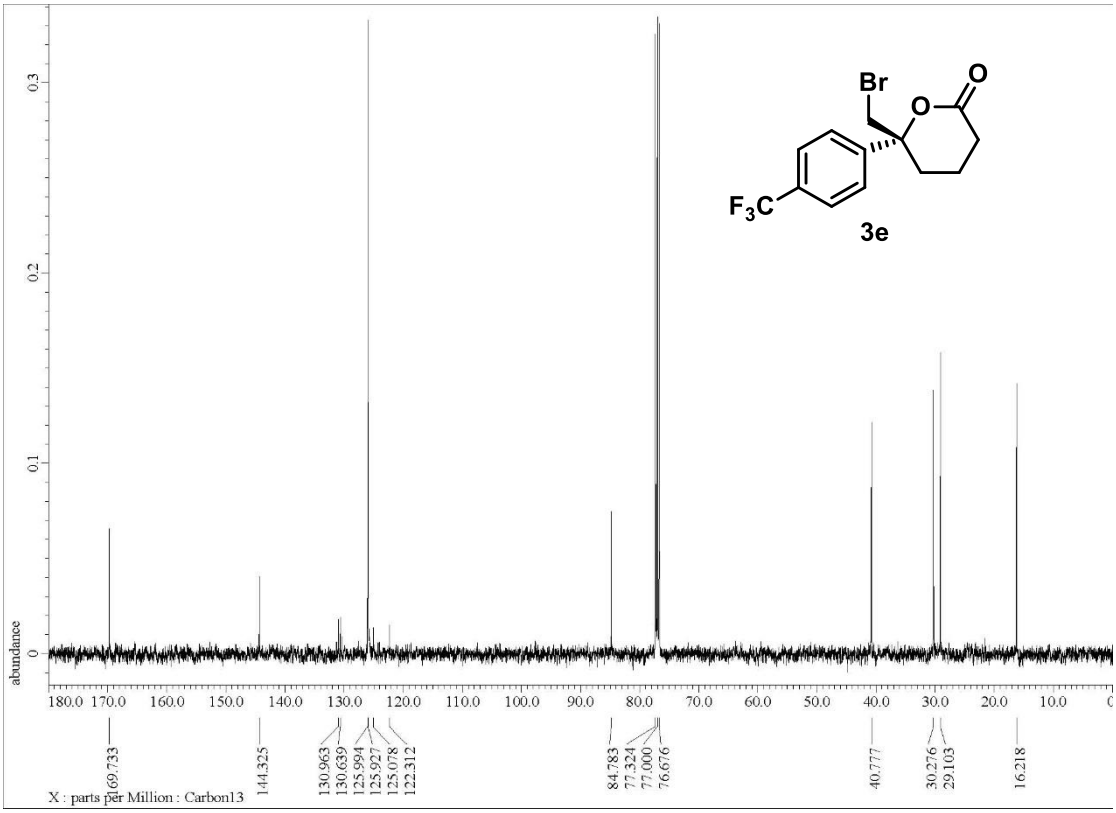

Figure S36. [13]C-NMR of **(*R*)-3e**, related to **Table S2**.

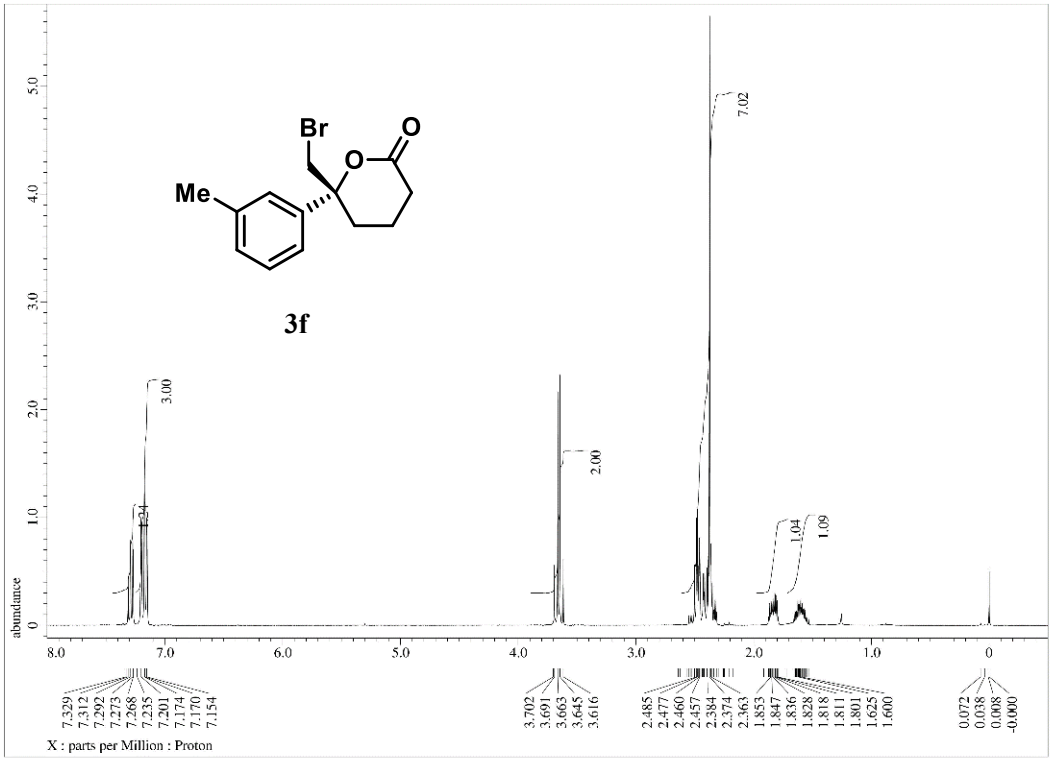

Figure S37. [1]H-NMR of **(*R*)-3f**, related to **Table S2**.

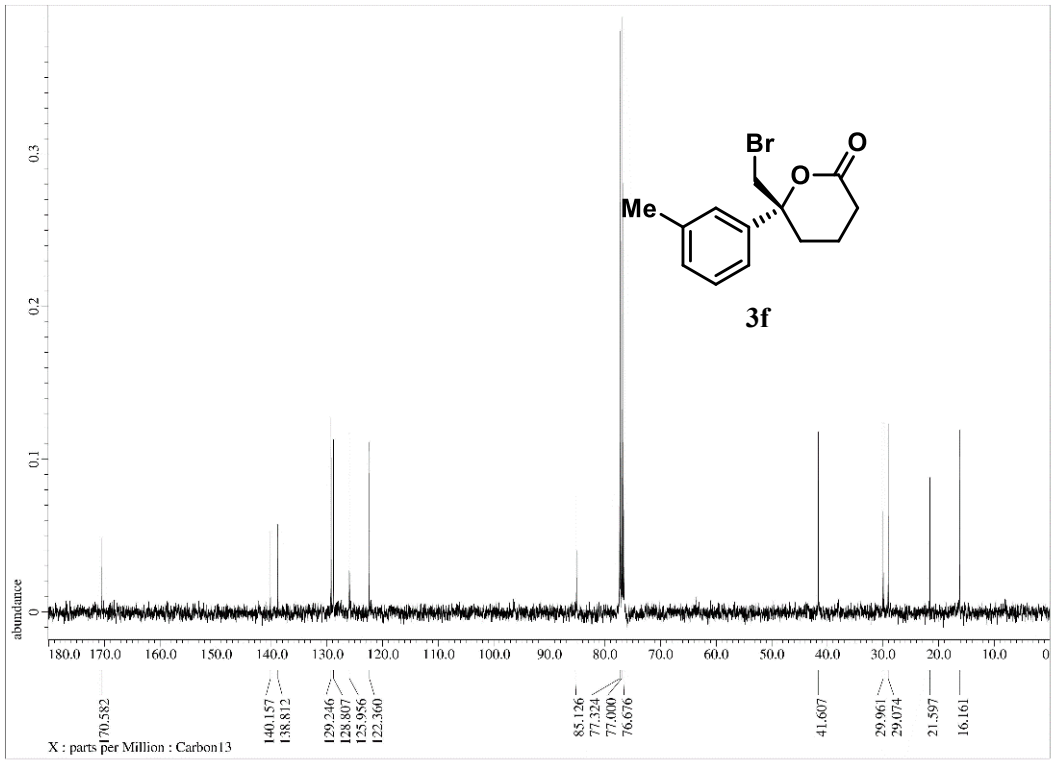

Figure S38. [13]C-NMR of **(*R*)-3**f related to **Table S2**.

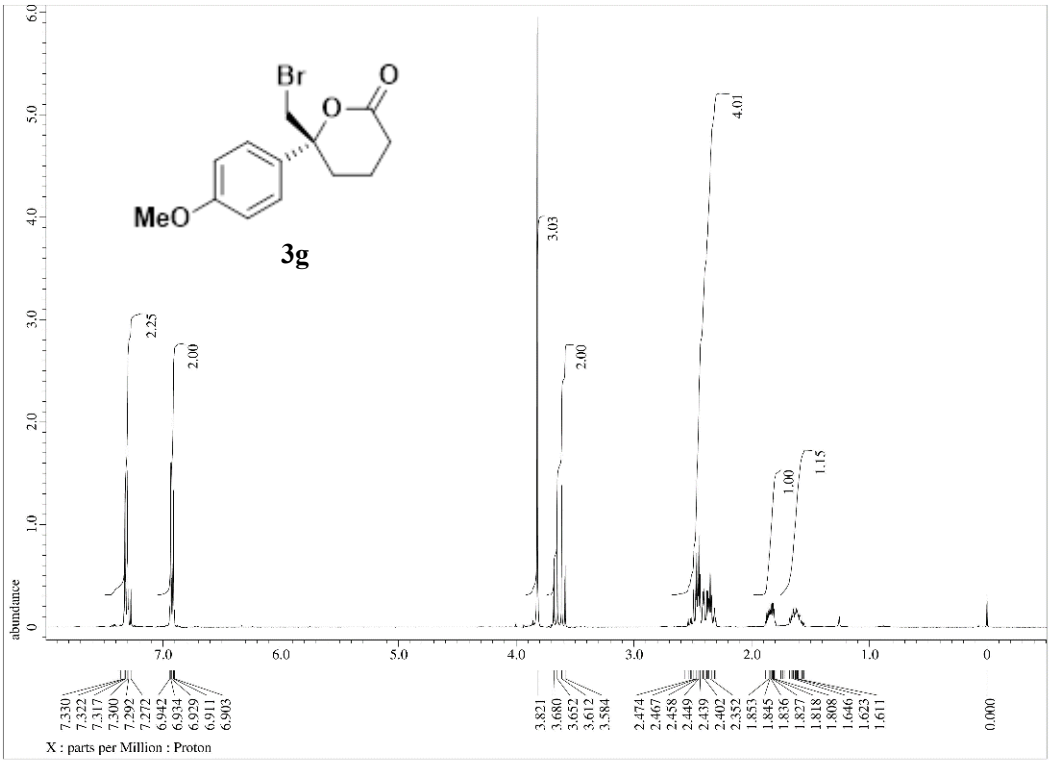

Figure S39. [1]H-NMR of **(*R*)-3g**, related to **Table S2**.

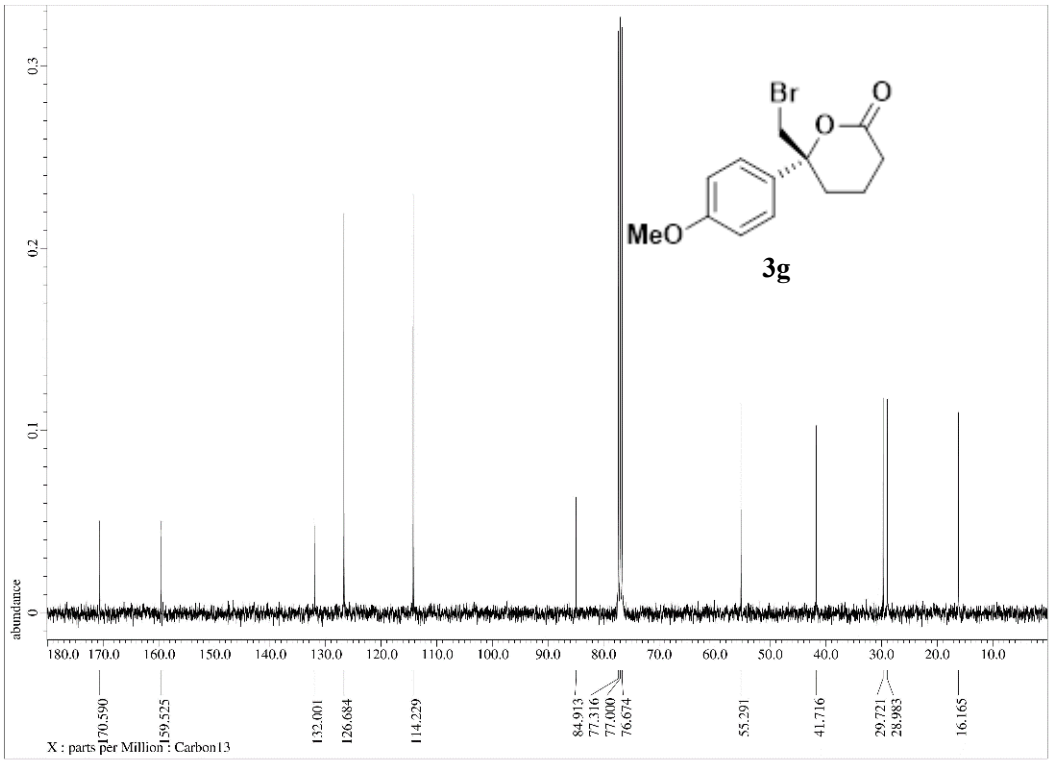

Figure S40. [13]C-NMR of **(*R*)-3g**, related to **Table S2**.

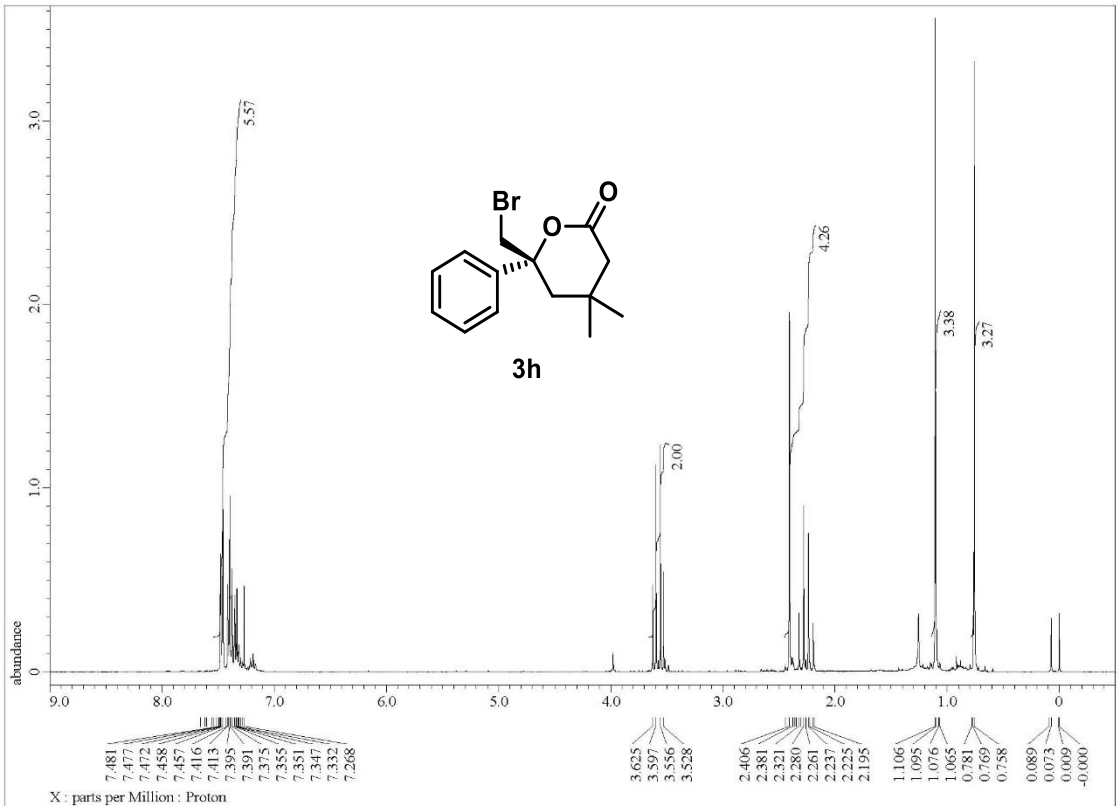

Figure S41. [1]H-NMR of **(*R*)-3h**, related to **Table S2**.

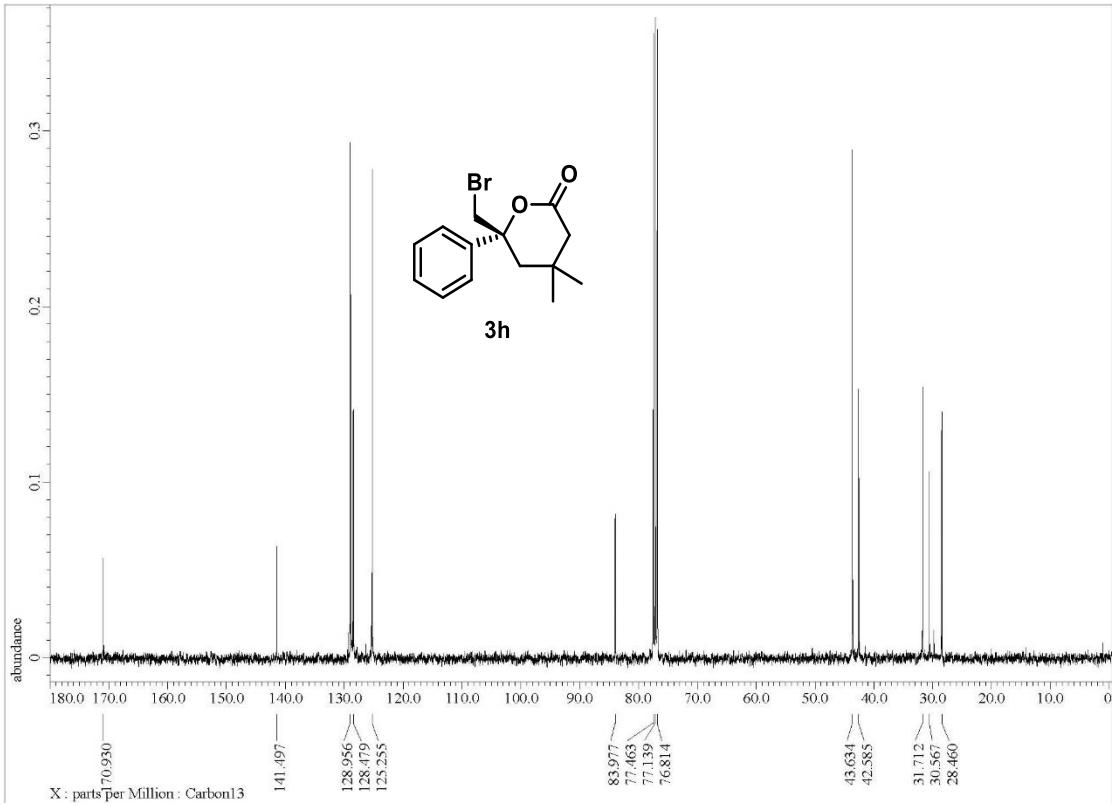

Figure S42. [13]C-NMR of **(*R*)-3h**, related to **Table S2**.

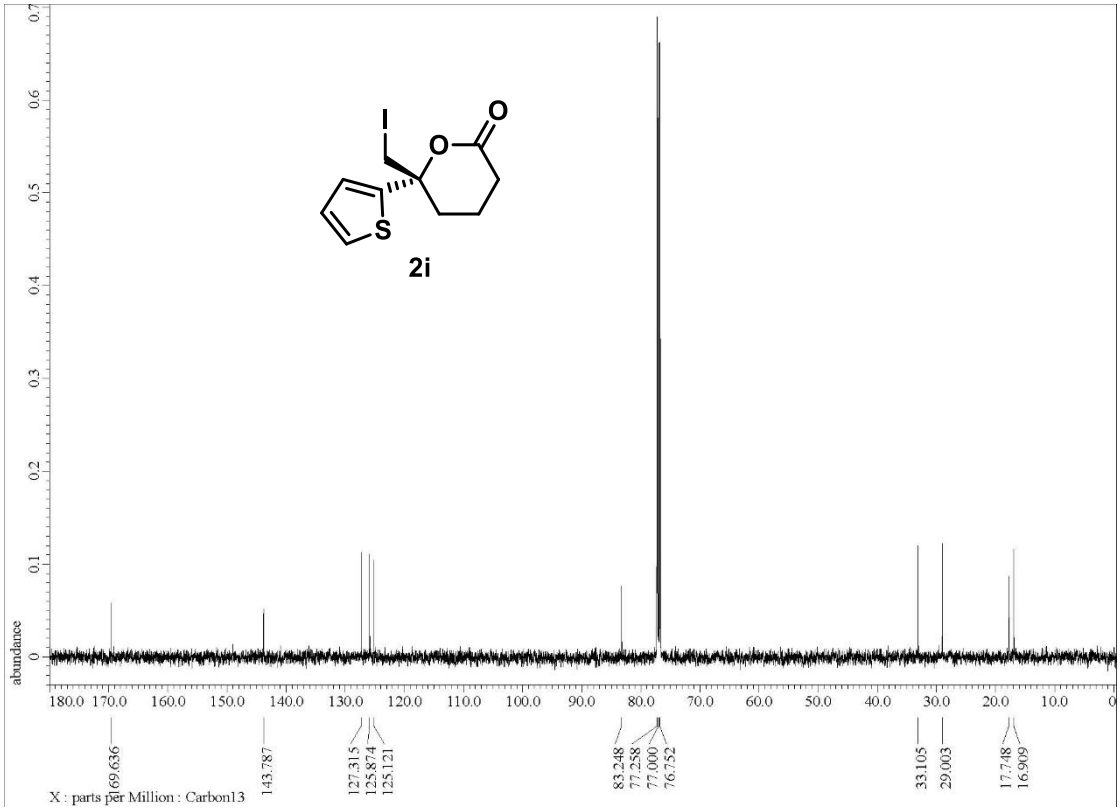

Figure S43. [1]H-NMR of **(*R*)-2i**, related to **Table S2**.

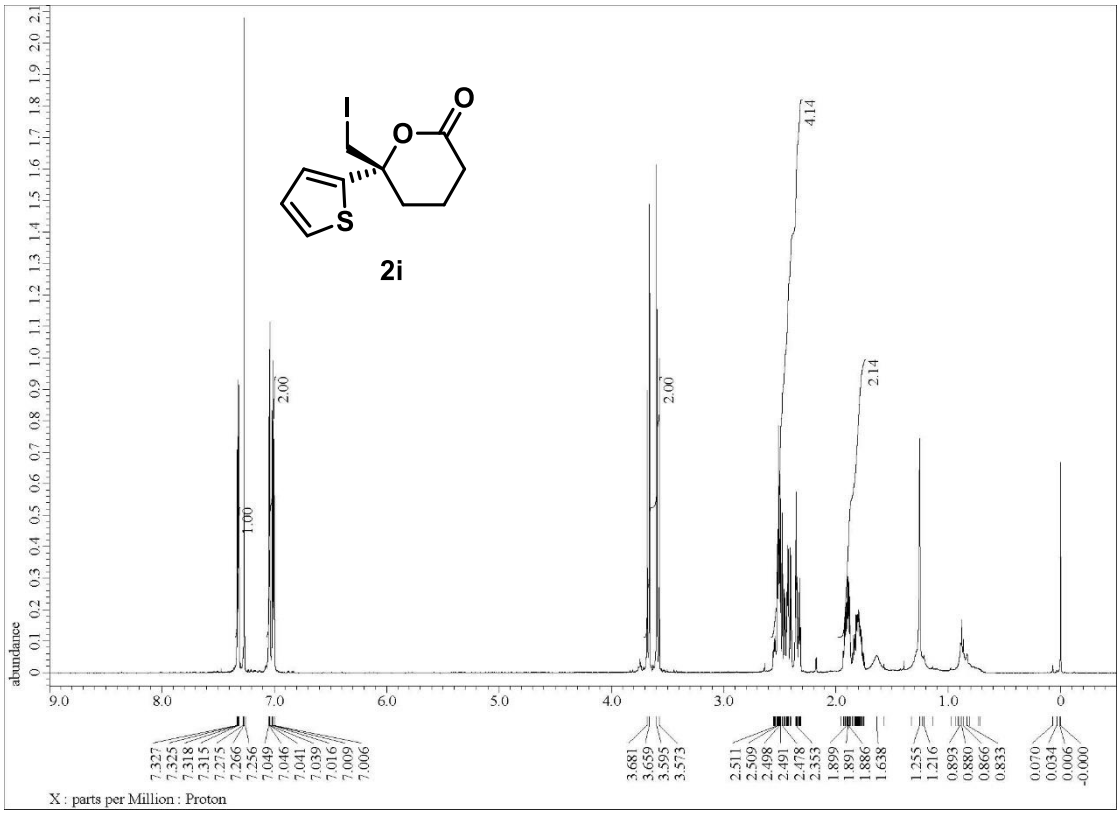

Figure S44. [13]C-NMR of **(*R*)-2i**, related to **Table S2**.

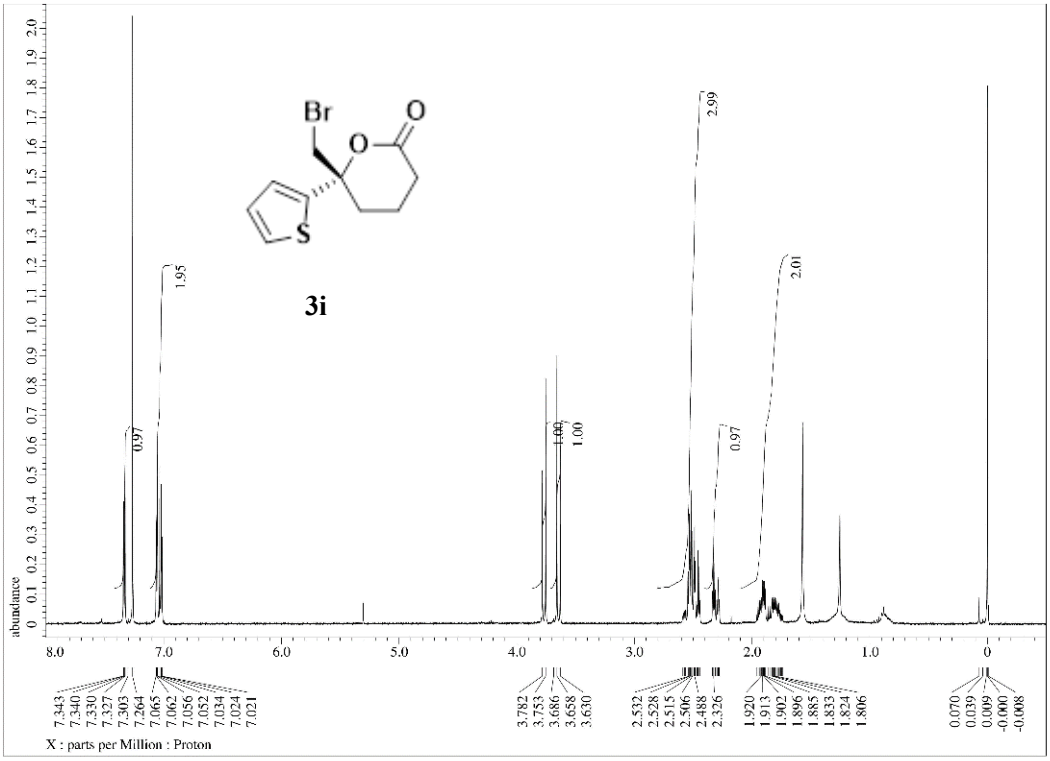

Figure S45. ^{1}H-NMR of **(*R*)-3i**, related to **Table S2**.

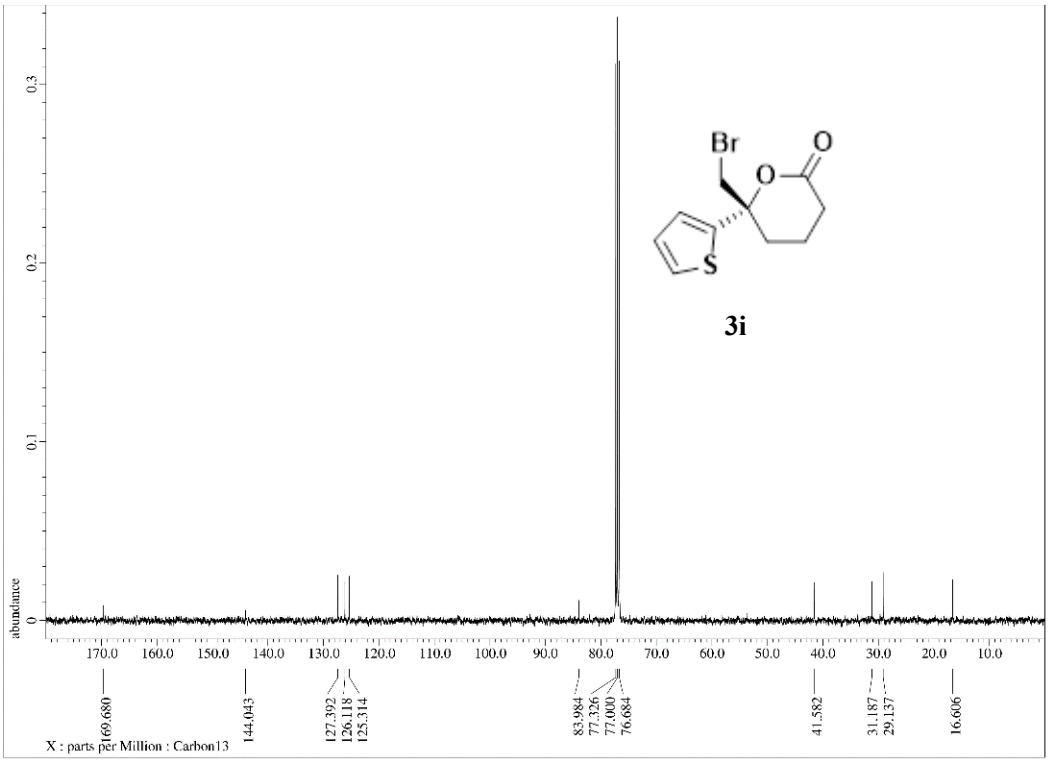

Figure S46. ^{13}C-NMR of **(*R*)-3i**, related to **Table S2**.

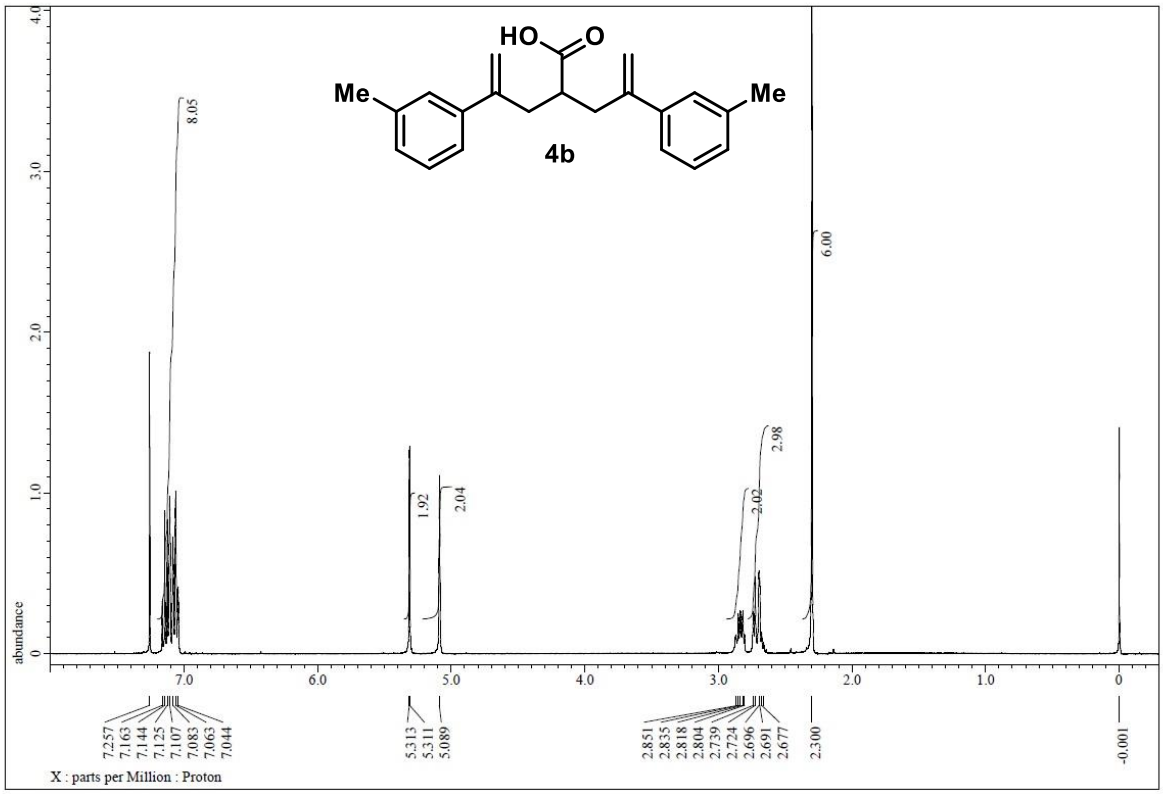

Figure S47. [1]H-NMR of **4b**, related to **Figure 5**.

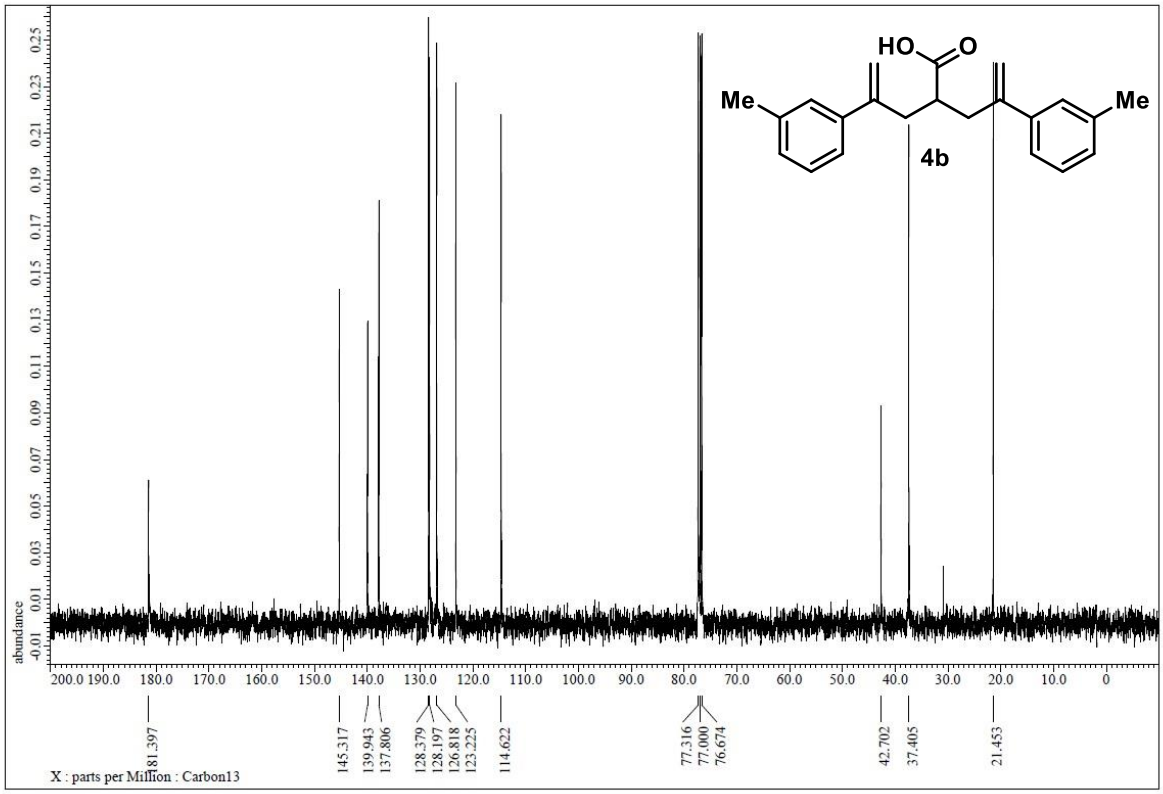

Figure S48. [13]C-NMR of **4b**, related to **Figure 5**.

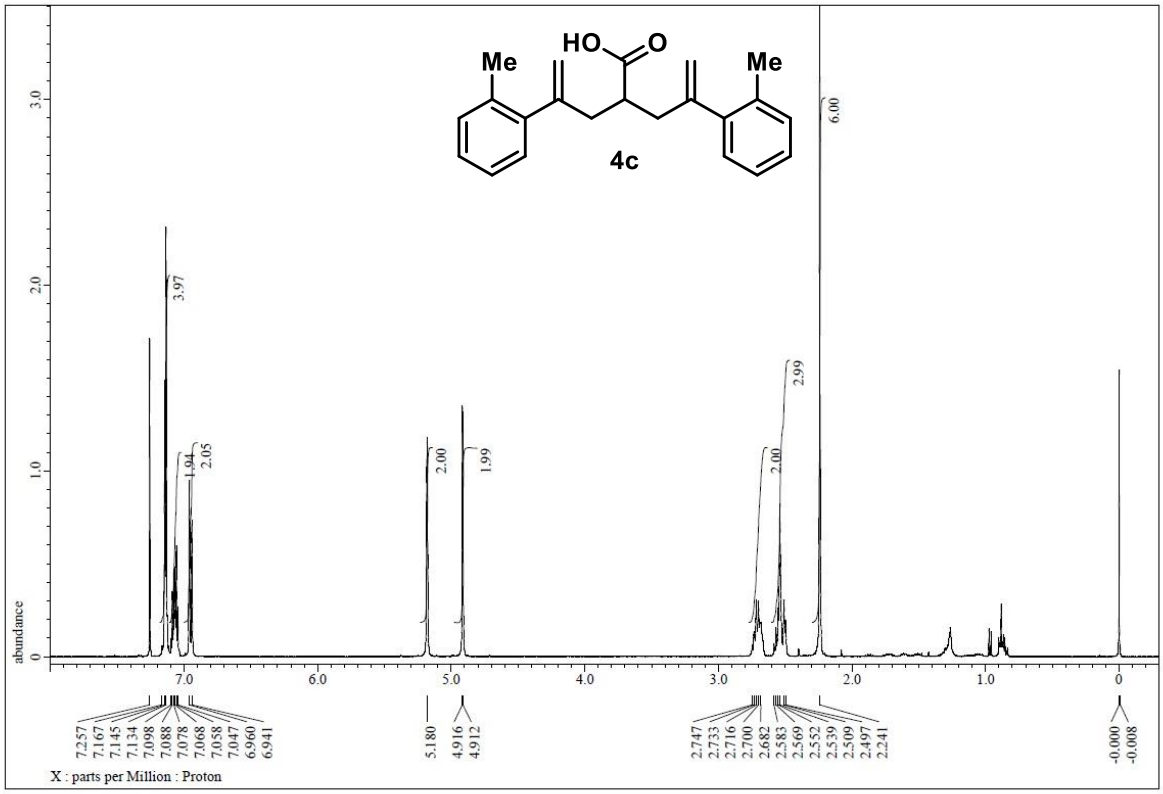

Figure S49. [1]H-NMR of **4c**, related to **Figure 5**.

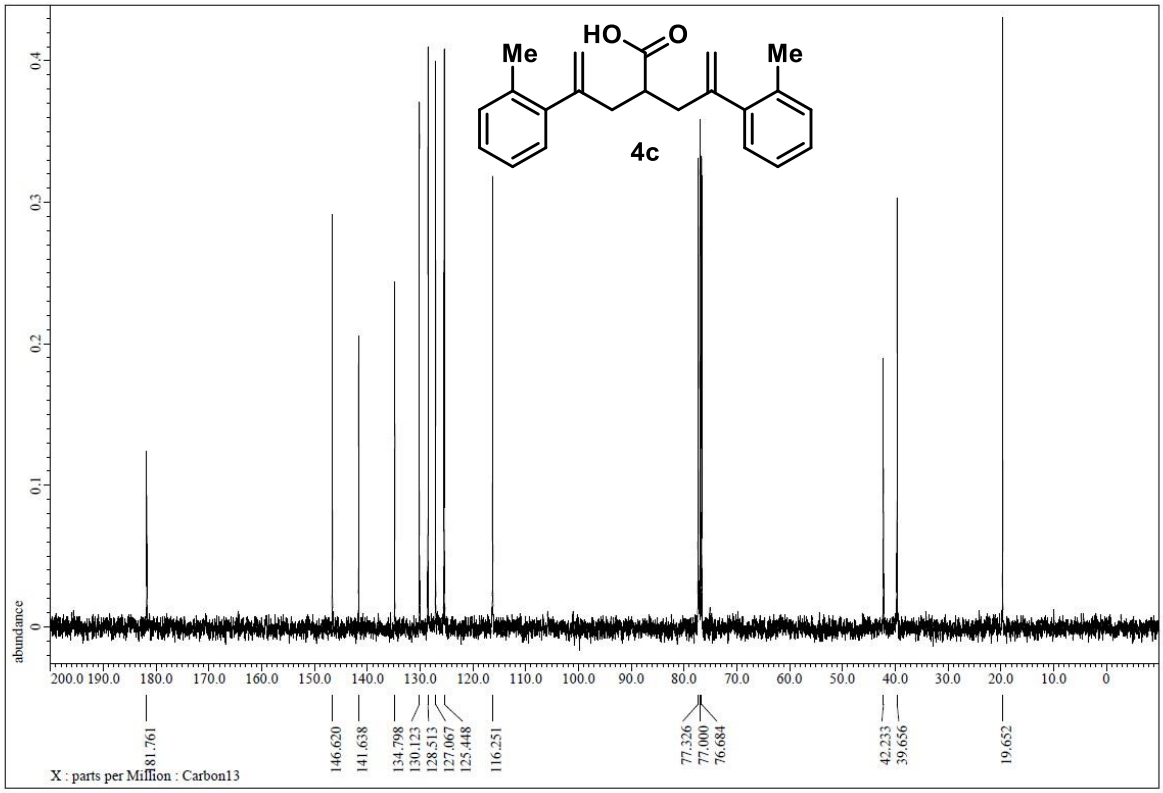

Figure S50. [13]C-NMR of **4c**, related to **Figure 5**.

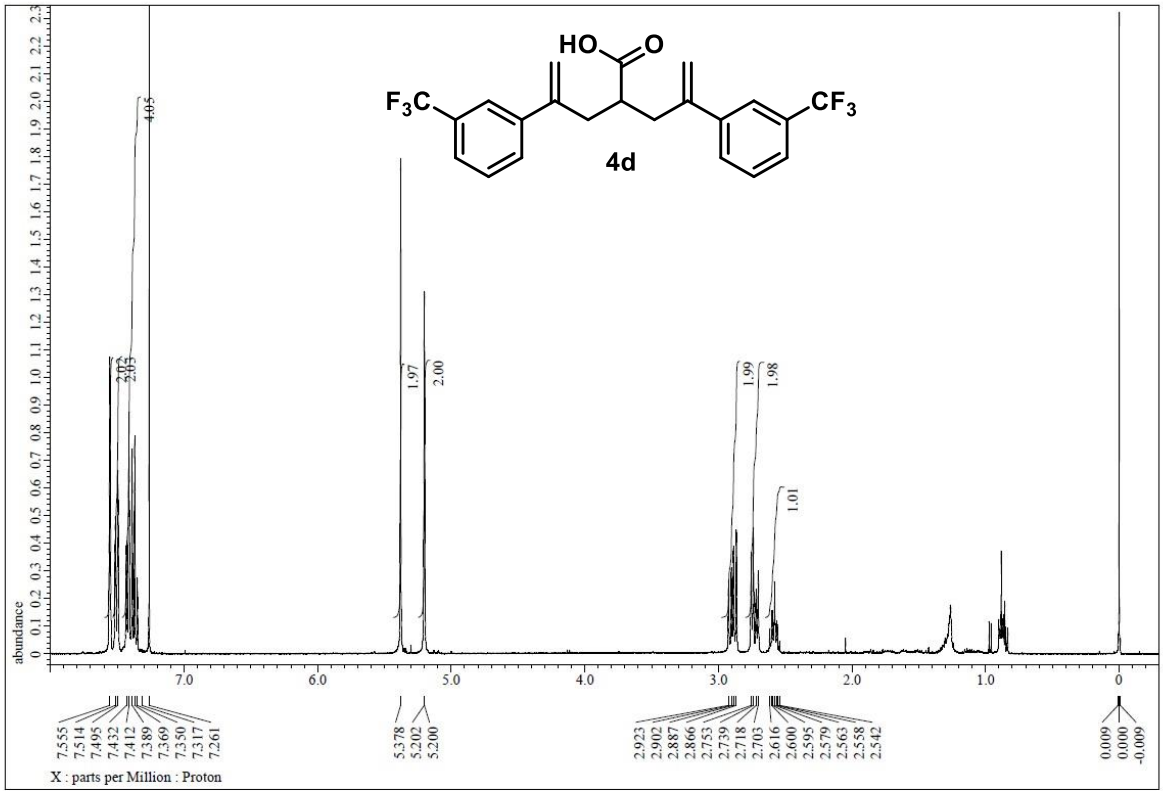

Figure S51. ^{1}H-NMR of **4d**, related to **Figure 5**.

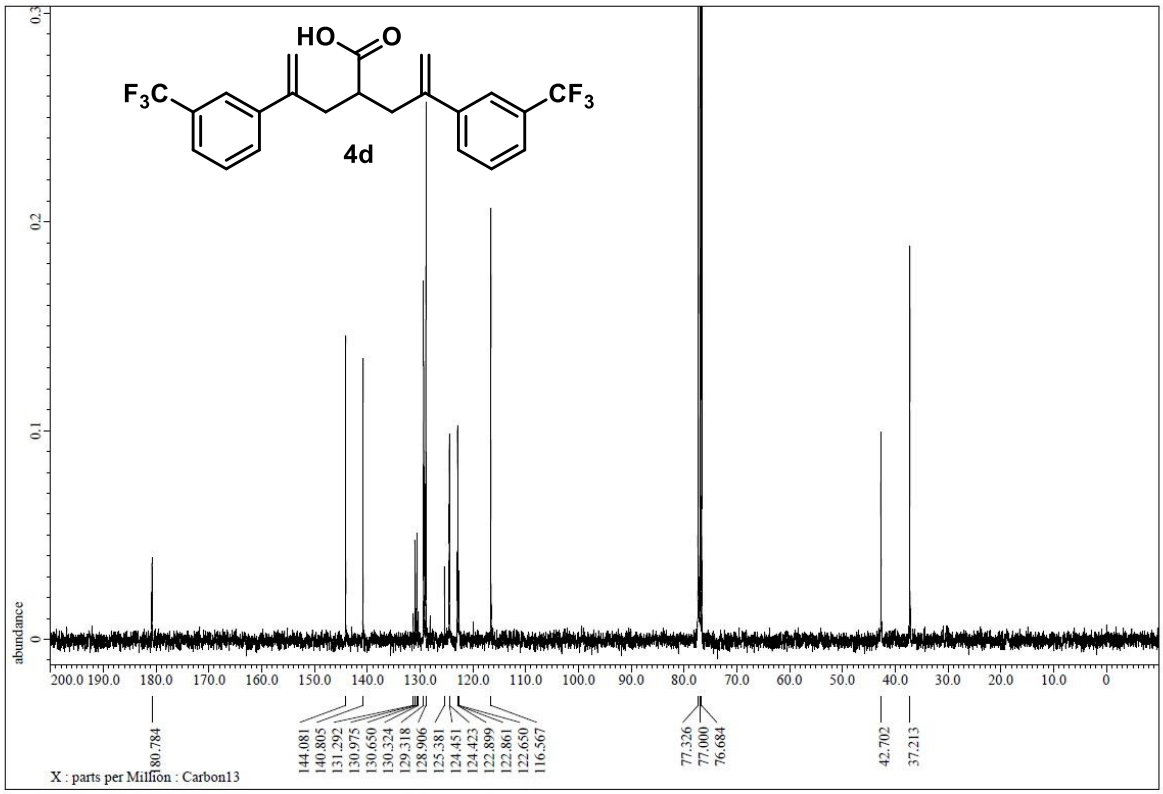

Figure S52. ^{13}C-NMR of **4d**, related to **Figure 5**.

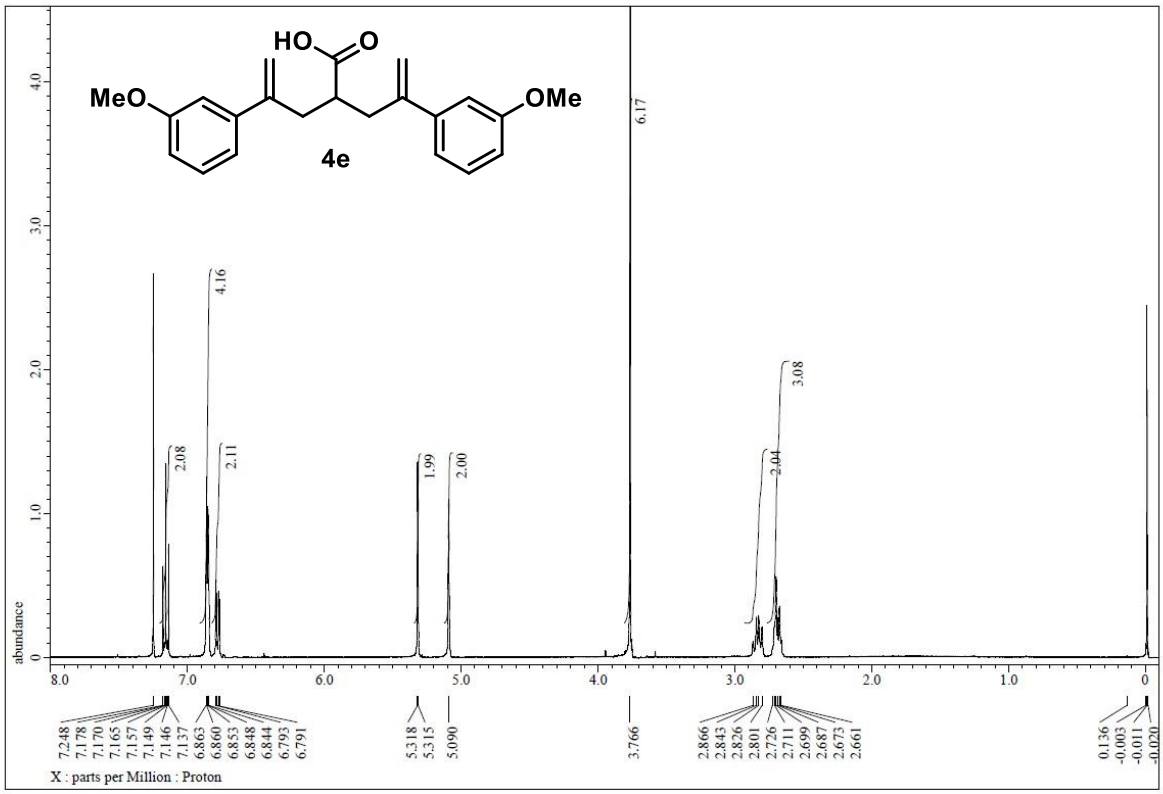

Figure S53. [1]H-NMR of **4e**, related to **Figure 5**.

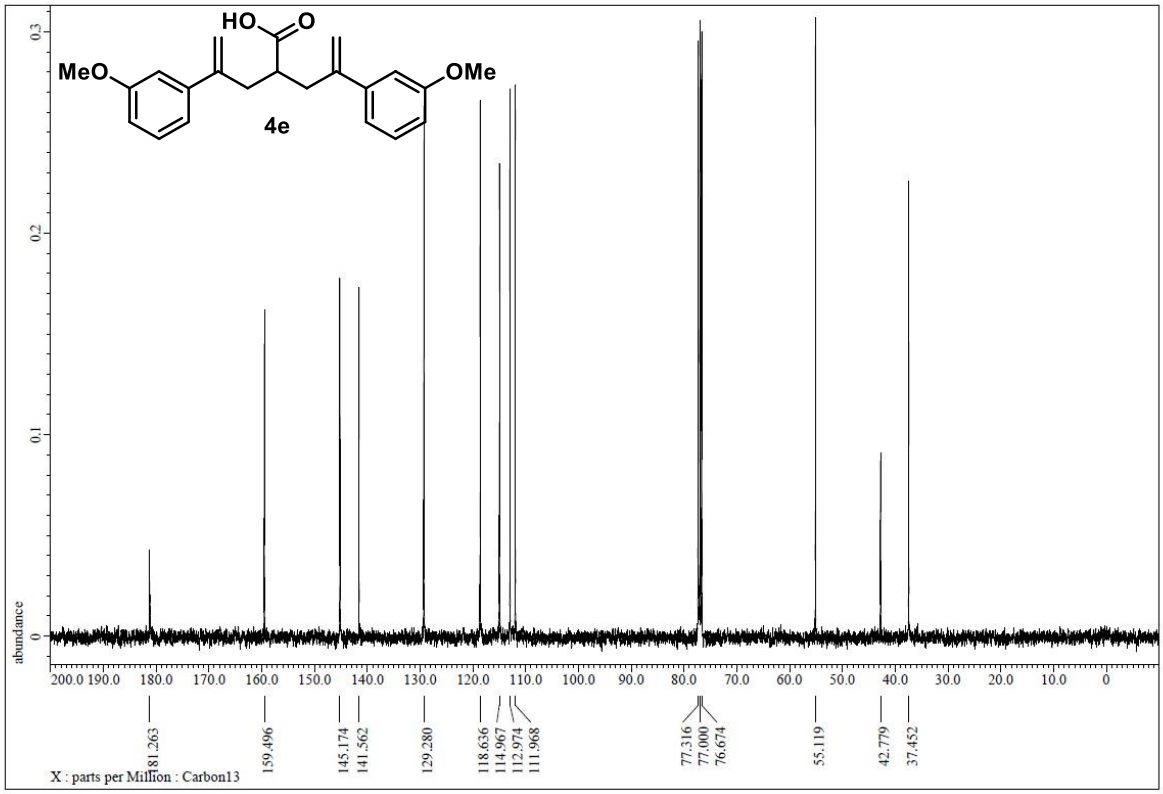

Figure S54. [13]C-NMR of **4e**, related to **Figure 5**.

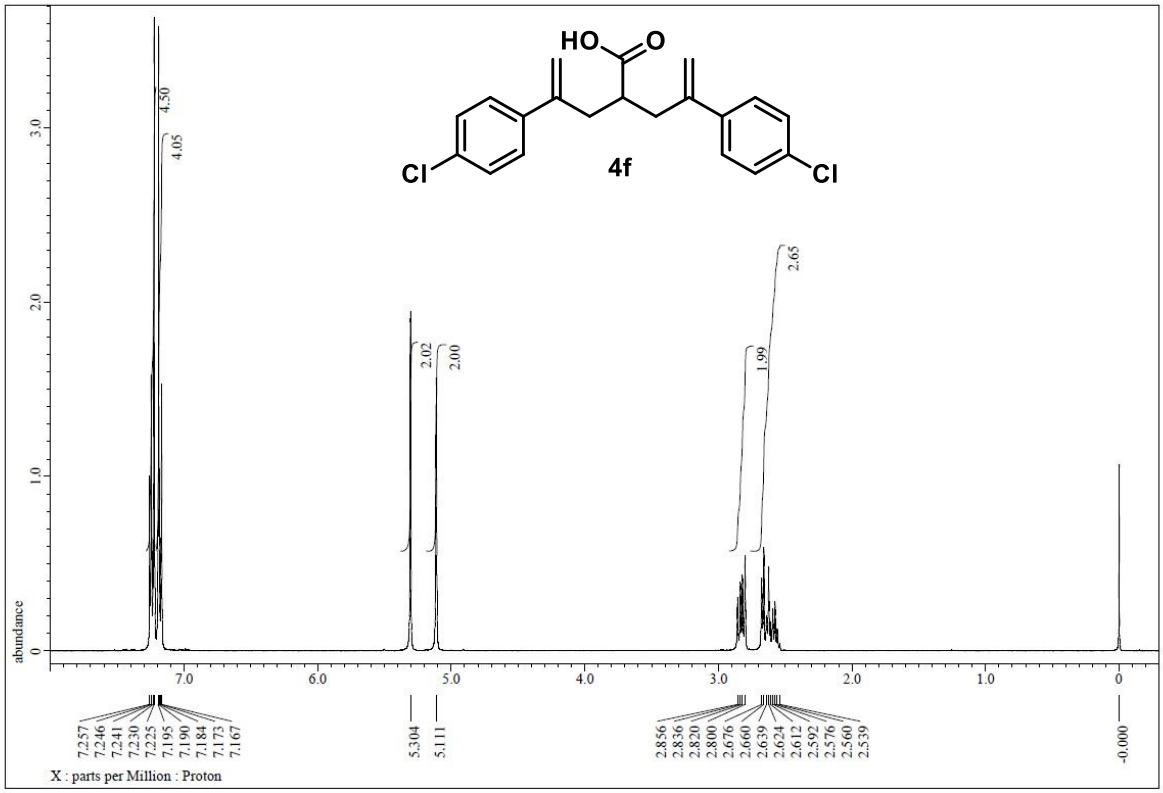

Figure S55. [1]H-NMR of **4f**, related to **Figure 5**.

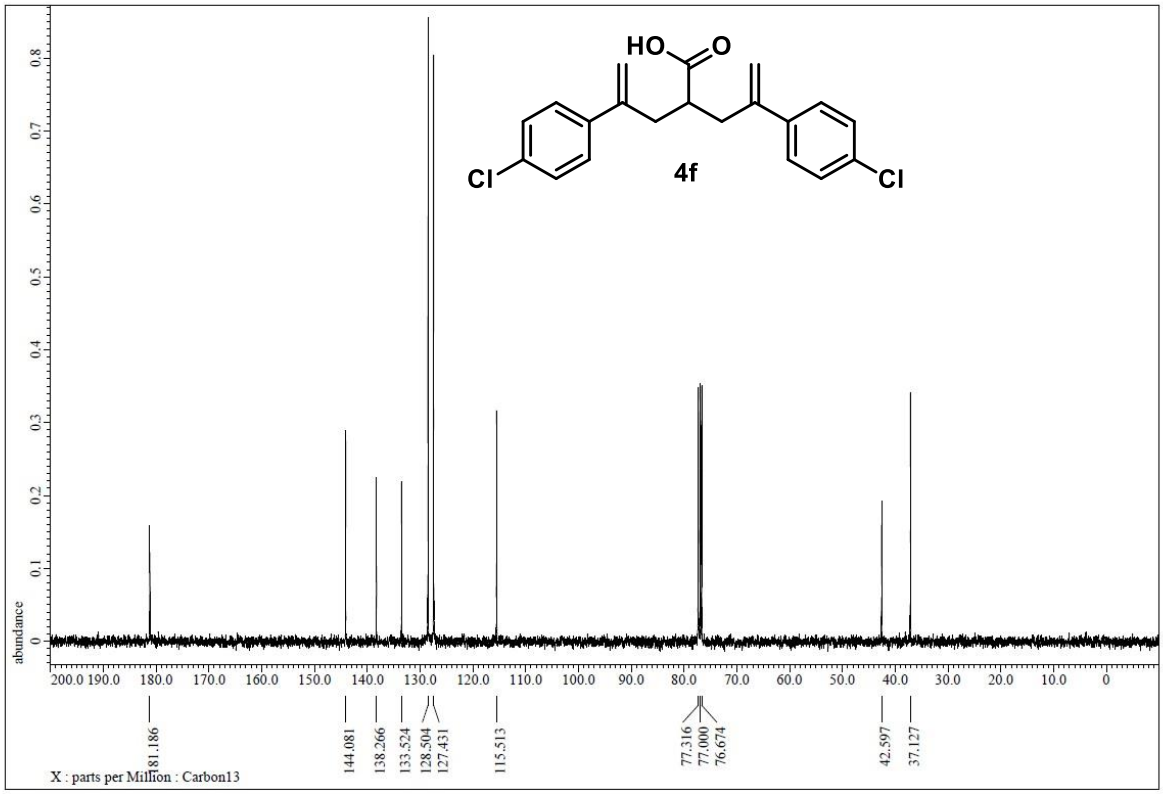

Figure S56. [13]C-NMR of **4f**, related to **Figure 5**.

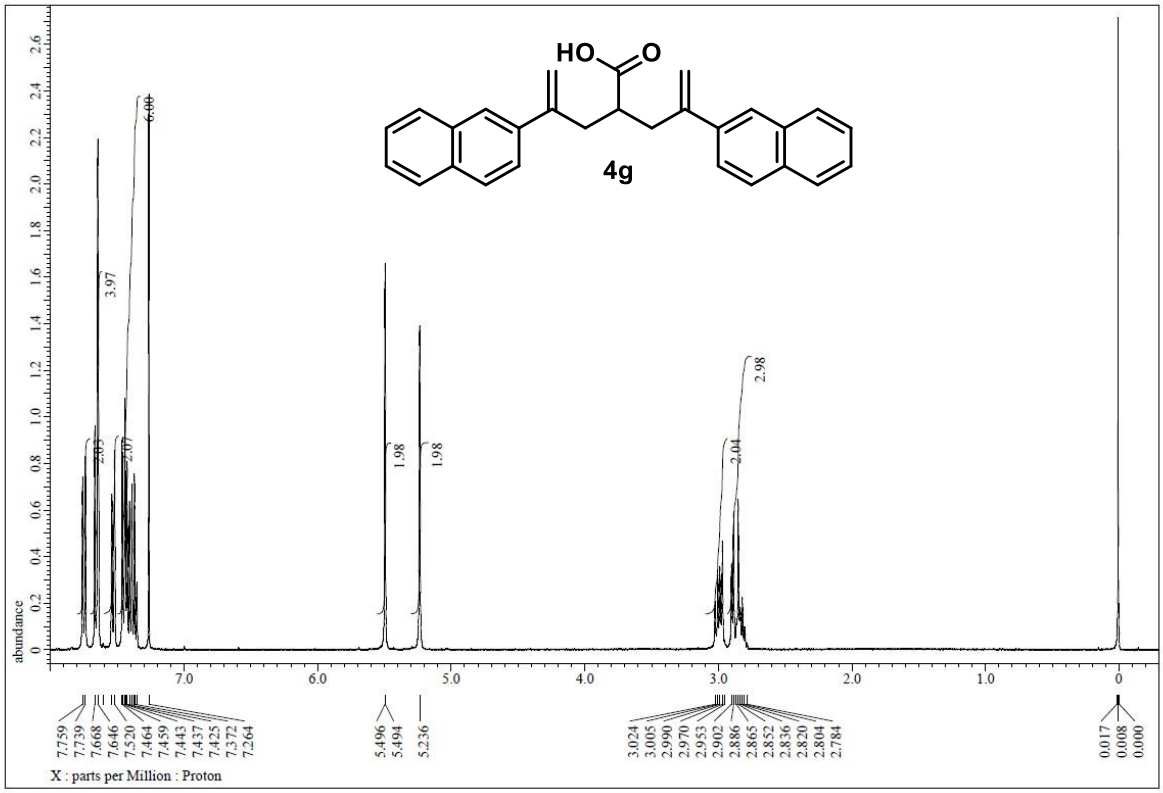

Figure S57. [1]H-NMR of **4g**, related to **Figure 5**.

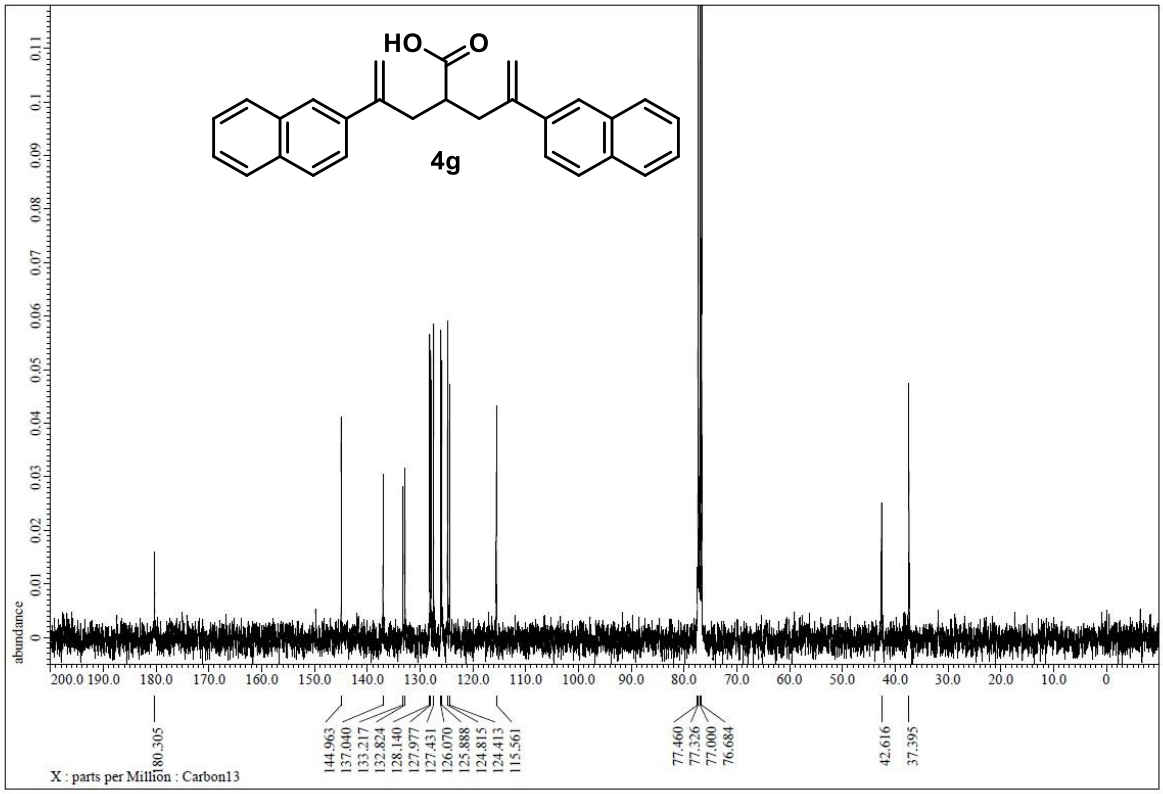

Figure S58. [13]C-NMR of **4g**, related to **Figure 5**.

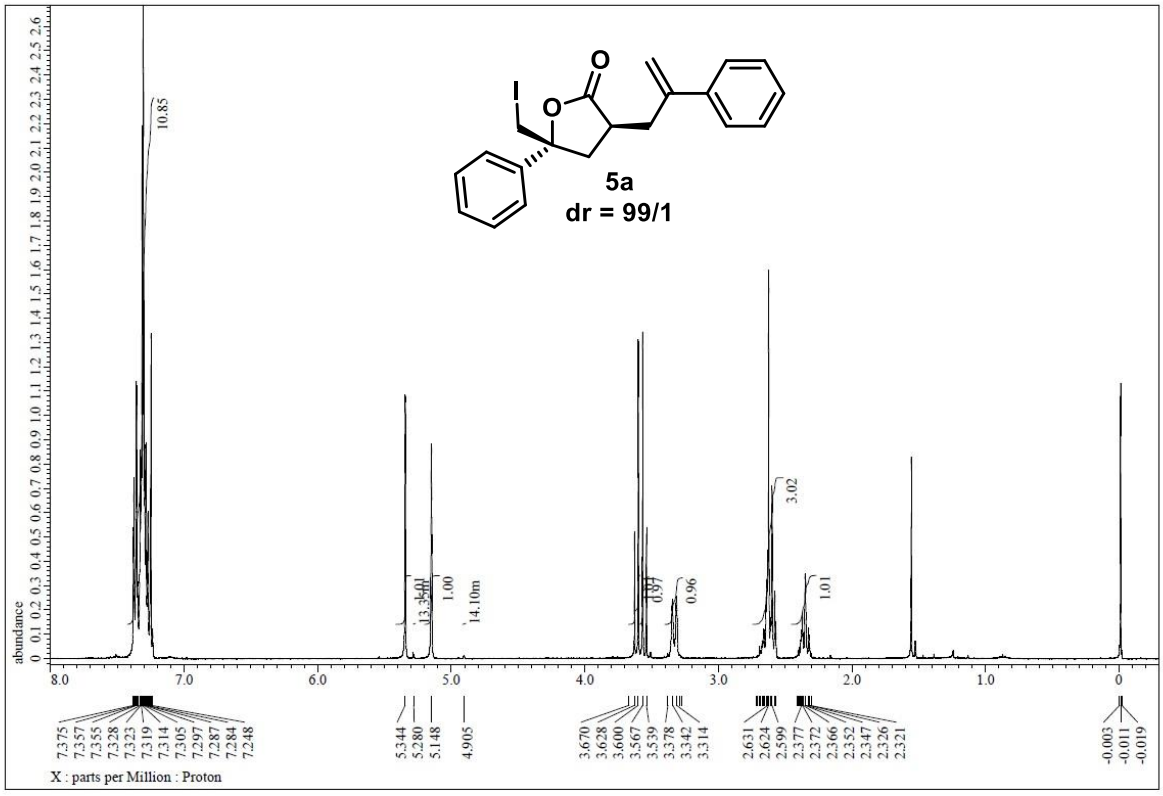

Figure S59. ^{1}H-NMR of **(3*S*,5*R*)-5a**, related to **Figure 5**.

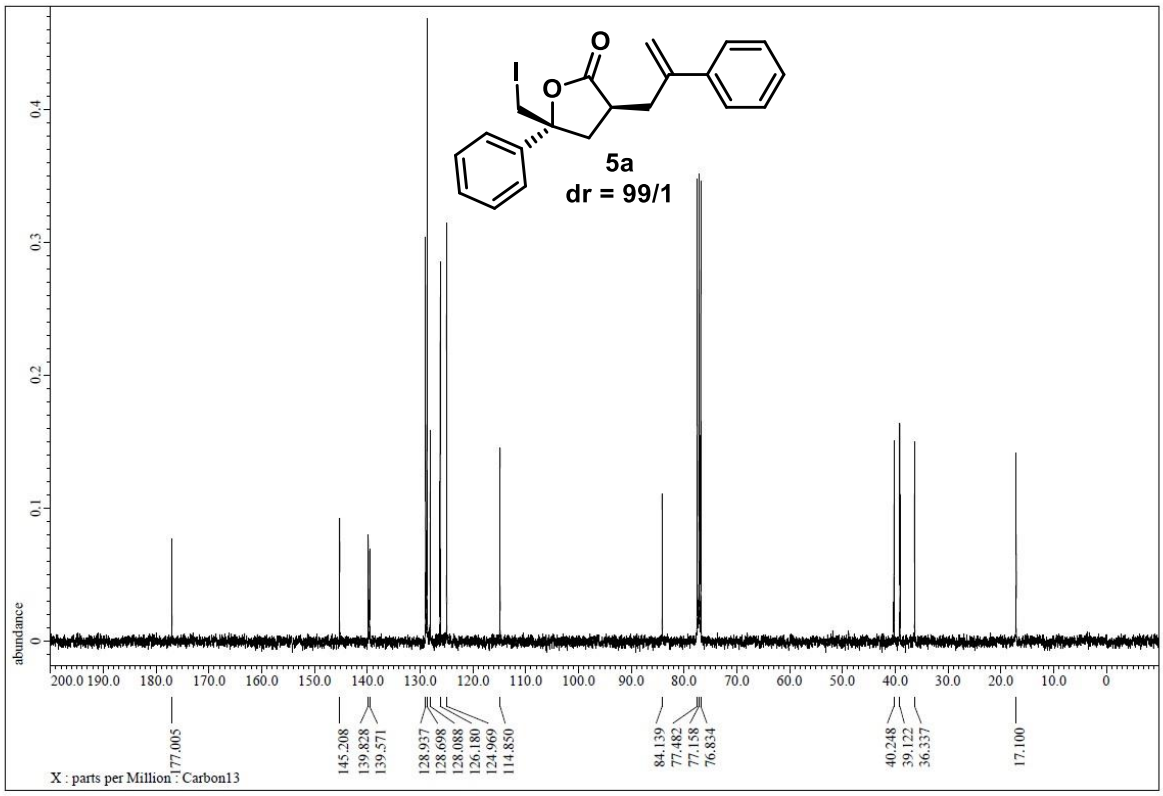

Figure S60. ^{13}C-NMR of **(3*S*,5*R*)-5a**, related to **Figure 5**.

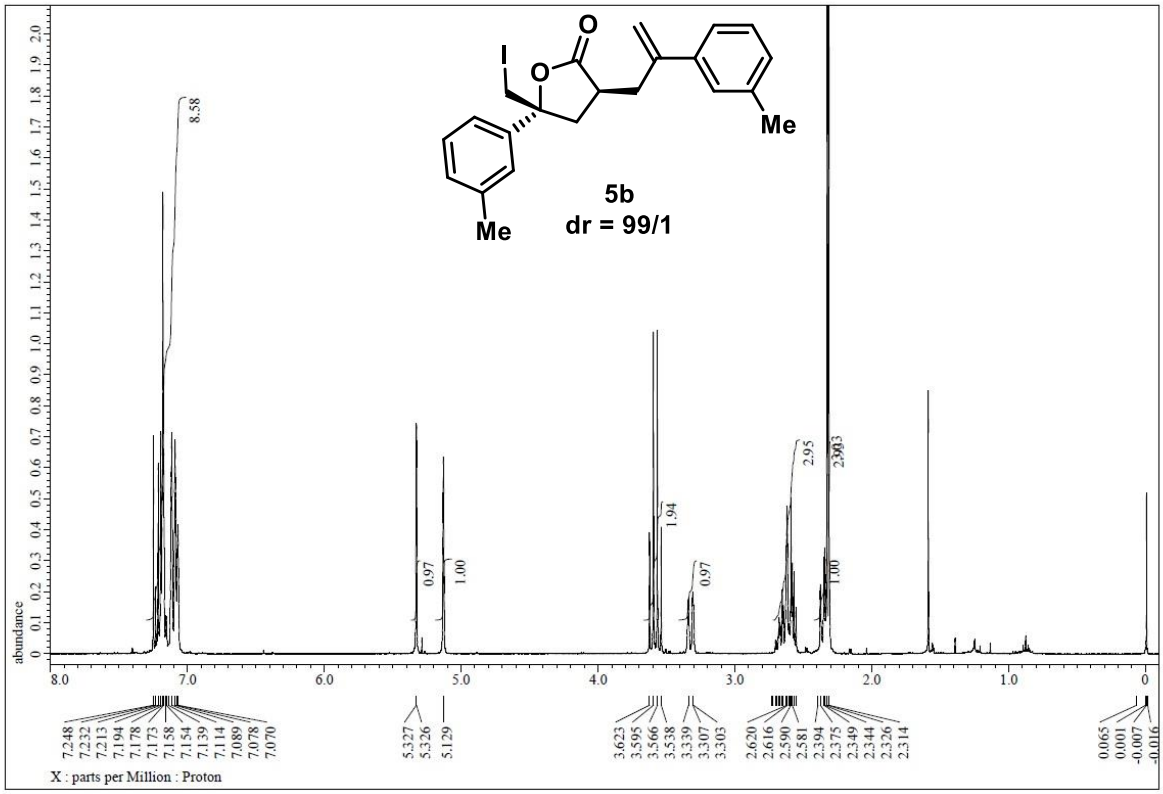

Figure S61. [1]H-NMR of **(3*S*,5*R*)-5b**, related to **Figure 5**.

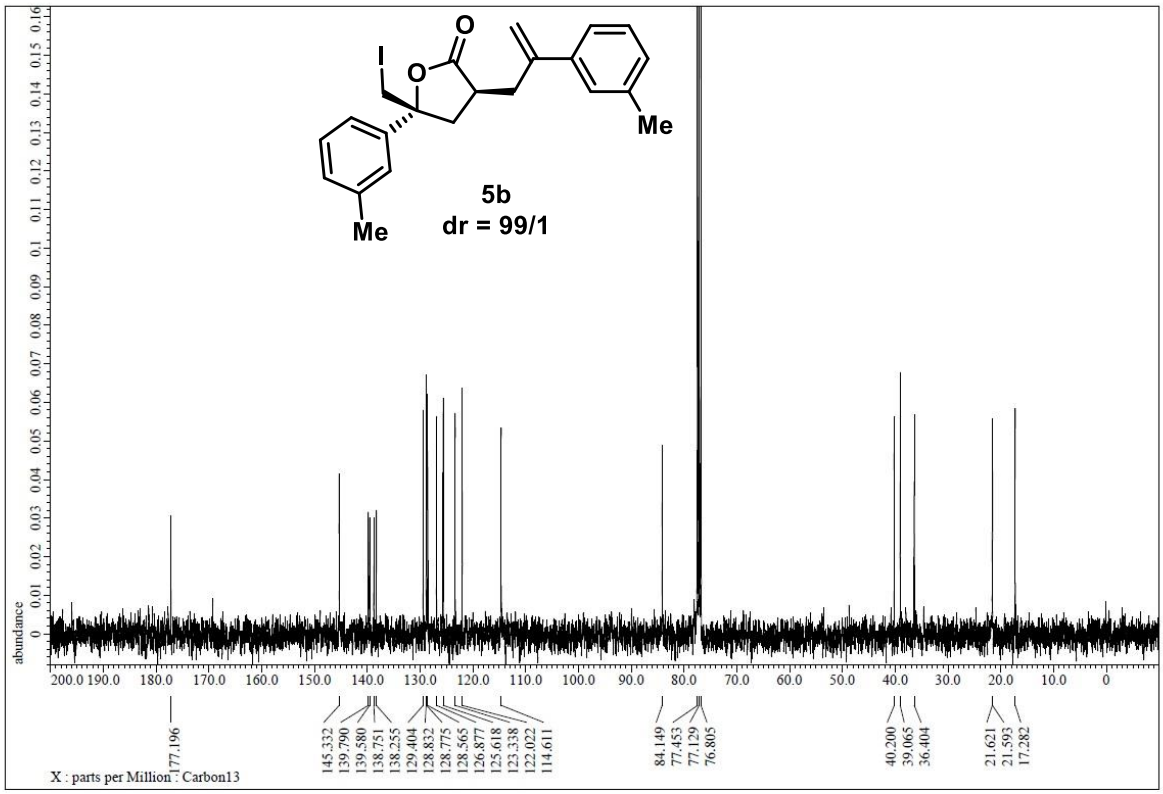

Figure S62. [13]C-NMR of **(3*S*,5*R*)-5b**, related to **Figure 5**.

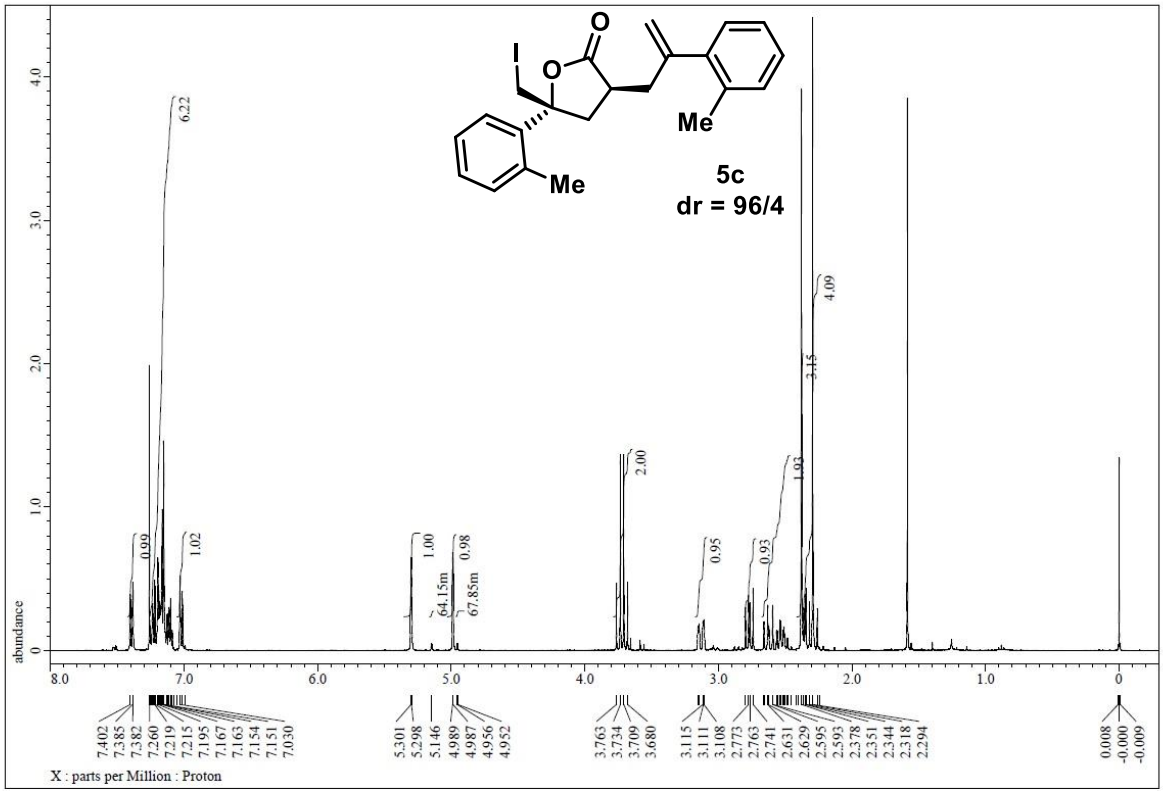

Figure S63. ^{1}H-NMR of **(3*S*,5*R*)-5c**, related to **Figure 5**.

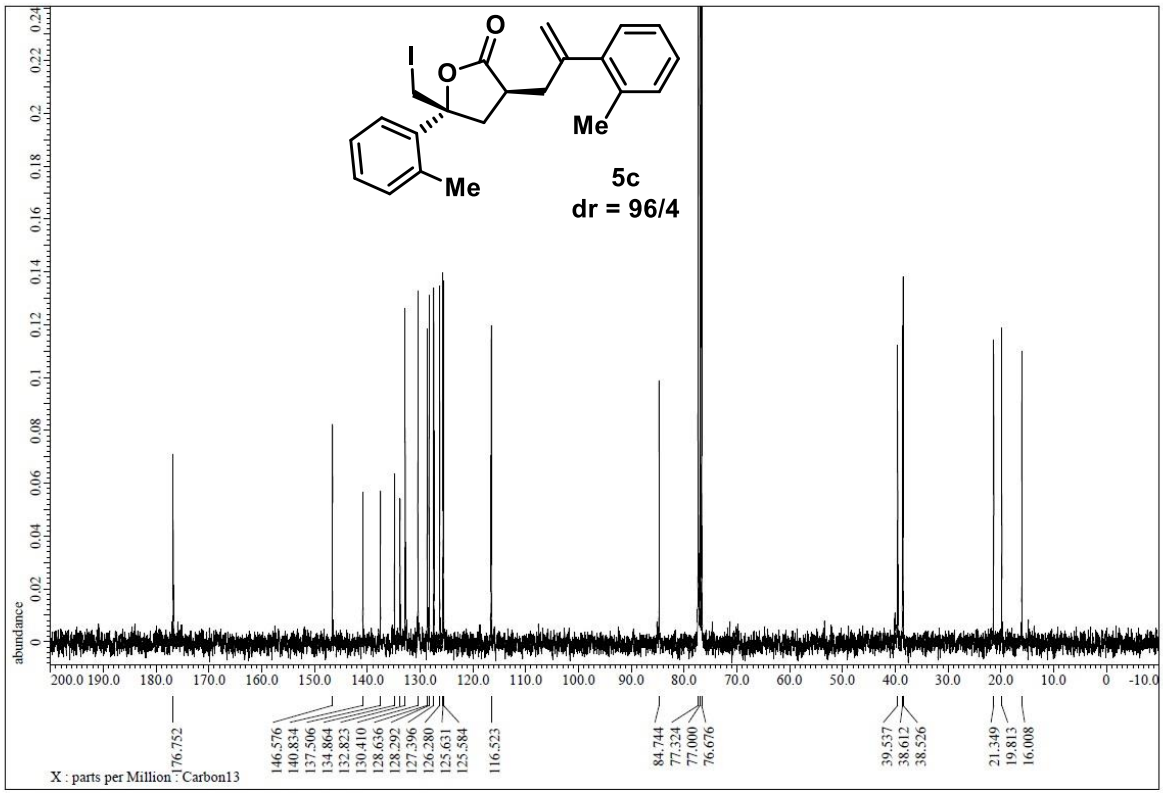

Figure S64. ^{13}C-NMR of **(3*S*,5*R*)-5c**, related to **Figure 5**.

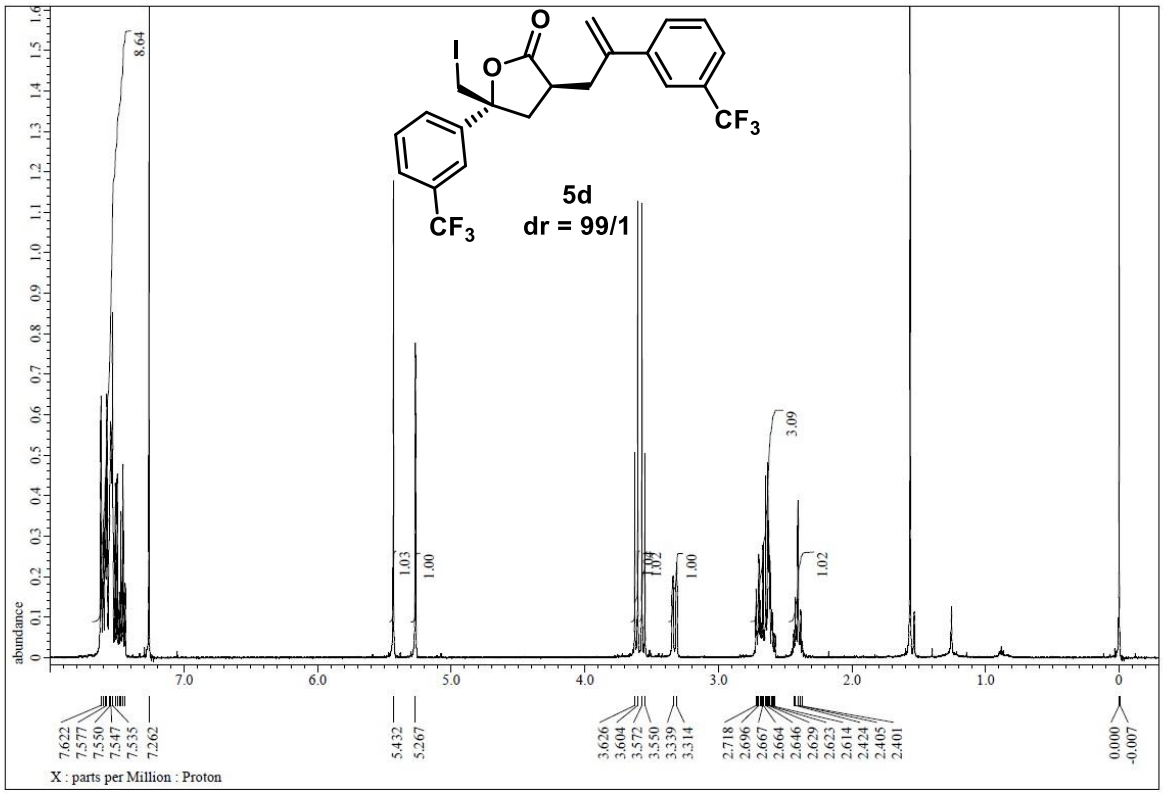

Figure S65. ^{1}H-NMR of **(3*S*,5*R*)-5d**, related to **Figure 5**.

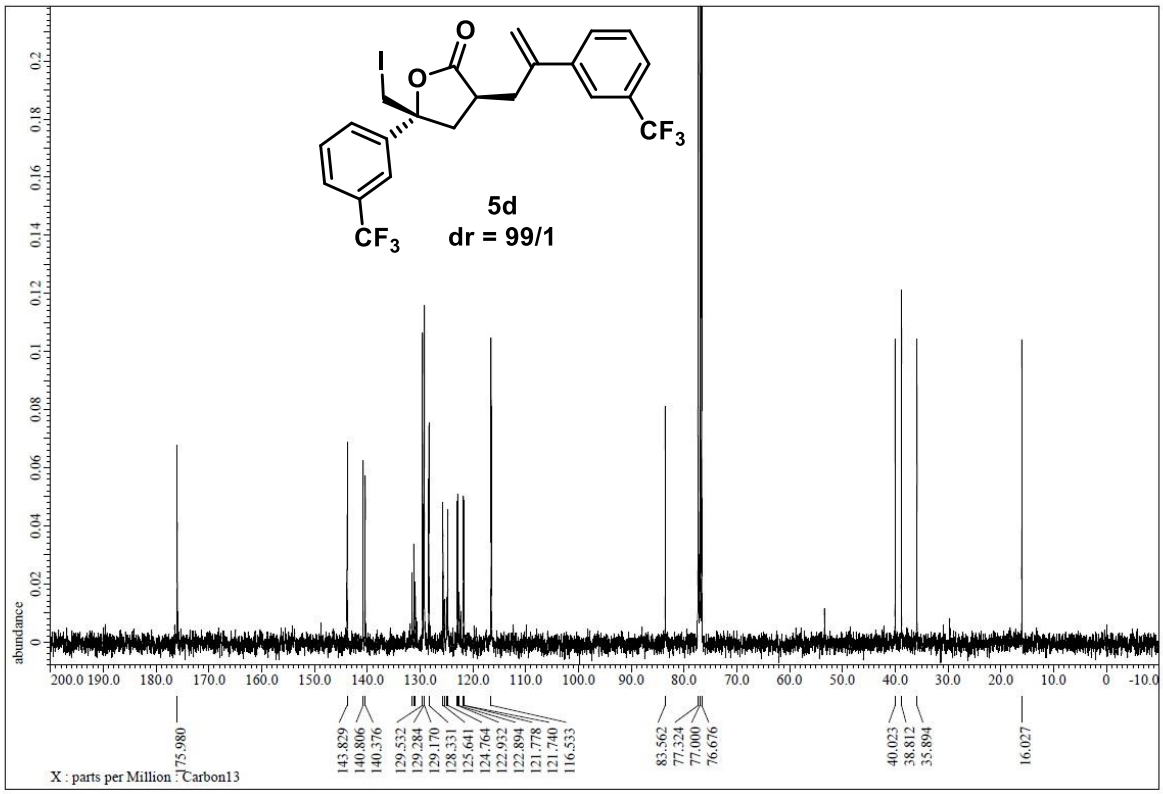

Figure S66. ^{13}C-NMR of **(3*S*,5*R*)-5d**, related to **Figure 5**.

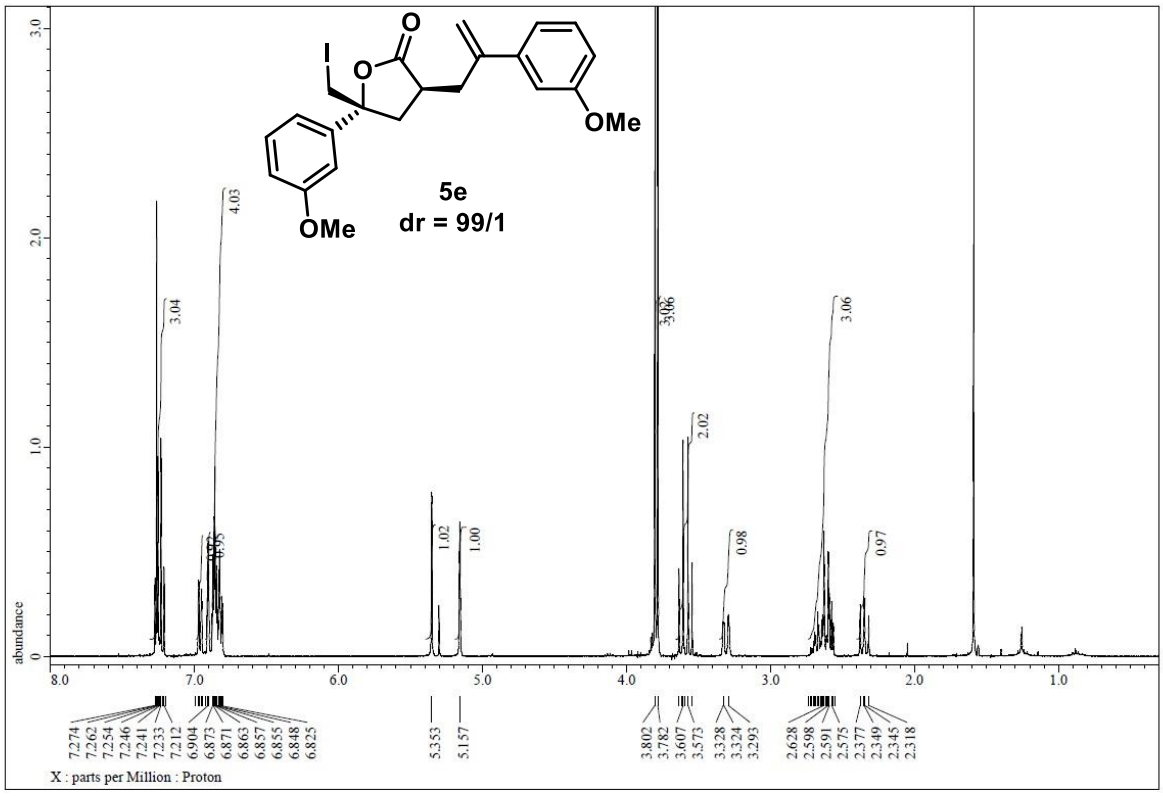

Figure S67. ^{1}H-NMR of **(3*S*,5*R*)-5e**, related to **Figure 5**.

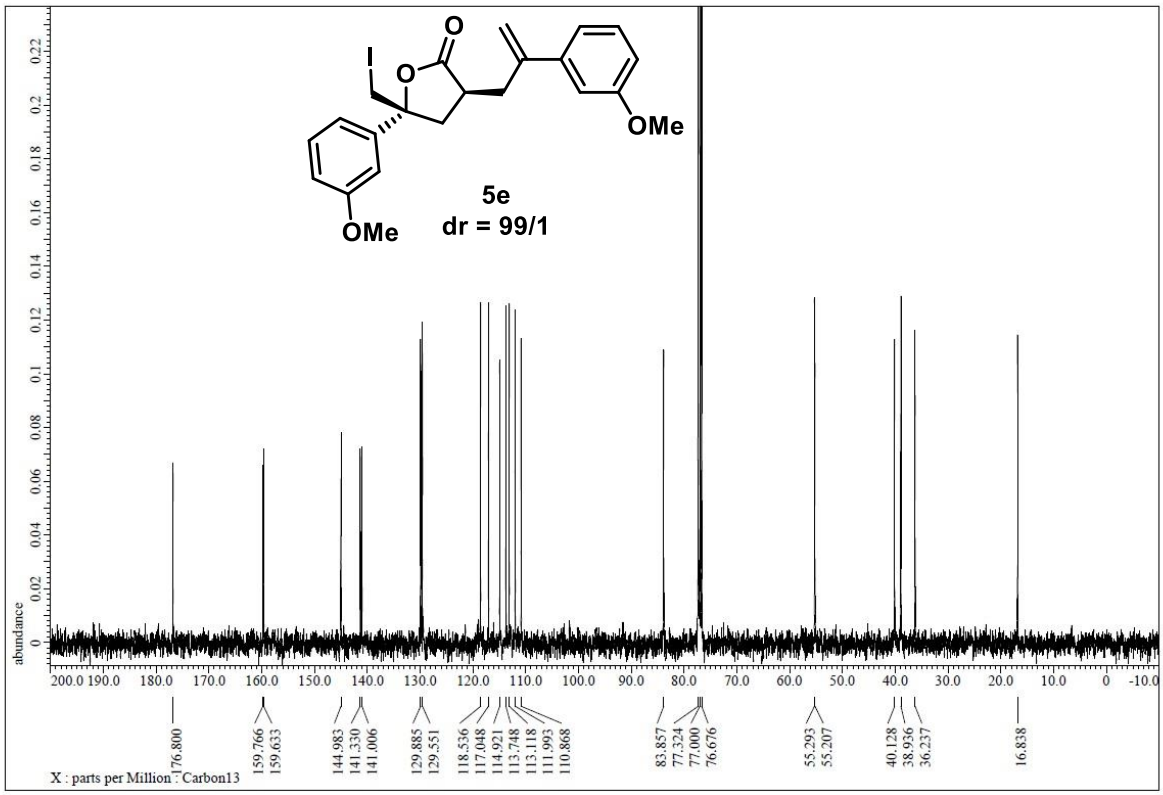

Figure S68. ^{13}C-NMR of **(3*S*,5*R*)-5e**, related to **Figure 5**.

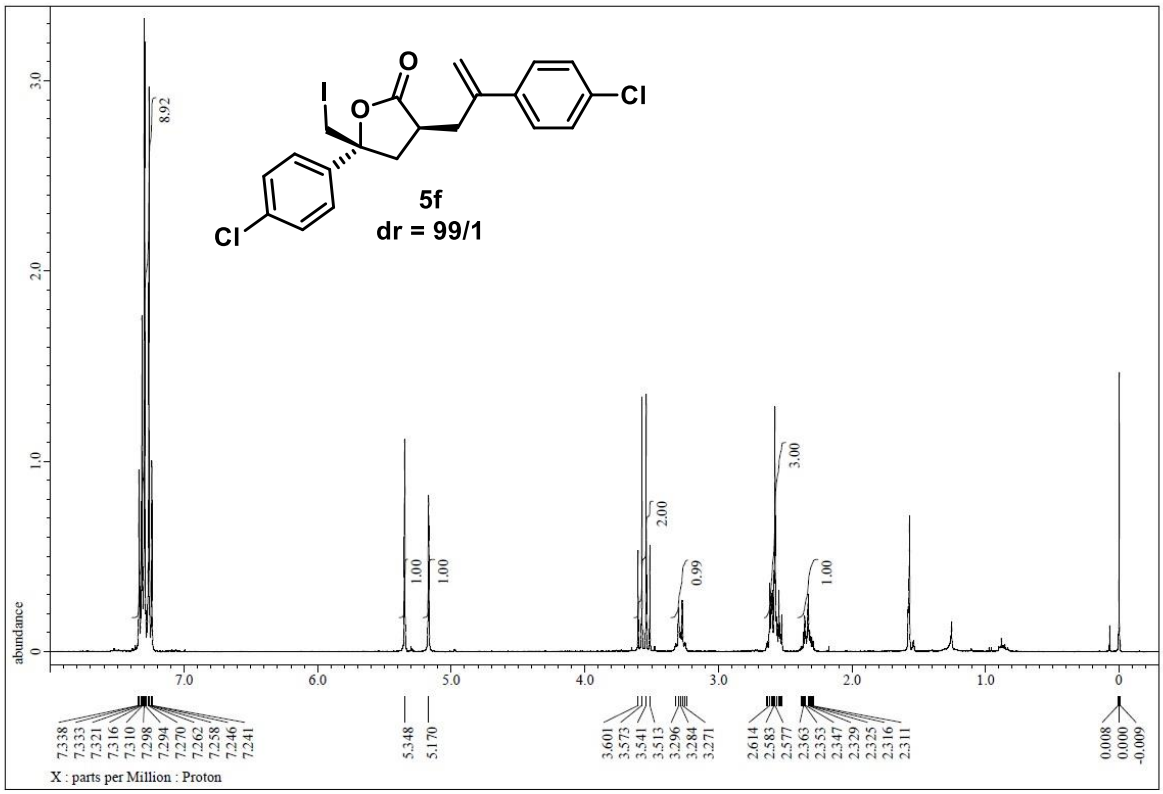

Figure S69. ^{1}H-NMR of **(3*S*,5*R*)-5f**, related to **Figure 5**.

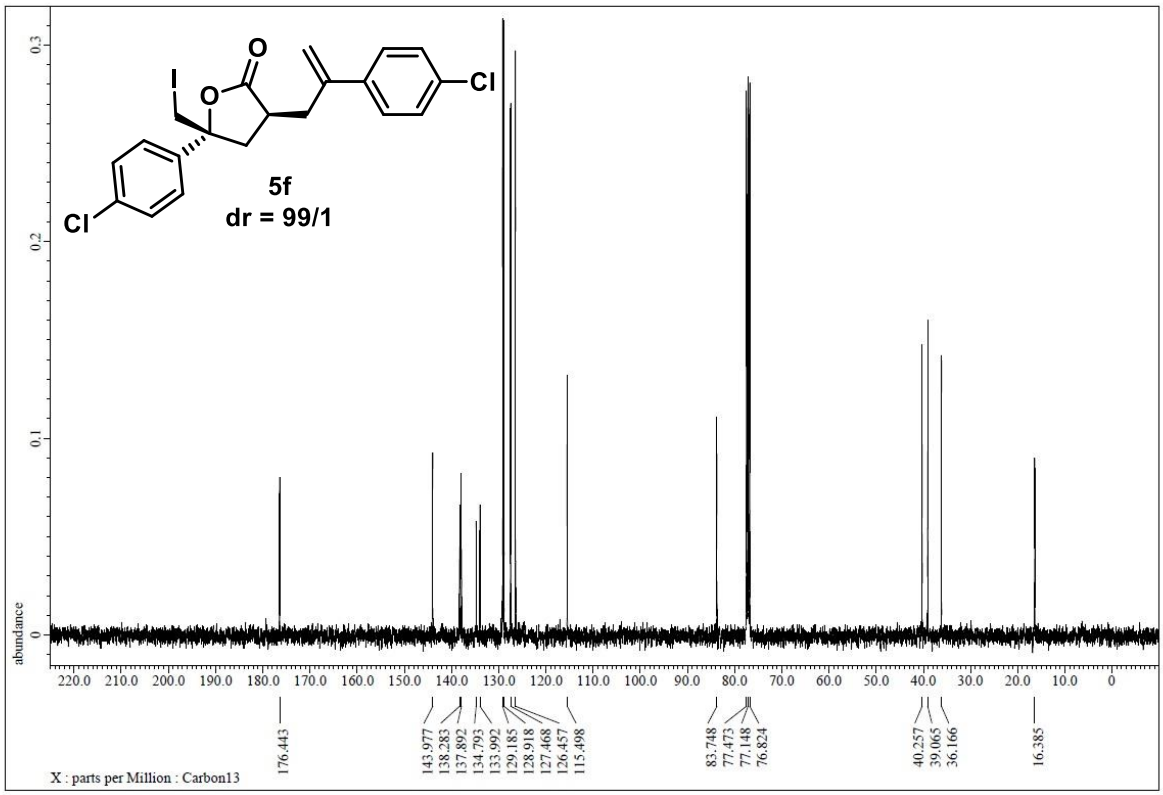

Figure S70. ^{13}C-NMR of **(3*S*,5*R*)-5f**, related to **Figure 5**.

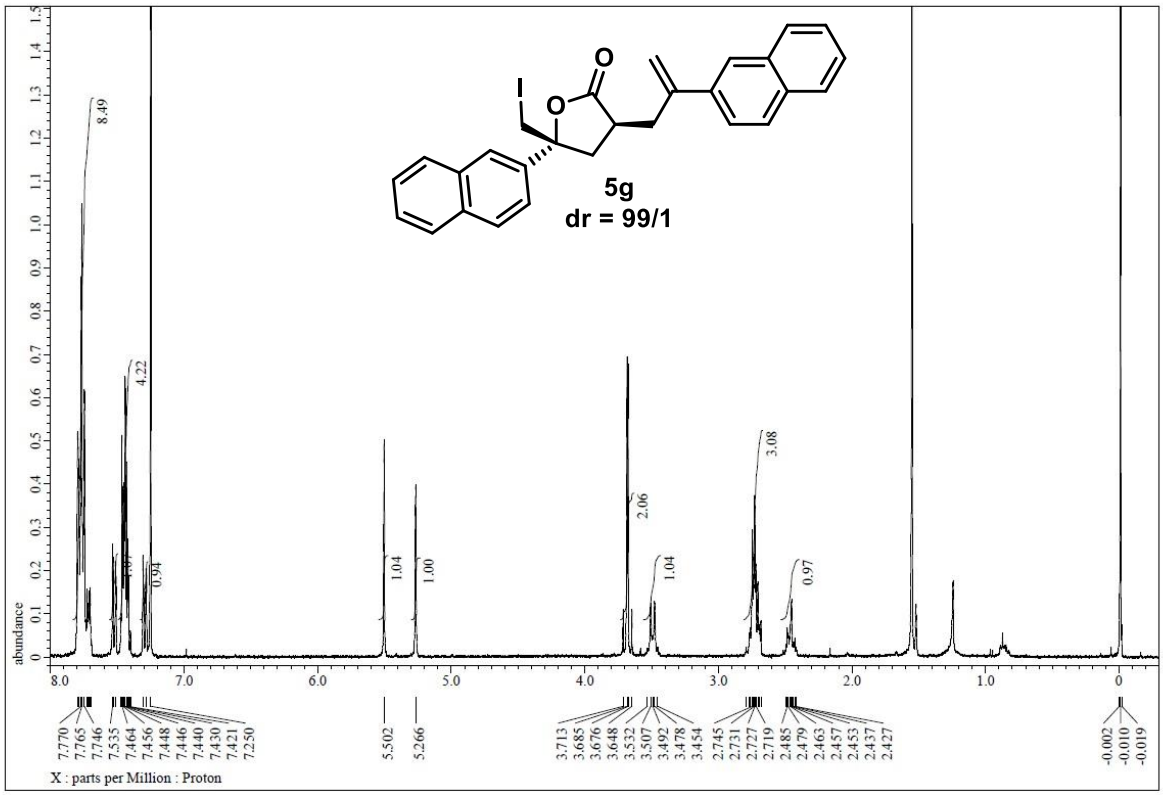

Figure S71. ^{1}H-NMR of **(3*S*,5*R*)-5g**, related to **Figure 5**.

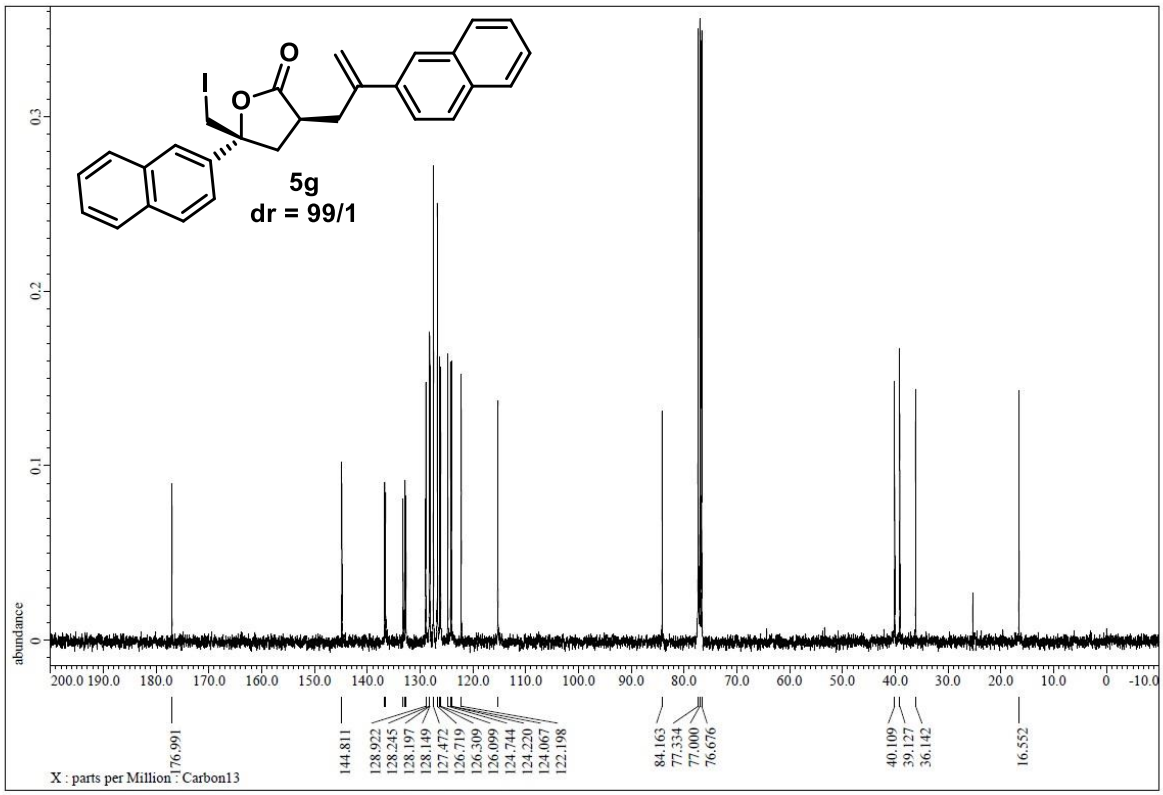

Figure S72. ^{13}C-NMR of **(3*S*,5*R*)-5g**, related to **Figure 5**.

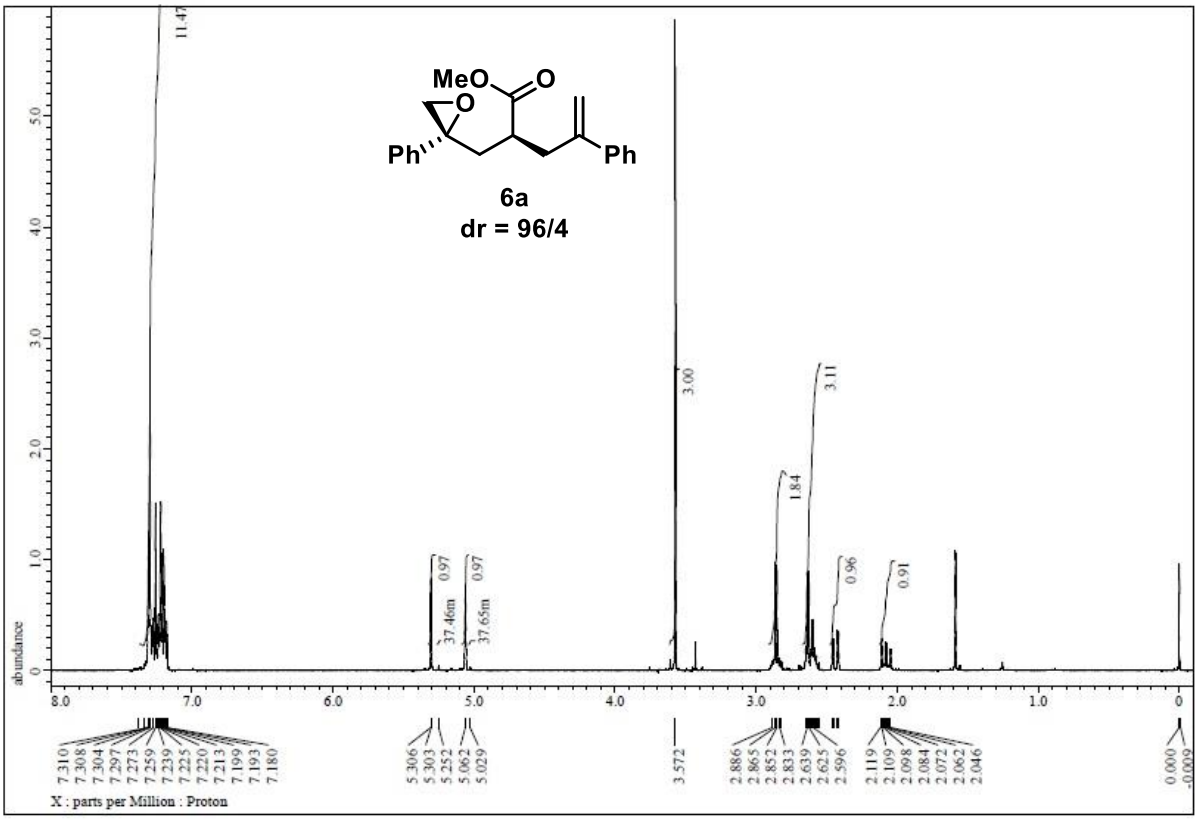

Figure S73. ^{1}H-NMR of **6a**, related to **Scheme 1**.

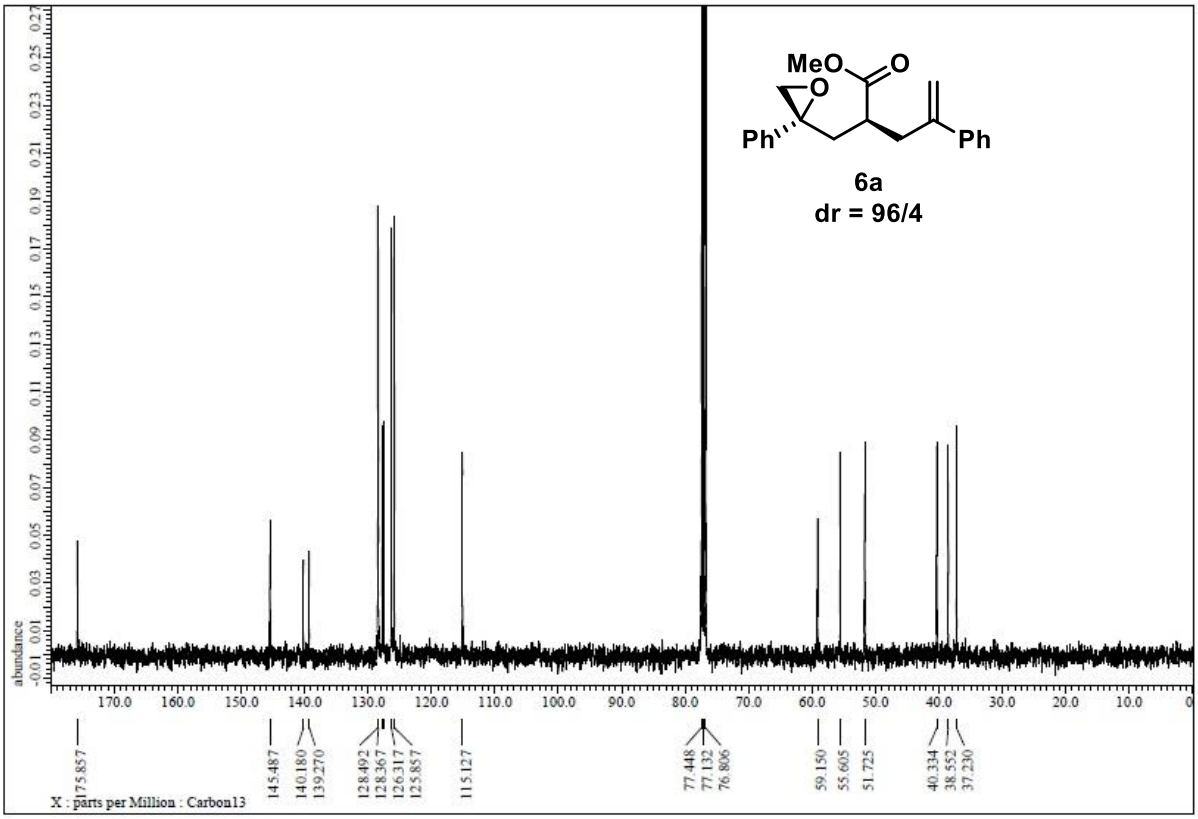

Figure S74. ^{13}C-NMR of **6a**, related to **Scheme 1**.

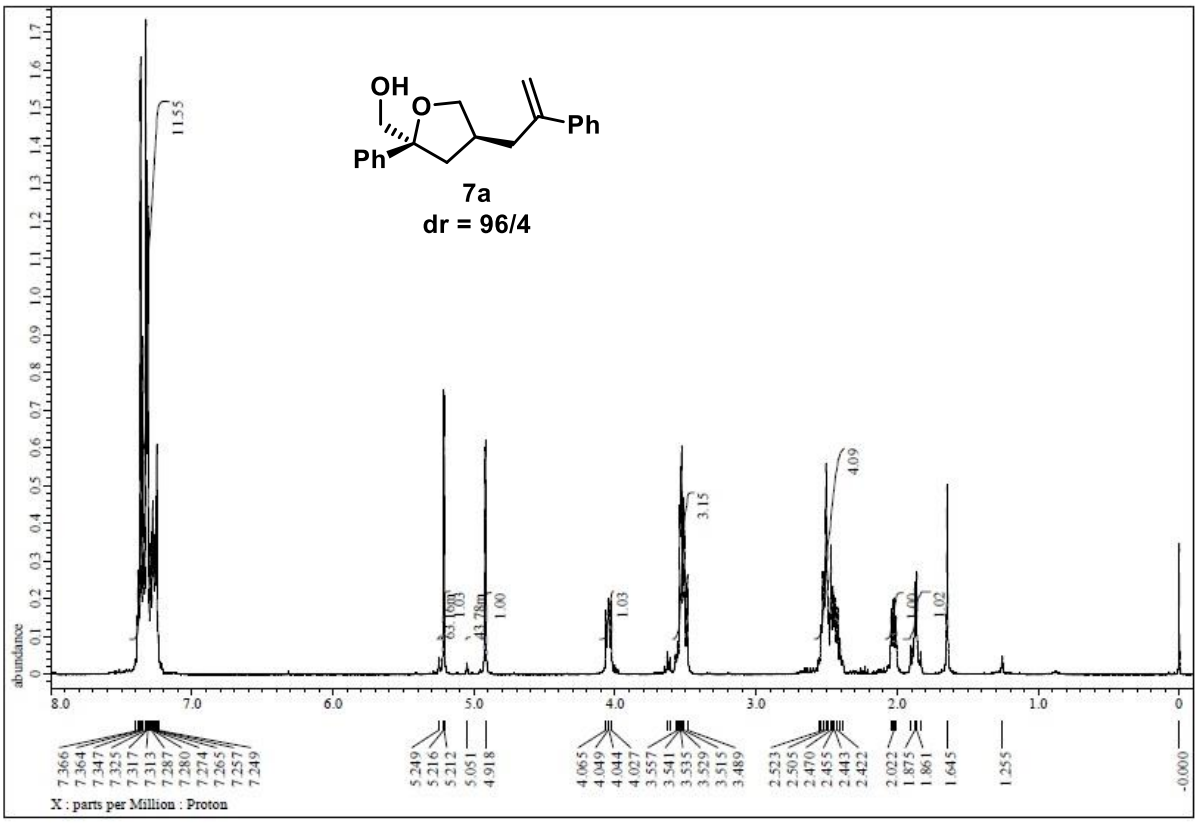

Figure S75. [1]H-NMR of **7a**, related to **Scheme 1**.

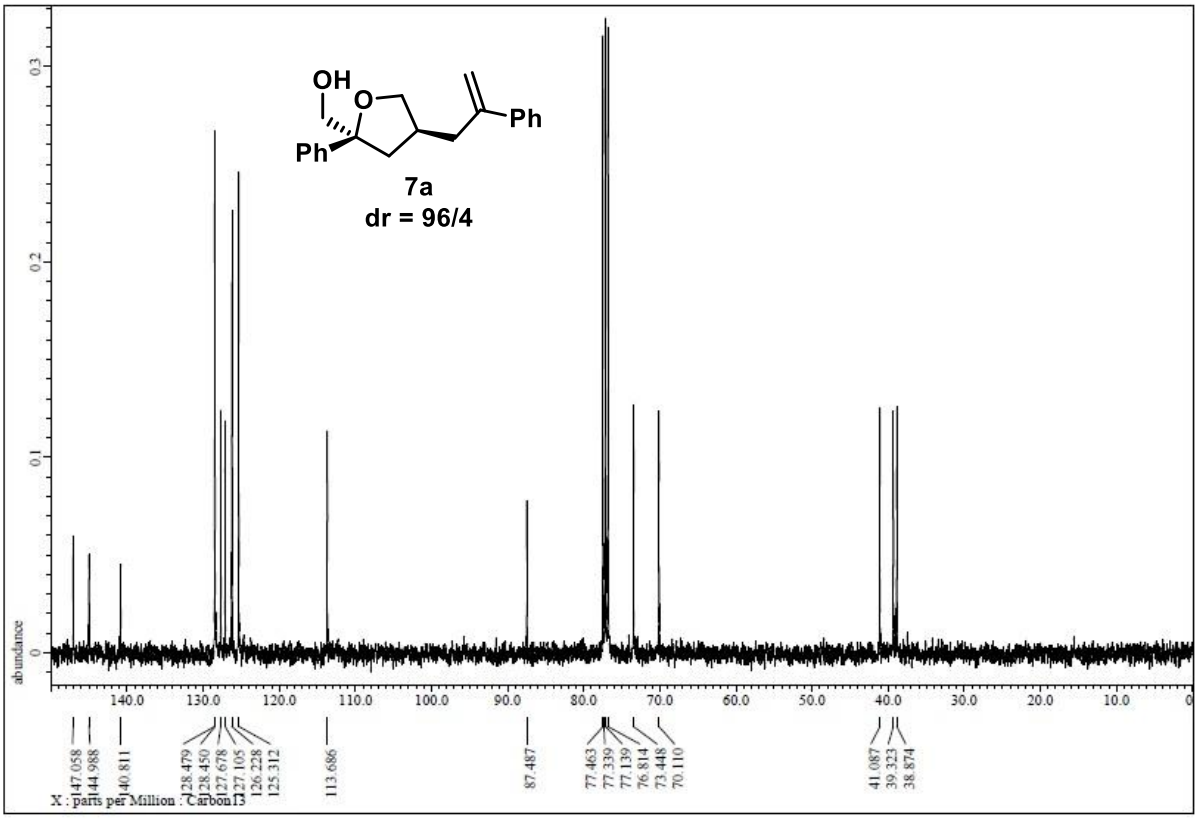

Figure S76. [13]C-NMR of **7a**, related to **Scheme 1**.

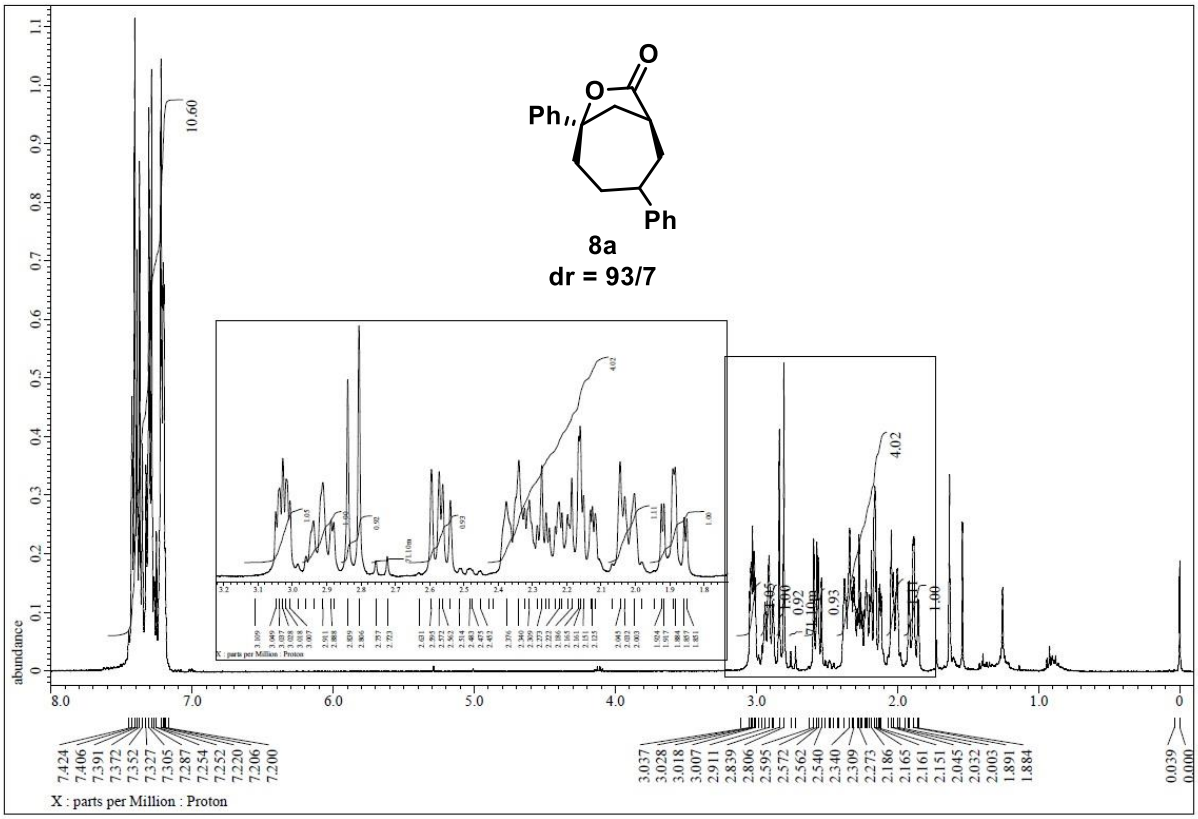

Figure S77. ^{1}H-NMR of **8a**, related to **Scheme 1**.

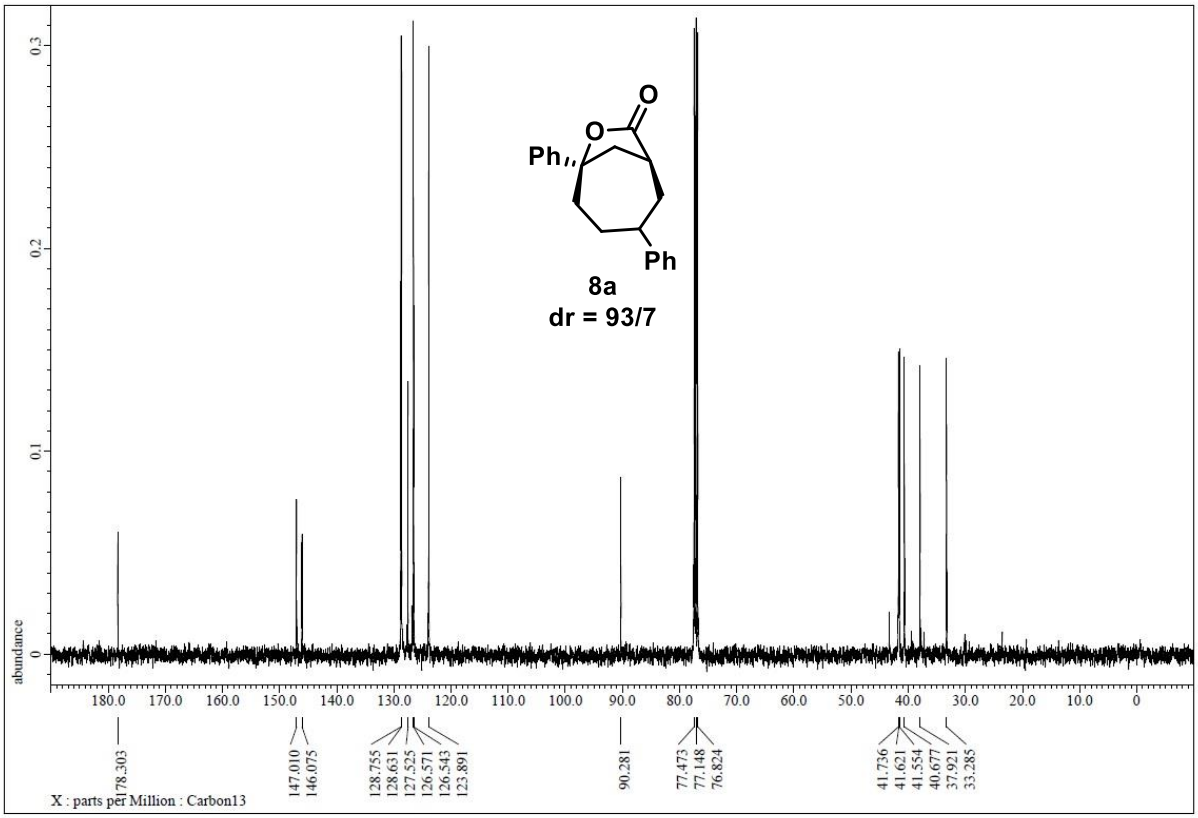

Figure S78. ^{13}C-NMR of **8a**, related to **Scheme 1**.

16. HPLC spectra

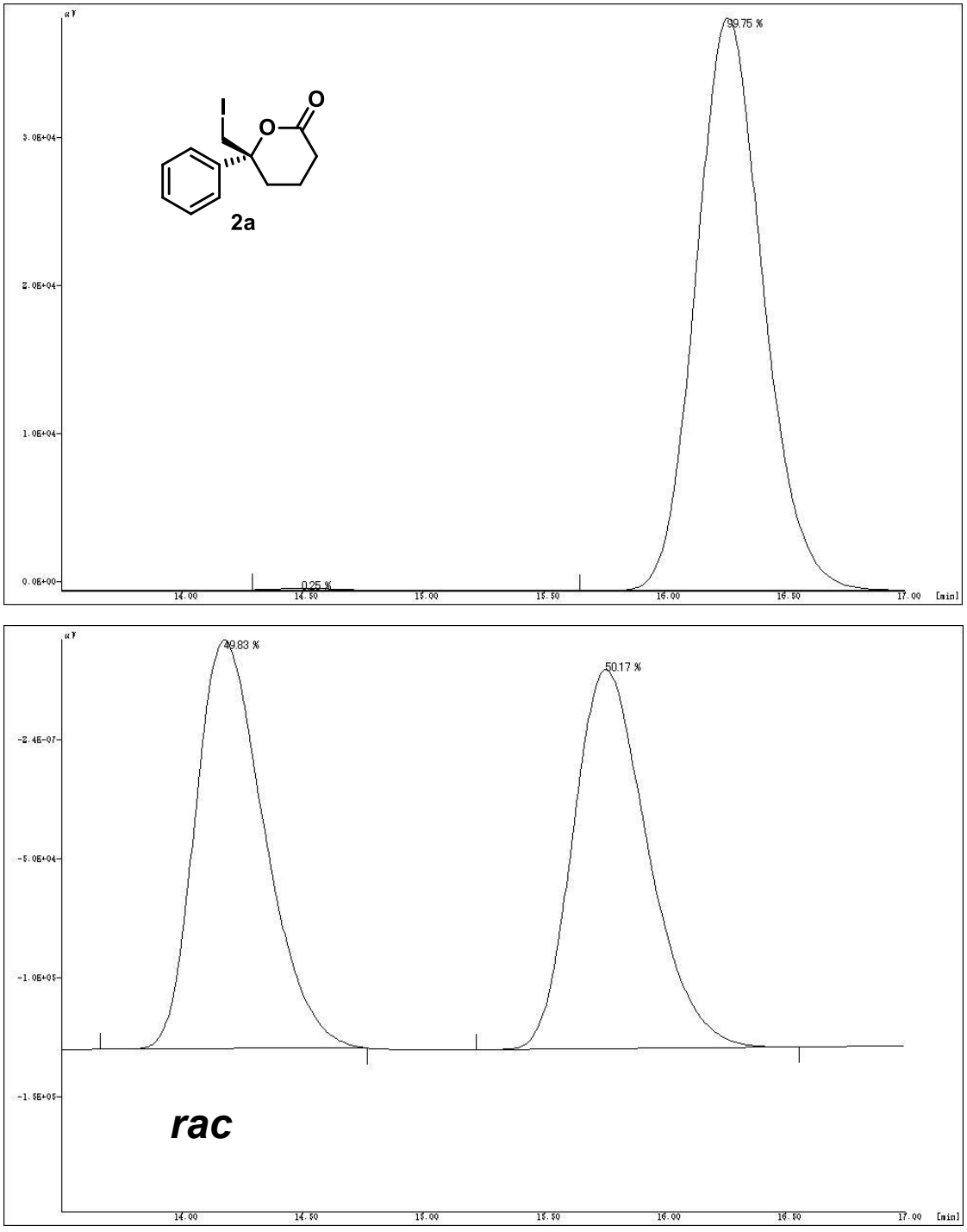

Chiralpack AD-H column (95:5 hexane: 2-propanol, 1.0 mL/min, 254 nm)

Figure S79. HPLC of **2a**, related to **Table 1**.

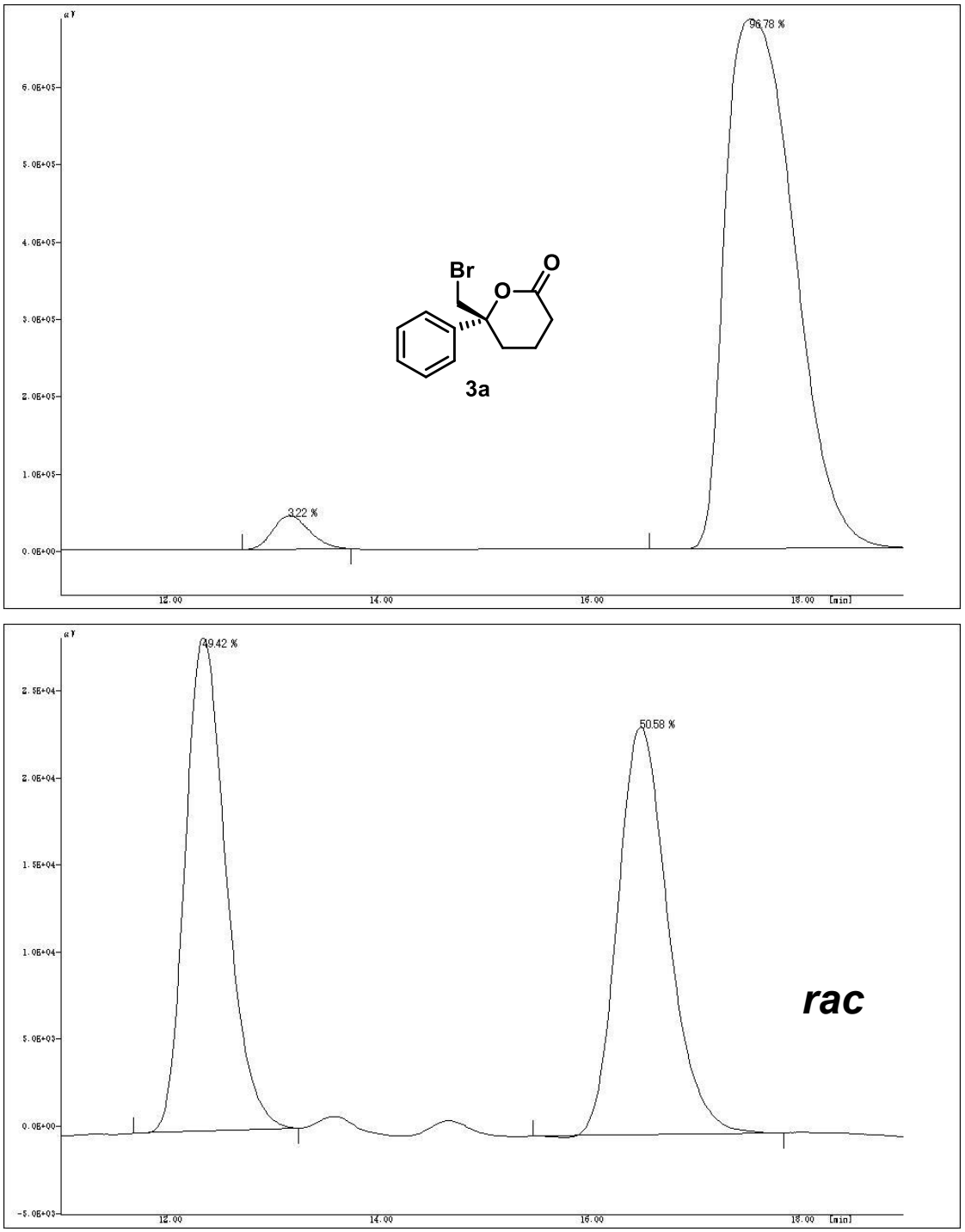

Chiralcel OD-H column (92:8 hexane: 2-propanol, 1.0 mL/min, 210 nm)

Figure S80. HPLC of **3a**, related to **Table 2**.

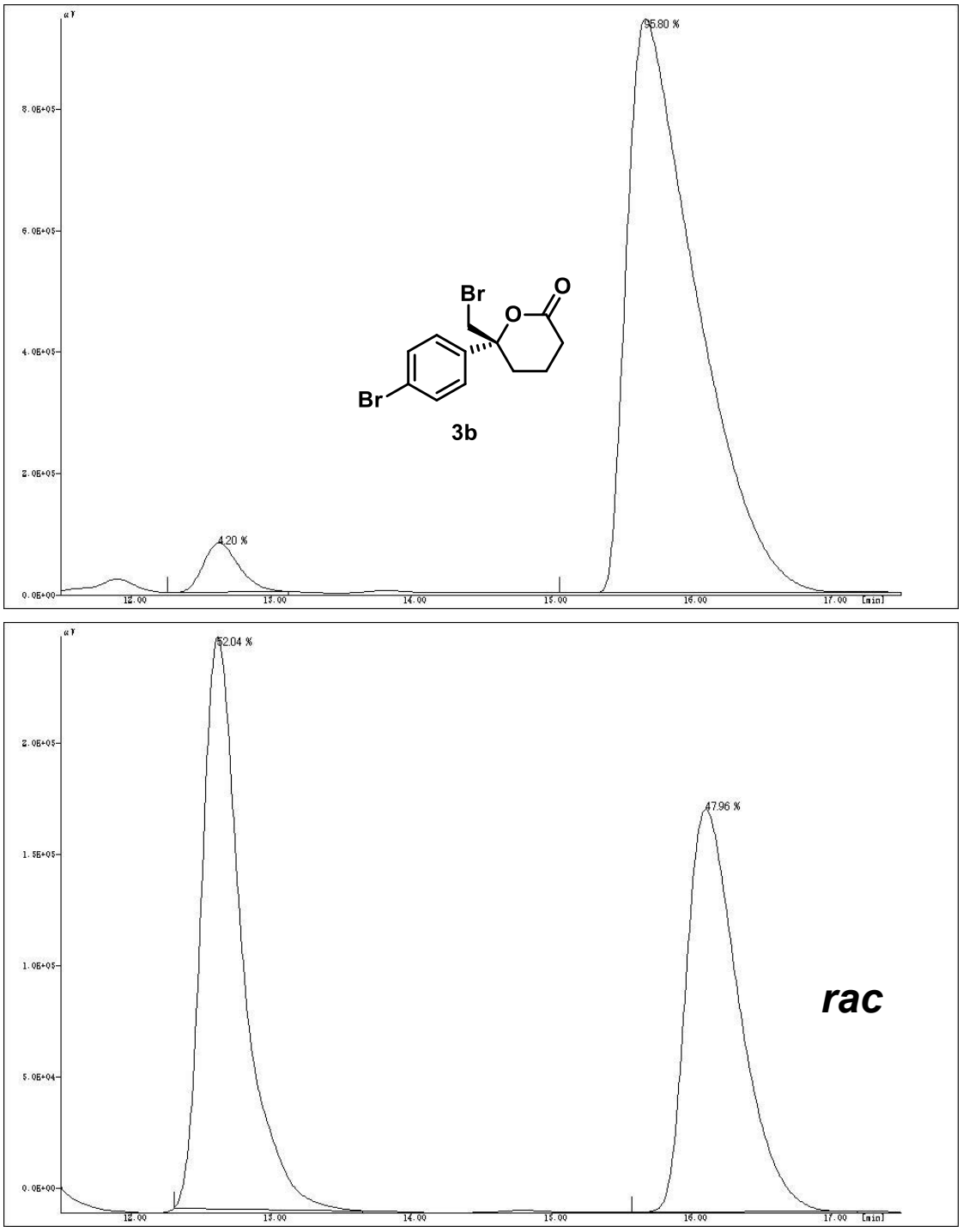

Chiralpack AD-H column (92:8 hexane: 2-propanol, 1.0 mL/min, 210 nm)

Figure S81. HPLC of **3b**, related to **Table S2**.

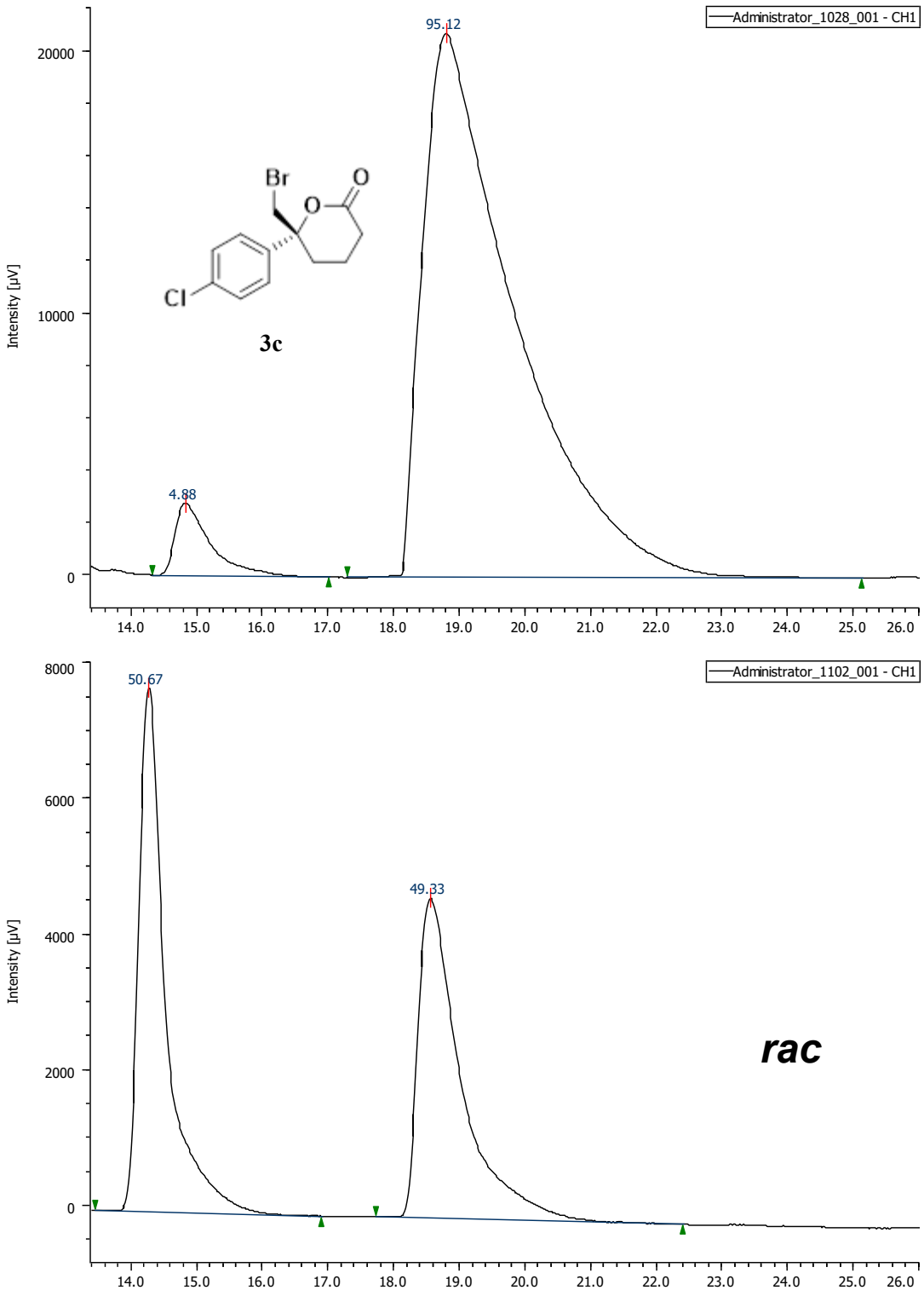

Chiralpack AD-H column (95:5 hexane: 2-propanol, 1.0 mL/min, 254 nm)

Figure S82. HPLC of **3c**, related to **Table S2**.

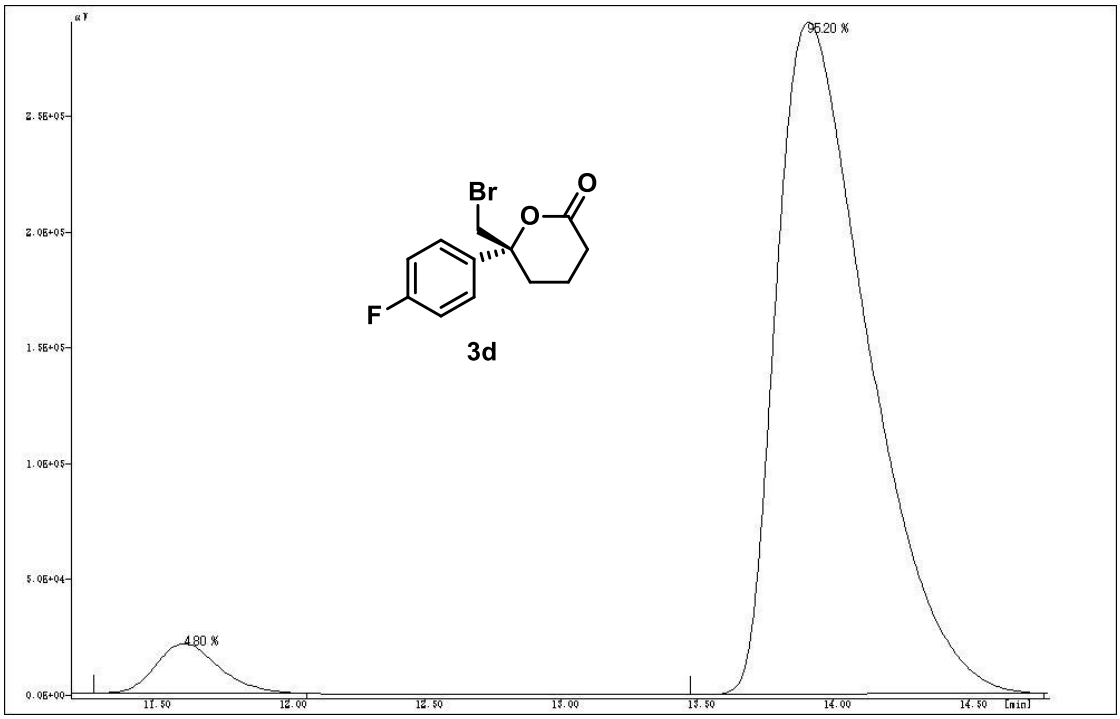

Chiralpack AD-H column (92:8 hexane: 2-propanol, 1.0 mL/min, 210 nm)

Figure S83. HPLC of **3d**, related to **Table S2**.

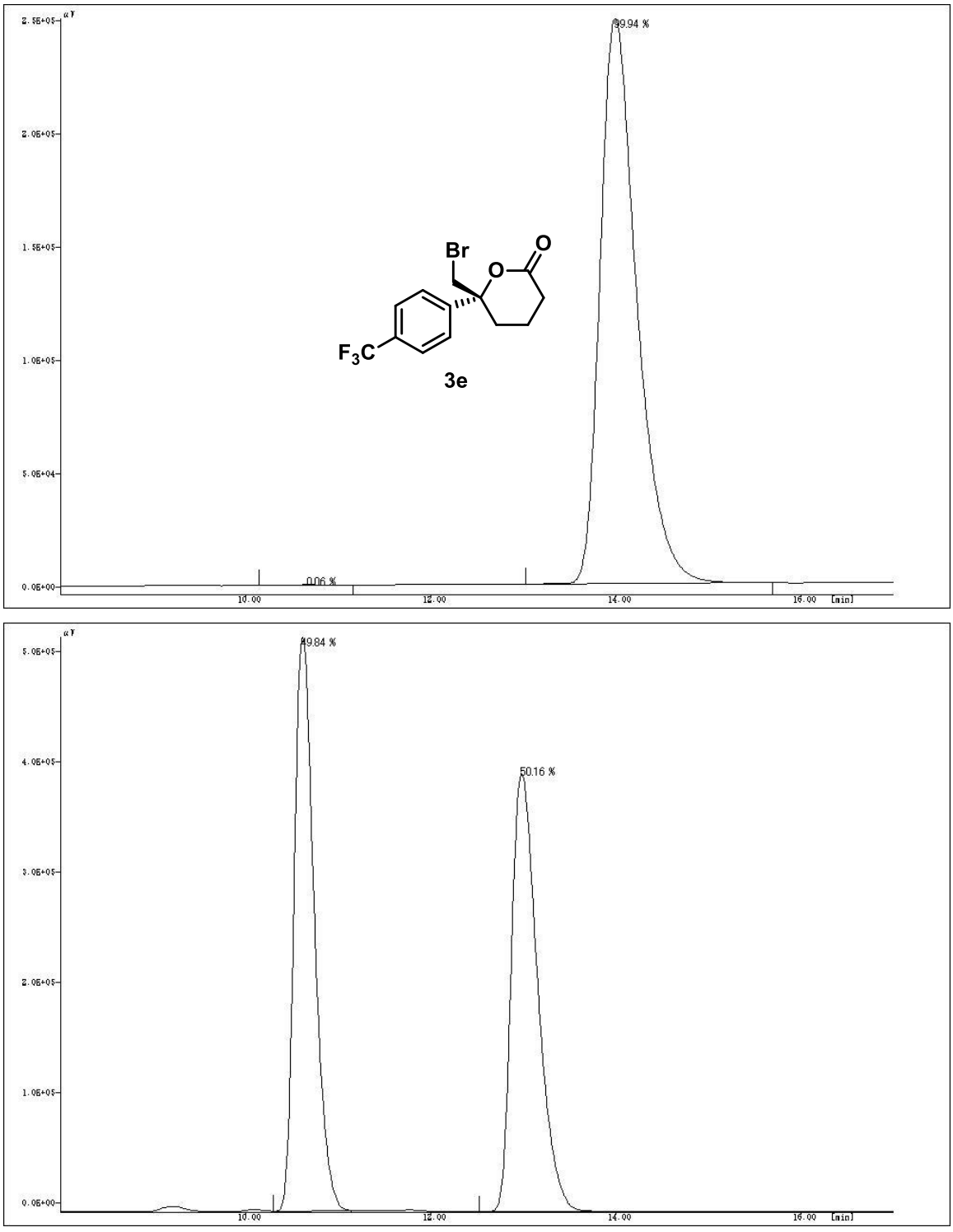

Chiralpack AD-H column (92:8 hexane: 2-propanol, 1.0 mL/min, 210 nm)

Figure S84. HPLC of **3e**, related to **Table S2**.

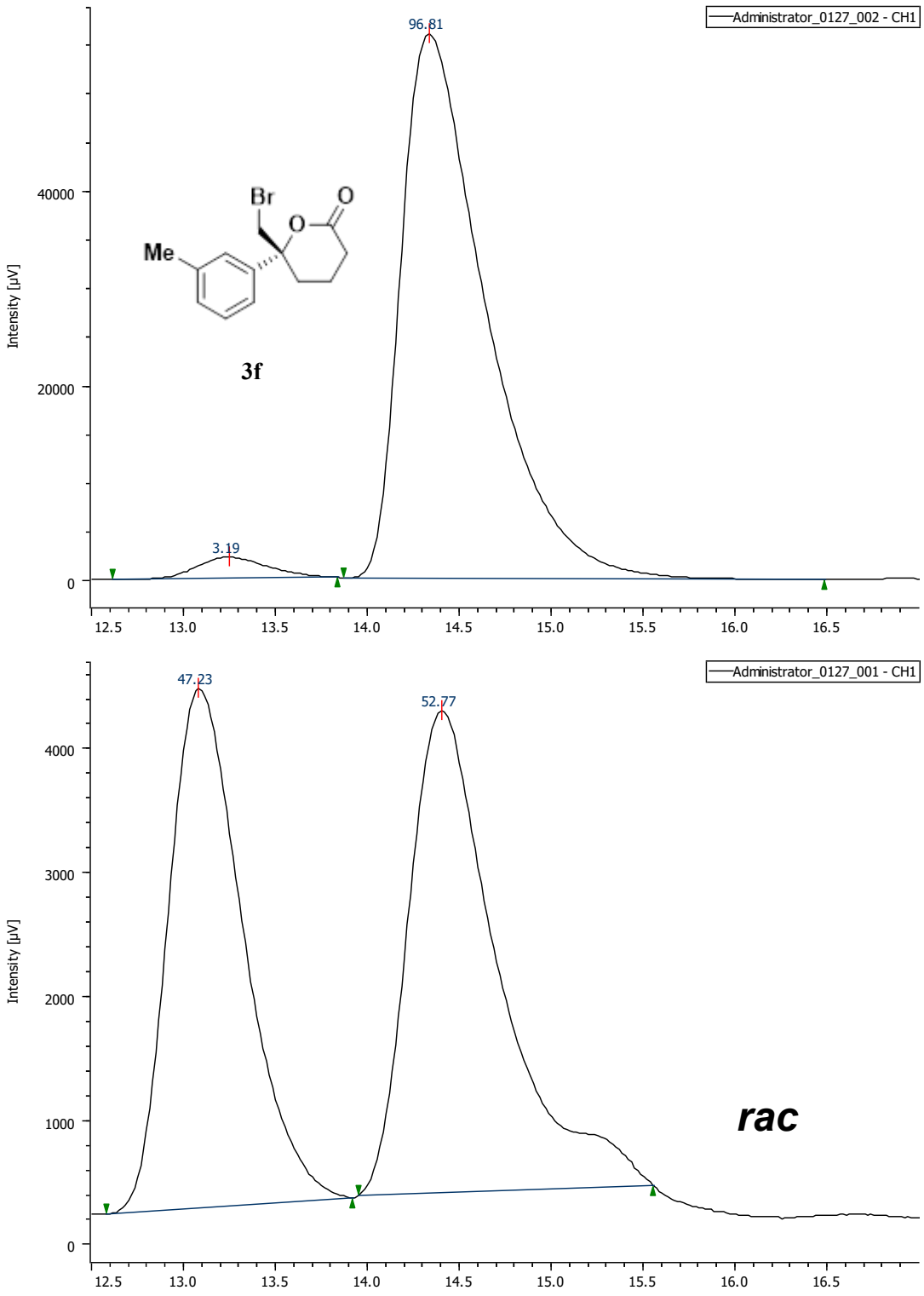

Chiralpack AD-H column (95:5 hexane: 2-propanol, 1.0 mL/min, 254 nm)

Figure S85. HPLC of **3f**, related to **Table S2**.

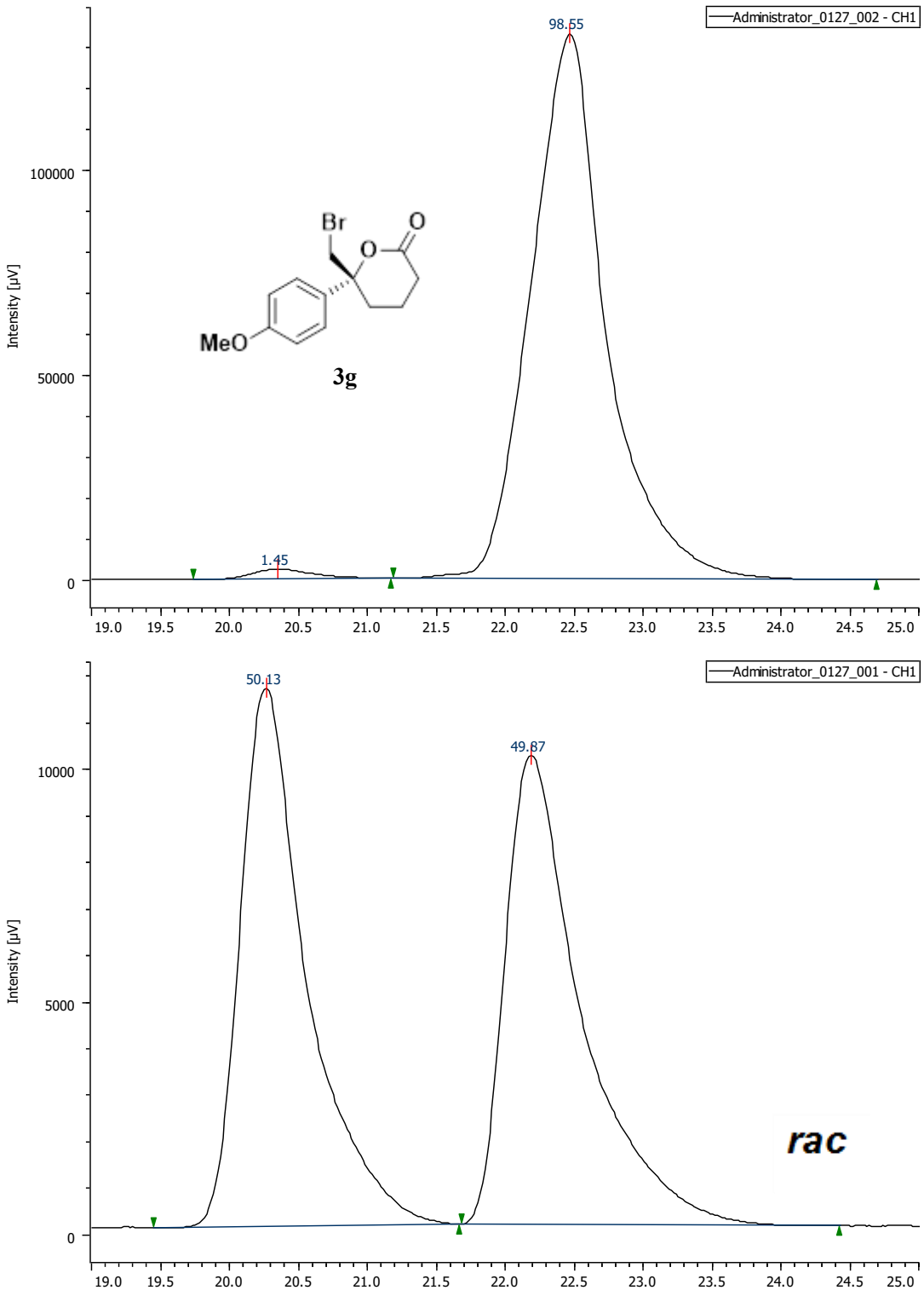

Chiralpack AD-H column (95:5 hexane: 2-propanol, 1.0 mL/min, 254 nm)

Figure S86. HPLC of **3g**, related to **Table S2**.

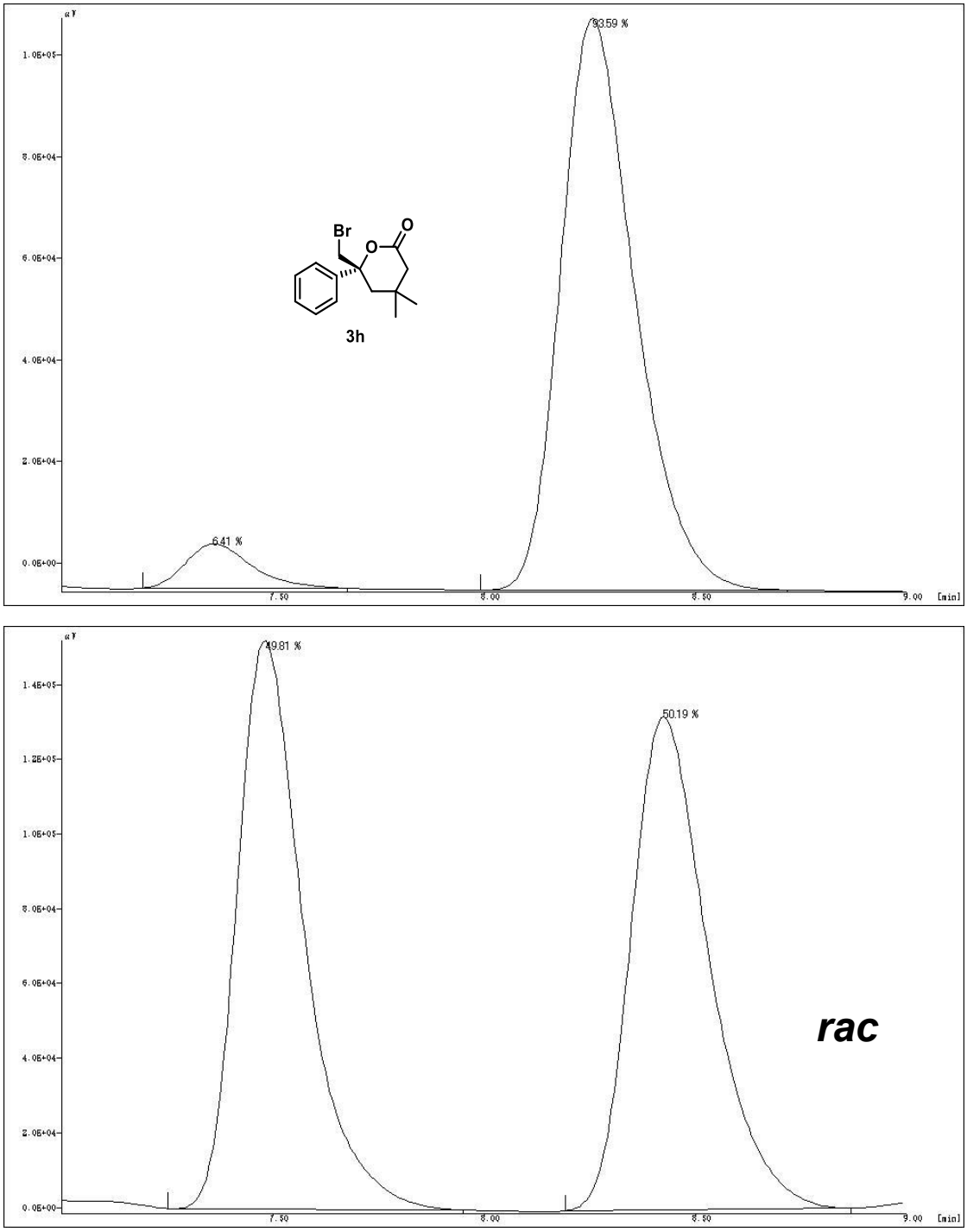

Chiralpack AD-H column (92:8 hexane: 2-propanol, 1.0 mL/min, 210 nm)

Figure S87. HPLC of **3h**, related to **Table S2.**

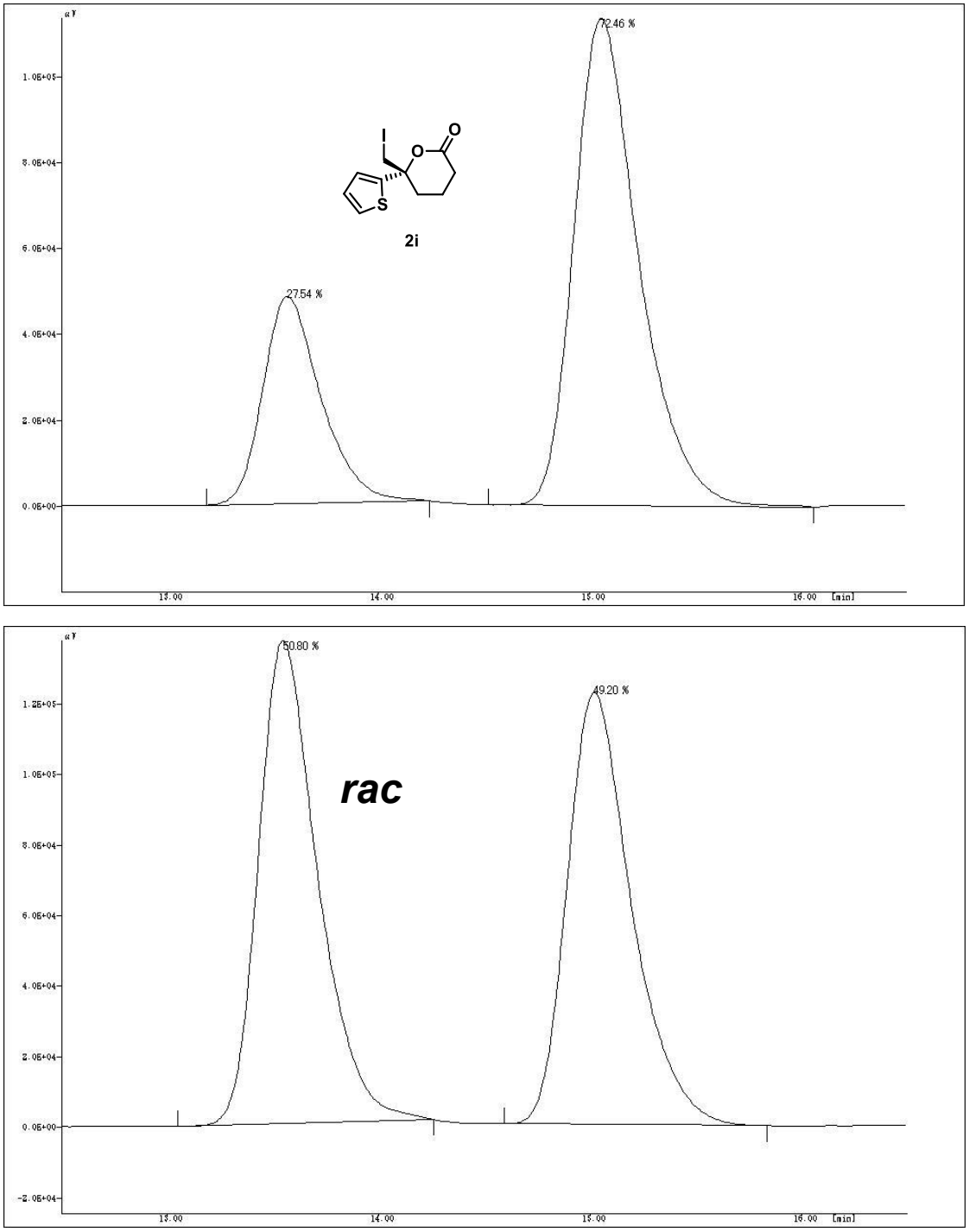

Chiralpack AD-H column (95:5 hexane: 2-propanol, 1.0 mL/min, 254 nm)

Figure S88. HPLC of **2i**, related to **Table S2.**

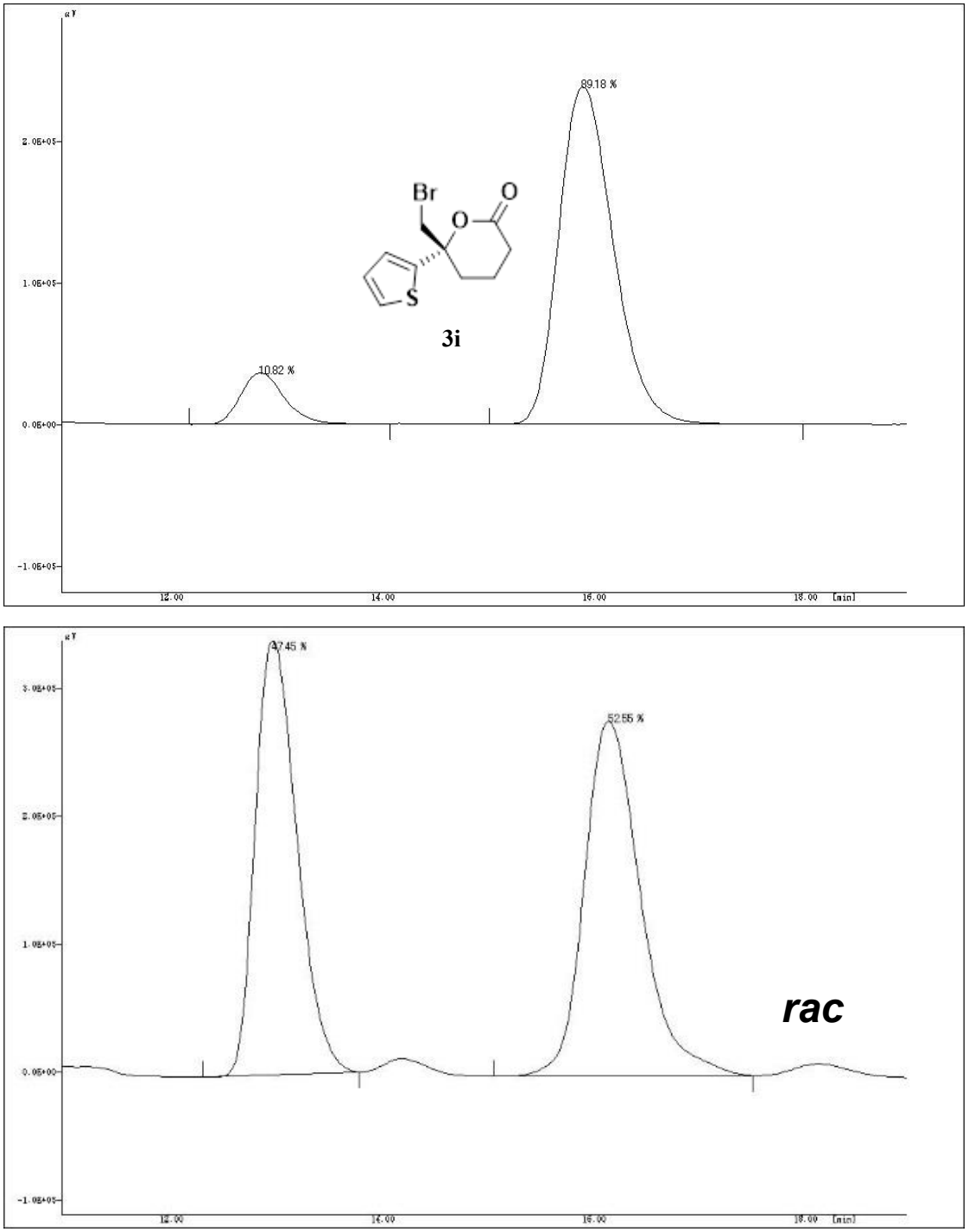

Chiralpack OD-H column (90:10 hexane: 2-propanol, 1.0 mL/min, 254 nm)

Figure S89. HPLC of **3i**, related to **Table S2.**

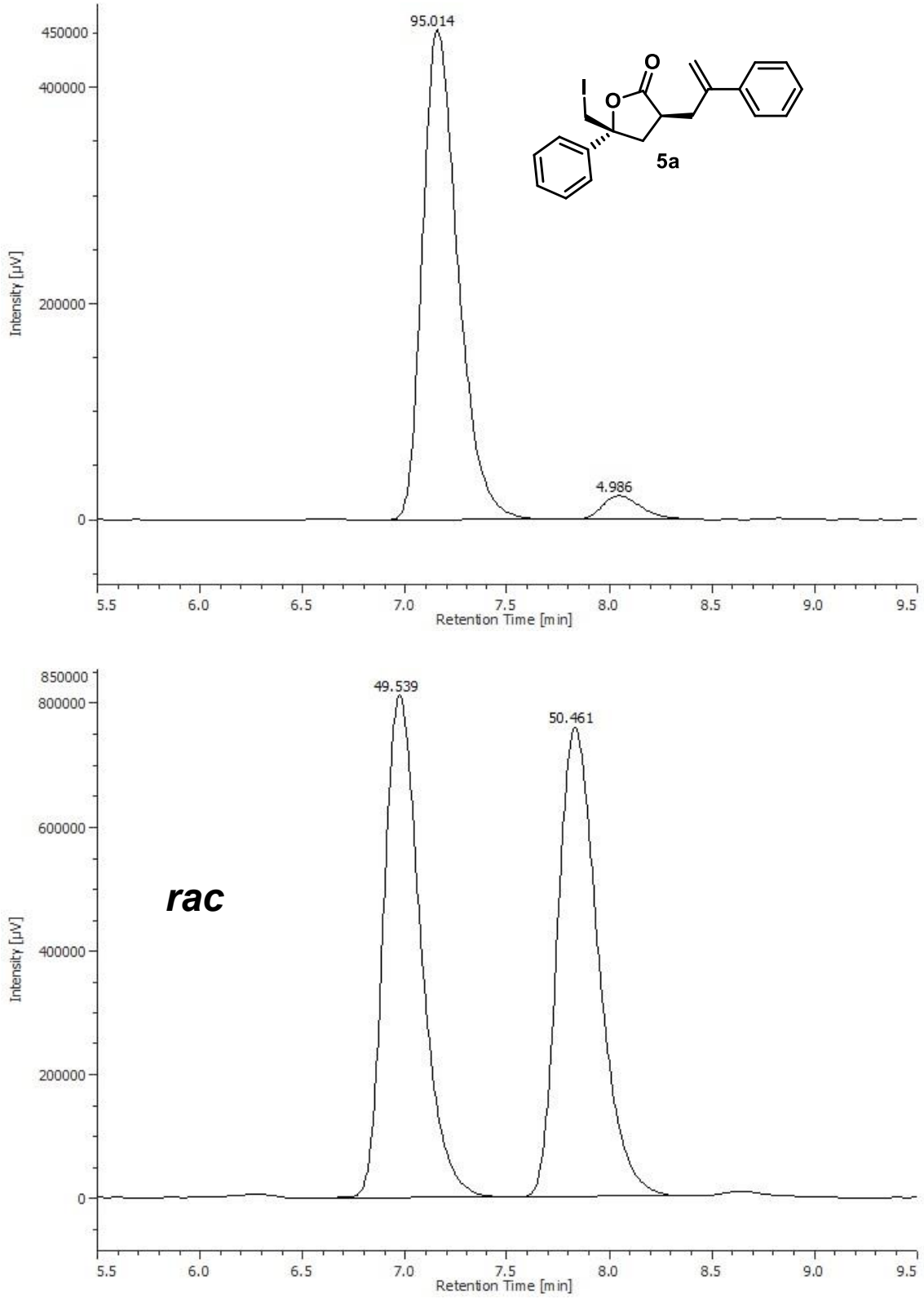

Chiralpack AD-3 column (90:10 hexane: 2-propanol, 1.0 mL/min, 254 nm)

Figure S90. HPLC of **5a**, related to **Figure 5**.

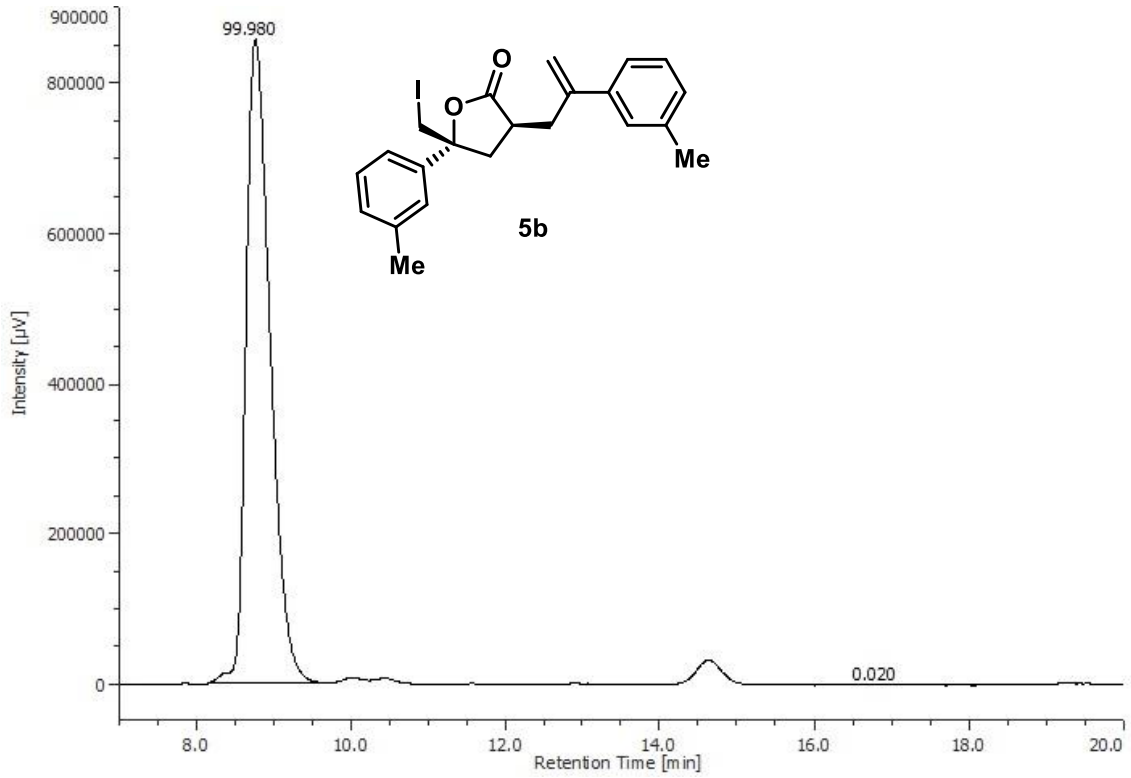

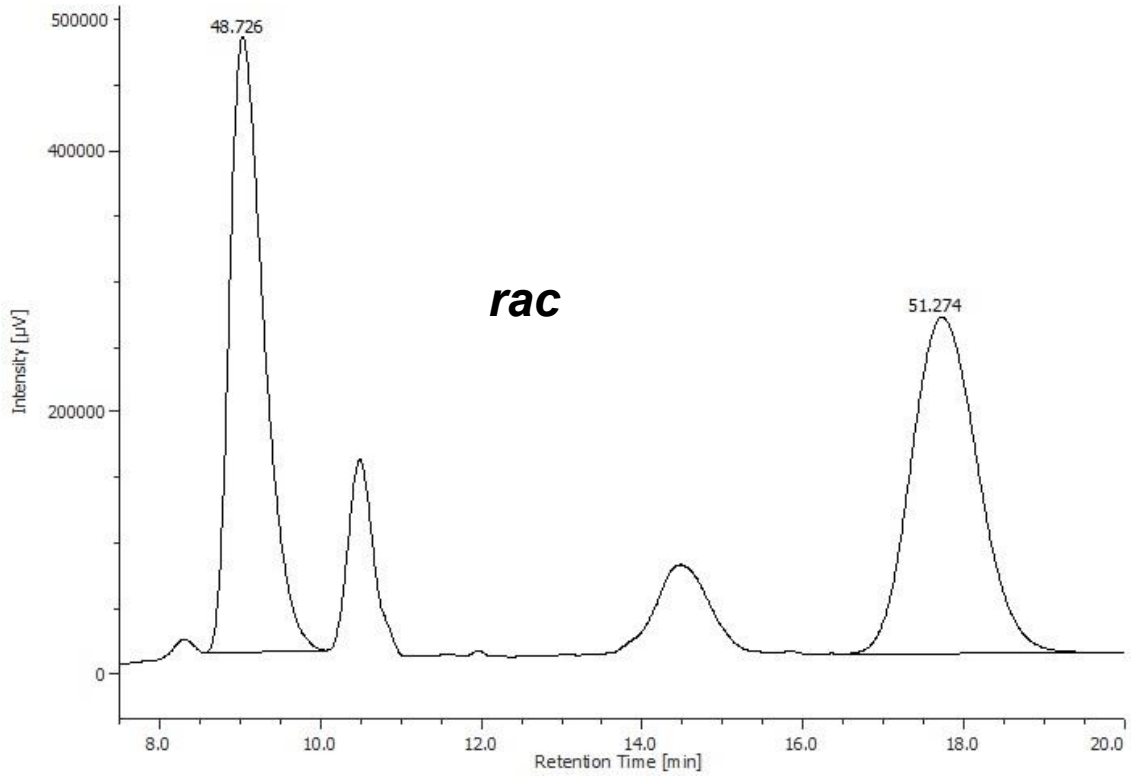

Chiralpack AS-H column (95:5 hexane: 2-propanol, 1.0 mL/min, 254 nm)

Figure S91. HPLC of **5b**, related to **Figure 5.**

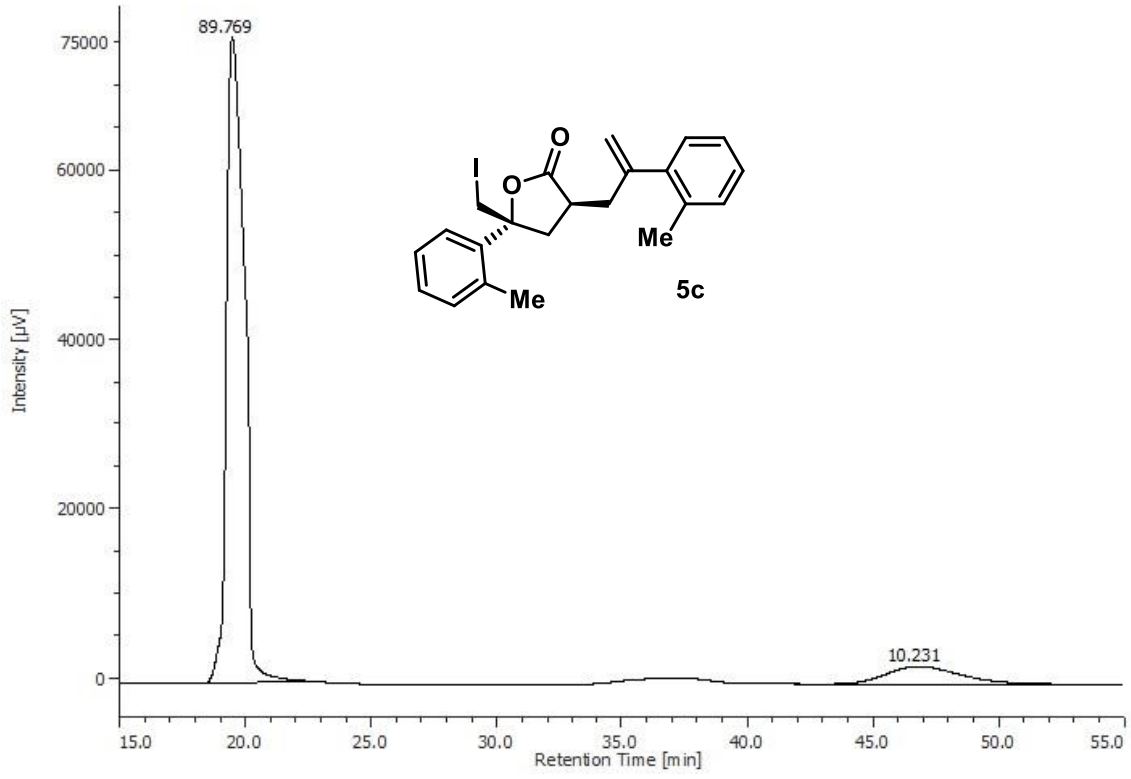

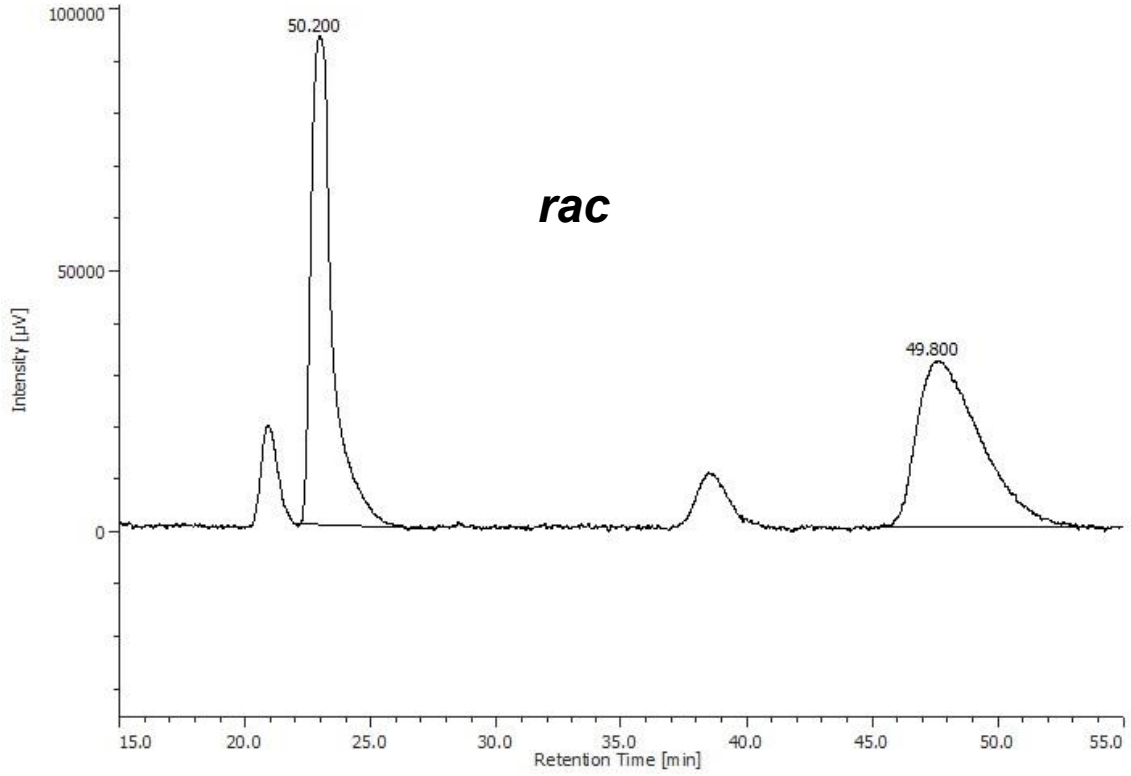

Chiralpack AS-H column (99:1 hexane: 2-propanol, 1.0 mL/min, 254 nm)

Figure S92. HPLC of **5c**, related to **Figure 5**.

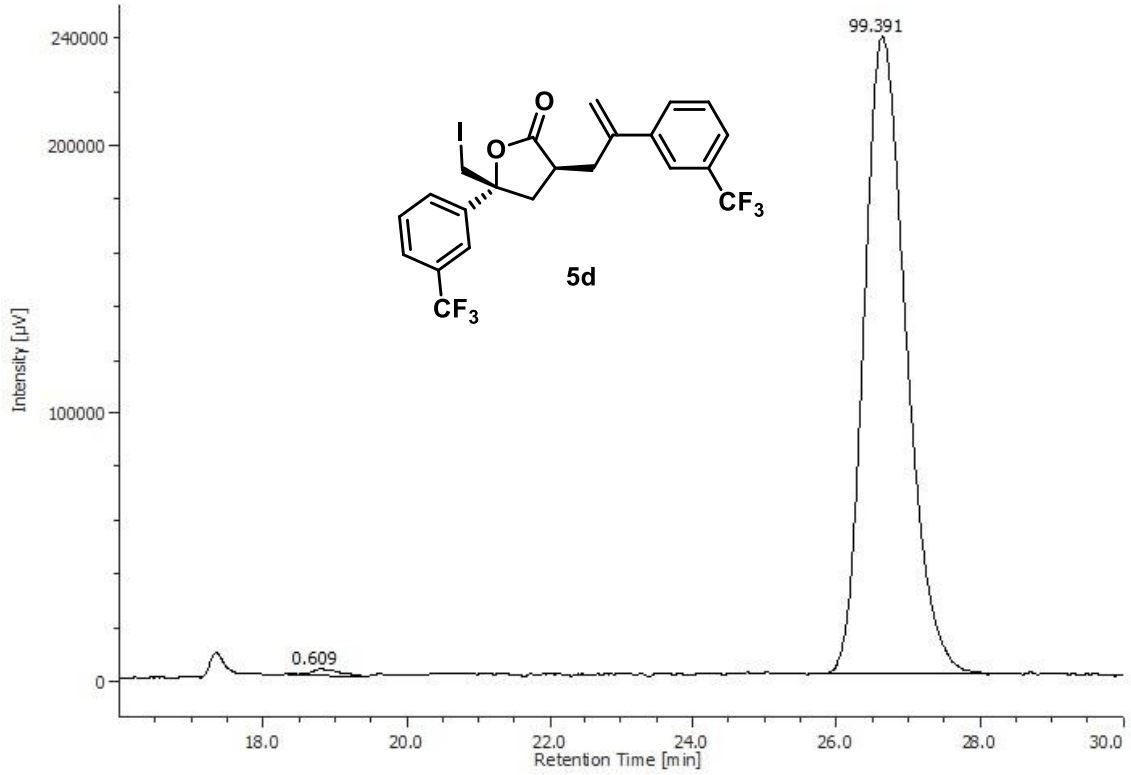

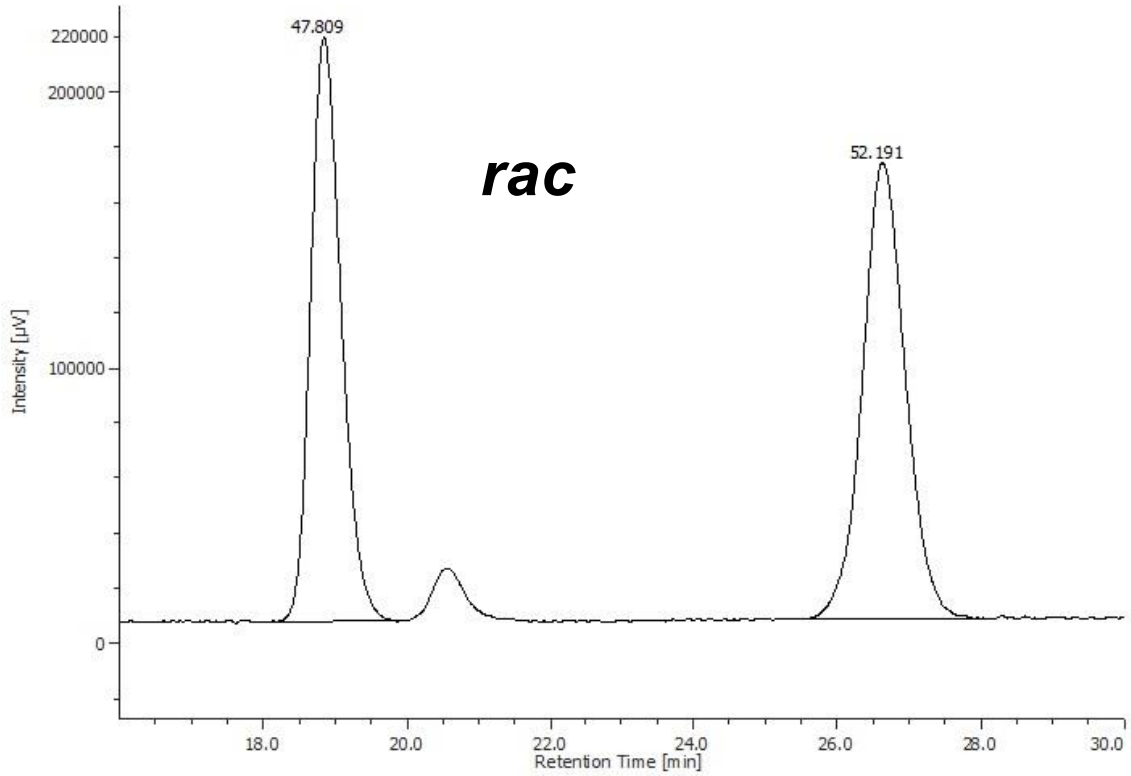

Two Chiralcel OD-H columns (95:5 hexane: 2-propanol, 1.0 mL/min, 254 nm)

Figure S93. HPLC of **5d**, related to **Figure 5**.

rac

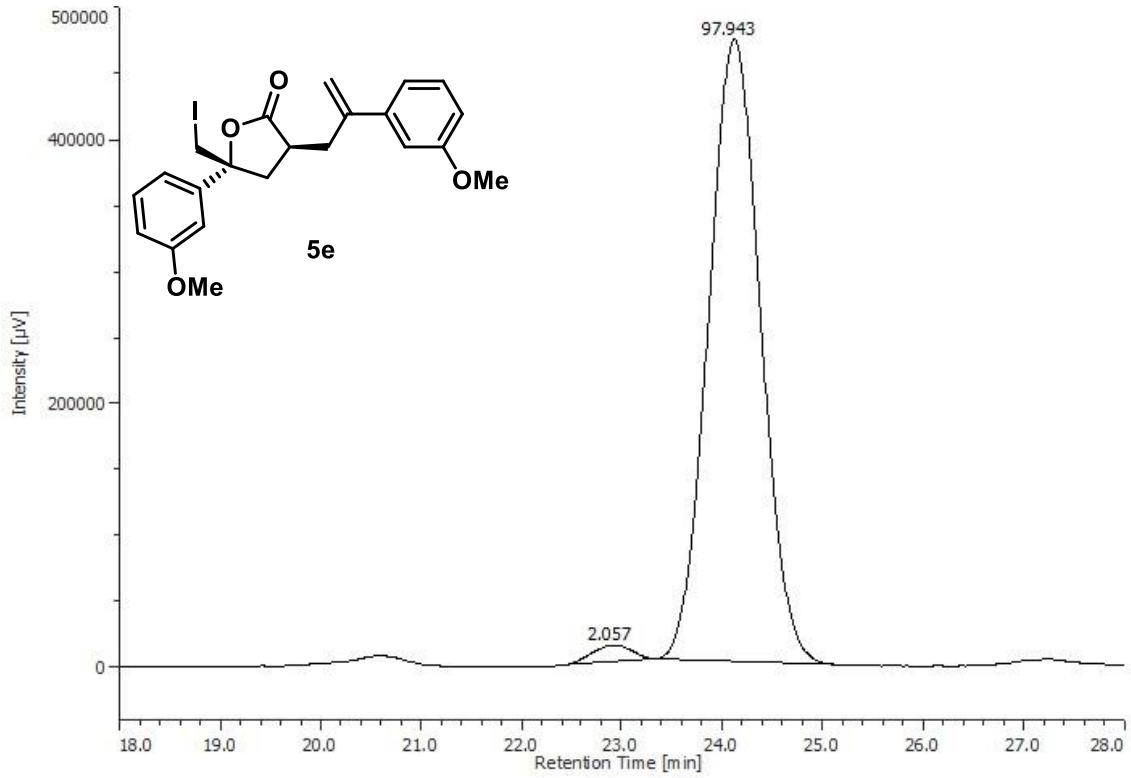

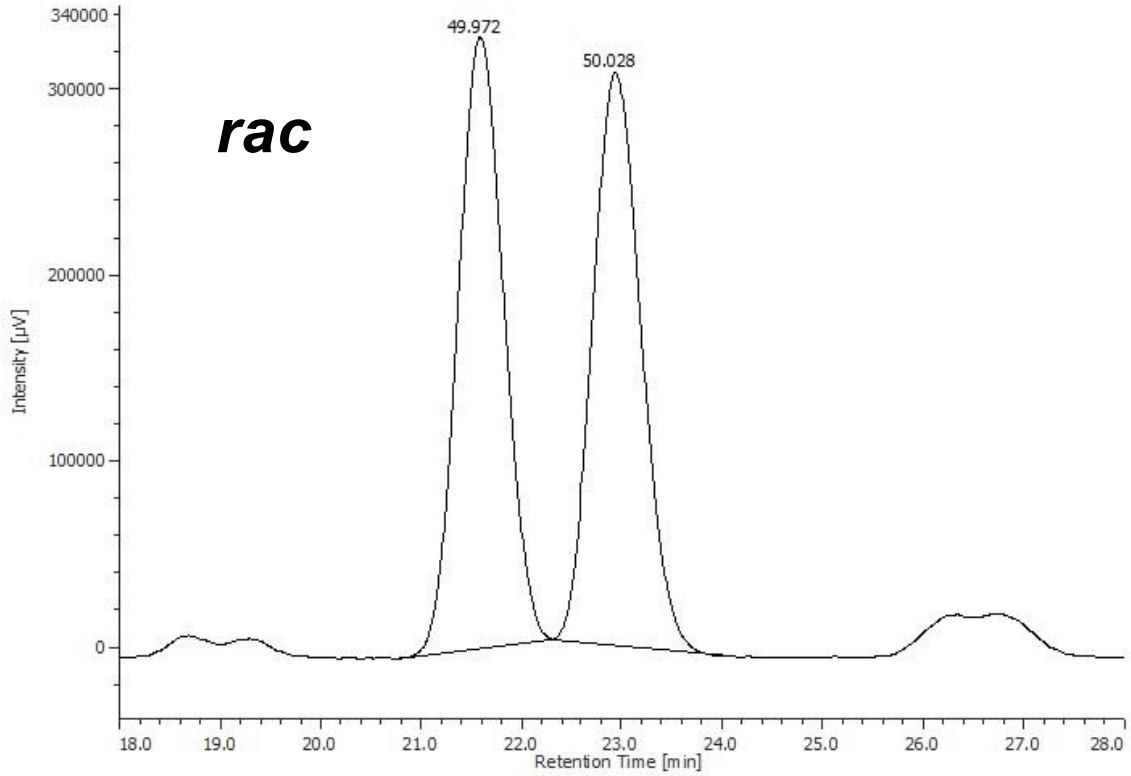

Chiralpack IC-3 column (95:5 hexane: 2-propanol, 1.0 mL/min, 254 nm)

Figure S94. HPLC of **5e**, related to **Figure 5.**

rac

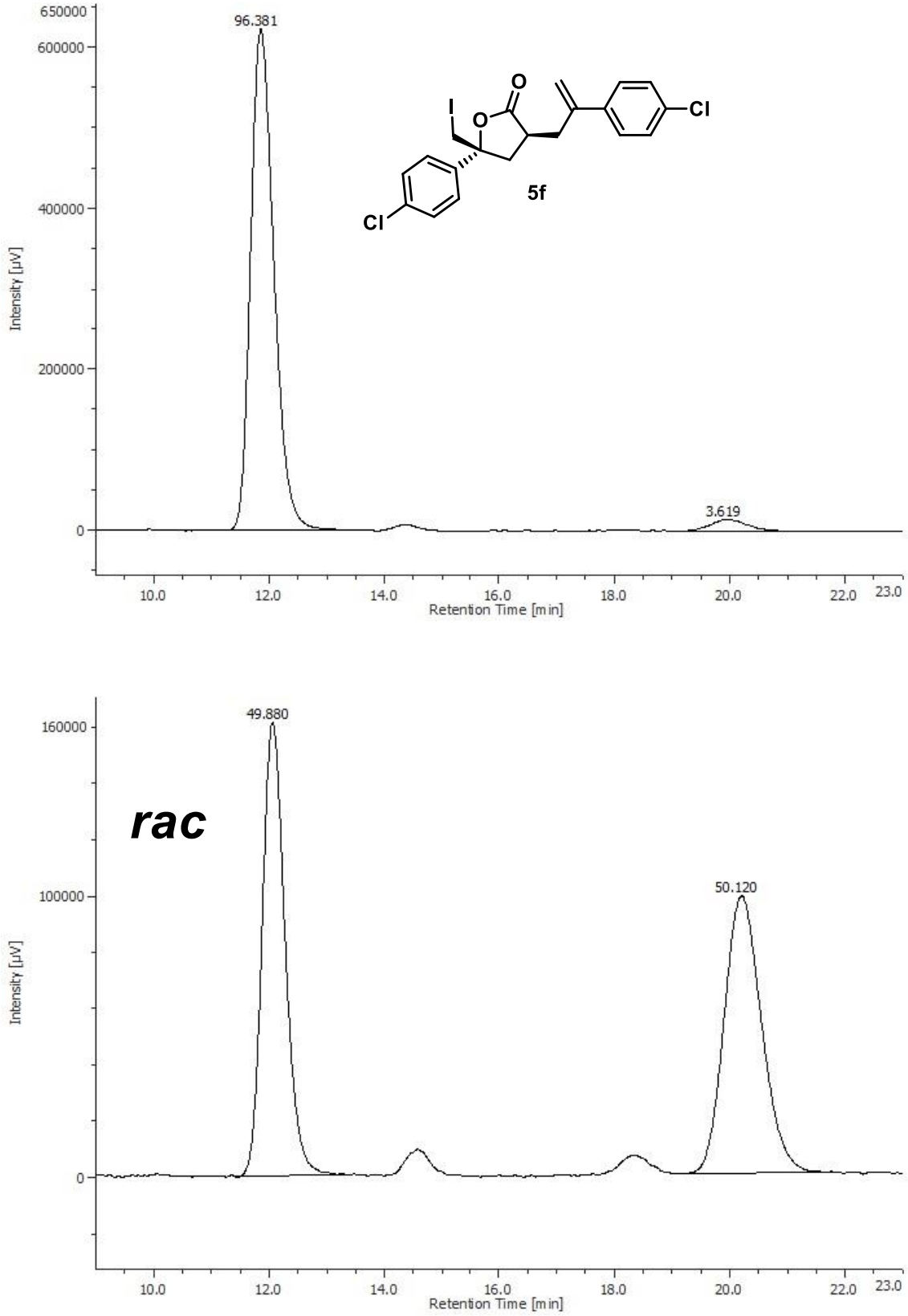

Chiralpack AS-H column (90:10 hexane: 2-propanol, 1.0 mL/min, 254 nm)

Figure S95. HPLC of **5f**, related to **Figure 5.**

rac

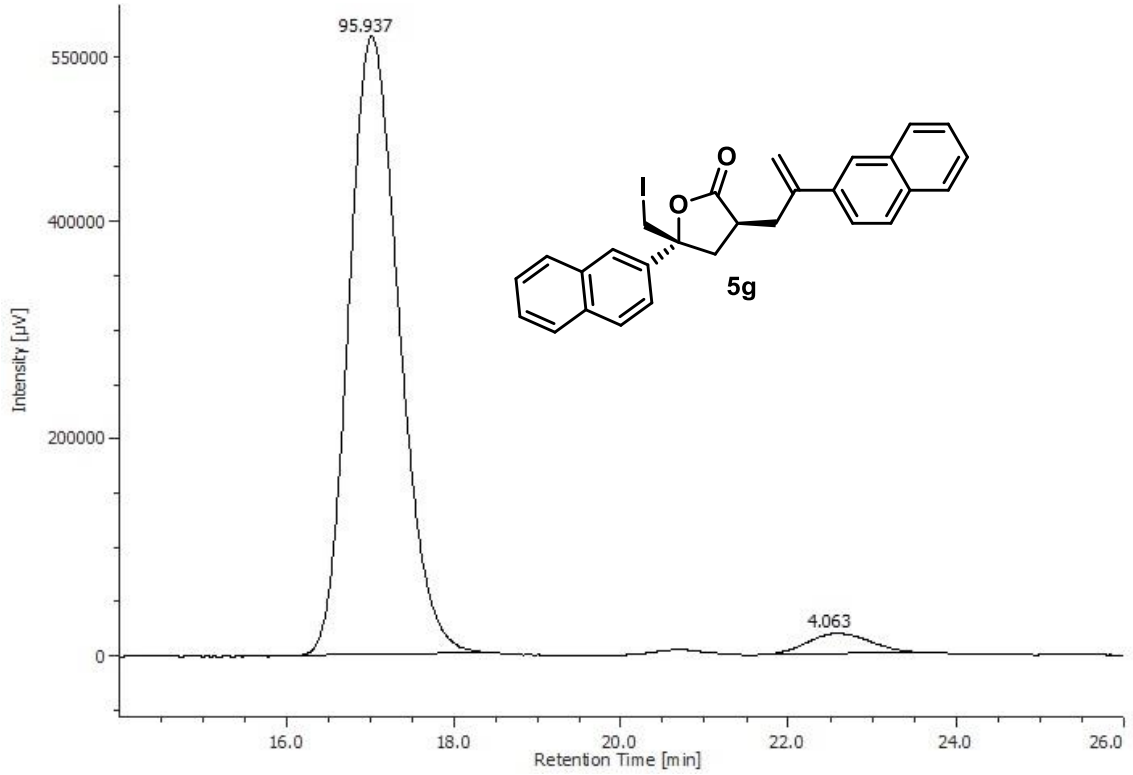

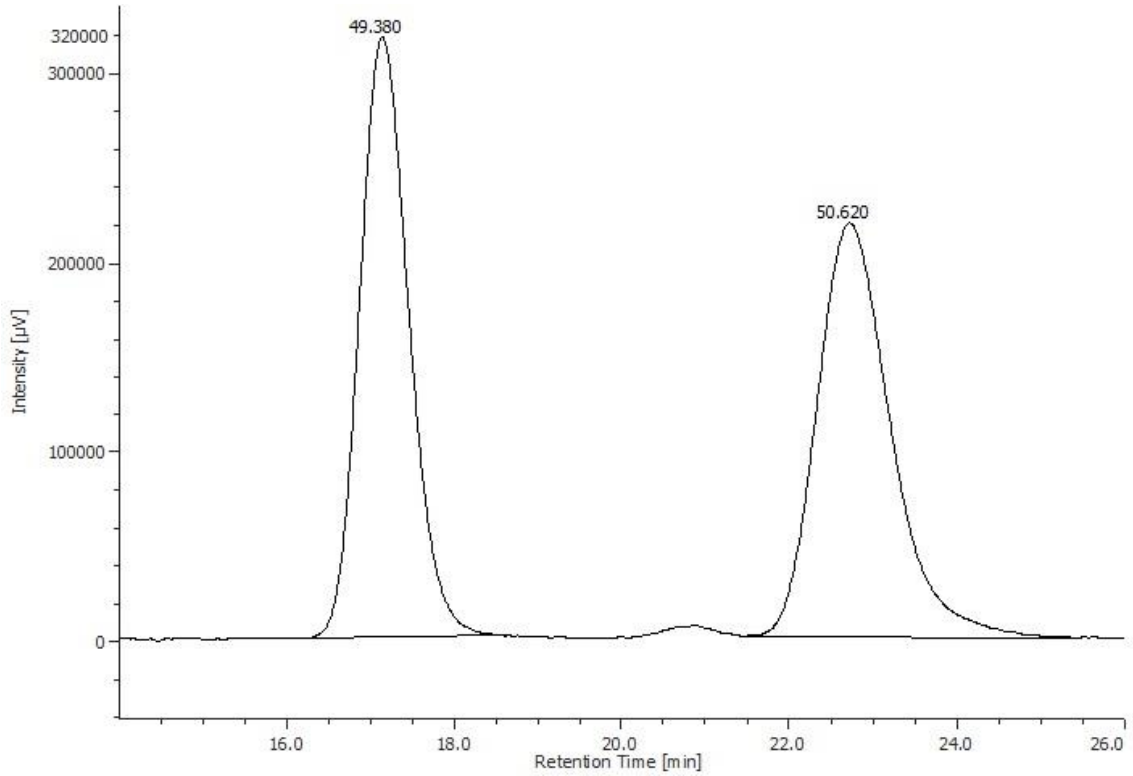

Chiralpack AS-H column (90:10 hexane: 2-propanol, 1.0 mL/min, 254 nm)

Figure S96. HPLC of **5g**, related to **Figure 5.**

rac

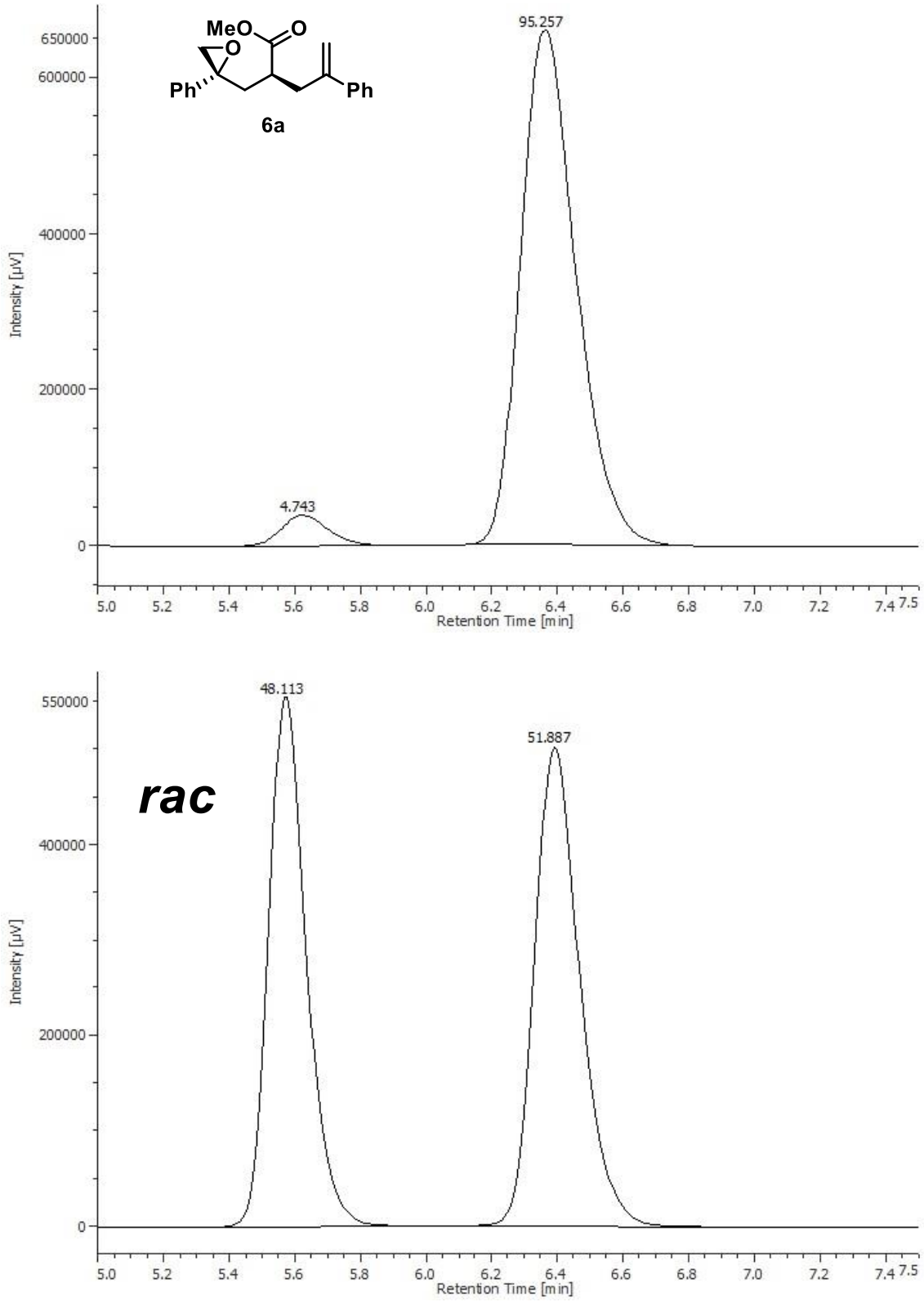

Chiralpack IC-3 column (70:30 hexane: 2-propanol, 1.0 mL/min, 254 nm)

Figure S97. HPLC of **6a**, related to **Table 1**.

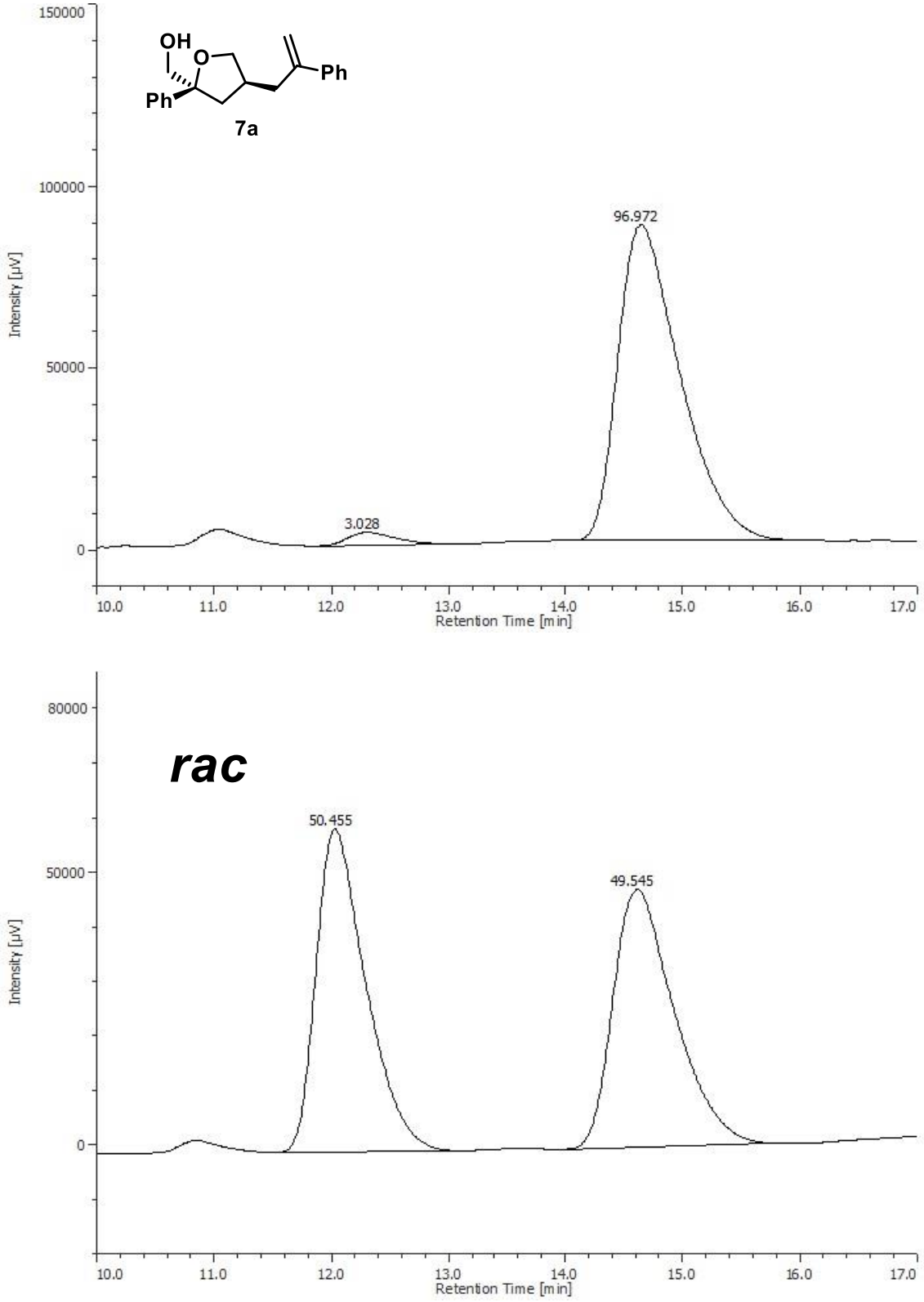

Chiralpack OJ-H column (90:10 hexane:2-propanol, 1.0 mL/min, 254 nm)

Figure S98. HPLC of **7a**, related to **Scheme 1**.

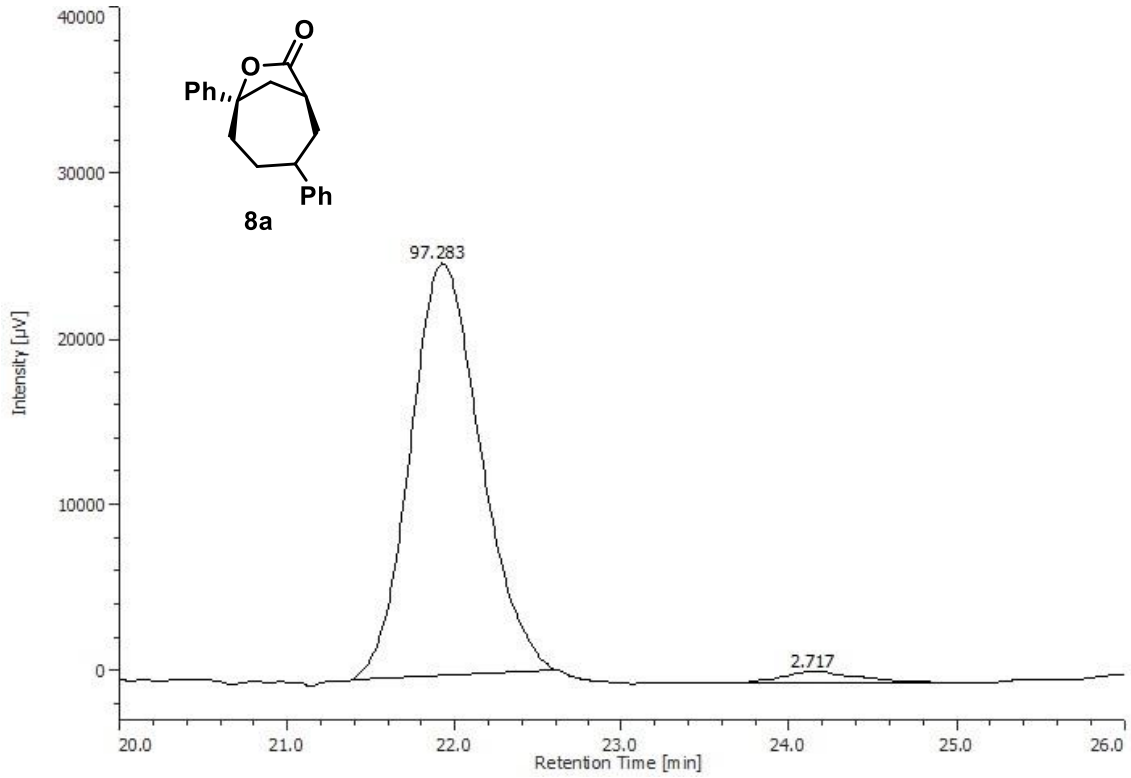

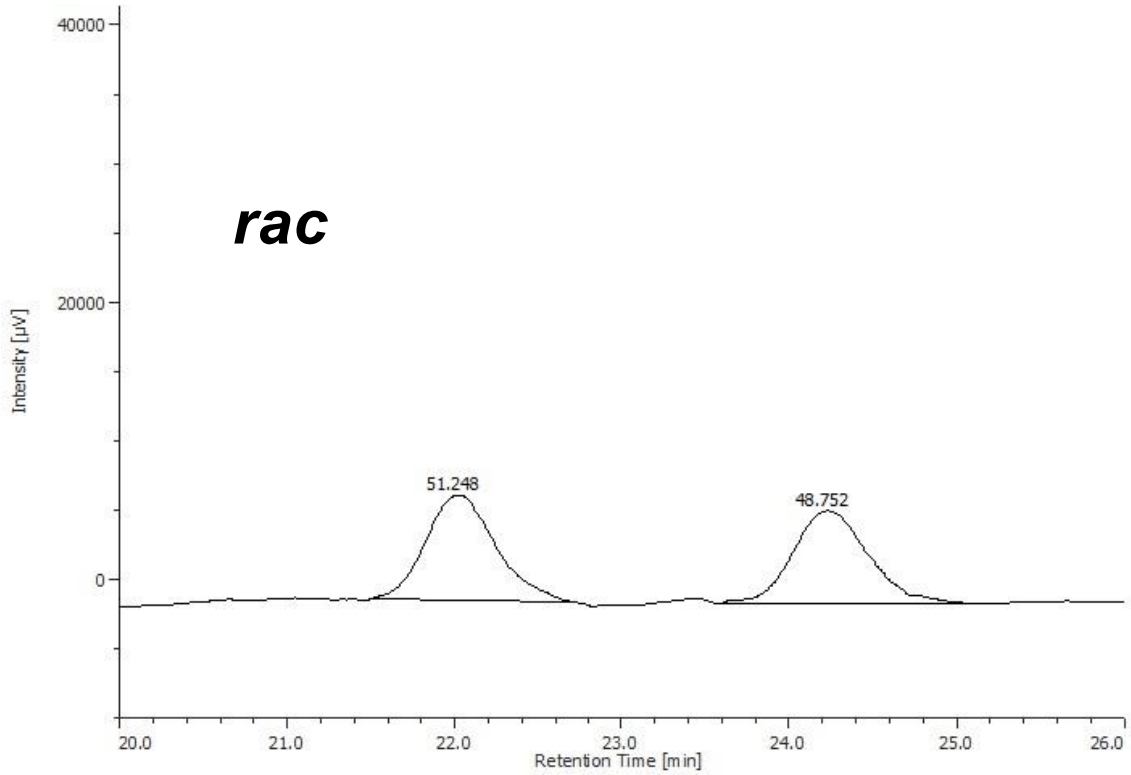

Chiralpack IC-3 column (90:10 hexane: 2-propanol, 1.0 mL/min, 254 nm)

Figure S99. HPLC of **8a**, related to **Scheme 1**.

17. X-Ray Crystallographic Data for γ-butyrolactone **5a** (**dataS1 related to Figure 5**)

_Identification code	CCDC 1825566
_chemical_formula_moiety	'C20 H19 I O2'
_chemical_formula_weight	418.25
_chemical_absolute_configuration	ad
_space_group_crystal_system	'orthorhombic'
_space_group_IT_number	19
_space_group_name_H-M_alt	'P 21 21 21'
_space_group_name_Hall	'P 2ac 2ab'
_cell_length_a	5.9572(11)
_cell_length_b	12.269(2)
_cell_length_c	23.607(5)
_cell_angle_alpha	90
_cell_angle_beta	90
_cell_angle_gamma	90
_cell_volume	1725.4(6)
_cell_formula_units_Z	4
_cell_measurement_reflns_used	3082
_cell_measurement_temperature	173
_cell_measurement_theta_max	24.4412
_cell_measurement_theta_min	2.3944
_shelx_estimated_absorpt_T_max	0.913
_shelx_estimated_absorpt_T_min	0.707
_exptl_absorpt_coefficient_mu	1.863
_exptl_absorpt_correction_T_max	0.91
_exptl_absorpt_correction_T_min	0.84
_exptl_absorpt_correction_type	empirical
_exptl_absorpt_process_details	'SADABS (Sheldrick 1996)'
_exptl_crystal_colour	colourless
_exptl_crystal_density_diffrn	1.610
_exptl_crystal_description	plate
_exptl_crystal_F_000	832
_exptl_crystal_size_max	0.2
_exptl_crystal_size_mid	0.05
_exptl_crystal_size_min	0.05
_exptl_special_details	'SADABS (Sheldrick 1996)'
_diffrn_reflns_av_R_equivalents	0.0356
_diffrn_reflns_av_unetI/netI	0.0505
_diffrn_reflns_Laue_measured_fraction_full	0.998
_diffrn_reflns_Laue_measured_fraction_max	0.932
_diffrn_reflns_limit_h_max	7
_diffrn_reflns_limit_h_min	-8
_diffrn_reflns_limit_k_max	14
_diffrn_reflns_limit_k_min	-16
_diffrn_reflns_limit_l_max	30
_diffrn_reflns_limit_l_min	-25

_diffrn_reflns_number	10190
_diffrn_reflns_point_group_measured_fraction_full	0.995
_diffrn_reflns_point_group_measured_fraction_max	0.900
_diffrn_reflns_theta_full	25.242
_diffrn_reflns_theta_max	28.771
_diffrn_reflns_theta_min	2.394
_diffrn_detector_area_resol_mean	8.3333
_diffrn_measured_fraction_theta_full	0.998
_diffrn_measured_fraction_theta_max	0.932
_diffrn_measurement_device_type	'Bruker APEXII CCD area detector'
_diffrn_measurement_method	'Phi and Omega scans'
_diffrn_radiation_type	MoK¥a
_diffrn_radiation_wavelength	0.71073
_reflns_Friedel_coverage	0.672
_reflns_Friedel_fraction_full	0.991
_reflns_Friedel_fraction_max	0.856
_reflns_number_gt	3601
_reflns_number_total	4033
_reflns_threshold_expression	'I > 2¥s(I)'
_refine_diff_density_max	0.413
_refine_diff_density_min	-0.347
_refine_diff_density_rms	0.082
_refine_ls_abs_structure_Flack	-0.017(16)
_refine_ls_goodness_of_fit_ref	1.036
_refine_ls_hydrogen_treatment	constr
_refine_ls_matrix_type	full
_refine_ls_number_parameters	208
_refine_ls_number_reflns	4033
_refine_ls_number_restraints	0
_refine_ls_R_factor_all	0.0379
_refine_ls_R_factor_gt	0.0304
_refine_ls_restrained_S_all	1.036
_refine_ls_shift/su_max	0.000
_refine_ls_shift/su_mean	0.000
_refine_ls_structure_factor_coef	Fsqd
_refine_ls_weighting_details	'w=1/[¥s^2^(Fo^2^)+(0.0111P)^2^+0.0059P] where P=(Fo^2^+2Fc^2^)/3'
_refine_ls_weighting_scheme	calc
_refine_ls_wR_factor_gt	0.0502
_refine_ls_wR_factor_ref	0.0532

18. References

Arai, T., Sugiyama, N., Masu, H., Kado, S., Yabe, S., and Yamanaka, M. (2014). A trinuclear $Zn_3(OAc)_4$-3,3'-bis(aminoimino)binaphthoxide complex for highly efficient catalytic asymmetric iodolactonization. Chem. Comm. 50, 8287.

Arai, T., Watanabe, M., Yanagisawa, A. (2007). Practical Asymmetric Henry Reaction Catalyzed by a Chiral Diamine-$Cu(OAc)_2$ Complex. Org. Lett. *9*, 3595.

Belkon, Y. N., Chusov, D., Borkin, D. A., Yashkina, L. V., Dmitriev, A. V., Katayev, D., North, M. (2006). Chiral Ti(IV) complexes of hexadentate Schiff bases as precatalysts for the asymmetric addition of TMSCN to aldehydes and the ring opening of cyclohexene oxide. Tetrahedron: Asymmetry *17*, 2328.

Frisch, M. J., Trucks, G. W., Schlegel, H. B., Scuseria, G. E., Robb, M. A., Cheeseman, J. R., Scalmani, G., Barone, V., Mennucci, B., Petersson, G. A., Nakatsuji, H., Caricato, M., Li, X., Hratchian, H. P., Izmaylov, A. F., Bloino, J., Zheng, G., J. Sonnenberg, L., Hada, M., Ehara, M., Toyota, K., Fukuda, R., Hasegawa, J., Ishida, M., Nakajima, T., Honda, Y., Kitao, O., Nakai, H., Vreven, T., Montgomery Jr, J. A., Peralta, J. E., Ogliaro, F., Bearpark, M., Heyd, J. J., Brothers, E., Kudin, K. N., Staroverov, V. N., Keith, T., Kobayashi, R., Normand, J., Raghavachari, K., Rendell, A., Burant, J. C., Iyengar, S. S., Tomasi, J., Cossi, M., Rega, N., Millam, J. M., Klene, M., Knox, J. E., Cross, J. B., Bakken, V., Adamo, C., Jaramillo, J., Gomperts, R., Stratmann, R. E., Yazyev, O., Austin, A. J., Cammi, R., Pomelli, C., Ochterski, J. W., Martin, R. L., Morokuma, K., Zakrzewski, V. G., Voth, G. A., Salvador, P., Dannenberg, J. J., Dapprich, S., Daniels, A. D., Farkas, O., Foresman, J. B., Ortiz, J. V., Cioslowski, J., Fox, D. J. (2013) Gaussian 09, Revision D.01, Gaussian, Inc., Wallingford CT.

Hoffmann, J.; Kazmaier, U. (2014). A Straightforward Approach towards Cyclic Photoactivatable Tubulysin Derivatives. Angew. Chem. Int. Ed. *53*, 11356.

Kee, C. W., Wong, M. W. (2016). In Silico Design of Halogen-Bonding-Based Organocatalyst for Diels-Alder Reaction, Claisen Rearrangement, and Cope-Type Hydroamination. J. Org. Chem. *81*, 7459.

Legault, C. Y. (2009) CYLview, 1.0b, Université de Sherbrooke.

Niu, W., Yeung, Y.-Y. (2015). Catalytic and Highly Enantioselective Selenolactonization. Org. Lett. *17*, 1660.

Pratch, G., Overmann, L. E. (2015). Synthesis of 2,5-Diaryl-1,5-dienes from Allylic Bromides Using Visible-Light Photoredox Catalysis. J. Org. Chem. *80*, 11388.

Tay, D. W., Leung, G. Y. C., Yeung, Y.-Y. (2014). Desymmetrization of Diolefinic Diols by Enantioselective Amino-thiocarbamate-Catalyzed Bromoetherification: Synthesis of Chiral Spirocycles. Angew. Chem. Int. Ed. *53*, 5161.

Wünnemann, S., Frölich, R., Hoppe, D. (2008). Asymmetric Strecker Reaction of N-Benzhydrylimines Utilising New Tropos Biphenyldiol-Based Ligands. Eur. J. Org. Chem. 684.

Zhao, Y., Truhlar, D. G. (2008). The M06 suite of density functionals for main group thermochemistry, thermochemical kinetics, noncovalent interactions, excited states, and transition elements: two new functionals and systematic testing of four M06-class functionals and 12 other functionals. Theor. Chem. Acc. *120*, 215.